

REPORT 950

INVESTIGATION OF A SYSTEMATIC GROUP OF NACA 1-SERIES COWLINGS WITH AND WITHOUT SPINNERS

By MARK R. NICHOLS and ARVID L. KEITH, Jr.

SUMMARY

An investigation has been conducted in the Langley propeller-research tunnel to study cowlings-spinner combinations based on the NACA 1-series nose inlets and to obtain systematic design data for one family of approximately ellipsoidal spinners. In the main part of the investigation, 11 of the related spinners were tested in various combinations with 9 NACA open-nose cowlings, which were also tested without spinners. The effects of location and shape of the spinner, shape of the inner surface of the cowlings lip, and operation of a propeller having approximately oval shanks were investigated briefly. In addition, a study was conducted to determine the correct procedure for extrapolating design conditions determined from the low-speed test data to the design conditions at the actual flight Mach number.

The design conditions for the NACA 1-series cowlings and cowlings-spinner combinations are presented in the form of charts from which, for wide ranges of spinner proportions and rates of internal flow, cowlings with near-maximum pressure recovery can be selected for critical Mach numbers ranging from 0.70 to about 0.85. In addition, the characteristics of the spinners and the effects of the spinners and the propeller on the cowlings design conditions are presented separately to provide initial quantitative data for use in a general design procedure through which NACA 1-series cowlings can be selected for use with spinners of other shapes. By use of this general design procedure, correlation curves established from the test data, and derived compressible-flow equations relating the inlet-velocity ratio to the surface pressures on the cowlings and spinner, NACA 1-series cowlings and cowlings-spinner combinations can be designed for critical Mach numbers as high as 0.90.

INTRODUCTION

The NACA 1-series nose inlets are a systematic series of open-nose cowlings, each having a near-maximum critical speed for its particular value of length-diameter ratio and inlet-diameter ratio at the correct rate of internal flow. Reference 1 reports the development of these cowlings, presents a simple procedure for their selection, and demonstrates the general applicability of the ordinates used to the design of other high-critical-speed-inlet configurations such as wing inlets, air scoops, and cowlings-spinner combinations (D-type cowlings). Because of the great importance of the latter

type of inlet in the case of conventional engine and turbo-propeller installations, a tentative procedure for the design of cowlings-spinner combinations utilizing the NACA 1-series nose inlets as the basic component was also presented in reference 1. The usefulness of this procedure was seriously limited, however, by the lack of information defining quantitatively the effects of the spinner and the propeller on the performance of the cowlings and on the characteristics of the entering flow.

The present investigation was undertaken in the Langley propeller-research tunnel to make a detailed study of cowlings-spinner combinations based on the NACA 1-series nose inlets and to obtain systematic design data for one family of approximately ellipsoidal spinners. For the main part of the investigation, in which 11 of the related spinners were tested in various combinations with 9 NACA 1-series open-nose cowlings, the maximum diameter of the spinner was located at the cowlings inlet. A representative configuration was tested, however, with the spinner projected somewhat farther ahead of the inlet, as might be used for a dual-rotating-propeller installation, and also with spinner withdrawn into the inlet, as is typical in the case of rotating cowlings (E-type cowlings) and jet-propulsion nacelles. Additional tests were conducted to study the characteristics of a conical spinner, designed to have a smaller pressure rise along its surface than that for the corresponding approximately ellipsoidal spinner, and to study the characteristics of a revised cowlings inner lip using NACA 1-series ordinates to eliminate the internal flow separation which occurs at the higher inlet-velocity ratios in the case of the standard NACA 1-series cowlings. The nine NACA 1-series cowlings were also tested in the open-nose condition to establish a base for determining the effects of the spinners.

The effects of propeller operation on the aerodynamic characteristics of a typical cowlings-spinner combination were studied through the use of a propeller with approximately oval shanks. Although other propeller configurations were not investigated, some information relative to the effects of propeller-shank configuration is provided by reference 2 and a beginning to the solution of the general propeller-cowlings-interference problem is afforded by reference 3 which presents a detailed study of the speeds and directions of the flow in the immediate field of seven of the cowlings configurations discussed herein.

Inasmuch as the present tests were conducted at low air-speeds, the investigation necessarily included a study of the procedure required to determine the design operating conditions at the design flight Mach number from the low-speed-test results. In this study, relations originally derived by German investigators for open-nose cowlings (for example, references 4 and 5) were generalized for the case of the cowling-spinner combination and extended to obtain a solution for compressible flow. The derived relations were then used to calculate the effect of Mach number on the design inlet-velocity ratio and to establish a simple correction procedure.

The method of analyzing the test data for use in the preparation of design charts is described, and design charts are given for the open-nose cowlings and for these cowlings when used in combination with each spinner of the related family. In addition, the characteristics of the spinners and the effects of the spinners and the propeller on the cowling design conditions are presented separately to provide initial quantitative data for use in a general design procedure from which NACA 1-series cowlings can be selected for use with spinners of other shapes.

SYMBOLS

| | |
|------------|---|
| A | area of stream tube containing internal flow |
| b | chord of propeller section |
| C | a function of M_0 and V_i/V_0 (see fig. 44) |
| d | cowling inlet diameter (see table I) |
| D | maximum diameter |
| f | skin-friction drag |
| F | maximum frontal area of cowling |
| H | total pressure |
| ΔH | total pressure loss between free stream and measuring station |
| h | thickness of propeller section |
| m | mass rate of internal air flow |
| M | Mach number |
| n | propeller rotational speed |
| p | static pressure |
| P | static-pressure coefficient $\left(\frac{p-p_0}{q_0}\right)$ |
| q | dynamic pressure $\left(\frac{1}{2} \rho V^2\right)$ |
| Q_c | propeller torque disk-loading coefficient $\left(\frac{\text{Torque}}{2q_0 D_p^3}\right)$ |
| R | radius of propeller tip |
| r | radius from model center line unless otherwise specified |
| T_c | propeller thrust disk-loading coefficient $\left(\frac{\text{Thrust}}{2q_0 D_p^2}\right)$ |
| V | velocity |
| x | distance from inlet along cowling axis |
| x_s | distance from nose of spinner along cowling axis |
| X | length of cowling from inlet to maximum-diameter station |
| X_f | length of cowling-inner-lip shape from nose to maximum-thickness station (see fig. 4) |
| X_s | length of spinner from nose to maximum-diameter station |

| | |
|----------|---|
| Y | maximum ordinate of cowling measured perpendicular to reference line at maximum-diameter station |
| Y' | thickness of cowling $\left(\frac{D_c-d}{2}\right)$ |
| Y_f | maximum ordinate of cowling-inner-lip shape measured perpendicular to reference line |
| Y_s | maximum radius of spinner $(D_s/2)$ |
| y | ordinate of cowling measured from reference line |
| y_s | radius to spinner surface |
| α | angle of attack of center line of model |
| β | propeller section blade angle measured from plane of rotation |
| γ | ratio of specific heat at constant pressure to specific heat at constant volume (1.4 for air) |
| δ | nominal boundary-layer thickness (defined as normal distance from surface to point where $\frac{H_t-p_0}{q_0} = 0.95$) |
| η | propulsive efficiency $\left(\frac{T_c}{2\pi Q_c} \left(\frac{V_0}{nD_p}\right)\right)$ |
| ρ | mass density of air |

Subscripts:

| | |
|-------|--|
| av | average value weighted according to mass flow in case of internal flow and according to frontal area in case of flow along surface |
| c | cowling |
| cr | condition corresponding to predicted critical Mach number |
| i | cowling inlet |
| min | minimum |
| 0 | free stream |
| p | propeller |
| s | spinner |
| t | condition corresponding to test Mach number |
| u | condition in propeller slipstream just outside cowling boundary layer |

COWLING AND SPINNER CONFIGURATIONS

The NACA 1-series nose-inlet ordinates (from reference 1) and relations for their application to the cowlings used in the present investigation are given in table I. As in reference 1, cowlings conforming to these ordinates are identified by a three-number designation, for example, 1-70-150. The first number indicates that the NACA 1-series ordinates are used; the second group and third group of numbers give the inlet diameter and cowling length, respectively, as percentages of the maximum cowling diameter. The cowling specified, therefore, has a 1-series profile with an inlet-diameter ratio d/D_c of 0.70 and a length ratio X/D_c of 1.50. The approximately ellipsoidal spinners of the family investigated were arbitrarily designed by revolving NACA 1-series nose-inlet ordinates about their reference line (table I) and are therefore identified by similar designations; for example, the NACA 1-40-060 spinner has a 1-series profile with $\frac{D_s}{D_c} = 0.40$ and $\frac{X_s}{D_c} = 0.60$.

The 9 NACA 1-series cowlings and 11 NACA 1-series spinners investigated are shown in figure 1. Each cowling was tested in conjunction with all spinners shown in the same horizontal row; in each case the maximum diameter of the spinner was located at the cowling inlet unless otherwise specified. The configurations tested to study the effects of varying the longitudinal location of the spinner with respect to the inlet are shown in figure 2. Modifications to the spinner and cowling shapes tested in attempts to obtain improved operational characteristics are presented in figures 3 and 4, respectively.

MODEL ARRANGEMENT AND TESTS

Views of the model installed in the Langley propeller-research tunnel are shown in figure 5. The internal-flow system (fig. 6) included an axial-flow fan which was necessary to obtain the higher inlet-velocity ratios. The internal flow was controlled by varying the speed of the fan motor and the position of the butterfly-type shutters. Flow quantities were measured by means of the total- and static-pressure tubes at the throat of the venturi and were checked by a rake at the exit. A thermocouple attached to the exit rake was used to measure the temperature rise through the fan.

Prior to the tunnel tests, the venturi in the tail of the model was carefully calibrated to assure the accuracy of the internal-flow-quantity measurements. It was found that accurate measurements could be obtained so long as the fan did not introduce appreciable rotation in the flow through the throat of the venturi. It was also determined that such rotation could be avoided for any desired flow quantity by simultaneous adjustment of the resistance of the system (by means of the shutters) and the rotational speed of the fan.

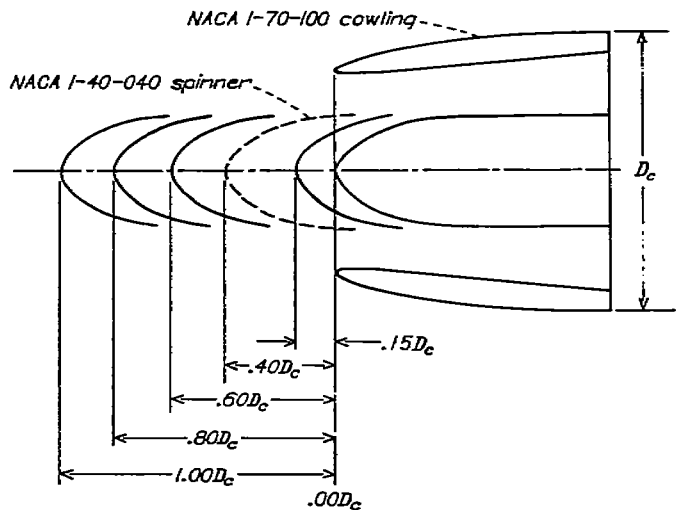


FIGURE 2.—Test configurations with longitudinally displaced spinner.

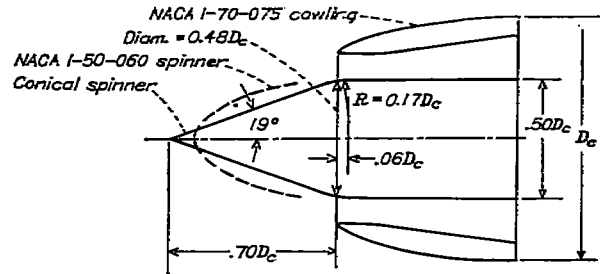


FIGURE 3.—Test configuration with conical spinner.

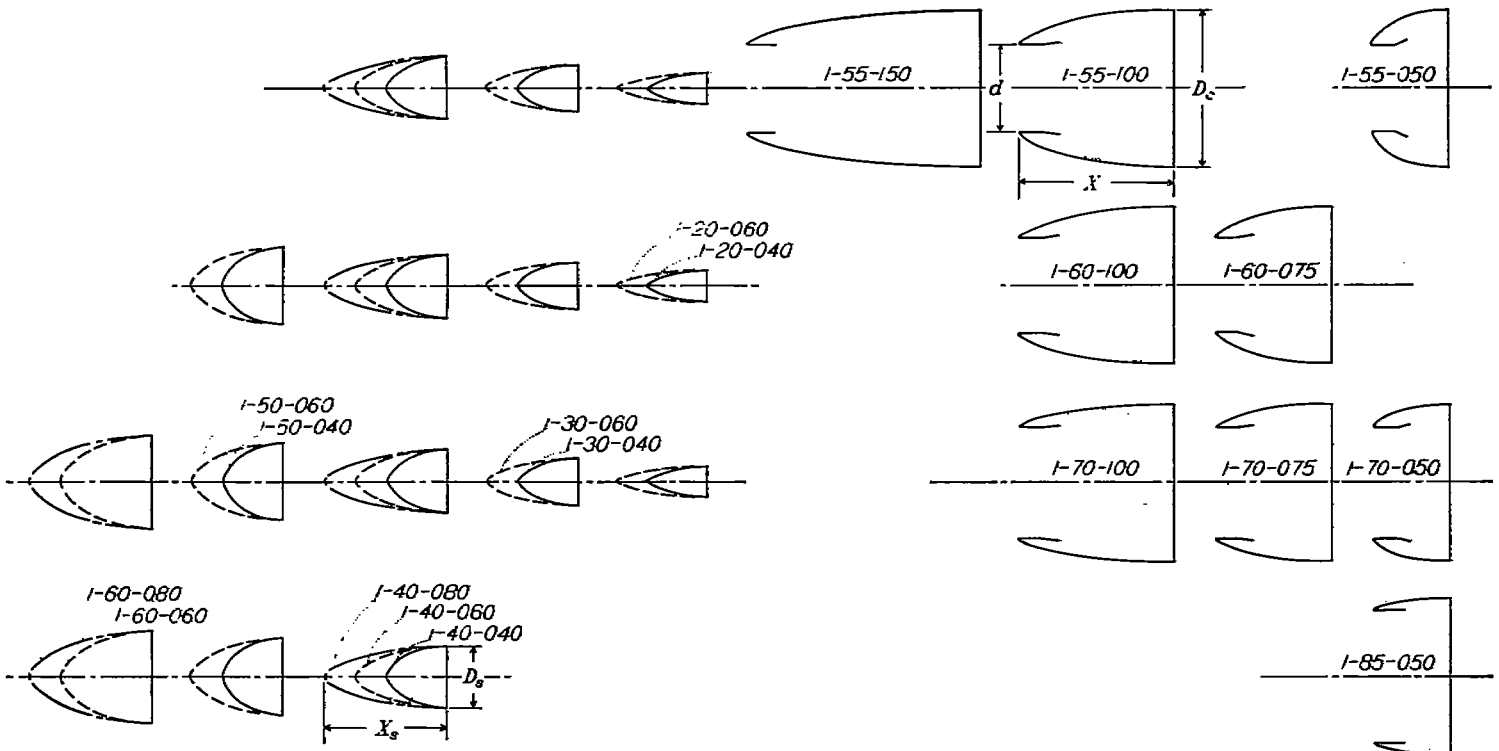


FIGURE 1.—NACA 1-series cowlings and spinners tested. Each cowling was tested in conjunction with all spinners in same horizontal row.

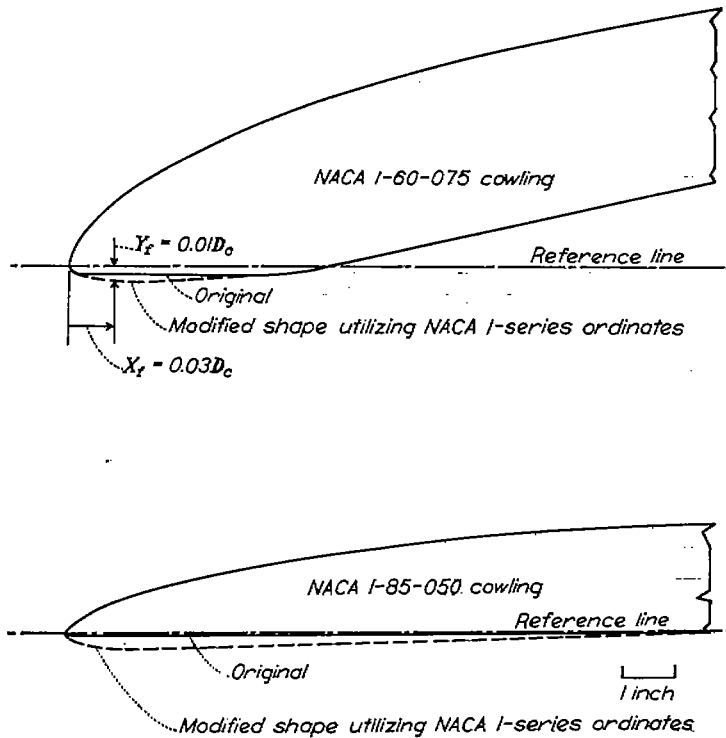


FIGURE 4.—Modified inner-lip shape tested on two basic cowlings.

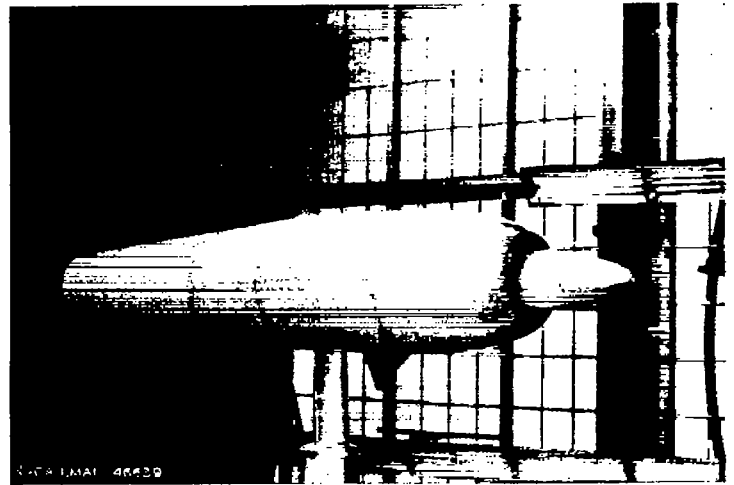
During the tunnel tests, uniform nonrotational flow in the venturi throat was obtained for each test condition by adjusting the shutter position and the fan speed until the static-pressure distribution across the venturi throat was uniform. Visual observation of a multitube manometer was used to establish this uniformity.

A three-blade 5.7-foot-diameter propeller (figs. 5 (b), 5 (c), and 7) driven by a variable-speed motor was used to investigate the effects of propeller operation on the aerodynamic characteristics of a typical cowling-spinner combination. The approximately oval shanks of this propeller were similar to those in general use. The propeller blade angle at the 0.75-radius station was fixed at 32° throughout the tests as this angle gave reasonable values of the thrust-torque relationship over the test range of thrust coefficient. The propeller operating conditions were as follows:

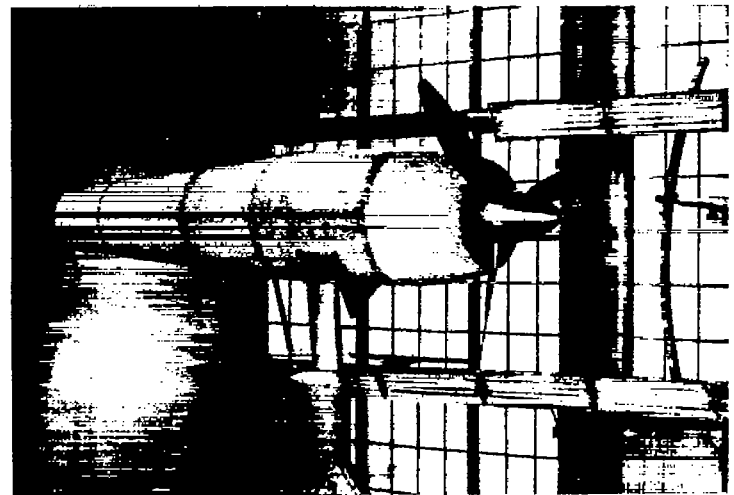
| T_c | Q_c | V_0/nD_p | η |
|-------|--------|------------|--------|
| 0.02 | 0.0058 | 1.46 | 0.81 |
| .06 | .0137 | 1.22 | .86 |
| .12 | .0237 | 1.03 | .83 |

The lowest thrust disk-loading coefficient, 0.02, is typical for the high-speed-flight condition of current airplanes but this value is probably an upper limit to the high-speed-flight values for future high-speed aircraft.

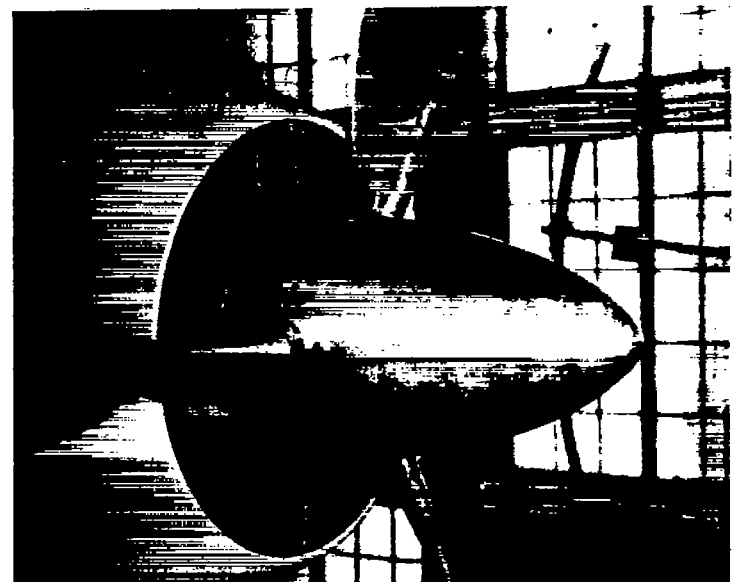
Surface pressures were measured by means of 11 flush orifices distributed along the top center line of each spinner and 22 orifices installed in the top section of each cowling. With propeller removed, pressure surveys were made at a station 0.75 inch inside the inlet by means of 10 total-pressure



(a) NACA 1-65-100 cowling with 1-40-030 spinner installed.



(b) Propeller installed; NACA 1-70-075 cowling with 1-40-030 spinner.



(c) Detail view of inlet showing propeller and instrumentation; NACA 1-70-075 cowling with 1-40-030 spinner.

FIGURE 5.—Views of model installed in Langley propeller-research tunnel.

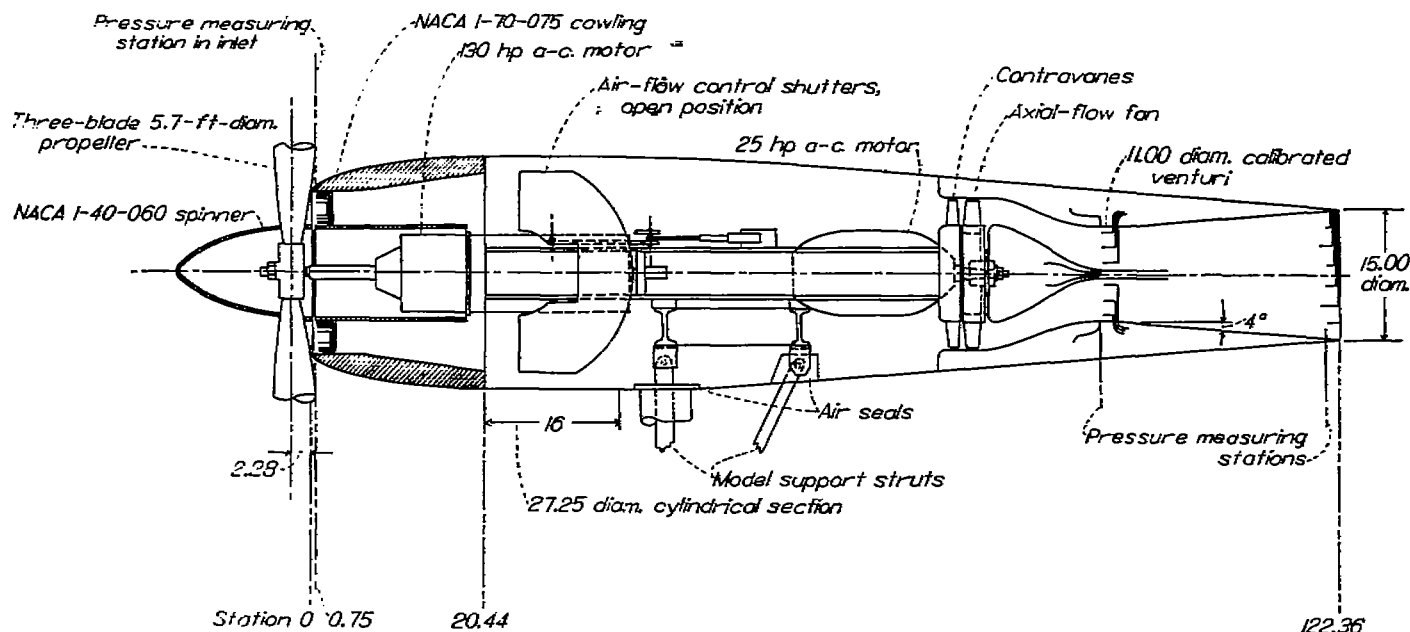


FIGURE 6.—General arrangement and principal dimensions of model. (All dimensions are in inches.)

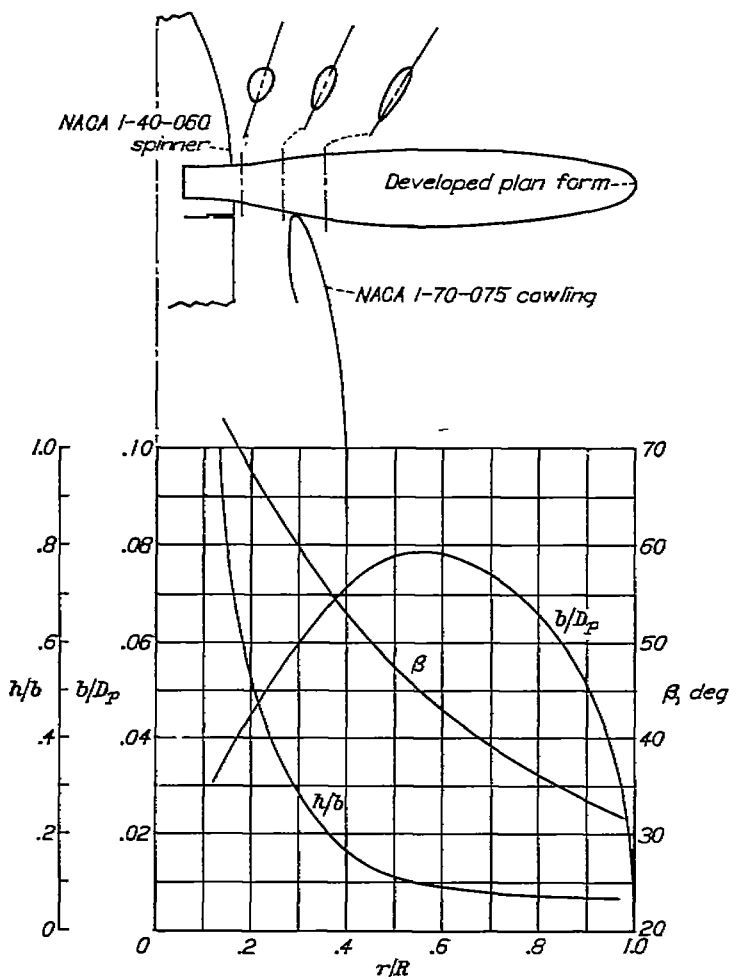


FIGURE 7.—Plan-form and blade-form curves for the test three-blade 5.7-foot-diameter propeller.

tubes extending across the annulus at the top of the inlet and 3 total-pressure tubes located 0.12, 0.25, and 0.50 inch from the cowling inner surface at the bottom of the inlet. For the propeller-installed tests, this inlet instrumentation was replaced by rakes of shielded total-pressure tubes supplemented at each end by boundary-layer rakes of four total-pressure tubes immediately adjacent to the annular surfaces. (See fig. 5 (c).) Two rakes of shielded total-pressure tubes at the top of the cowling (fig. 5 (c)) also were used in the propeller-installed tests to measure the total pressure of the flow in the vicinity of the surface orifices. All pressure measurements obtained by such instrumentation were recorded by photographing a multitube manometer. Pressures measured by the venturi instrumentation were read visually from a second multitube manometer.

With propeller removed, pressure surveys of each configuration were conducted for 11 to 18 values of inlet-velocity ratio at angles of attack of 0°, 2°, 4°, and 6°; angles of attack of 8° and 12° were also investigated in two instances. With propeller installed, pressure surveys were conducted for similar ranges of inlet-velocity ratio at angles of attack of 0° and 6° for propeller thrust disk-loading coefficients of 0.02, 0.06, and 0.12. A tunnel speed of 100 miles per hour, which corresponds to a Mach number of 0.13 and a Reynolds number of about 2×10^6 based on the maximum cowling diameter, was used for the majority of the tests for inlet-velocity ratios less than 1.3. For the configurations having very large inlet areas, the tunnel speed was reduced to 70 miles per hour to obtain the higher inlet-velocity ratios with the limited capacity of the fan.

RESULTS AND DISCUSSION

FLOW OVER SPINNERS

Surface pressures on NACA 1-series spinners.—Static-pressure distributions representative of those measured along the tops of the NACA 1-series cowling-spinner combinations are presented in figures 8 to 15. Sharp negative-pressure peaks did not occur in the distributions over the spinners for any of the conditions investigated, and the minimum pressures on the spinners were rarely less than that of the free stream except for very high values of inlet-velocity ratio. For given values of inlet-velocity ratio, the peak velocities on the spinners, indicated by the minimum pressure coefficients as summarized in figures 16 and 17, generally increased with increases in spinner diameter and angle of attack; except for the very high inlet-velocity ratios, increases in spinner length also caused increases in these peak velocities by moving the spinner nose farther ahead of the retarded flow in the immediate vicinity of the inlet.

The abrupt breaks which occurred in some of the spinner pressure distributions in the vicinity of the inlet at the lower inlet-velocity ratios (figs. 8 to 15) were caused by boundary-layer separation. For given values of inlet-velocity ratio and angle of attack, the shapes of the pressure distributions for the NACA 1-series spinners (see distributions for NACA 1-40-060 spinner which was typical) were changed somewhat by variations in both cowling length and cowling inlet diameter; however, the over-all pressure rise from the point of minimum pressure to the inlet was essentially unaffected by these cowling variables. The phenomenon of separation for these spinners, therefore, would be expected to be a function mainly of the spinner proportions, the inlet-velocity ratio, and the angle of attack so long as the inlet lip is located at a reasonable distance ($0.075D_c$ or greater) from the spinner surface. This conclusion may not apply for other types of spinners that might have, for example, more severe pressure gradients.

Effect of spinner location.—In order to determine the effect of spinner location, the NACA 1-40-040 spinner was tested in several longitudinal positions relative to the NACA 1-70-100 cowling. (See fig. 2.) The configurations with the nose of the spinner located near the inlet are of interest for the case of the rotating (E-type) cowling, whereas the configurations with the nose of the spinner located at $0.8D_c$ and $1.0D_c$ resemble the design frequently proposed for dual-rotating-propeller installations.

Static-pressure distributions over the cowling-spinner combinations of figure 2 are shown in figure 18. Insofar as the spinner was concerned, the most important effect of shifting its nose ahead of the inlet in successive increments was to increase successively the severity of the minimum pressure peak on its surface (fig. 19). Such increases, as

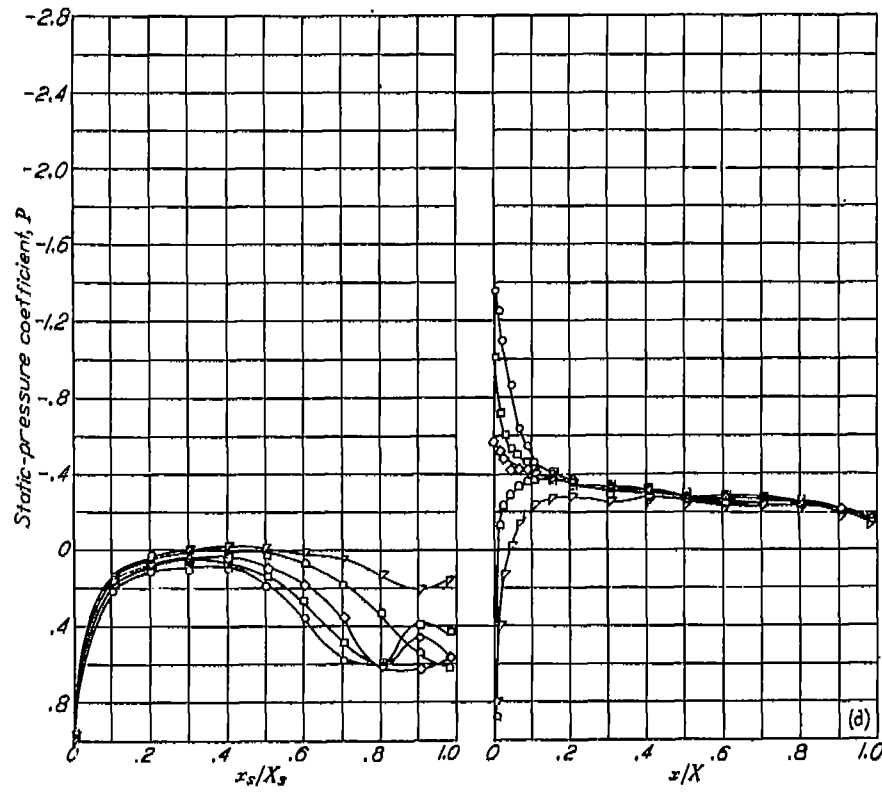
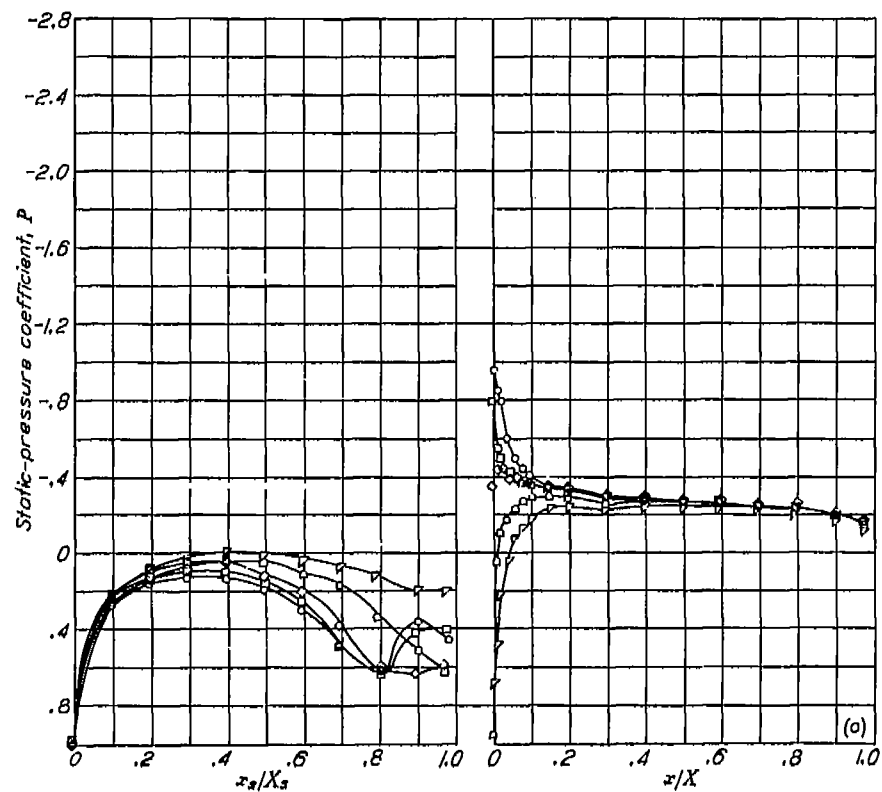
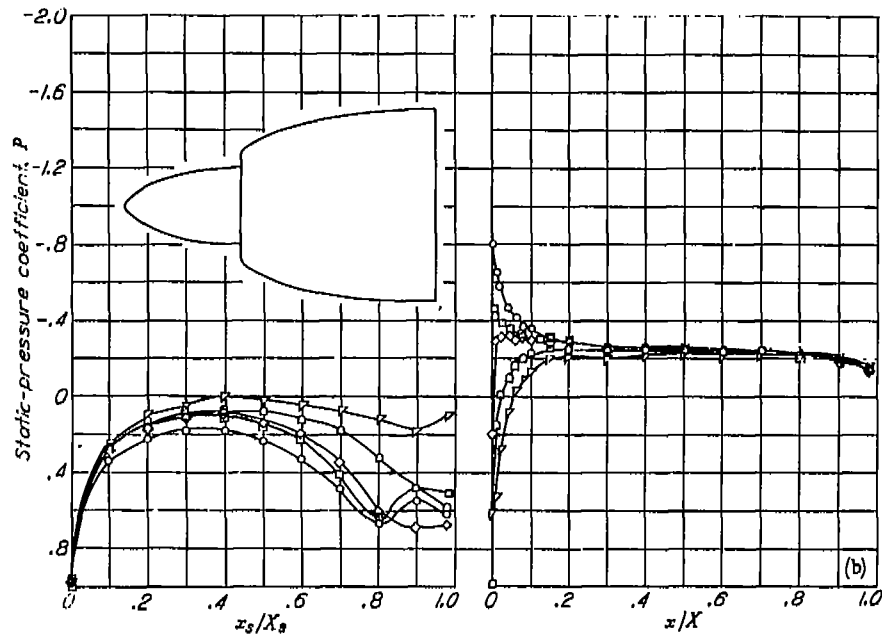
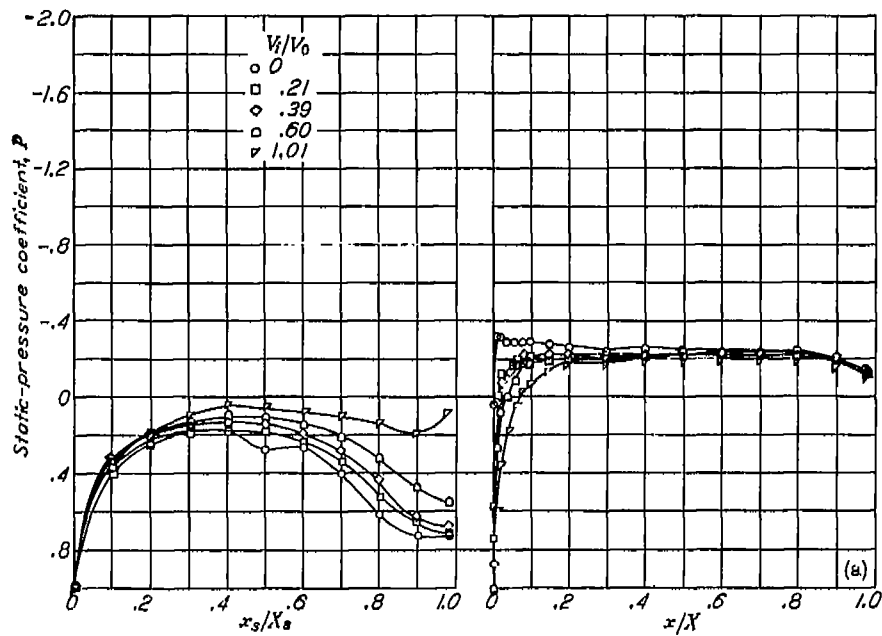
shown by the measurements of P. Ruden in the similar tests of reference 4, would cause corresponding increases in the pressure losses at the inlet at the lower inlet-velocity ratios and successive increases in the value of the minimum inlet-velocity ratio required to avoid such losses.

A comparison of the data of figures 18 and 8 to 15 shows that the minimum pressure peaks on the NACA 1-40-040 spinner when its nose was located at $0.60D_c$ and $0.80D_c$ ahead of the inlet were much more negative than those for the normally located $0.60D_c$ - and $0.80D_c$ -length spinners of the same or larger maximum diameter. Thus, for dual-rotating-propeller installations, the long normally located NACA 1-series spinners are superior to spinners having cylindrical base sections just ahead of the inlet with regard to the minimum value of inlet-velocity ratio, which can be used without incurring flow separation.

Effect of conical spinner.—A study of the surface pressure distributions over the NACA 1-series spinners (figs. 8 to 15) showed that appreciable pressure rises occurred ahead of the inlet at low values of inlet-velocity ratio. A conical spinner (fig. 3) was therefore tested in conjunction with the NACA 1-70-075 cowling to determine whether such a modification to the spinner shape would reduce the velocities along the spinner and thereby reduce the pressure rise acting on the spinner boundary layer. A comparison of the surface pressure distributions over the conical spinner with corresponding pressure distributions over NACA 1-series spinners of the same maximum diameter (fig. 20) shows that the desired result was obtained at all test values of inlet-velocity ratio. Such spinners are therefore superior to the NACA 1-series spinners with regard to the minimum value of inlet-velocity ratio, for which flow separation from the spinner surface is avoided, and are worthy of further research.

INTERNAL FLOW

Total-pressure distributions at inlet.—Total-pressure distributions across the annulus at the top of the inlet of a typical NACA 1-series cowling-spinner combination with propeller removed are shown in figure 21. At an angle of attack of 0° , a pressure-recovery coefficient of unity was obtained over most of the inlet at the higher inlet-velocity ratios. As the test inlet-velocity ratio was decreased below 0.5, however, the boundary layer on the spinner thickened rapidly and soon separated under the influence of the increasingly severe adverse pressure rise; this separation caused large losses in total pressure (fig. 22). The effect of increasing the angle of attack was to increase the severity of the flow separation from the spinner at the lower-inlet-velocity ratios and to require the use of a higher value of inlet-velocity ratio in order to avoid such separation. It should be noted that the losses in inlet total pressure caused by flow separation from the spinners would become increasingly severe with successive reductions in the width of the inlet annulus.



(a) $\alpha = 0^\circ$
(c) $\alpha = 4^\circ$

(b) $\alpha = 2^\circ$
(d) $\alpha = 6^\circ$

FIGURE 8.—Static-pressure distributions over top of NACA 1-65-100 cowling with 1-40-060 spinner. Propeller removed; $M_1 = 0.18$.

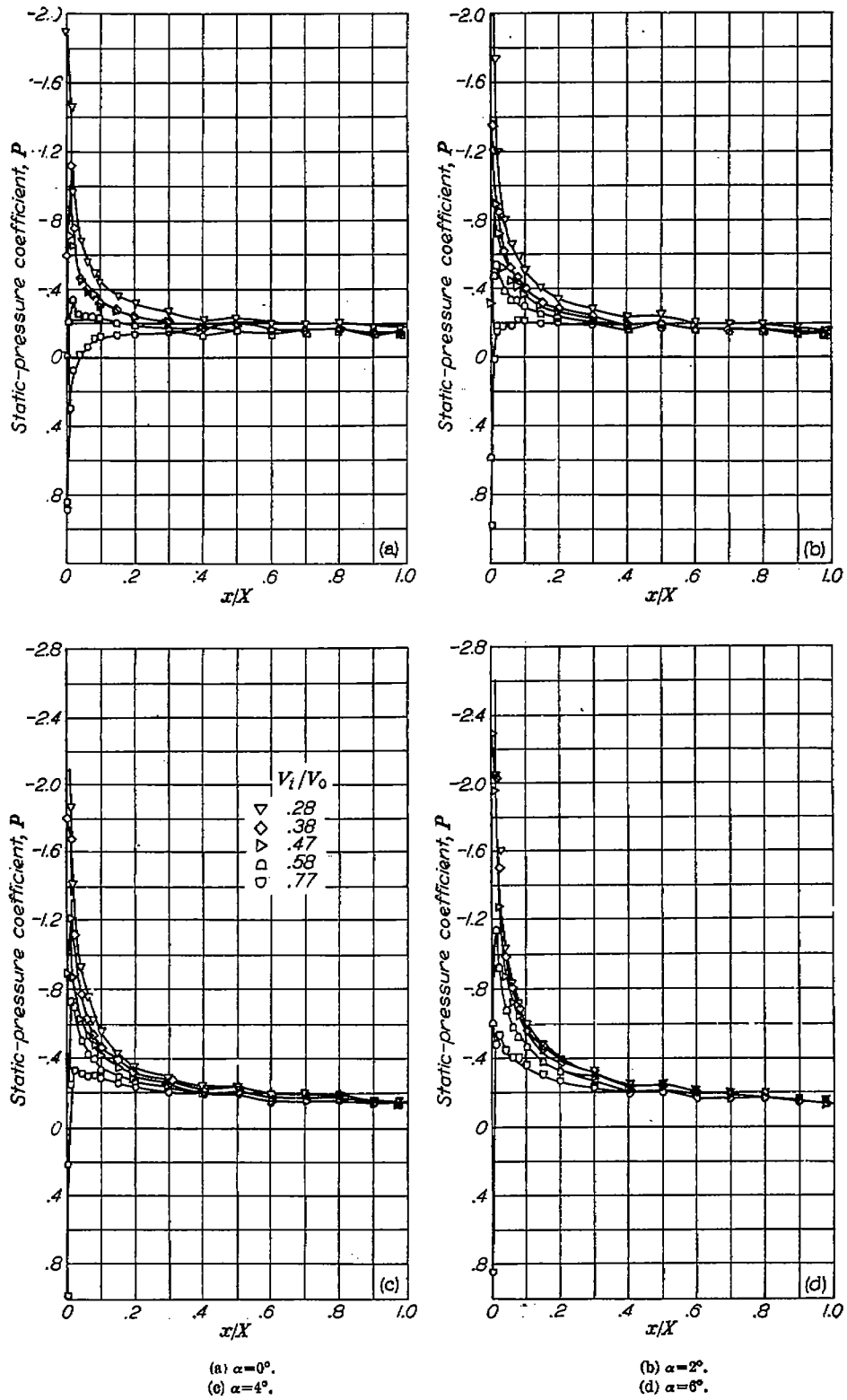


FIGURE 9.—Static-pressure distributions over top of NACA 1-70-100 cowling. Propeller removed; $M_1=0.13$.

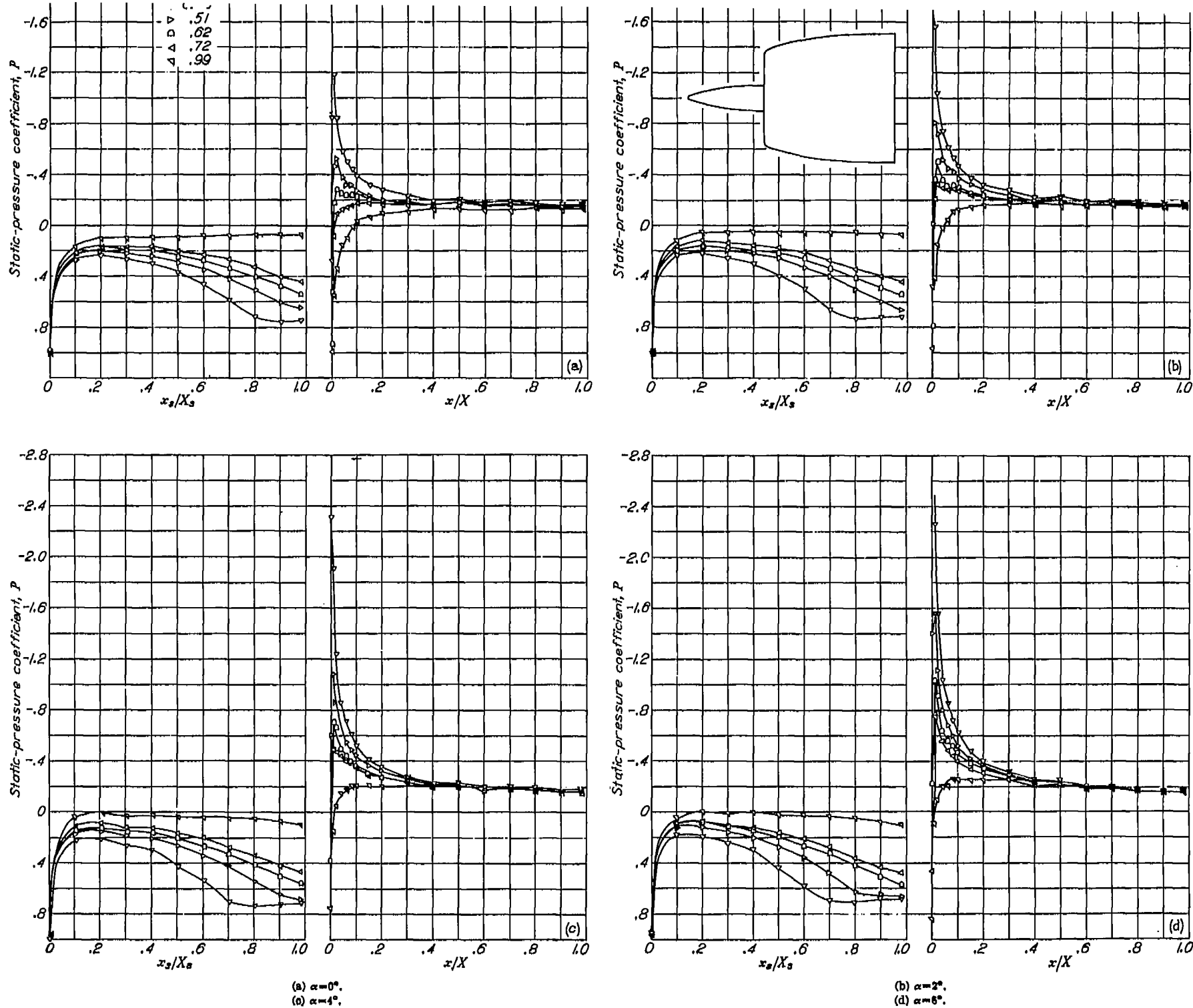


FIGURE 10.—Static-pressure distributions over top of NACA 1-70-100 cowlings with 1-20-060 spinner. Propeller removed; $M_1=0.13$.

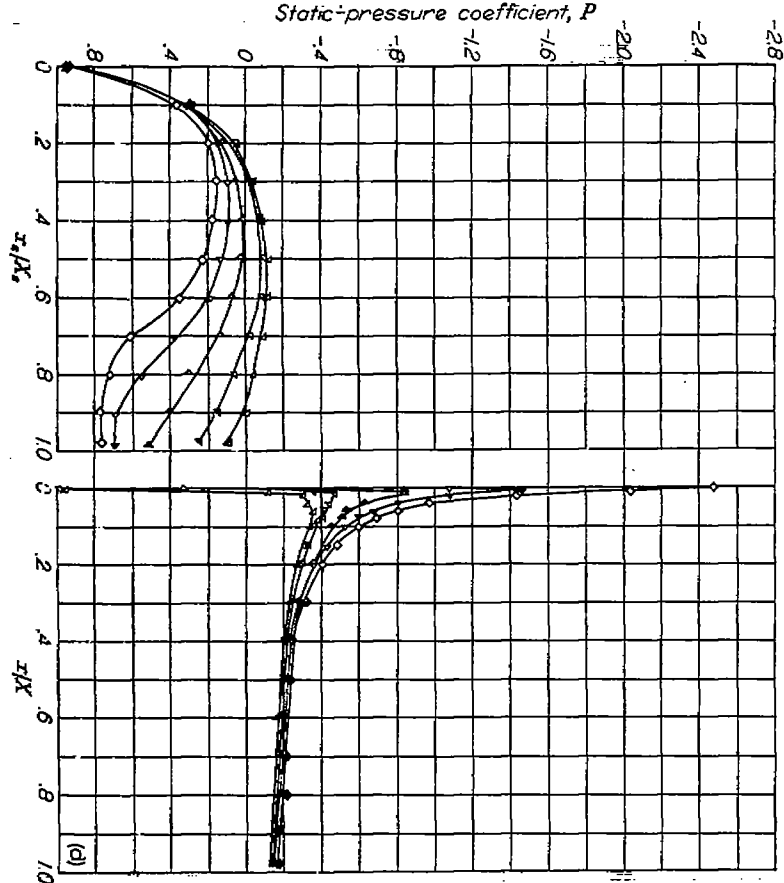
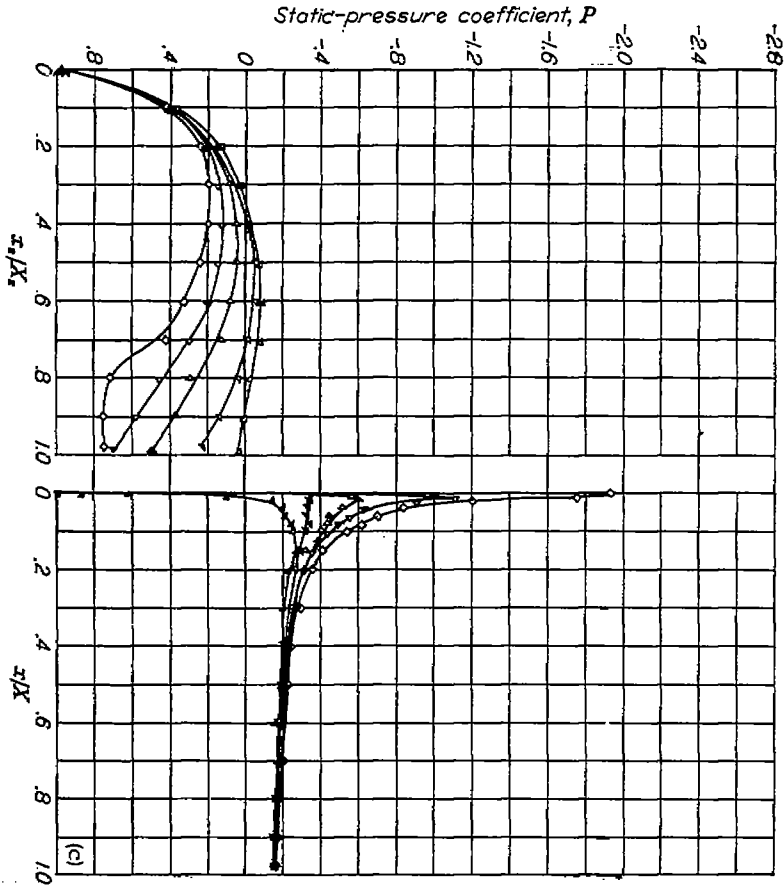
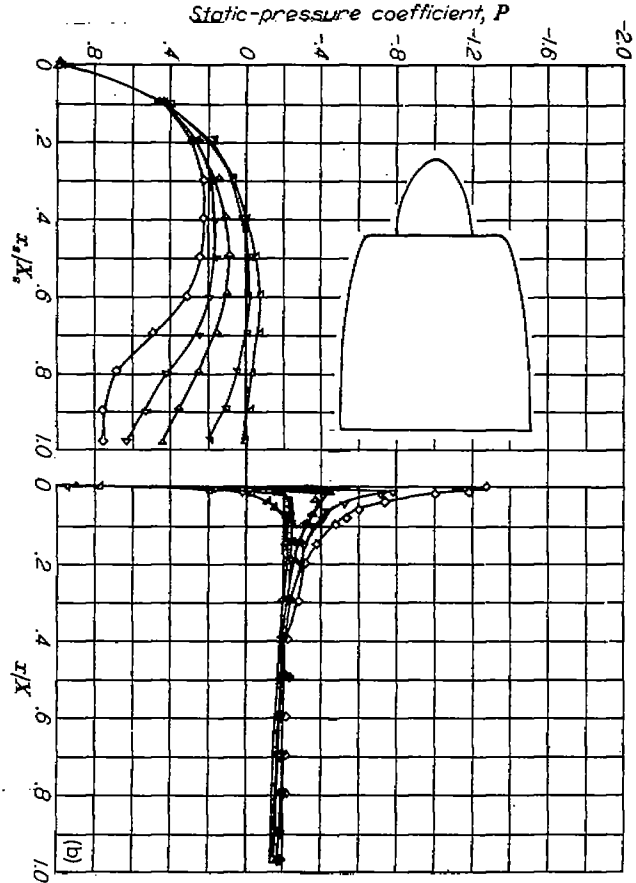
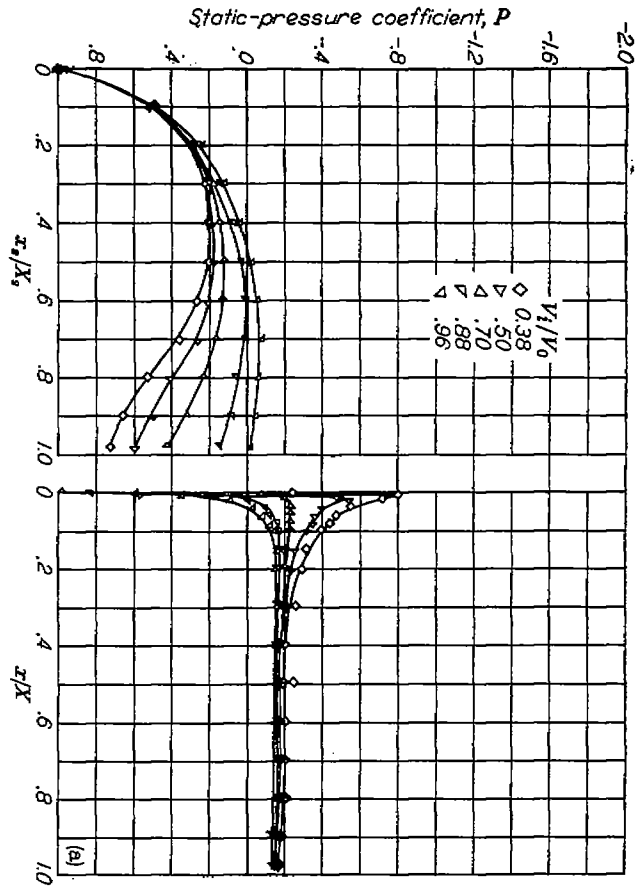


FIGURE 11.—Static-pressure distributions over top of NACA 1-70-300 airfoil with 1-40-040 splader. Preroller removed; $M_\infty = 0.13$.

(a) $\alpha = 0^\circ$,
(b) $\alpha = 2^\circ$.

(c) $\alpha = 0^\circ$,
(d) $\alpha = 2^\circ$.

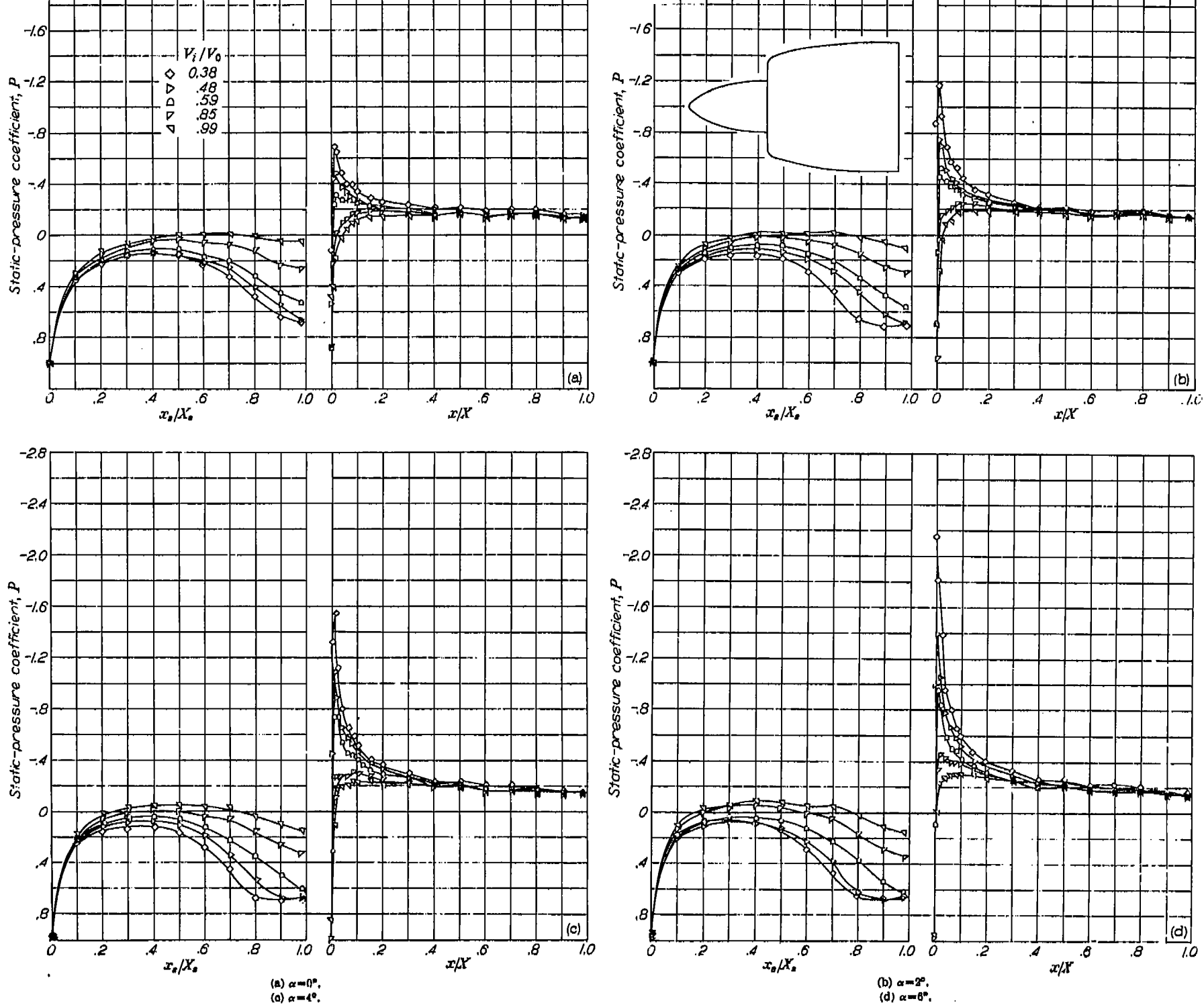


FIGURE 12.—Static-pressure distributions over top of NACA 1-70-100 cowling with 1-40-000 spinner. Propeller removed; $M_1 \approx 0.13$.

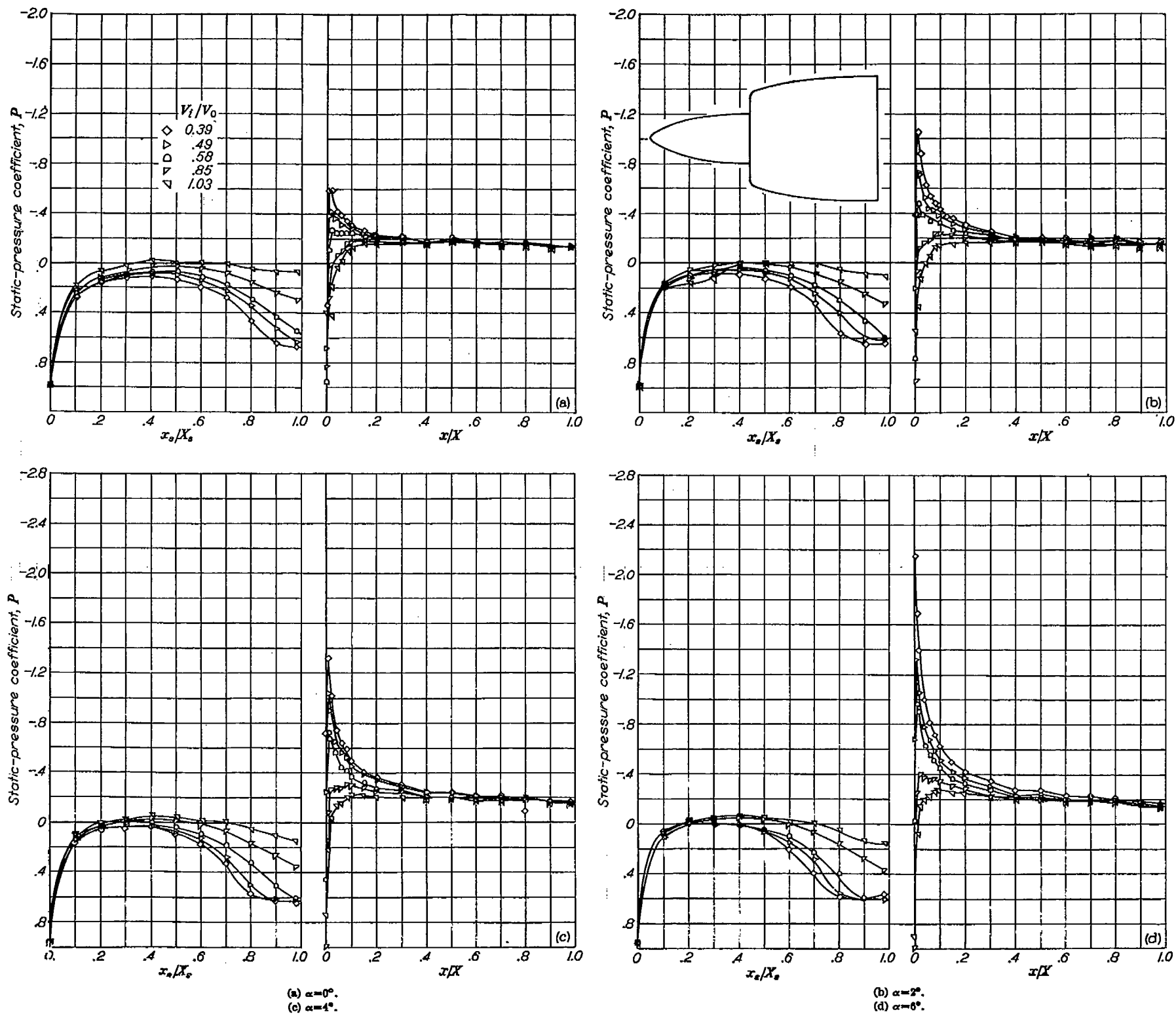


FIGURE 11.—Static-pressure distributions over top of NACA 170-140 cowling with 1-40-080 spinner. Propeller removed; $M_1=0.13$.

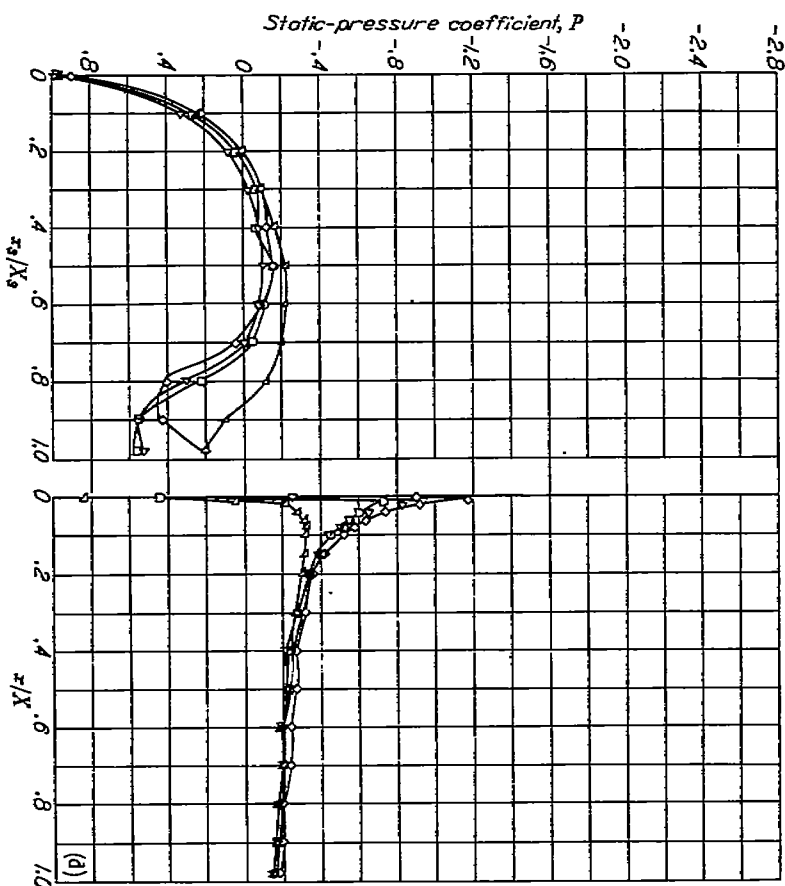
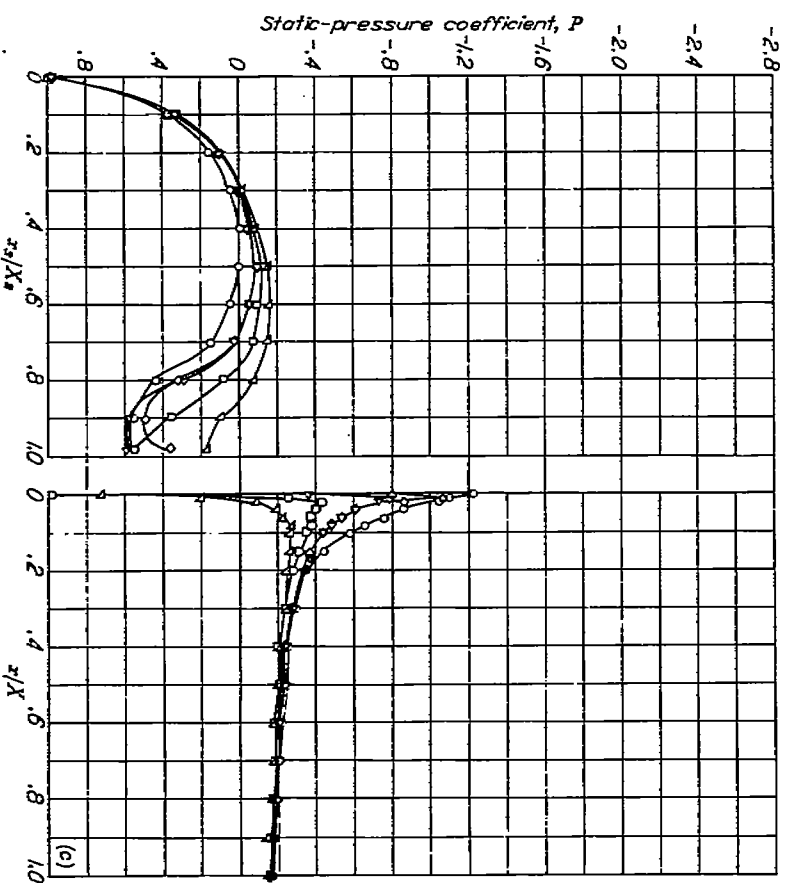
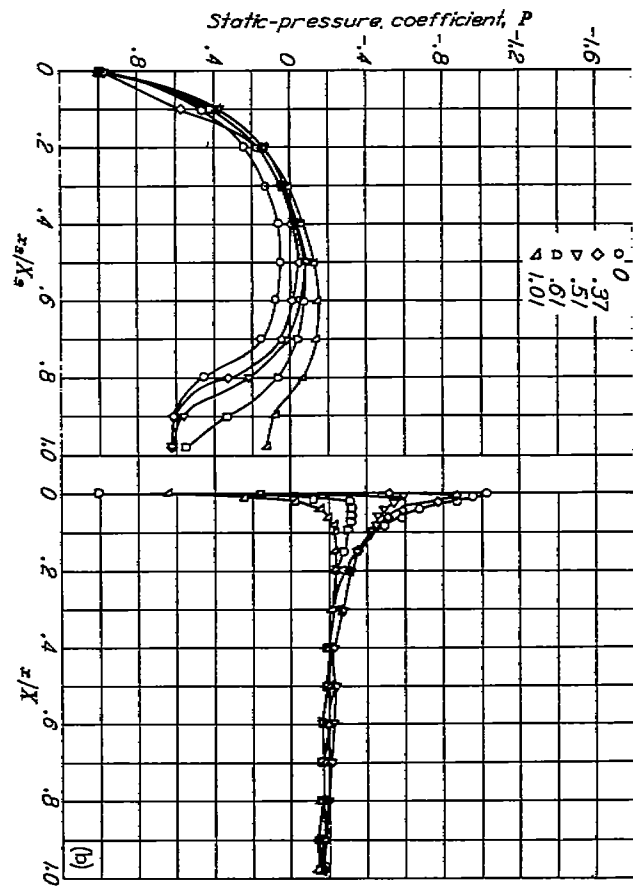
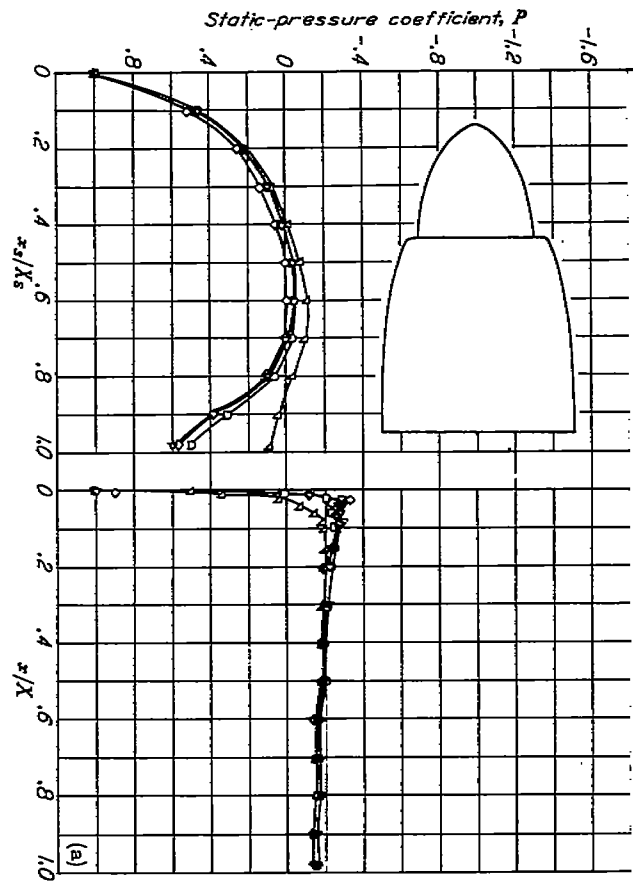
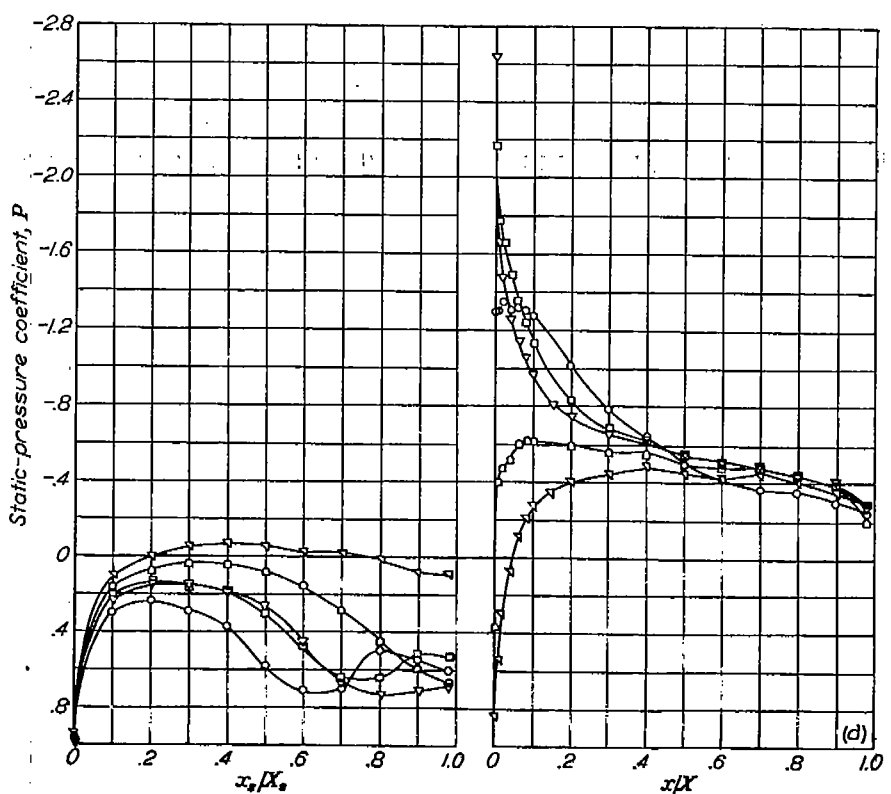
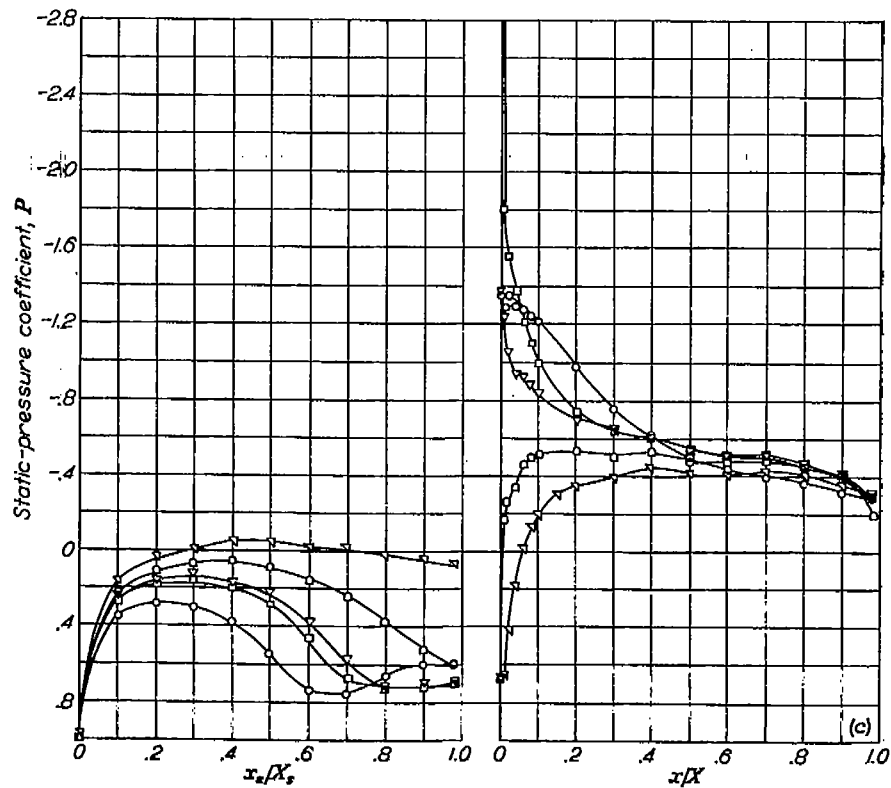
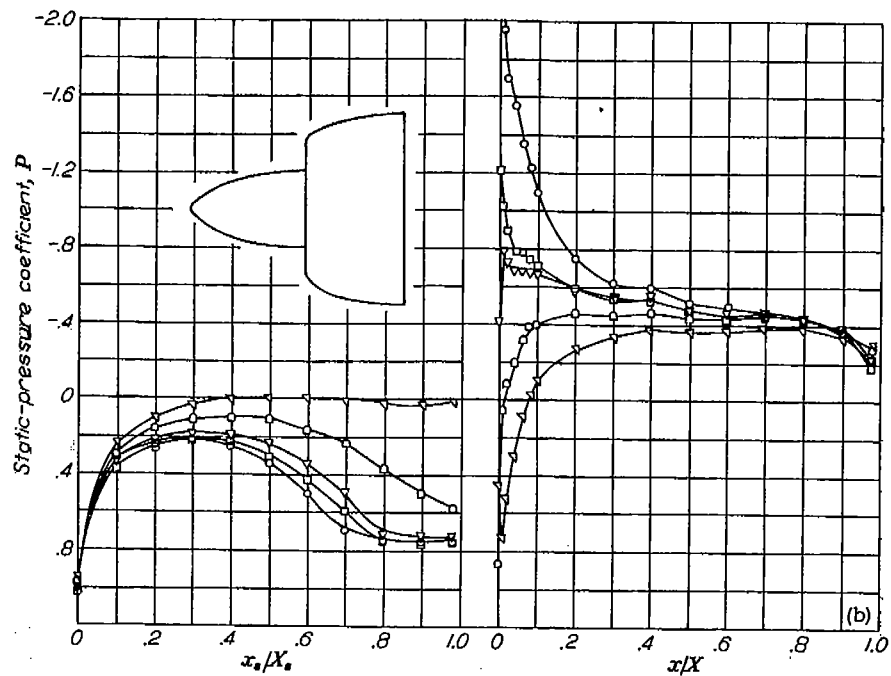
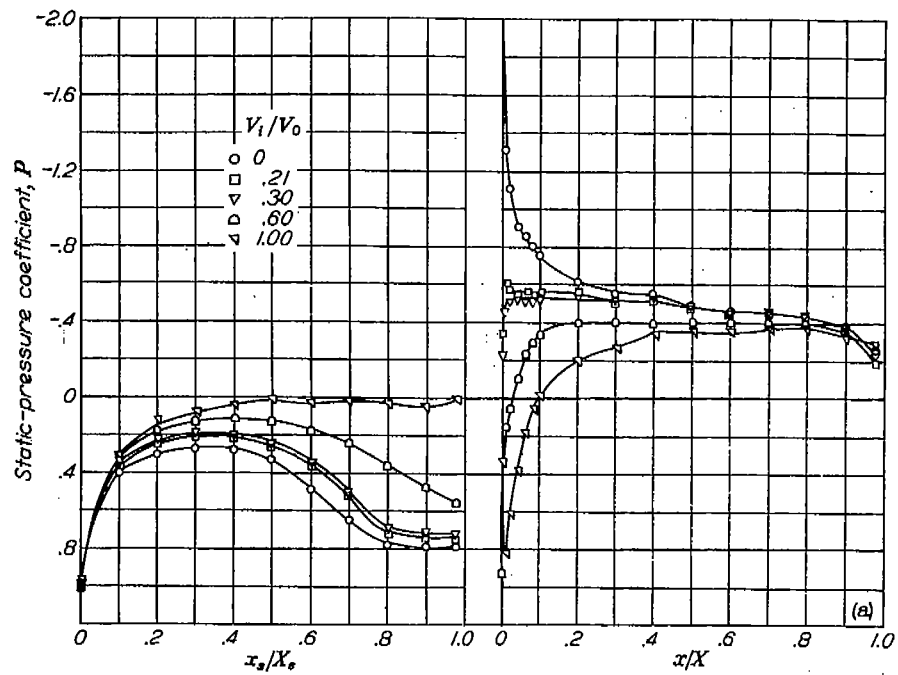


FIGURE 14.—Static-pressure distributions over top of NACA 1-70-100 cowling with 1-60-90 spinner. Propeller removed; $M_\infty=0.18$.

(a) $\alpha=0^\circ$
 (c) $\alpha=1^\circ$

(b) $\alpha=2^\circ$
 (d) $\alpha=8^\circ$



(a) $\alpha = 0^\circ$.
(c) $\alpha = 4^\circ$.

(b) $\alpha = 2^\circ$.
(d) $\alpha = 8^\circ$.

Figure 12. Static-pressure coefficient P versus x/X and x_s/X_s for various values of V_1/V_0 and α .

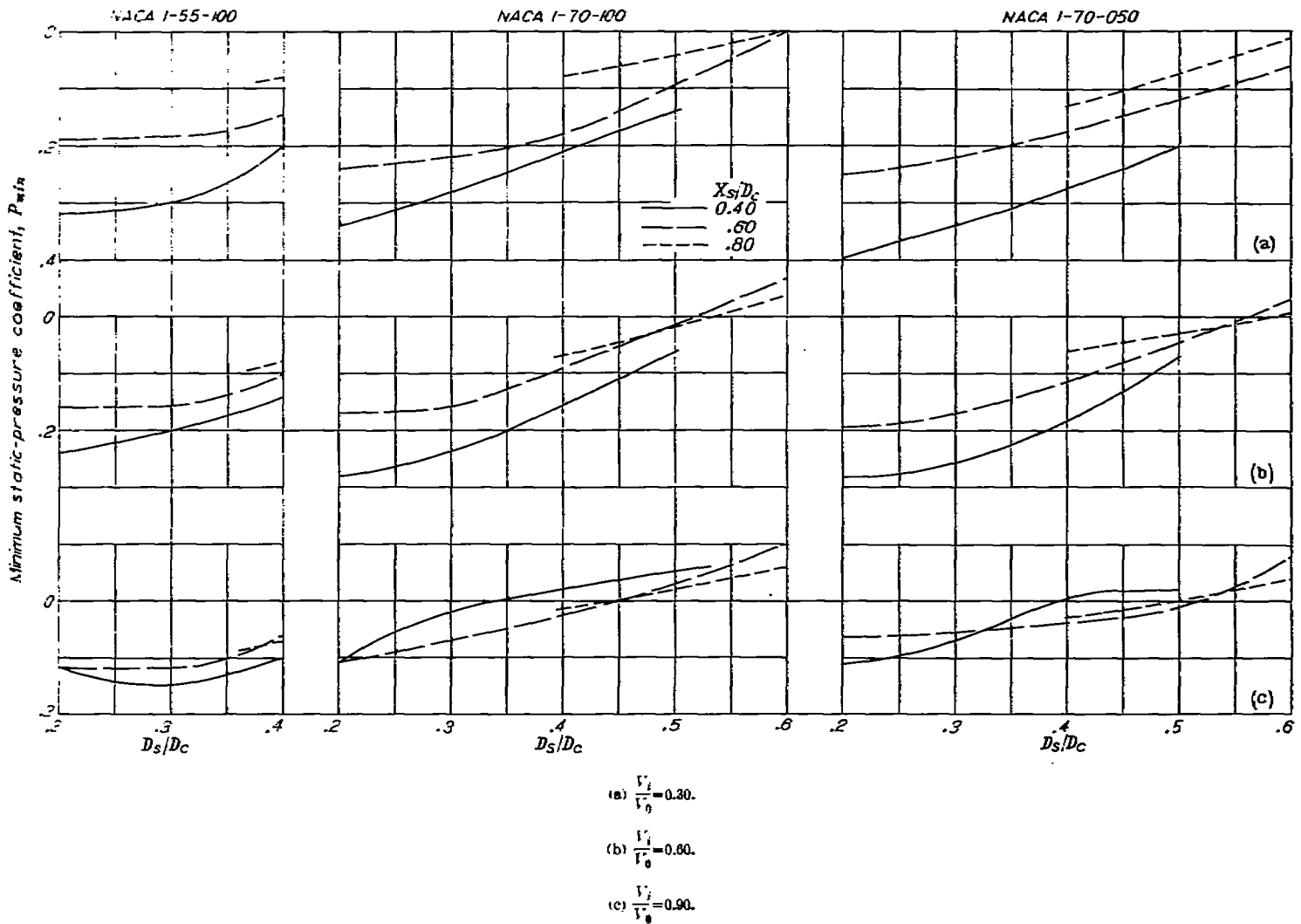


FIGURE 16.—Minimum pressure coefficients for top of spinners of representative NACA 1-series cowling-spinner combinations. Propeller removed; $M_1 = 0.13$; $\alpha = 0^\circ$.

Propeller operation effected large changes in the shapes of the total-pressure distributions at the top of the inlet (figs. 23 and 24). In general, the total pressures in the vicinity of the cowling lip were increased, whereas those near the spinner were reduced. This radial total-pressure gradient, which to a lesser extent would be present even with thinner-airfoil-type propeller shanks, would cause increases in pressure recovery with increases in the width of the inlet annulus and might be expected to encourage separation from the spinner at the lower inlet-velocity ratios. Such separation was not observed, however, and propeller operation either had a negligible effect upon or actually reduced the value of inlet-velocity ratio below which the mean inlet total pressure decreased rapidly. (See fig. 22.) It appears, therefore, that with a conventional propeller any destabilizing effects of the propeller on the boundary layer are compensated for by additional effects possibly including: (1) the removal of the spinner boundary layer along the propeller blade surfaces, (2) the introduction of large-scale turbulent mixing, and (3) the effect of the swirl introduced by the

propeller in reducing the pressure rise acting on the boundary layer. Further research is necessary to establish the effectiveness of these compensating effects for the case of a propeller with thin-airfoil-type propeller shanks. Since only one propeller blade angle was investigated, tests are desirable with propellers set at high blade angles such as will be used by high-subsonic-speed turbine-powered aircraft.

Minimum inlet-velocity ratio for high pressure recovery.—Boundary-layer thicknesses at the top of the spinner of the typical configuration being examined are presented in figures 25 and 26 as a function of inlet-velocity ratio. The curves are of the same general shape and the breaks in the curves, which are indicative of the onset of separation, occur at nearly the same inlet-velocity ratio regardless of the definition of boundary-layer thickness used. Hence, the boundary-layer thickness δ has been defined as the normal distance from the surface to the point where $\frac{H_t - p_0}{q_0} = 0.95$. The minimum inlet-velocity ratio for avoiding flow separation also is defined arbitrarily as a value 0.04 greater than

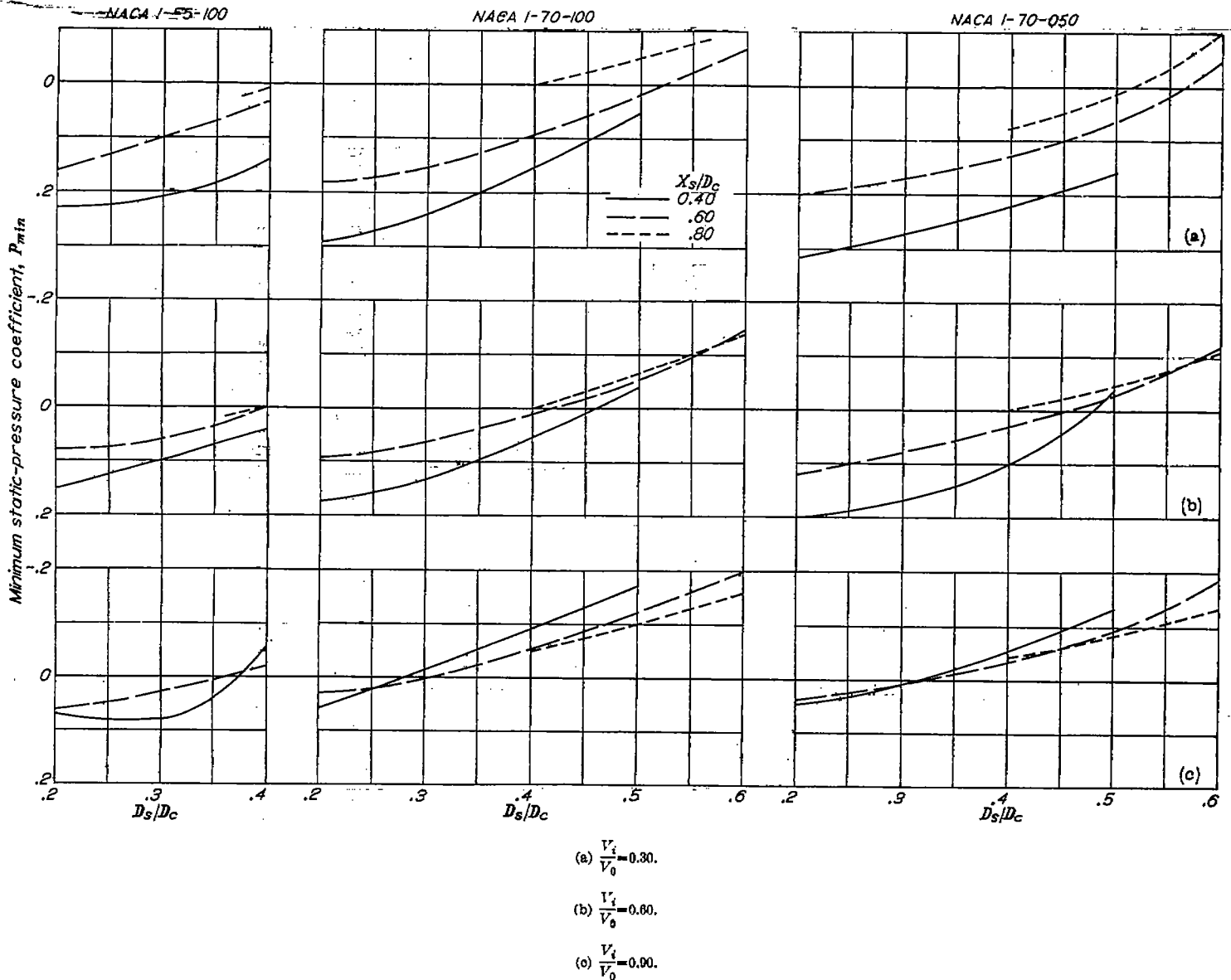


FIGURE 17.—Minimum pressure coefficients for top of spinners of representative NACA 1-series cowling-spinner combinations. Propeller removed; $M_1 = 0.18$; $\alpha = 6^\circ$.

that corresponding to the intersection of tangents to the inclined and approximately horizontal parts of this boundary-layer-thickness curve.

In correspondence with the discussion in the preceding section, it is noted in figures 25 and 26 that propeller operation either did not affect or actually reduced the separation value of inlet-velocity ratio. Propeller-removed data for a high-critical-speed fuselage scoop (reference 6) show that such separation values of inlet-velocity ratio are essentially unaffected by large changes in test Mach number and by reasonable changes in boundary-layer thickness such as might be introduced by variations in the transition point. A large increase in Reynolds number might decrease the separation value of inlet-velocity ratio; however, any such decrease would be expected to be small. Therefore, inasmuch as a maximum pressure recovery in the ducting generally is obtained at an inlet-velocity ratio just greater than

the maximum value for which the inlet flow is separated, the experimentally determined minimum values of inlet-velocity ratio for avoiding flow separation in the propeller-removed condition are considered to be optimum-design values.

Boundary-layer thicknesses on the tops of the spinners of a number of NACA 1-series cowling-spinner combinations are shown in figures 27 and 28. So long as the inlet lip was located at a reasonable distance ($0.075D_c$ or greater) from the spinner surface, the inlet-velocity ratios below which the boundary layers thickened rapidly were essentially a function only of the proportions of the spinner and the angle of attack, as previously deduced from the pressure distributions on the spinners. Hence, within the useful range of inlet-annulus widths, it was possible at each angle of attack to determine a single minimum inlet-velocity ratio for which separation from each spinner was avoided

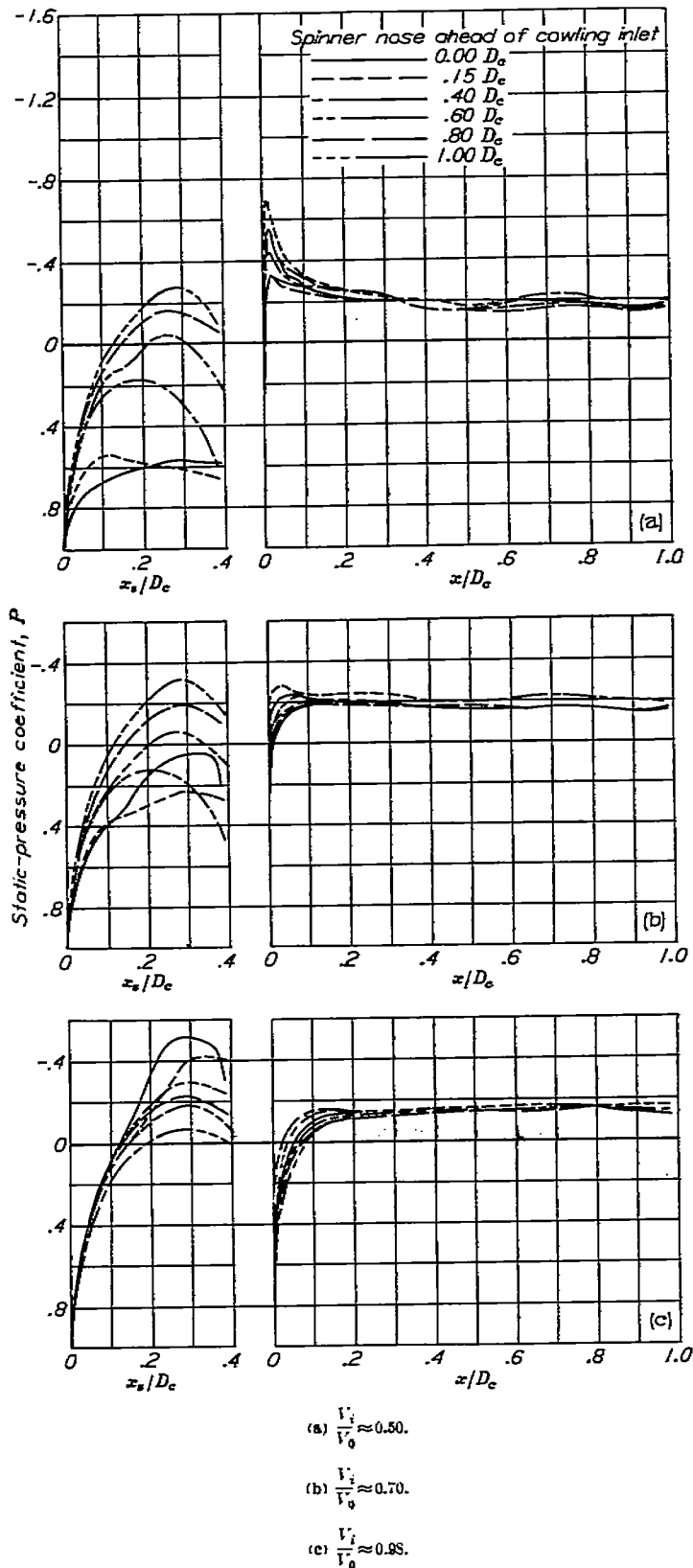


FIGURE 18.—Effect of spinner location on static-pressure distribution over NACA 1-70-100 cowling with 1-40-040 spinner. $\alpha=0^\circ$; $M_i=0.13$.

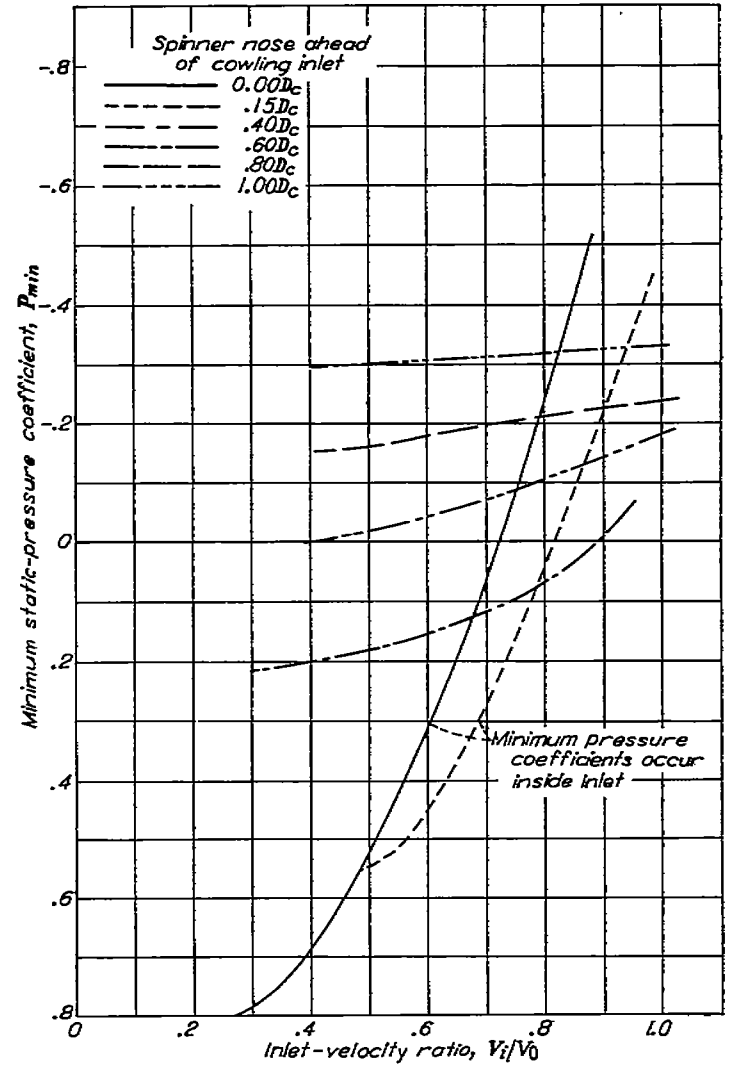


FIGURE 19.—Variation of minimum static-pressure coefficient for the NACA 1-40-040 spinner with inlet-velocity ratio for several spinner positions. NACA 1-70-100 cowlings; $\alpha=0^\circ$; $M_i=0.13$.

regardless of the proportions of the cowling used. Such minimum values, which increase with increases in spinner-diameter ratio, spinner-length ratio, and angle of attack, are summarized in figure 29.

It was not possible to determine single minimum values of inlet-velocity ratio for avoiding flow separation from the spinners where the width of the inlet annulus was less than $0.075D_c$, because the separation inlet-velocity ratio then was no longer a function only of the proportions of the spinner. No attempt was made to determine more accurate design conditions for such configurations; they are seldom used because the large thickness of the spinner boundary layer relative to the inlet annulus results in a low pressure recovery.

The minimum inlet-velocity ratios necessary for avoiding separation from the NACA 1-series spinners (fig. 29) were higher than generally would be desirable for high pressure recovery. In reference 1, values of 0.35 to 0.40 were indicated for the particular cowling-spinner combinations considered. Further gains in internal pressure recovery appear

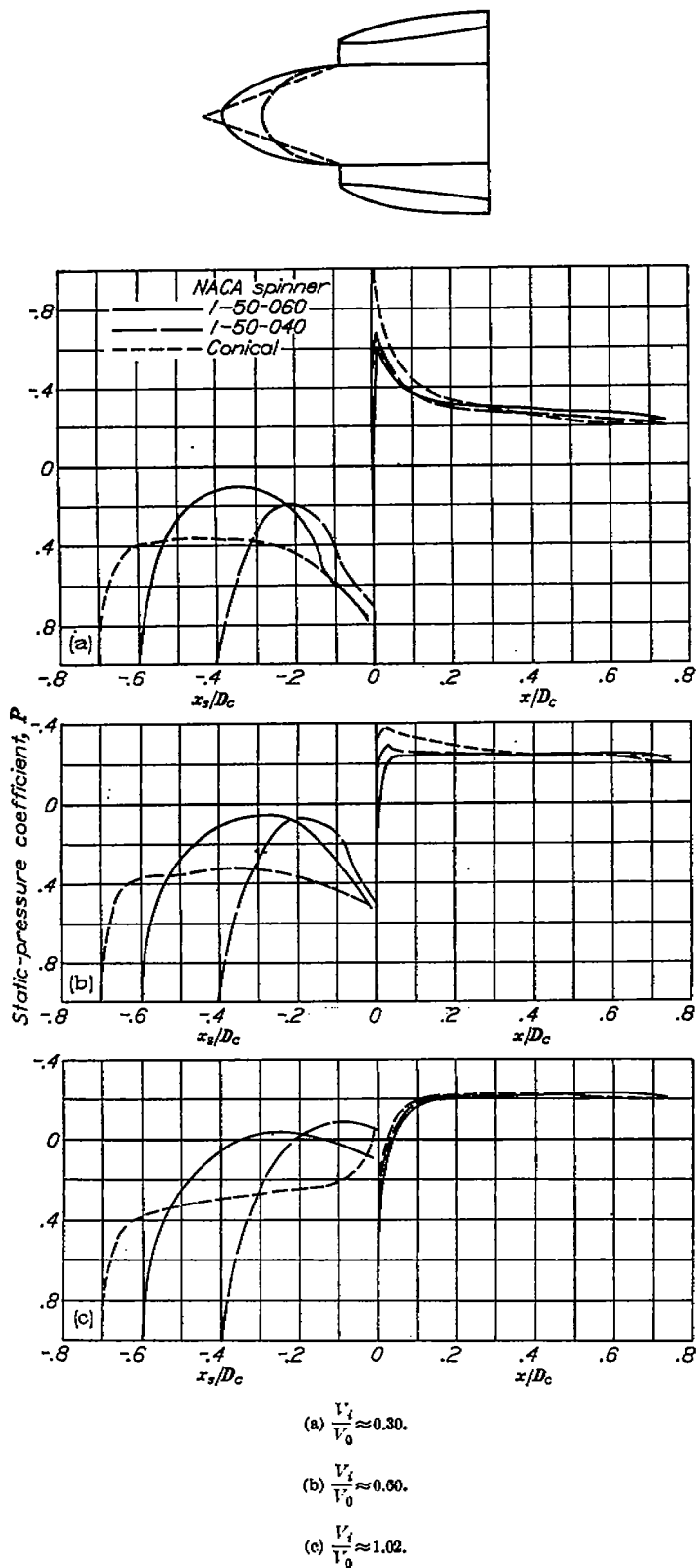


FIGURE 20.—Effect of spinner shape on static-pressure distribution over spinner and NACA 1-70-075 cowling. $\alpha=0^\circ$; $M_1=0.13$.

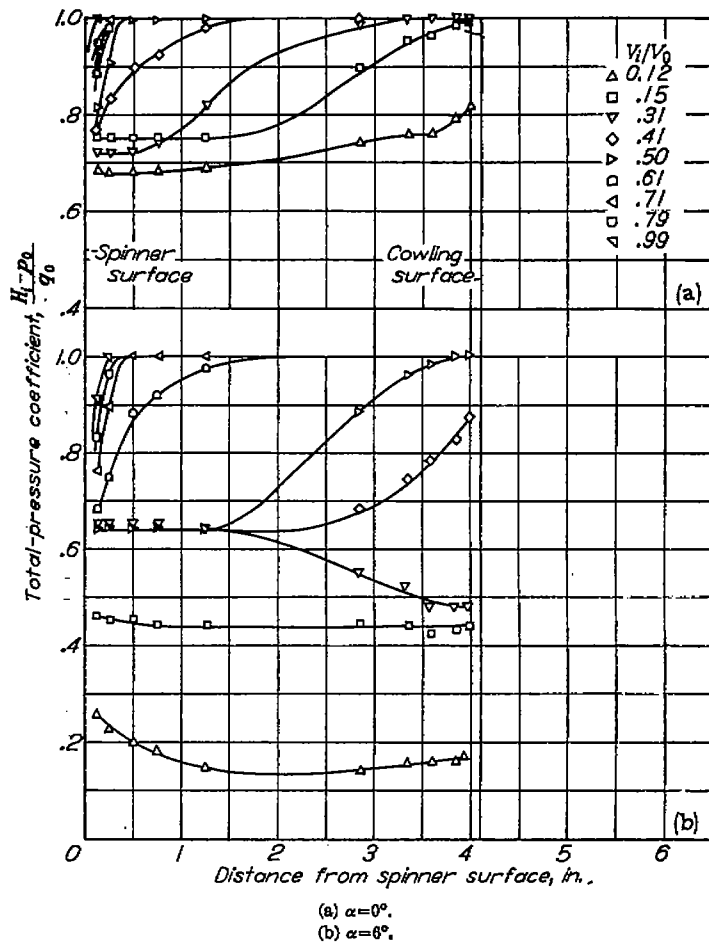


FIGURE 21.—Total-pressure distributions at station 0.75 at top of inlet. NACA 1-70-075 cowling with 1-40-060 spinner; propeller removed.

possible through the development of new families of spinners with lower separation inlet-velocity ratios. In this regard, the conical spinner of figures 3 and 20 is of interest inasmuch as the previously noted decreases in the severity of the pressure rise ahead of the inlet, obtained by substituting this spinner for comparable NACA 1-series spinners, resulted (fig. 30) in reductions of 0.05 to 0.10 in the minimum usable value of inlet-velocity ratio. Such reductions would cause important gains in the ultimate pressure recovery at the end of the diffuser; where not limited by the geometry of the propeller hub, additional gains could undoubtedly be obtained by increasing the cone angle.

Maximum inlet-velocity ratio for avoiding separation from inside of lip.—At the higher inlet-velocity ratios the outward displacement of the stagnation point on the inlet lip (figs. 31 and 32) caused high local pressure peaks at the inside of the lip for both the open-nose and spinner-installed configurations. These minimum pressure coefficients are summarized in figure 33. Although appreciable scatter of the experimental data occurred, presumably because of both the necessarily limited number of pressure orifices in the lip radii and

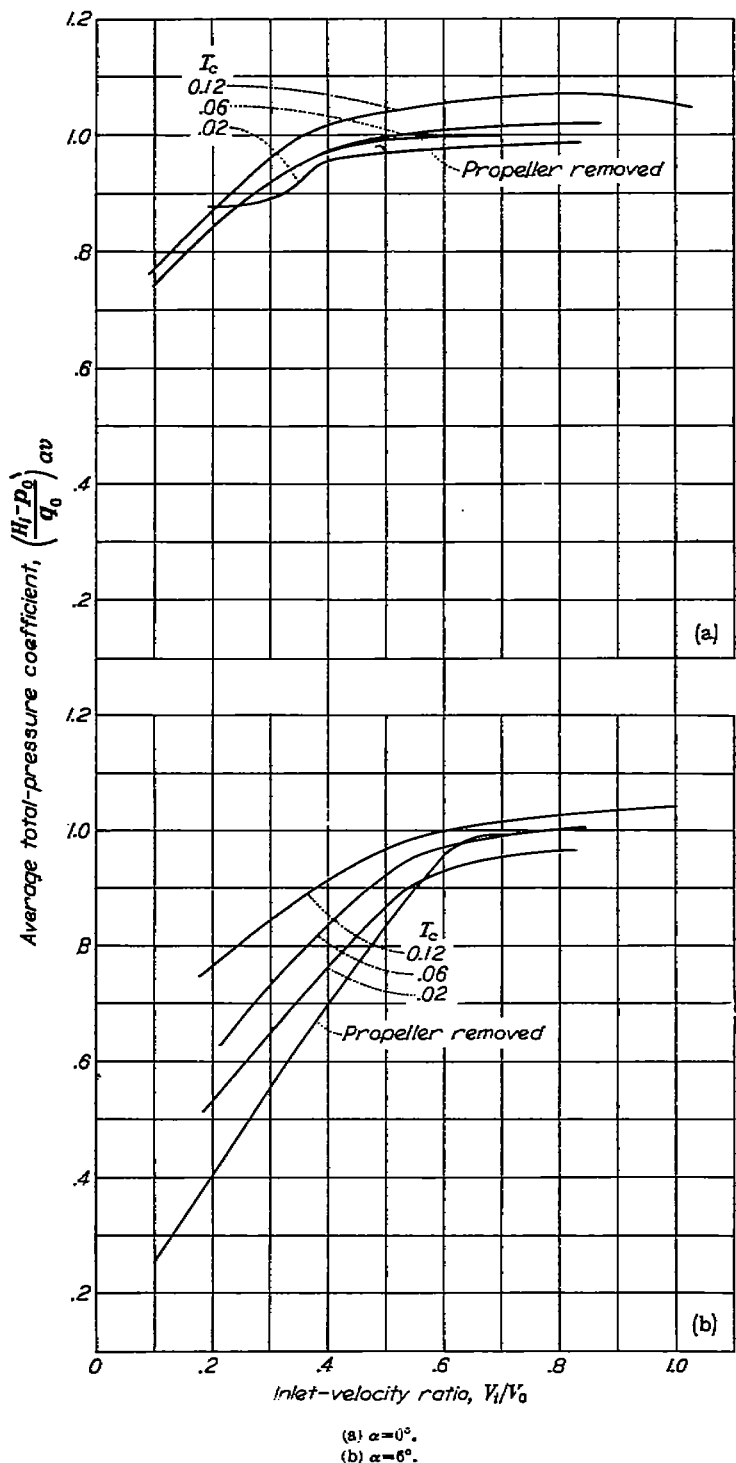


FIGURE 22.—Effect of inlet-velocity ratio and propeller operation on weighted average total-pressure coefficient at station 0.75 at top of inlet. NACA 1-70-075 cowling with 1-40-060 spinner.

the unsteady nature of the flow, a definite effect of spinner size is discernible when, as shown, an attempt is made to fair separate lines through the points for the different spinner

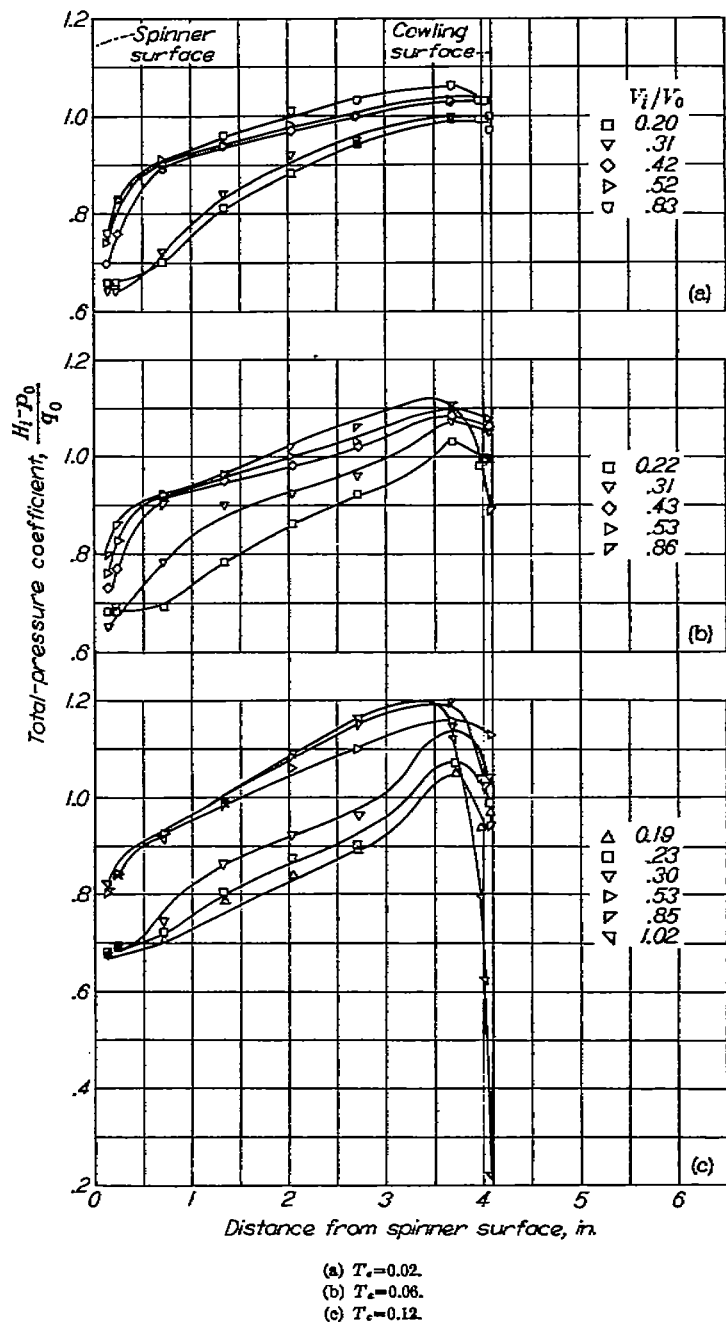


FIGURE 23.—Total-pressure distributions at station 0.75 at top of inlet. NACA 1-70-075 cowling with 1-40-060 spinner; propeller installed; $\alpha = 0^\circ$.

diameters. When the spinner diameter was small with respect to the inlet diameter, small variations in spinner proportions had little effect on the velocities along the inner cowling-lip surface. When the spinner diameter was increased to the point where the inlet annulus width was $0.075D_c$ or less, however, these flow velocities increased markedly, possibly because of the effect of the spinner

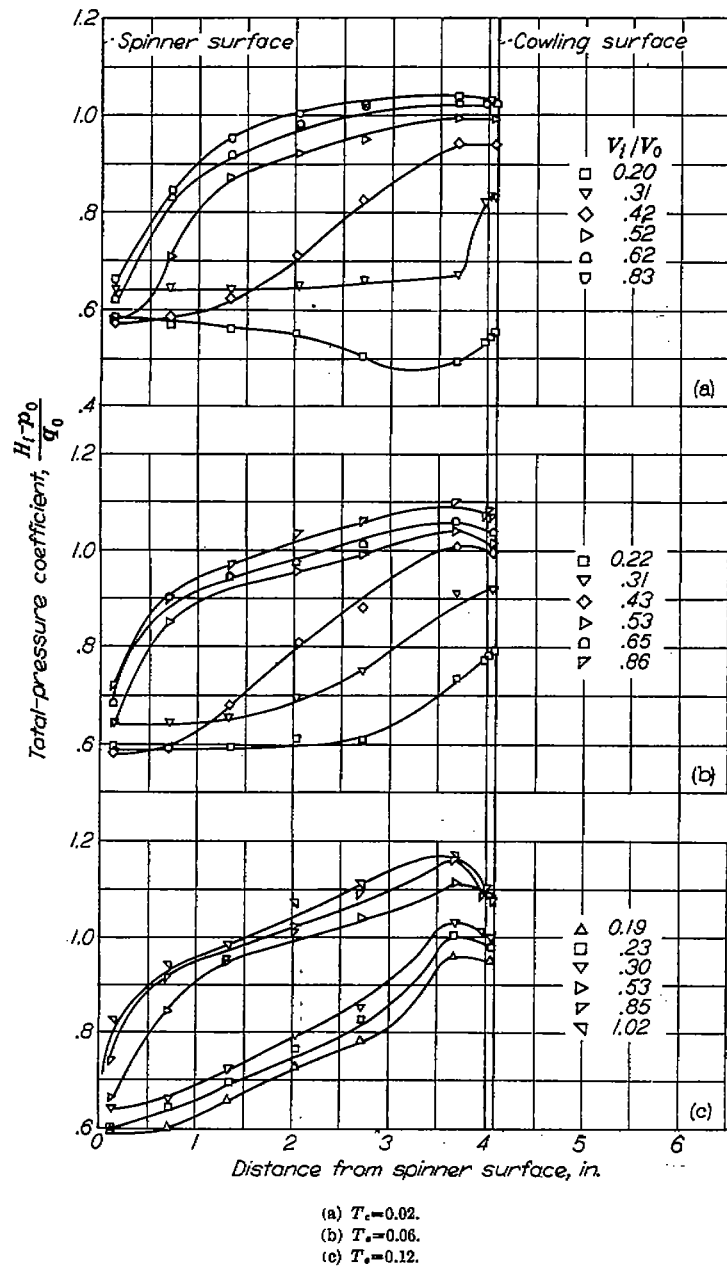


FIGURE 24.—Total-pressure distributions at station 0.75 at top of inlet. NACA 1-70-075 cowling with 1-40-060 spinner; propeller installed; $\alpha=6^\circ$.

boundary layer on the direction of the flow at the cowling lip. Propeller operation (fig. 34) also caused appreciable increases in the flow velocities along this surface by distorting the radial total-pressure distribution in the inlet (figs. 23 and 24) and by reducing the effective angle of attack of the cowling lip.

Representative total-pressure-loss coefficients measured by a total-pressure tube 0.12 inch from the inner surface of the bottom section of the inlet lip (the section where the most severe separation losses are likely to be initiated in the cruise and climb conditions) are presented in figure 35 for an angle of attack of 6° . The formation of bubbles of separation is indicated by the abrupt breaks in these curves beyond which the losses increased rapidly until the local total-pressure coefficients became approximately equal to the local surface-pressure coefficients. These data, which are typical for all cases investigated, show that the inlet-velocity ratios at

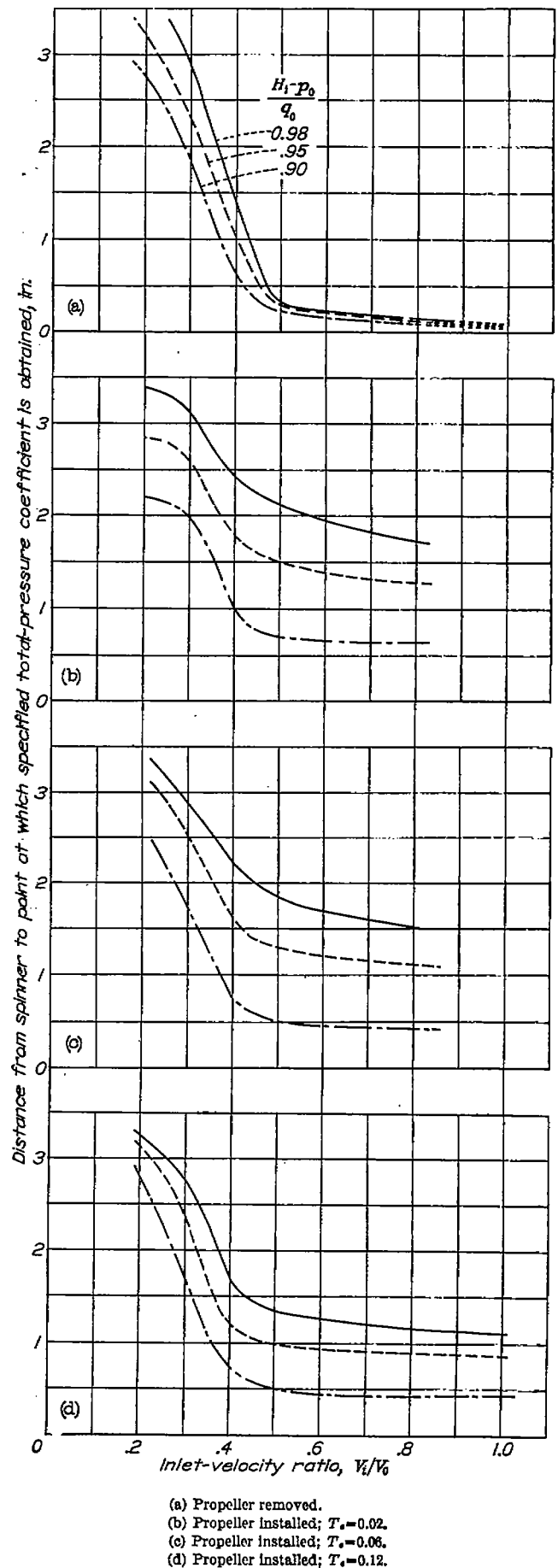
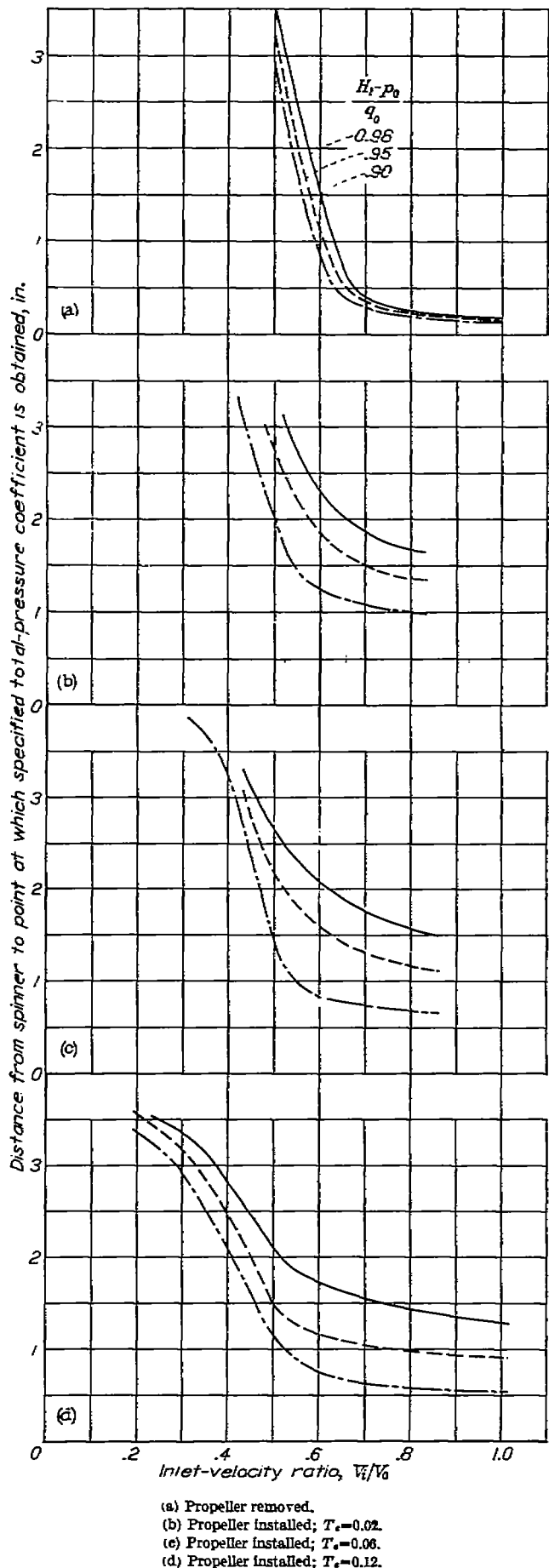


FIGURE 25.—Effect of inlet-velocity ratio and propeller operation on boundary-layer thickness on spinner at station 0.75 at top of inlet. NACA 1-70-075 cowling with 1-40-060 spinner; $\alpha=6^\circ$.



(a) Propeller removed.
 (b) Propeller installed; $T_c=0.02$.
 (c) Propeller installed; $T_c=0.06$.
 (d) Propeller installed; $T_c=0.12$.

FIGURE 26.—Effect of inlet-velocity ratio and propeller operation on boundary-layer thickness on spinner at station 0.75 at top of inlet. NACA 1-70-075 cowling with 1-40-060 spinner; $\alpha=6^\circ$.

which separation bubbles first occurred were again essentially a function only of the proportions of the spinner. For a given spinner the locations of the breaks in these curves were shifted by as much as $\pm 0.03 \frac{V_t}{V_0}$ from the mean value by changes in cowling proportions; however, no consistent trends were observed.

The inlet-velocity ratios for which the total-pressure-loss coefficient was 0.1, determined from plots of the type of figure 35, have been arbitrarily taken as the maximum values for which appreciable separation bubbles did not occur. These limiting values for high pressure recovery (fig. 36) increased with increases in spinner diameter and decreases in spinner length and were undesirably low for the angles of attack encountered in low-speed flight. As discussed in the section entitled "Critical Mach Number Characteristics," the effect of an increase in flight Mach number at any fixed inlet-velocity ratio less than 1.0 is to decrease the effective angle of attack of the cowling lip and, consequently, to reduce these already low limiting values. However, propeller operation, as shown in figure 37 by data obtained with shielded total-pressure tubes, has an opposing favorable effect which, at the high propeller thrust disk-loading coefficients encountered in the low-speed cruise and climb conditions, would more than counterbalance the growth of the local pressure peaks with increases in Mach number. Furthermore, the inlet total-pressure distributions of figures 23 and 24 strongly indicate that the internal flow would separate from the inner surface of the diffuser rather than from the cowling lip at reasonably high values of inlet-velocity ratios. It is concluded therefore that flow separation from the inner portion of the cowling lip, while of major importance in the case of the NACA open-nose inlets, is not of significant importance in the case of the NACA 1-series cowling-spinner combinations, except for extremely severe combinations of high inlet-velocity ratio and high angle of attack such as are encountered in the take-off condition.

Because of the importance of avoiding separation of the internal flow in low-speed flight, tests were conducted on two representative cowlings to determine whether the upper limit of the separation-free operating range of inlet-velocity ratio (fig. 36) could be raised by the addition of an inner-lip fairing. The NACA 1-series ordinates inverted with respect to the reference line through the cowling lip (table I) were used in this fairing (fig. 4) because the general applicability of these ordinates to high-critical-speed configurations had already been established and because the use of these ordinates would permit the region of high curvature to be kept well forward. The addition of this fairing caused large reductions in the peak negative pressure coefficient on this surface at the higher inlet-velocity ratios (figs. 38 and 39) and corresponding large increases in the limiting values of inlet-velocity ratio (fig. 40). A fairing of this type therefore is desirable for installations in which separation of the internal flow from the inlet lip is likely to be encountered. In the case of cowling-spinner combinations, it appears that such a fairing need only be applied as a "glove" in the bottom quarter of the inlet.

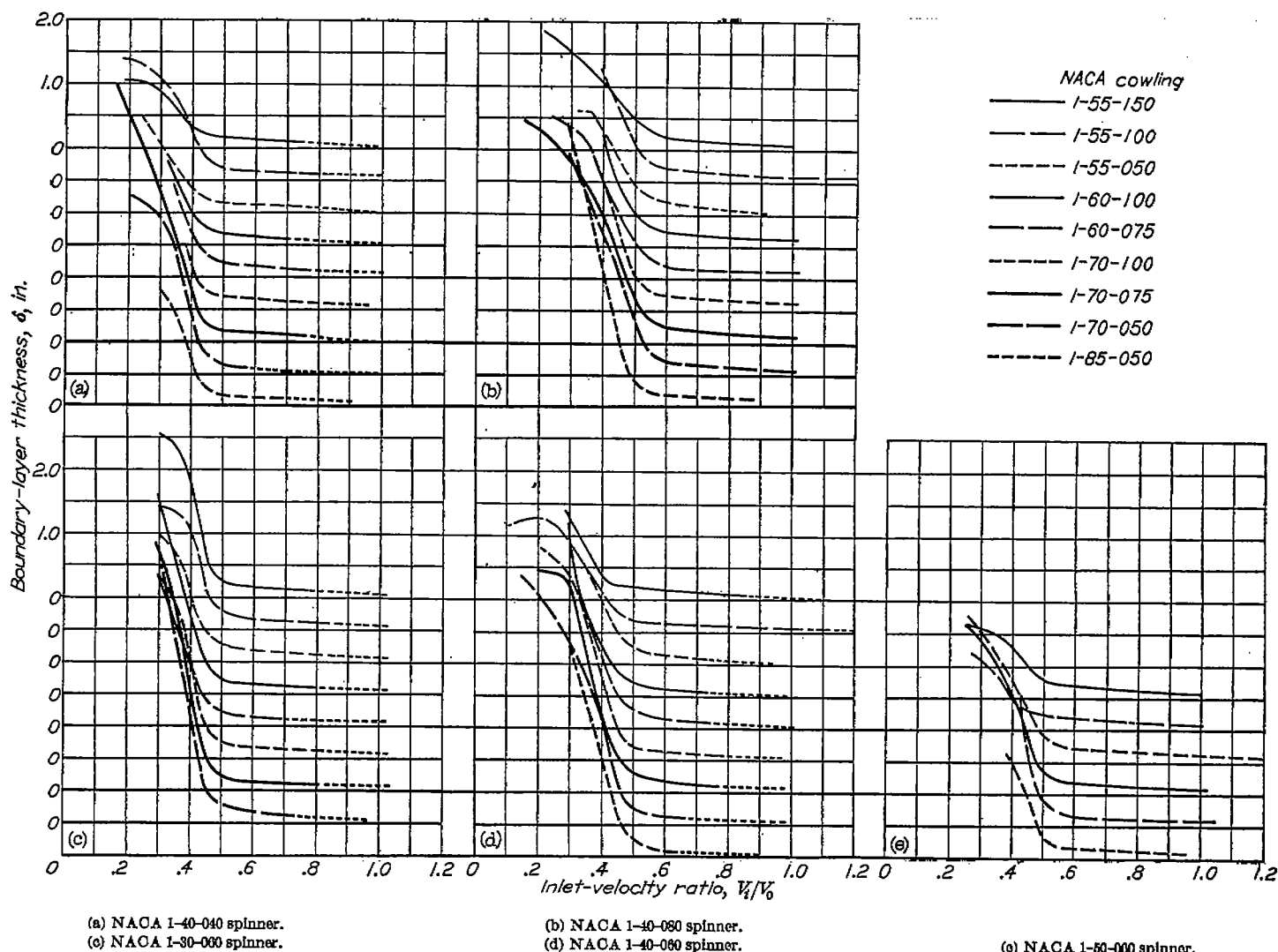


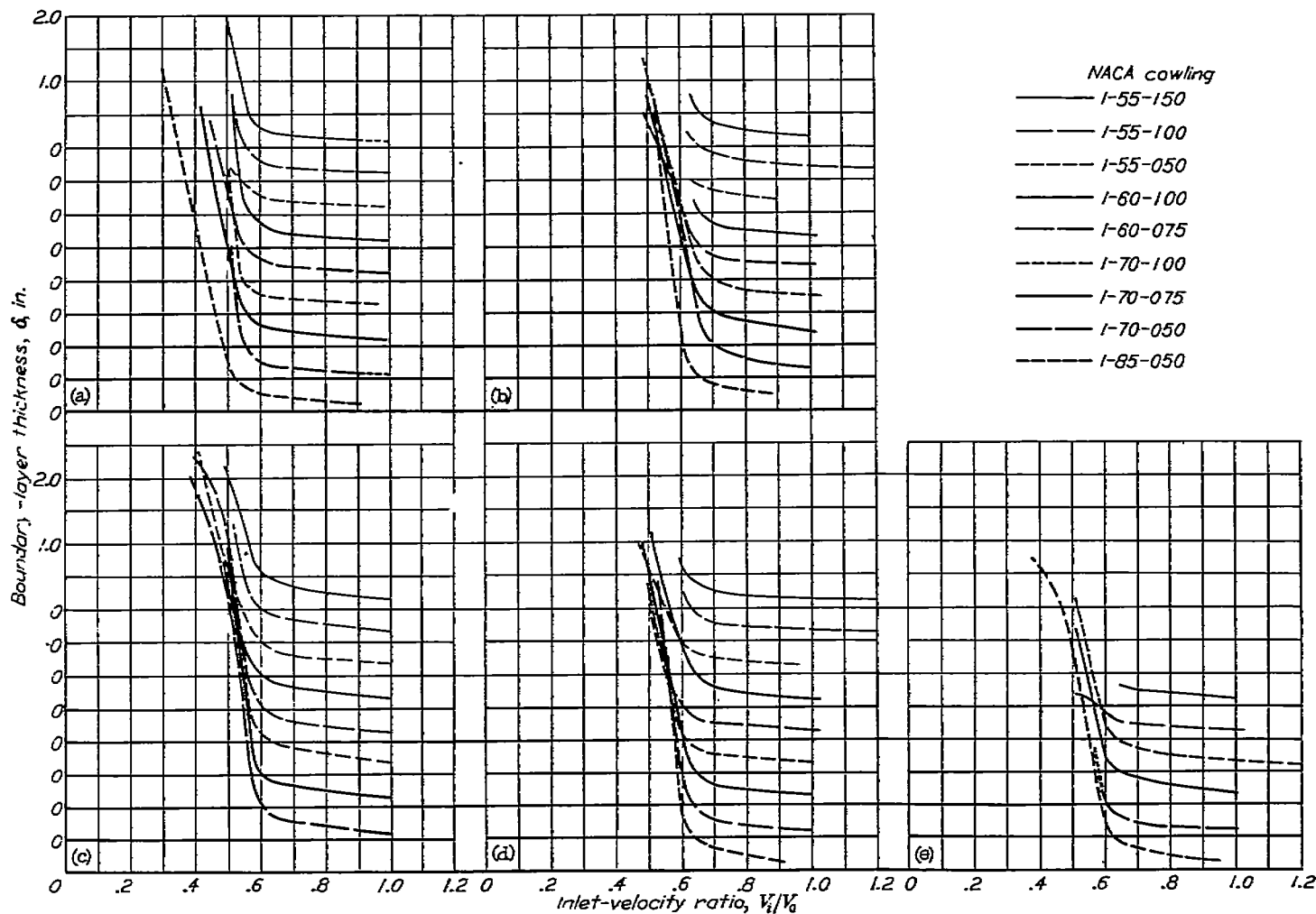
FIGURE 27.—Boundary-layer thicknesses on top of a number of spinners at station 0.75 as a function of inlet-velocity ratio and cowling proportions. Propeller removed; $\alpha = 0^\circ$.

EXTERNAL FLOW OVER COWLING

Static-pressure distributions over the external cowling surfaces of several of the test configurations are shown in figures 8 to 15, 18, and 20. The phenomena shown are generally similar to those discussed in reference 1. At the lower inlet-velocity ratios, high negative pressure peaks usually occurred on the cowling lips because of their high effective angle of attack, and in the case of some of the sharper lipped cowlings these peaks initiated separation of the external flow. As the inlet-velocity ratio was increased, these negative pressure peaks decreased progressively in severity until at particular values, determined by the cowling and spinner shapes and the angle of attack, the pressure distributions became essentially uniform. The surface pressures decreased only slightly and the distributions of these pressures were essentially unaffected by large additional increases in inlet-velocity ratio; thus, for each cowling, the critical speed increased only slightly and, presumably, the external friction drag decreased only slightly over a wide range of inlet-velocity ratio above the value necessary to eliminate the pressure

peak on the cowling lip. The effect of increasing the angle of attack was to increase the severity of the pressure peak on the top section of the cowling lip at the lower inlet-velocity ratios and to increase the inlet-velocity ratio required to eliminate this peak.

Some effects of cowling and spinner geometry on the distribution and magnitudes of the surface pressures on the cowling are shown in figures 8 to 15, 18, and 20. The inlet-velocity ratio required to avoid a negative pressure peak on the cowling lip increased with increases in both cowling length and cowling inlet diameter; at inlet-velocity ratios above the critical values, increases in these same variables decreased the minimum surface pressure coefficients. In general, the addition of a small-diameter spinner or a long spinner to the basic open-nose cowling did not cause important changes in the cowling pressure distributions. The addition, however, of a spinner with a large rate of decrease of cross-sectional area just ahead of the inlet, such as a short large-diameter spinner or a conical spinner, tended to cause the formation of a negative pressure peak on the cowling lip even at very high values of inlet-velocity ratio.



(a) NACA 1-40-040 spinner.
(c) NACA 1-30-060 spinner.

(b) NACA 1-40-080 spinner.
(d) NACA 1-40-060 spinner.

(e) NACA 1-60-060 spinner.

FIGURE 23.—Boundary-layer thicknesses on top of a number of spinners at station 0.75 as a function of inlet-velocity ratio and cowling proportions. Propeller removed; $\alpha = 6^\circ$.

The inlet-velocity ratio for which the surface pressure distribution on the cowling first becomes essentially uniform is a function of the free-stream Mach number. A detailed discussion of the effects of cowling and spinner proportions on this important operating condition is therefore delayed pending an evaluation of the effect of Mach number.

Propeller operation effected increases in both the static and total pressures in the vicinity of the cowling surface. The increases in static pressure (fig. 41) were large near the leading edge but were small near the position of maximum diameter. The increases in total pressure just outside the cowling boundary layer (fig. 42) were approximately the same at the fore and aft rake locations (fig. 5 (b)) and were somewhat less than values calculated for the ideal case of uniform propeller disk loading. Because the increases in total pressure were greater than the increases in static pressure, except in the region of the lip, there was a net increase in the maximum flow velocity along the surface which became of significant magnitude at the higher propeller thrust disk-loading coefficients.

CRITICAL MACH NUMBER CHARACTERISTICS

The critical Mach number has important design significance in that it is the lower limit of the range of Mach number within which significant force changes due to shock can occur. Numerous tests of wings and bodies have indicated that an appreciable margin may exist between the critical Mach number and the force-break Mach number, especially when the critical Mach number is determined by pressures ahead of the maximum thickness station; hence, the critical Mach number may be unnecessarily conservative for design purposes. The present discussion must be limited to the critical Mach number, however, because of the lack of data defining the margin between the two Mach numbers.

Extrapolation of low-speed test data.—In estimating the high-speed operational characteristics of a particular cowling from low-speed test data, such as those of the present investigation, it is necessary to consider the effect of increasing the free-stream Mach number on the magnitude of the surface-pressure coefficients and on the minimum value of

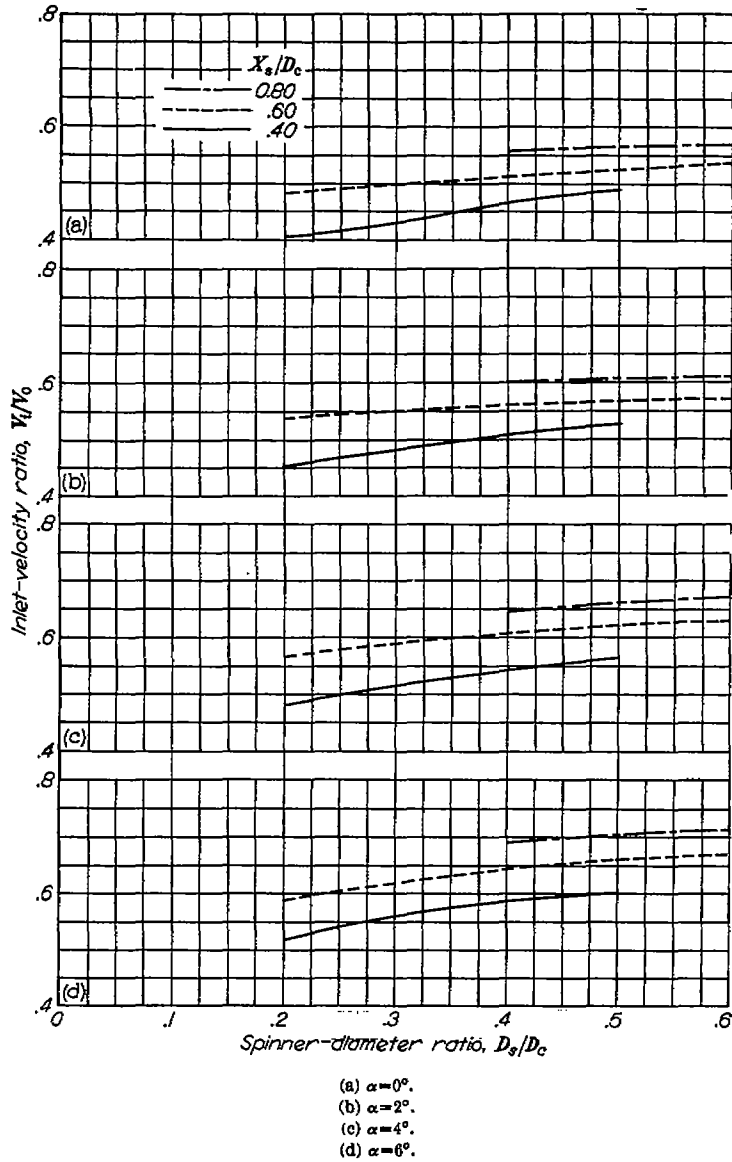


FIGURE 29.—Minimum inlet-velocity ratios for which unseparated boundary layers were obtained at station 0.75 on top of NACA 1-series spinners. Propeller removed.

inlet-velocity ratio for which the surface pressure distribution is essentially uniform. Previous discussion has pointed out that the inlet-velocity ratio required to avoid flow separation from the spinner need not be considered as it is essentially unaffected by increases in the free-stream Mach number.

The Von Kármán method of extrapolating the measured surface-pressure coefficients (reference 7) was shown in reference 1 to be valid for cowling data obtained at test Mach numbers as low as 0.3 so long as sharp forwardly located peaks did not occur in the measured pressure distributions. A comparison in figure 43 of the results predicted from the present data with the higher-speed results of reference 1 shows that the Von Kármán method likewise is applicable, with the same reservation, to the present data obtained at a test Mach number of 0.13; hence, this method has been used to predict the critical Mach numbers for all test configurations.

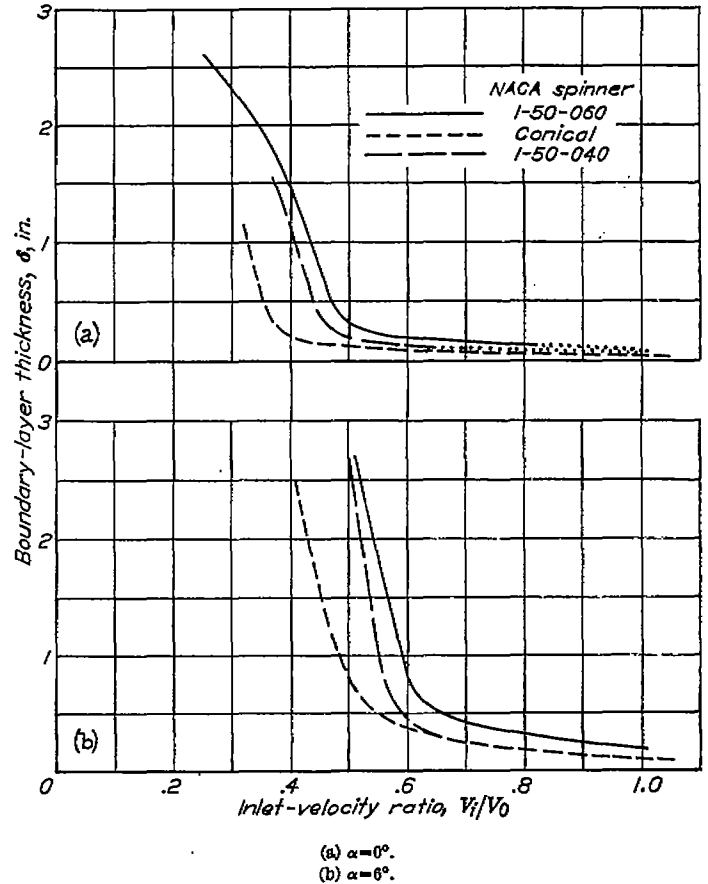
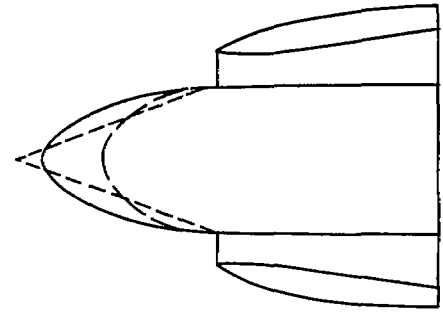
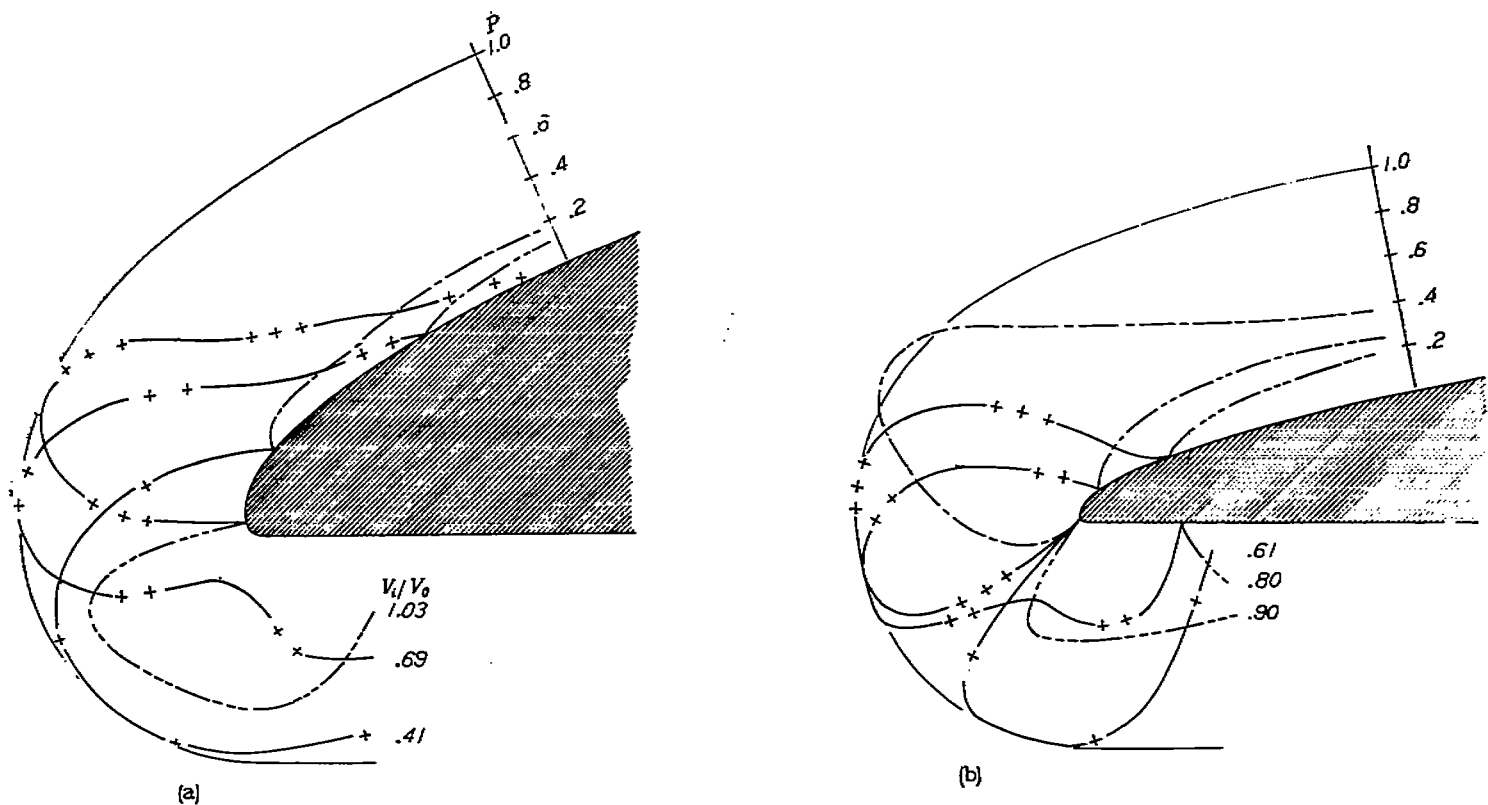
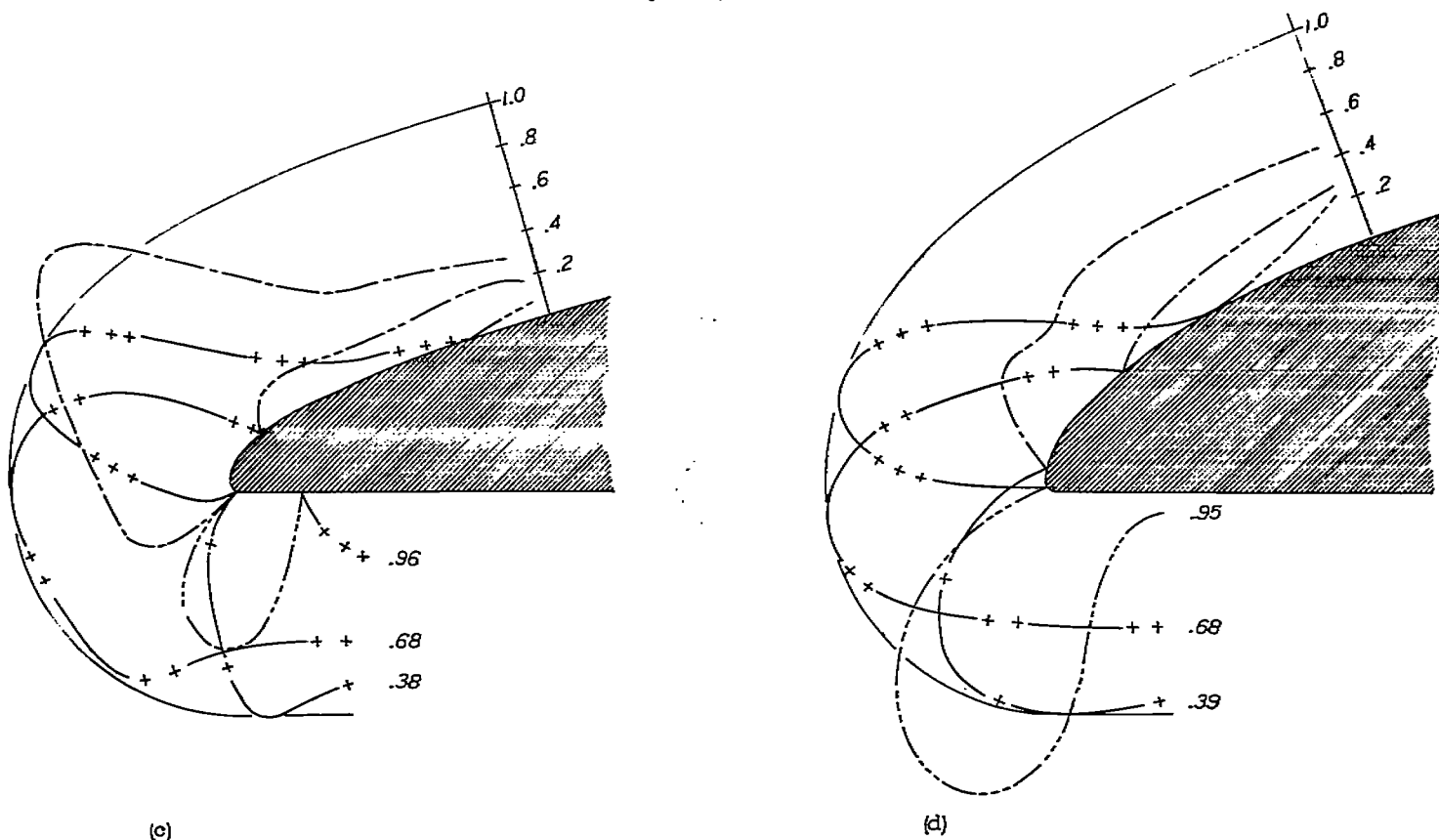


FIGURE 30.—Effect of spinner shape on boundary-layer thickness on spinner at station 0.75 at top of inlet. NACA 1-70-076 cowling; propeller removed.

The data contained in figure 43 show the important influence that the test Mach number has on the minimum value of inlet-velocity ratio for which the surface pressure distribution is essentially uniform and below which the predicted critical Mach number decreases rapidly owing to the formation of a negative pressure peak on the cowling lip. The decrease with increasing Mach number shown was ignored in making the selection charts of reference 1, because the shift was in a conservative direction and appeared small for those tests and because theoretical justification for a correction was lacking. This shift, however, must be taken into account in analyzing and applying the low-speed data of the present investigation.



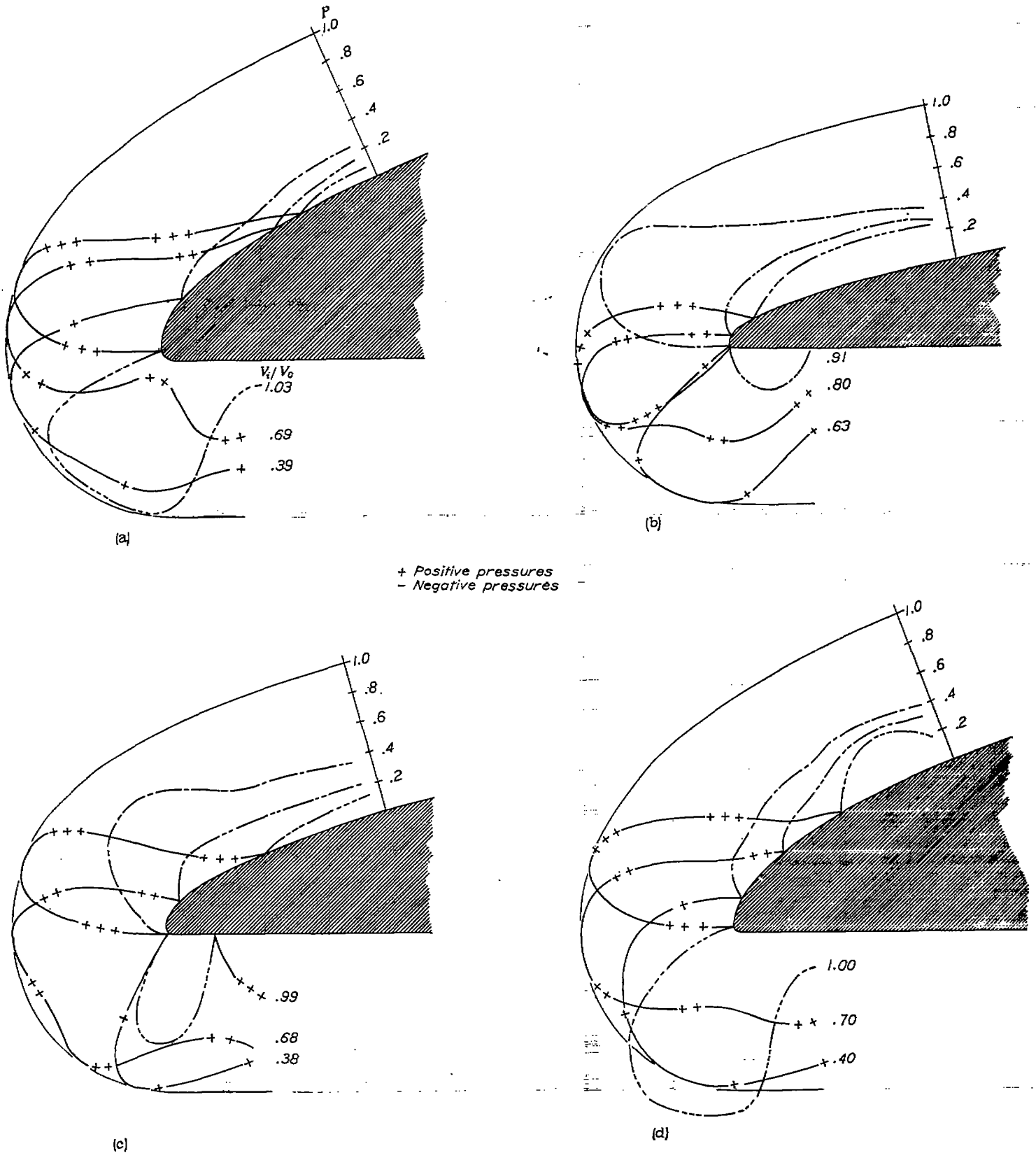
+ Positive pressures
- Negative pressures



(a) NACA 1-55-100 cowling.
(c) NACA 1-70-100 cowling.

(b) NACA 1-85-050 cowling.
(d) NACA 1-70-050 cowling.

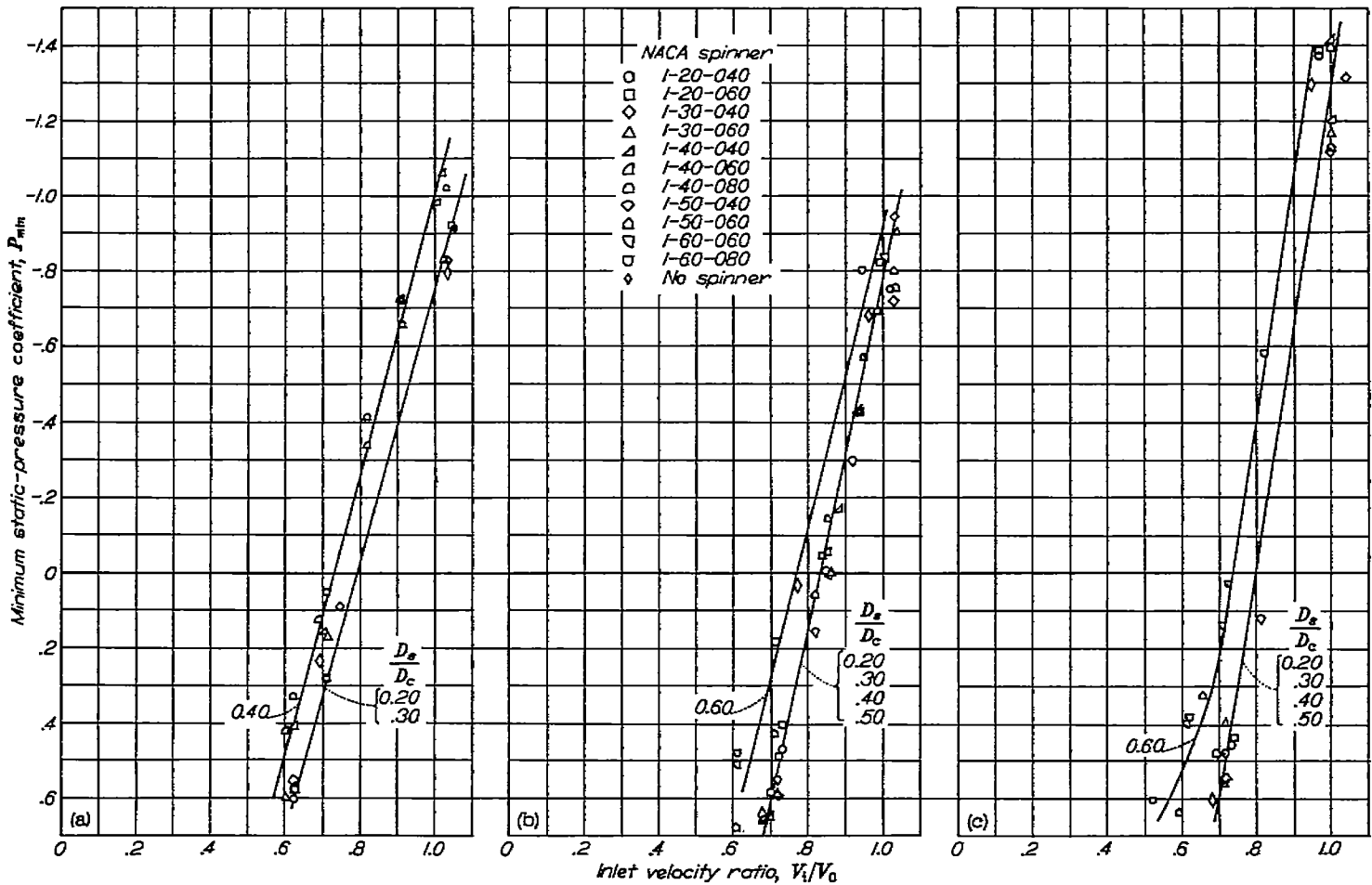
FIGURE 31.—Static-pressure distributions around nose sections of representative NACA 1-series cowlings. Propeller removed; no spinner; $\alpha=0^\circ$; $M_\infty=0.13$.



(a) NACA 1-55-100 cowling.
(c) NACA 1-70-100 cowling.

(b) NACA 1-85-050 cowling.
(d) NACA 1-40-050 cowling.

FIGURE 32.—Static-pressure distributions around nose sections of representative NACA 1-series cowlings. Propeller removed; NACA 1-40-050 spinner; $\alpha=0^\circ$; $M_1=0.13$.



(a) NACA 1-55-100 cowling. (b) NACA 1-70-100 cowling. (c) NACA 1-70-050 cowling.
 FIGURE 33.—Minimum static-pressure coefficients for inner lip surfaces of typical NACA 1-series cowlings and cowling-spinner combinations. Propeller removed; $\alpha=0^\circ$; $M_0=0.13$.

The problem of estimating the magnitude of the inlet-velocity-ratio shift just discussed may be attacked theoretically on the basis of an extension of the work of Ruden (references 4 and 5). (See appendix.) By relating the pressure force on the cowling to the change in pressure and rate of change of momentum of the entering air, Ruden obtained an incompressible-flow expression for an open-nose cowling which can be written in the form (equation (5) of the appendix)

$$P_{c_{av}} = \frac{\left(1 - \frac{V_i}{V_0}\right)^2}{1 - \left(\frac{D_c}{d}\right)^2}$$

where $P_{c_{av}}$ is the average pressure coefficient on the external cowling surface weighted with respect to frontal area. When compressible-flow conditions are assumed, this expression (as shown in the appendix, equation (10)) becomes

$$P_{c_{av}} = \frac{2C}{1 - \left(\frac{D_c}{d}\right)^2}$$

where

$$C = \frac{1}{\gamma M_0^2} \left\{ \left[\frac{\gamma-1}{2} M_0^2 - \frac{\gamma-1}{2} M_0^2 \left(\frac{V_i}{V_0}\right)^2 + 1 \right]^{\frac{\gamma}{\gamma-1}} - 1 \right\} + \left[\left(\frac{V_i}{V_0}\right)^2 - \frac{V_i}{V_0} \right] \left[\frac{\gamma-1}{2} M_0^2 - \frac{\gamma-1}{2} M_0^2 \left(\frac{V_i}{V_0}\right)^2 + 1 \right]^{\frac{1}{\gamma-1}}$$

The factor C is given in figure 44 as a function of the free-stream Mach number and the inlet-velocity ratio. If it is assumed that the low-speed surface pressure distributions can be extrapolated by the Von Kármán equation to obtain possible surface pressure distributions at higher Mach numbers, this expression can then be used to find the inlet-velocity ratios required by these higher-speed pressure distributions. In the case of the NACA 1-70-050 open-nose cowling, for example, the measured pressure distribution for which the predicted critical Mach number is 0.715 may be extrapolated to obtain pressure distributions for Mach numbers of 0.30 and 0.715. Then, the inlet-velocity ratios for the test Mach number (0.13) and these two higher Mach numbers can be calculated from equation (10) of the

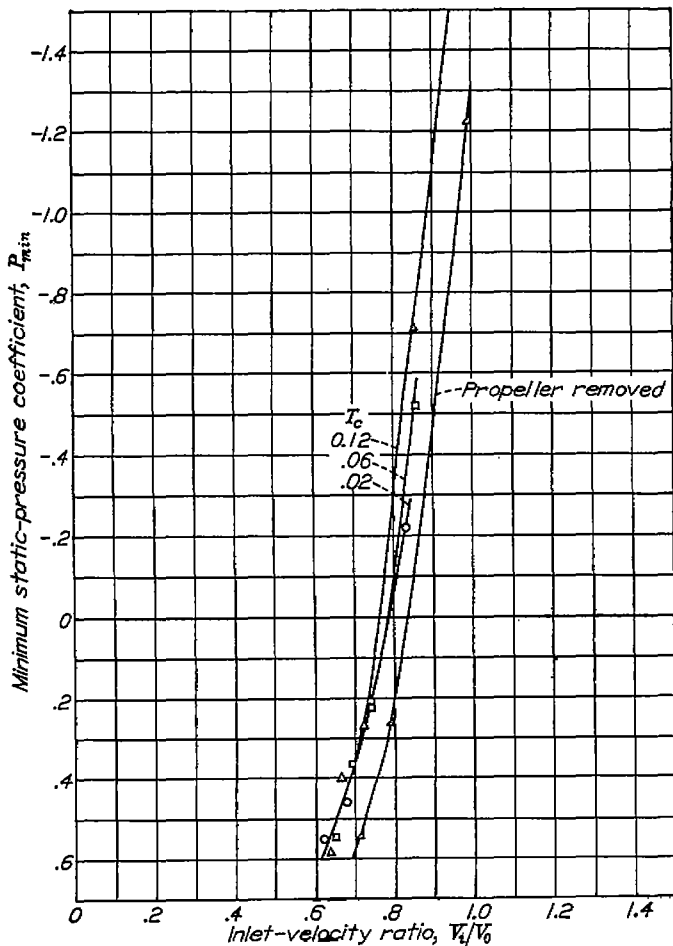


FIGURE 34.—Effect of propeller operation on minimum static-pressure coefficient for inner cowling-lip surface of NACA 1-70-075 cowling with 1-40-080 spinner. $\alpha=0^\circ$; $M_t=0.18$.

appendix after each pressure distribution is mechanically integrated to obtain the weighted average surface pressure coefficient. For this example case, the following comparison with the experimental results of figure 43 is obtained:

| Mach number | V_i/V_0 | |
|-------------|-----------|------------|
| | Test | Calculated |
| 0.13 | 0.39 | 0.36 |
| .30 | .32 | .32 |
| .715 | .23 | .32 |

The calculated inlet-velocity ratios are shown to be in excellent agreement with the values observed experimentally.

The foregoing results indicate that equation (10) of the appendix and the similar compressible-flow relation for cowling-spinner combinations (equation (9) of the appendix) can be used to calculate the increments of V_i/V_0 through which each point on the test curves of M_{cr} plotted against V_i/V_0 must be shifted to correct the low-speed test data. (See fig. 43.) However, the amount of work required to make such corrections is prohibitively large in the present case even if only the points near the knees of the curves are considered; also, the results for cowling-spinner combinations might be subject to appreciable error as a result of the failure of the Von Kármán relation to predict accurately the variation of large positive pressure coefficients with

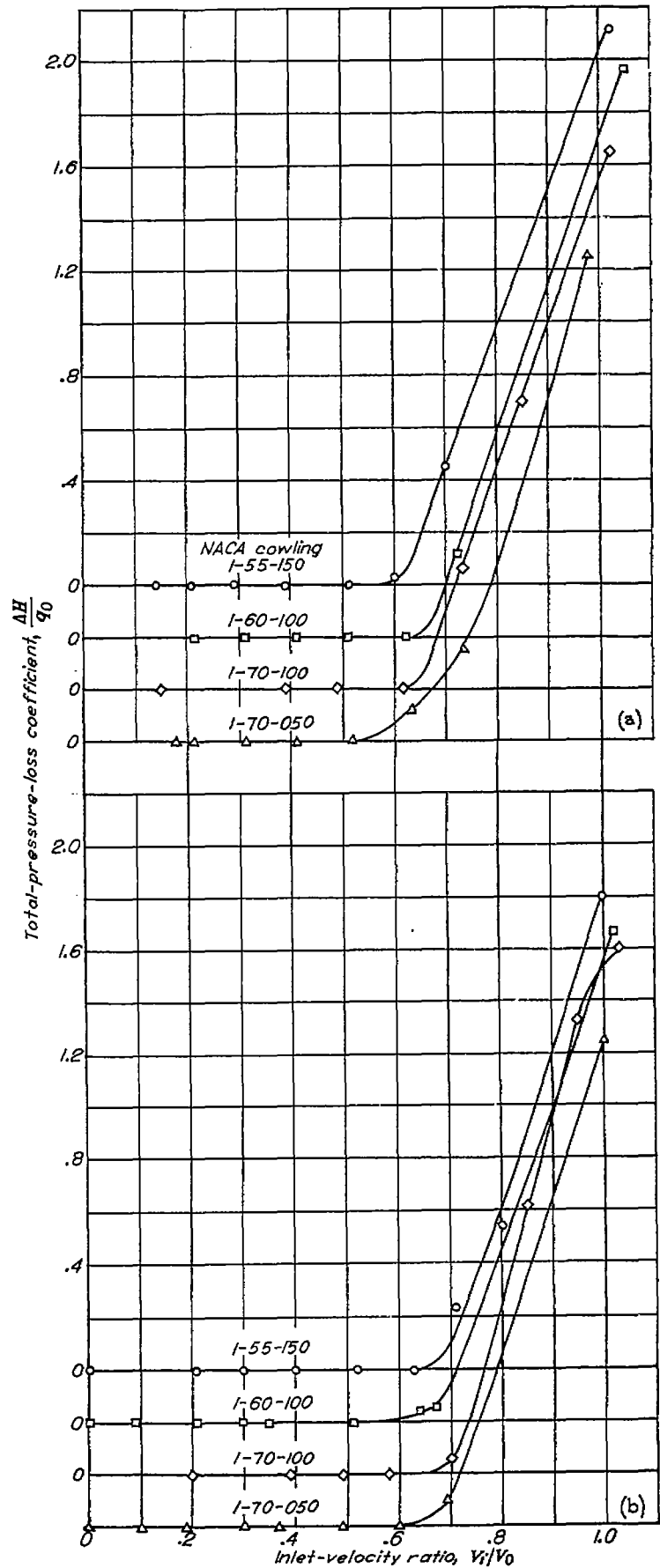


FIGURE 35.—Total-pressure-loss coefficients at reference tube 0.12 inch from inner surface of cowling at station 0.75 at bottom of inlet. Propeller removed; $\alpha=6^\circ$.
 (a) NACA 1-20-040 spinner.
 (b) NACA 1-40-080 spinner.

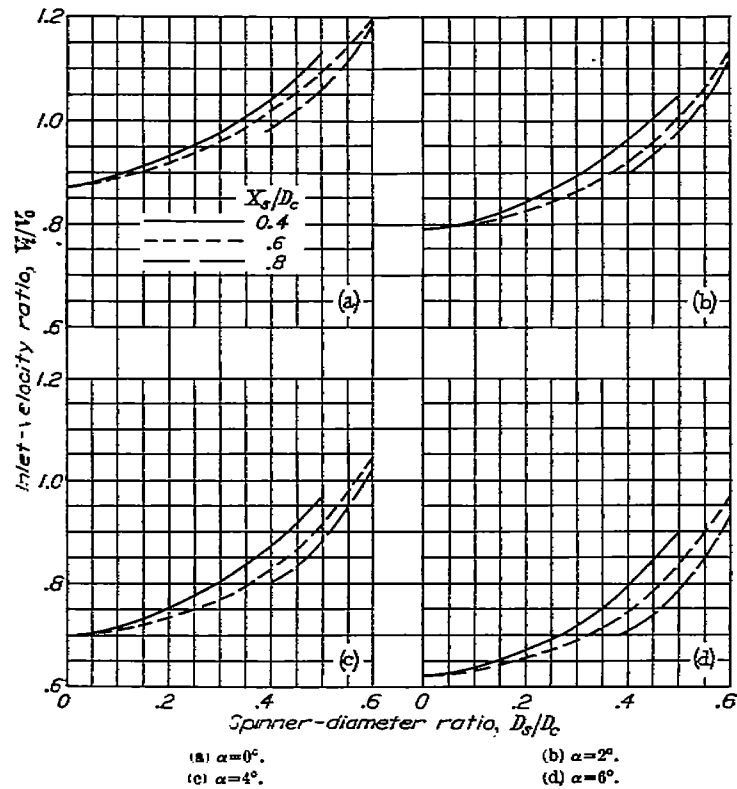


FIGURE 36.—Maximum inlet-velocity ratios for which an appreciable separation bubble was avoided at the bottom of the inlet. (Taken as the inlet-velocity ratio for which the total-pressure losses at station 0.75 were $0.10q_0$ at a reference tube 0.12 inch from the cowling inner surface.) Propeller removed.

Mach number. Hence, equations (9) and (10) of the appendix were examined in an attempt to determine a simple factor which would accurately predict the shifts of the knees of the curves. As a result of this study, it was found that the major parts of such shifts were caused by the change in inlet-density ratio ρ_i/ρ_0 which accompanies an increase in flight Mach number. This result can be explained physically (fig. 45) by considering that, for a constant inlet-velocity ratio, a change in inlet-density ratio requires a change ahead of the inlet in the area of the stream tube containing the internal flow and a corresponding change in the effective angle of attack of the cowling lip. At inlet-velocity ratios less than unity, the effective angle of attack is decreased, whereas at inlet-velocity ratios greater than unity the effective angle of attack is increased. Thus, the minimum value of inlet-velocity ratio required to obtain a uniform pressure distribution on the external surface (less than unity) decreases regularly with increases in flight Mach number.

Figure 46 shows the greatly improved correlation between the critical Mach number results obtained in the present tests and those of reference 1 when the test inlet-velocity ratios were multiplied by the inlet-density ratio ρ_i/ρ_0 . Extensive analysis failed to uncover any other simple factor which would more accurately predict the shift of the knees of the curves. In view of the previously discussed difficulty of calculating these shifts, therefore, this approximate but

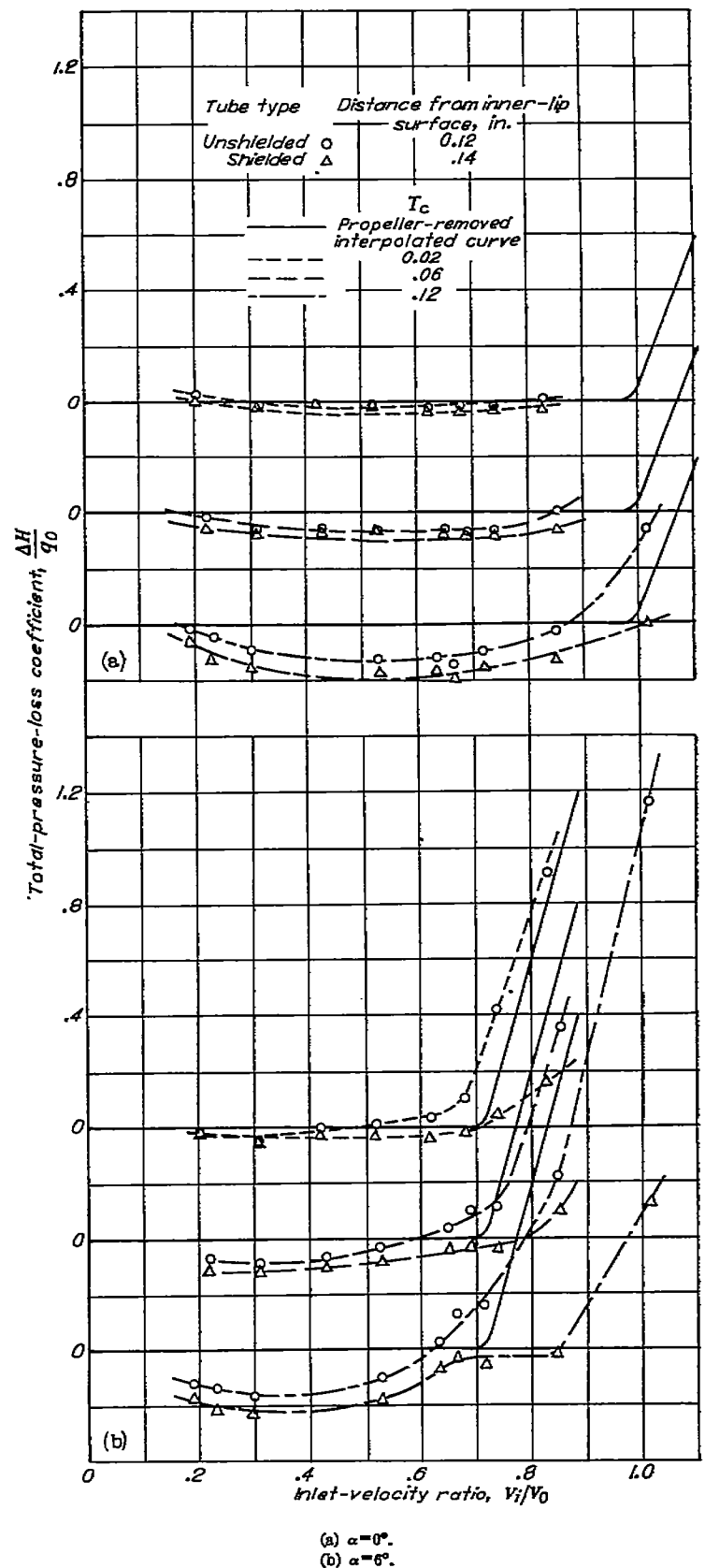


FIGURE 37.—Effect of propeller operation on total-pressure-loss coefficient at station 0.75 at bottom of inlet. NACA I-70-075 cowling with I-40-060 spinner.

always conservative correction factor was used; all critical Mach number results of the present report are presented as functions of the mass-flow coefficient

$$\frac{m}{\rho_0 F V_0} = \frac{A_0}{F} = \frac{A_t}{F} \times \frac{\rho_t V_t}{\rho_0 V_0}$$

or the inlet-velocity ratio $\left(\frac{V_t}{V_0}\right)_{cr}$ which corresponds to this mass-flow coefficient at the predicted critical Mach number.

Inlet-velocity ratios corresponding to the mass-flow coefficients given in the present report may be determined by use of an inlet-area chart (fig. 47) and a conversion chart (fig. 48). As an illustration of the use of these charts, suppose that a particular configuration with a spinner-diameter ratio D_s/D_c of 0.30 and an inlet-diameter ratio d/D_c of 0.72 has a predicted critical Mach number of 0.65 at a mass-flow coefficient of 0.165. The inlet-area ratio A_t/F is first determined to be 0.425 by reference to figure 47. Then, by proceeding through figure 48 as indicated by the short-dash line, the inlet-velocity ratio corresponding to this predicted critical Mach number and the test mass-flow

coefficient is found to be 0.325 as compared with the test value of 0.385.

NACA 1-series cowlings and cowling-spinner combinations.—The predicted critical Mach number characteristics of the NACA 1-series cowling-spinner combinations at angles of attack of 0°, 2°, 4°, and 6° are presented in figures 49 to 78 as a function of the mass-flow coefficient and compared with the characteristics of the basic open-nose cowlings. A key to these data is given as table II. The inlet-velocity ratios located by ticks on the curves are the minimum usable design values from the viewpoint of avoiding flow separation from the spinners (fig. 29) and are therefore optimum with respect to obtaining minimum internal losses. Except for the relatively thin lip cowlings, these inlet-velocity ratios usually occur above the knees of the curves and thus define the "design points" for the high-speed condition. However, when these ticks fall below the knees of the curves (figs. 64 to 66) or when no spinner is used, the most desirable rates of internal flow are determined by the locations of the knees, where the pressure distribution over the cowling first becomes essentially uniform. The method for determining the latter type of design condition is outlined in the section entitled "Envelope Values of M_{cr} and $(V_t/V_0)_{cr}$."

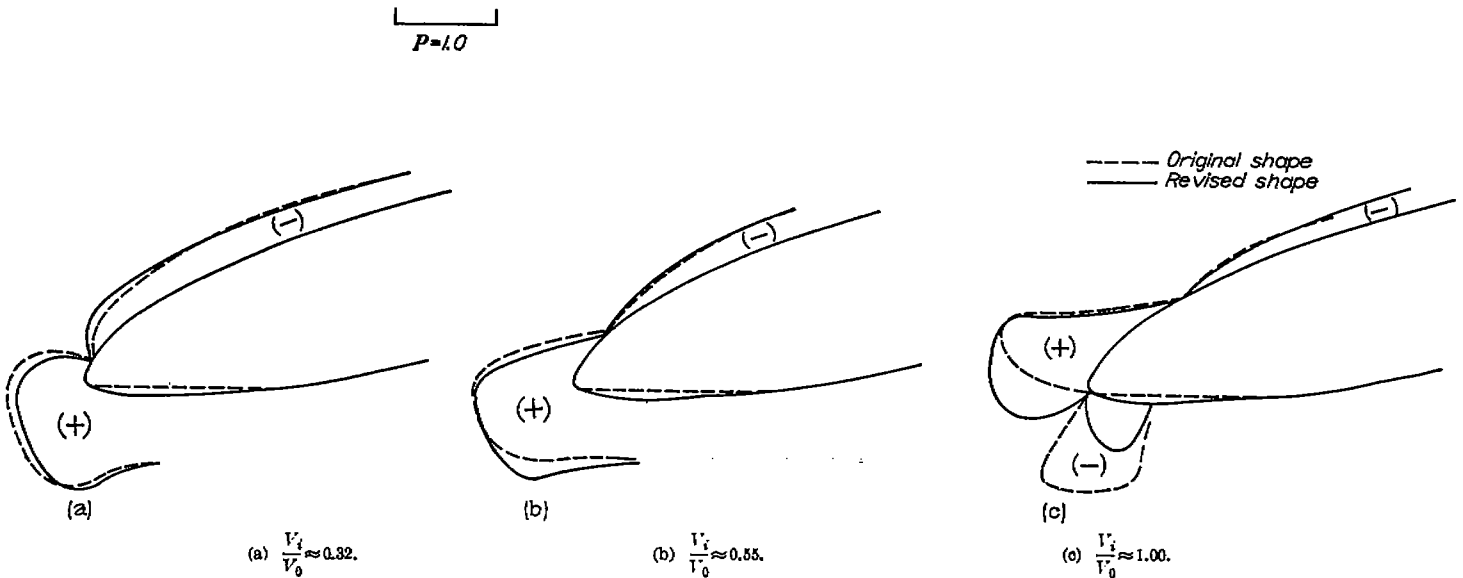


FIGURE 38.—Effect of inner lip shape on static-pressure distribution around NACA 1-60-075 cowling with 1-40-060 spinner. Propeller removed; $\alpha=0^\circ$; $M_t=0.13$.

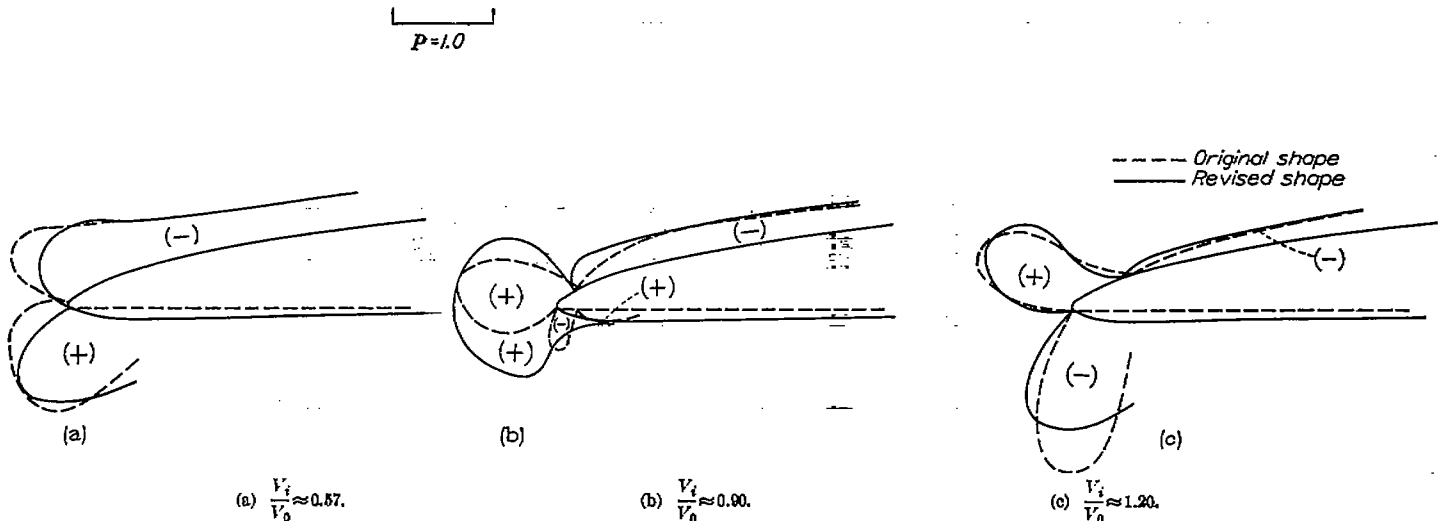


FIGURE 39.—Effect of inner lip shape on static-pressure distribution around NACA 1-60-050 cowling with 1-60-080 spinner. Propeller removed; $\alpha=0^\circ$; $M_t=0.13$.

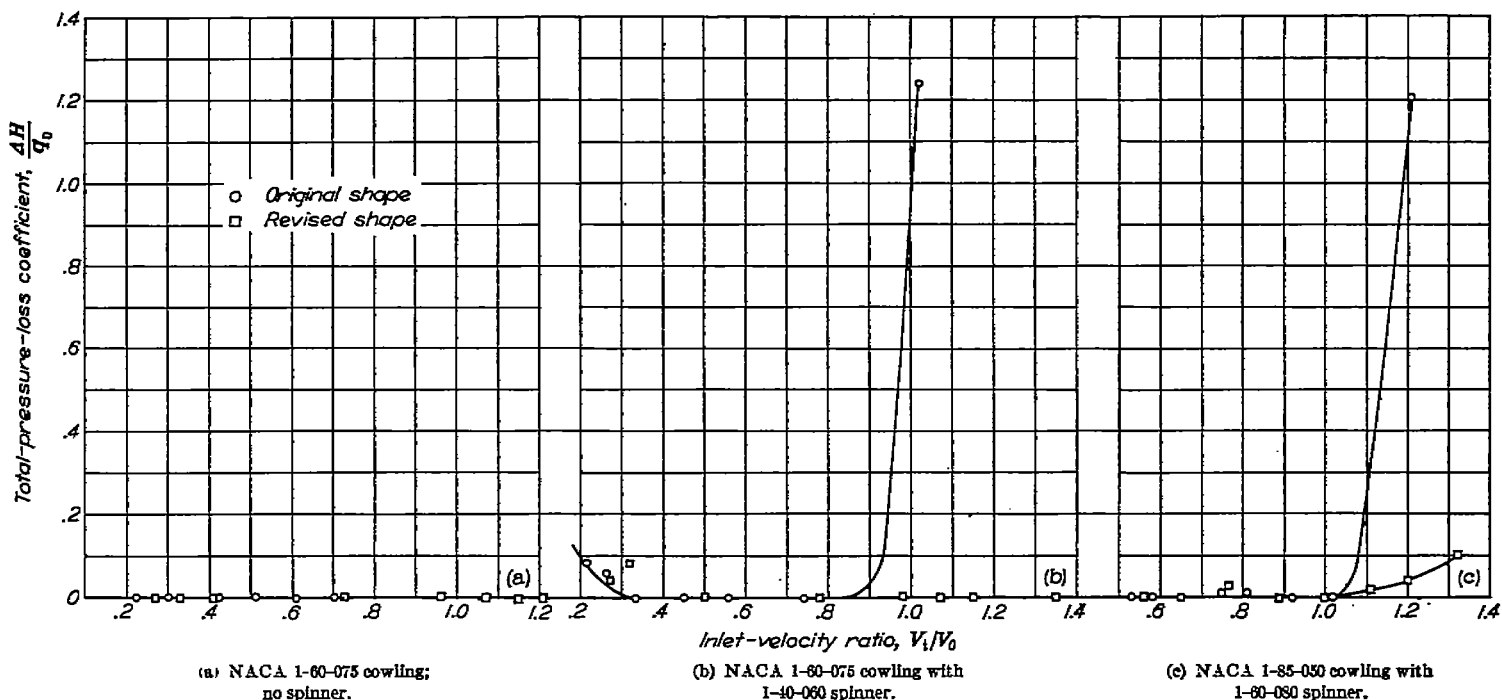


FIGURE 40.—Effect of inner lip shape on total-pressure-loss coefficient at reference tube 0.12 inch from inner surface of cowling at station 0.75 at top of inlet. Propeller removed; $\alpha=0^\circ$.

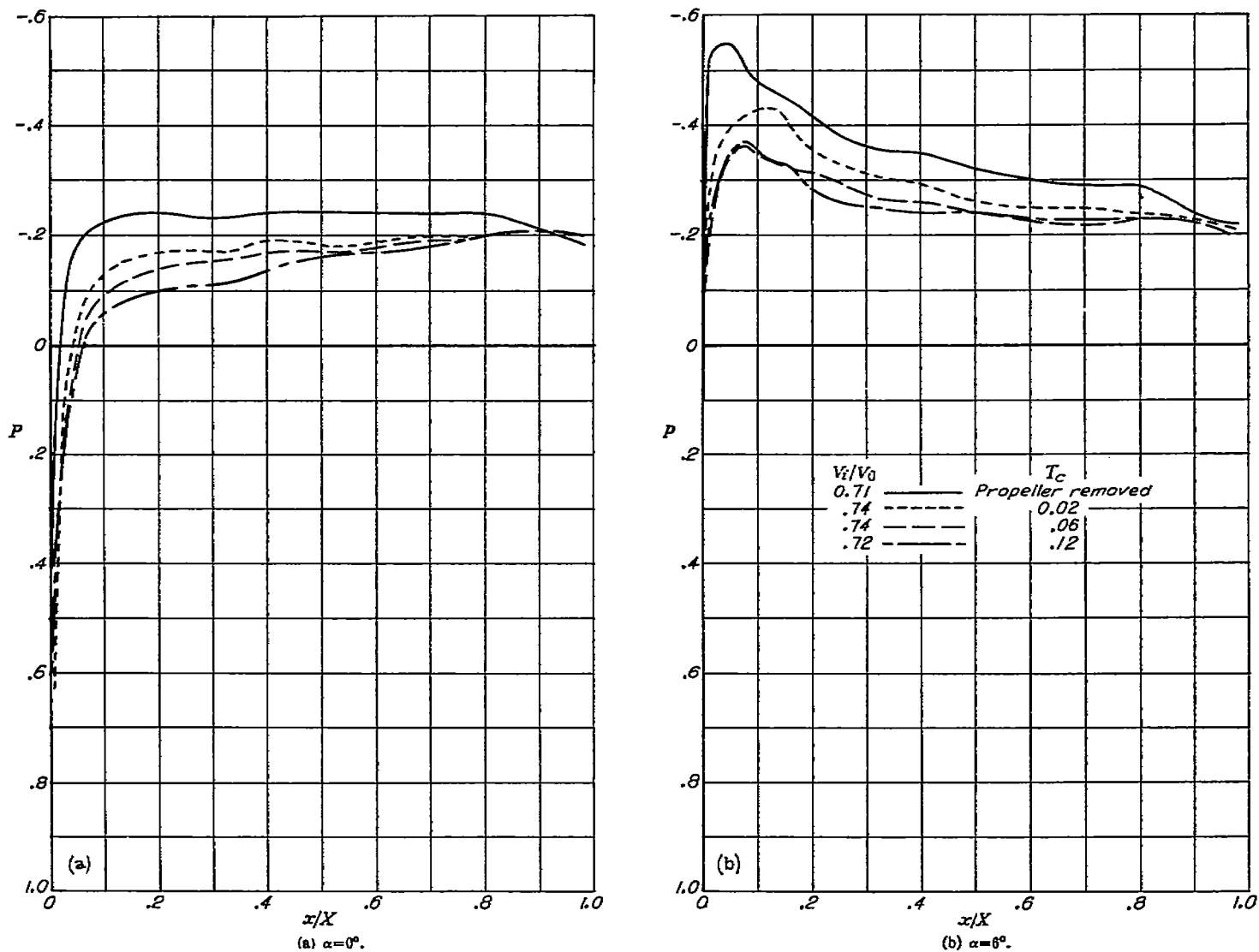


FIGURE 41.—Effect of propeller operation on static-pressure distribution over top surface of NACA 1-70-075 cowling with 1-40-060 spinner. $M_t=0.13$.

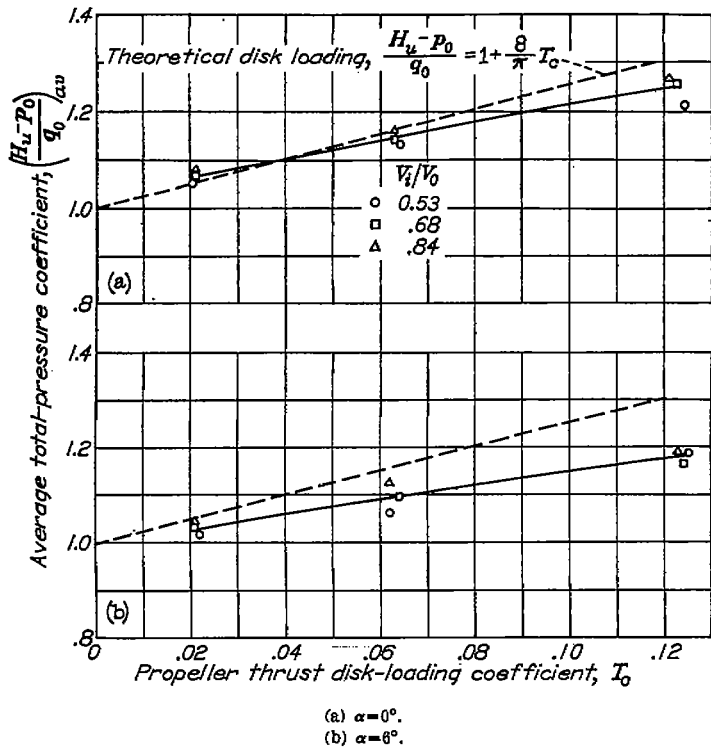


FIGURE 42.—Effect of propeller operation on average total-pressure coefficient for flow just outside boundary layer of cowling. NACA 1-70-075 cowling with 1-40-060 spinner; $M_t=0.13$.

Changes in spinner diameter shifted horizontally the knees of the curves of M_{cr} plotted against $m/\rho_0 FV_0$ of figures 49 to 78 because of resulting changes in the inlet area. The data for an angle of attack of 0° were therefore replotted in figures 79 to 83 as a function of $(V_i/V_0)_{cr}$ to show the effect of spinner configuration on the aerodynamic phenomena. In general, the addition of the smallest-diameter spinners ($\frac{D_s}{D_c}=0.2$) to the open-nose cowlings did not cause large changes in the critical Mach number characteristics. Further increases in spinner diameter and changes in the length of the larger-diameter spinners, however, frequently caused important changes in the location of the knees and in the critical Mach number above these knees. The nature of such changes depended primarily on the boundary-layer-separation characteristics of the spinners.

When the flow was separated from the spinner, successive increases in either spinner diameter or spinner length caused successive decreases in the inlet-velocity ratio at which the knee of the critical Mach number curve occurred. (See data in figs. 79 to 83, except those for the NACA 1-70-100 and 1-85-050 cowlings.) This trend is believed to have resulted from growth of the separation region on the spinner, which caused the divergence of the flow to take place farther ahead of the inlet. So long as the spinner flow was separated at the knee of the curve, the magnitude of the critical Mach number in the important design range above the knee was not appreciably affected by changes in spinner proportions.

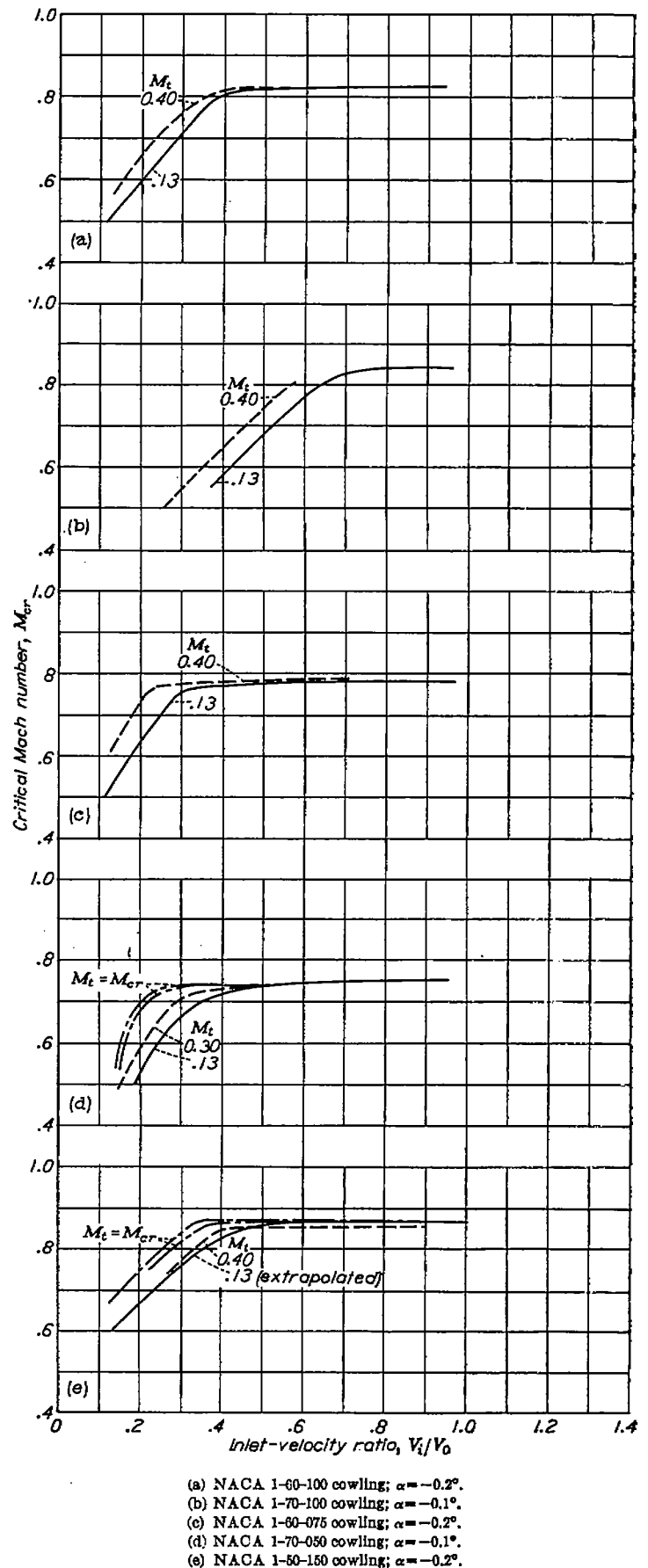


FIGURE 43.—Effect of test Mach number on predicted critical Mach number for NACA 1-series open-nose cowlings. $\frac{V_i}{V_0}$ used as independent variable. Results from reference indicated by broken lines.

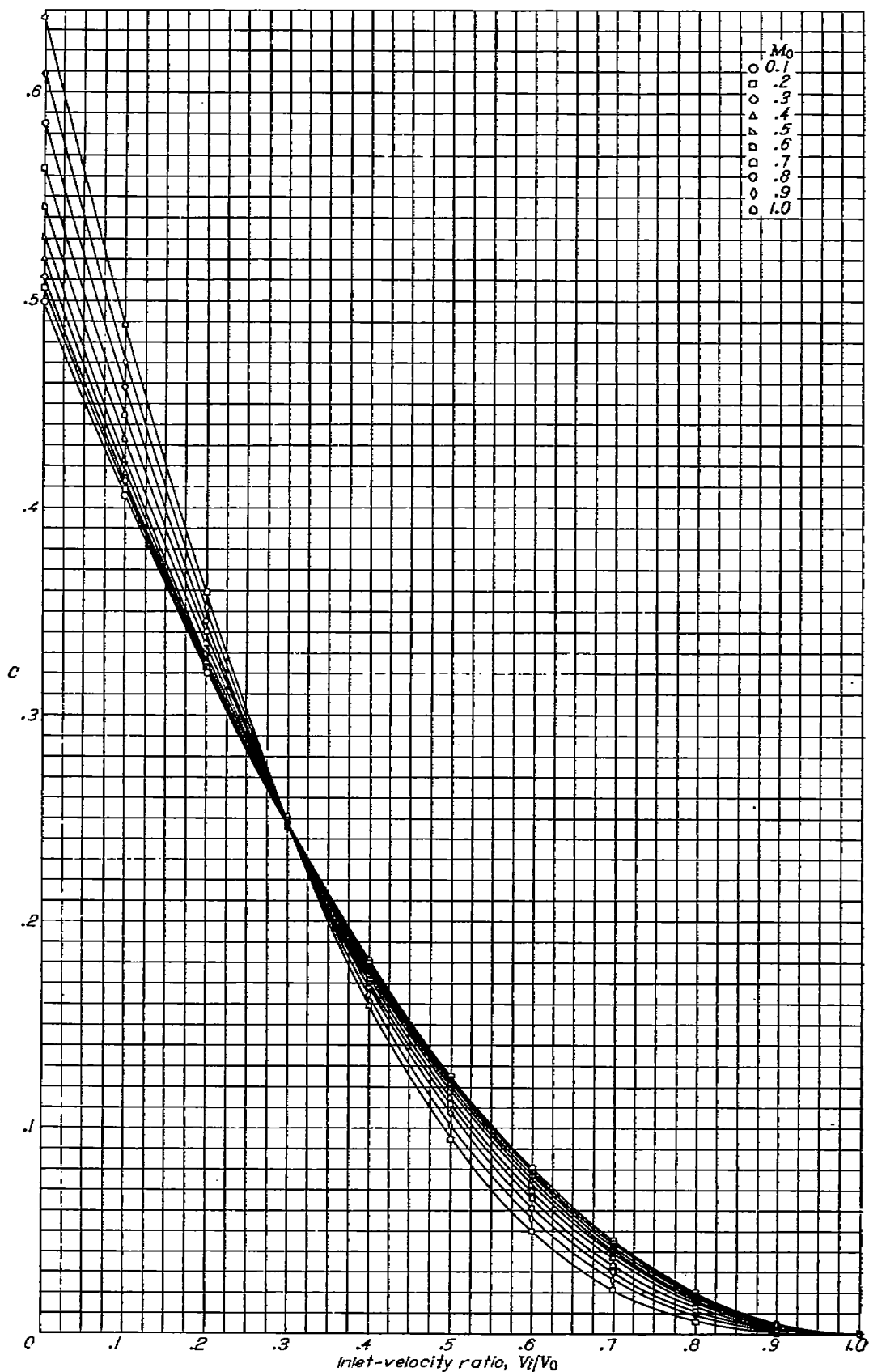


FIGURE 44.—Factor C in equations (9) and (10) of the appendix as a function of inlet-velocity ratio and free-stream Mach number. (Symbols are used only for purpose of identification.)

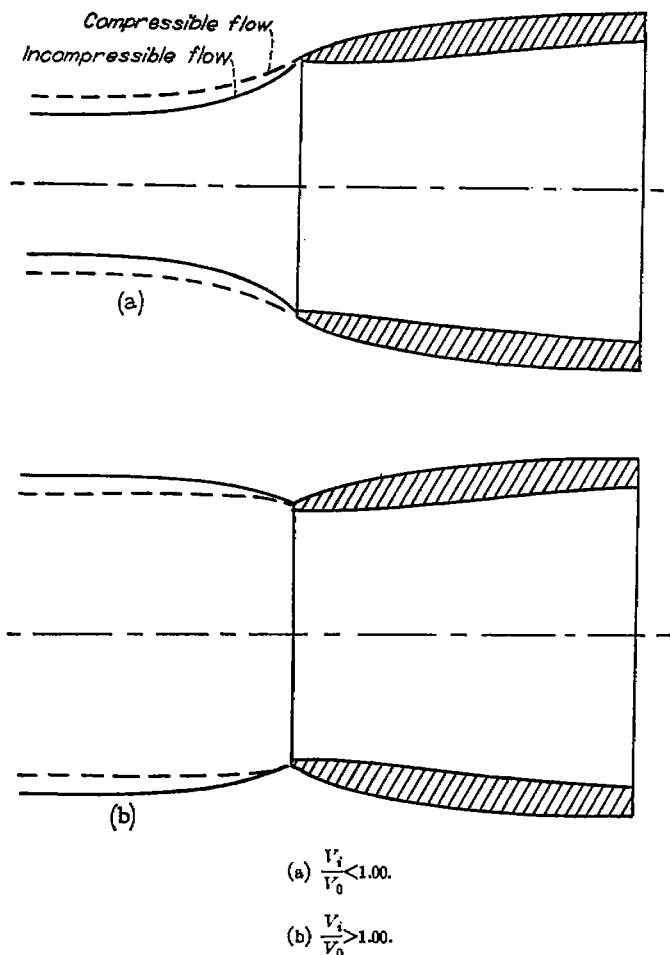


FIGURE 45.—Schematic diagram illustrating effect of compressibility on the stream tube containing the internal flow at a constant inlet-velocity ratio.

When the flow was not separated from the spinner at the inlet-velocity ratio corresponding to the knee of the critical Mach number curve for any particular open-nose cowling (for example, the NACA 1-70-100 and 1-85-050 cowlings, figs. 79 to 83), the phenomena were importantly different from those just discussed. Increasing the diameter of a given-length spinner or decreasing the length of a given-diameter spinner shifted the knee to a higher inlet-velocity ratio because the flow angle at the cowling lip increased in accordance with the change in slope of the spinner surface just ahead of the inlet. The spinner pressure distributions of figures 10 to 13 indicate that a steepening of the adverse pressure gradient just ahead of the inlet was responsible for a large part of such increases in flow divergence at the cowling lip. Above the knee of the curve, the flow divergence in the region of the cowling lip was still affected by the presence of the spinner so that a change in spinner proportions that shifted the knee to a higher inlet-velocity ratio also caused decreases in the critical Mach numbers above the knee. As these decreases and the magnitude of the shift of the knee both become important in the case of the large-diameter spinners, the desirability of conducting further research to develop spinner shapes with less severe adverse pressure gradients is again indicated.

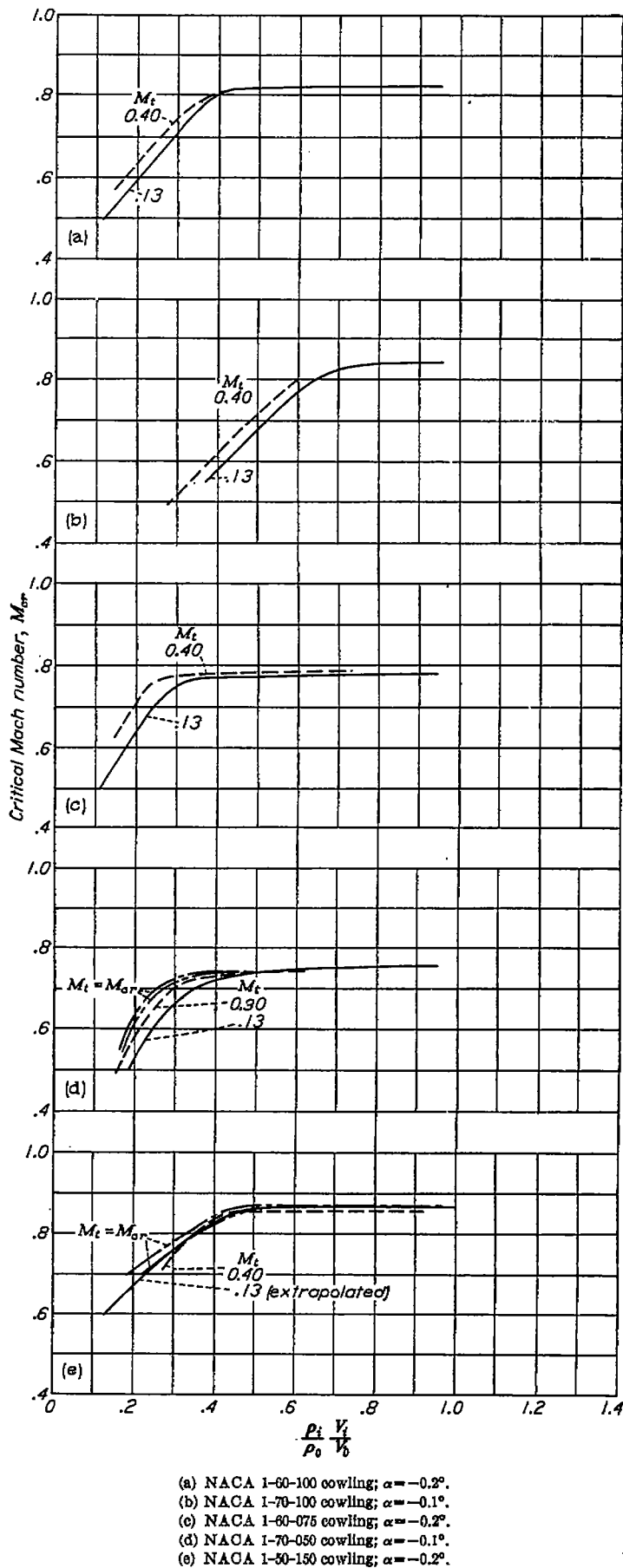


FIGURE 46.—Effect of test Mach number on predicted critical Mach number for NACA 1-series open-nose cowlings. $\frac{\rho_i V_i}{\rho_0 V_0} = \frac{m}{\rho_0 F V_0 A_i}$ used as independent variable. Results from reference 1 indicated by broken lines.

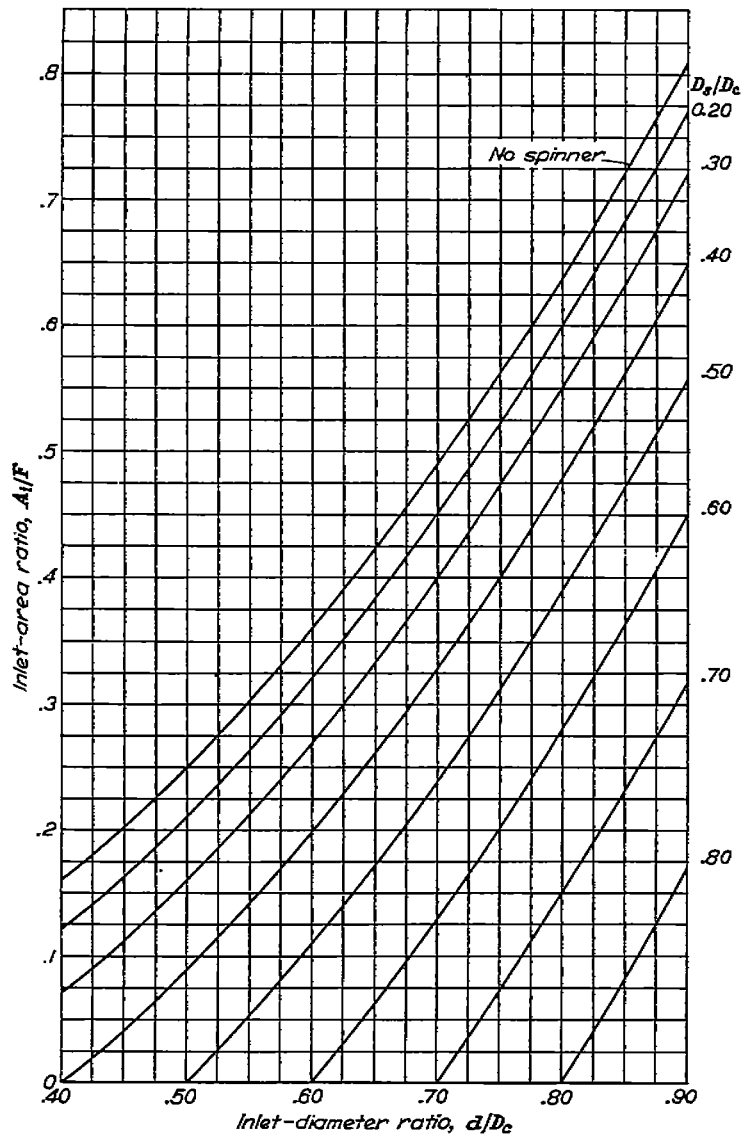


FIGURE 47.—Variation of inlet-area ratio with inlet-diameter ratio for several spinner-diameter ratios.

Except for these changes due to the spinner, the effects of cowling proportions on the critical Mach number characteristics of the NACA 1-series cowling-spinner combinations were generally similar to those for the NACA 1-series open-nose cowlings (figs. 79 to 83). As the trends shown have already been extensively discussed in reference 1, further discussion is omitted herein. The effects of cowling proportions on the design conditions are analyzed in detail, however, in a subsequent section of the report entitled "Envelope Values of M_{cr} and $(V_d/V_0)_{cr}$."

Effect of spinner location.—The effects of the longitudinal location of the NACA 1-40-040 spinner on the critical Mach number characteristics of the NACA 1-70-100 cowling are shown in figure 84. In order to be consistent with the rest of the report, the inlet area used in calculating the inlet-velocity ratio was always taken to be the unobstructed area in the most forward plane at which the diameter of the inner surface of the cowling was a minimum.

With the nose of the spinner at the inlet, the influence of the spinner on the flow field ahead of the inlet was small so that the critical Mach number characteristics were very nearly the same as those for the NACA 1-70-100 cowling.

(Compare figs. 81 (b) and 84.) This result indicates that the design data for the NACA open-nose cowlings are directly applicable to the design of rotating cowlings regardless of whether the propeller-hub fairing is located at or well inside the inlet.

When the nose of the spinner was located $0.15D_c$ ahead of the inlet or in its normal position ($\frac{x}{D_c}=0.40$), the knee of the critical Mach number curve was shifted to the right of the knee of the curve for the position $\frac{x}{D_c}=0$ (fig. 84) because of the previously discussed effect of the spinner in increasing the flow angle at the cowling lip. Also, when the nose of the spinner was moved to $0.60D_c$ and then farther forward to positions of interest for dual-rotating-propeller installations, the knee of the curve was shifted back to the left. This finding would appear to indicate that the spinner should be cylindrical for a short distance ahead of the inlet to reduce the flow angle at the cowling lip and thereby to increase the critical Mach number at the lower inlet-velocity ratios. As previously noted, however, the spinner flow became separated at the inlet-velocity ratio corresponding to the knee of the curve for these forward spinner locations. Such protruded spinners, therefore, are inferior to the corresponding normally located spinners of the same length, which have approximately the same knee inlet-velocity ratio with unseparated spinner flow. (See fig. 81.)

Effect of conical spinner.—The advantage of using a conical spinner to reduce the separation value of inlet-velocity ratio has previously been pointed out in the section entitled "Flow over Spinners." If the cowling used with a conical spinner of the type investigated (fig. 3) has a relatively blunt lip so that the knee of its critical Mach number curve occurs at a very low value of inlet-velocity ratio, the critical Mach number characteristics should not differ appreciably from those for the open-nose cowling. When such a spinner is used with a relatively thin-lipped cowling, however, the increase in flow angle at the cowling lip causes a marked reduction in critical Mach number so that the critical Mach number characteristics are inferior to those for the cowling with a comparable NACA 1-series spinner (fig. 85); this decrease in Mach number would be accentuated by an increase in cone angle. Further research appears to be required, therefore, to determine if this undesirable characteristic of the conical spinner can be overcome either by keeping the spinner cylindrical for a short distance ahead of the inlet or by modifying the cowling lip to allow for the change in the effective angle of attack.

Effect of cowling-inner-lip shape.—The effectiveness of a revised cowling-inner-lip shape incorporating the NACA 1-series ordinates of table I has previously been shown in the section entitled "Internal Flow." Data presented in figure 86 show that installation of the revised inner-lip shape did not appreciably affect the critical Mach number characteristics of several widely different cowling configurations. Hence, the design data for the standard NACA 1-series cowlings can be used to design NACA 1-series cowlings utilizing this revised shape provided that the change in inlet area is taken into account.

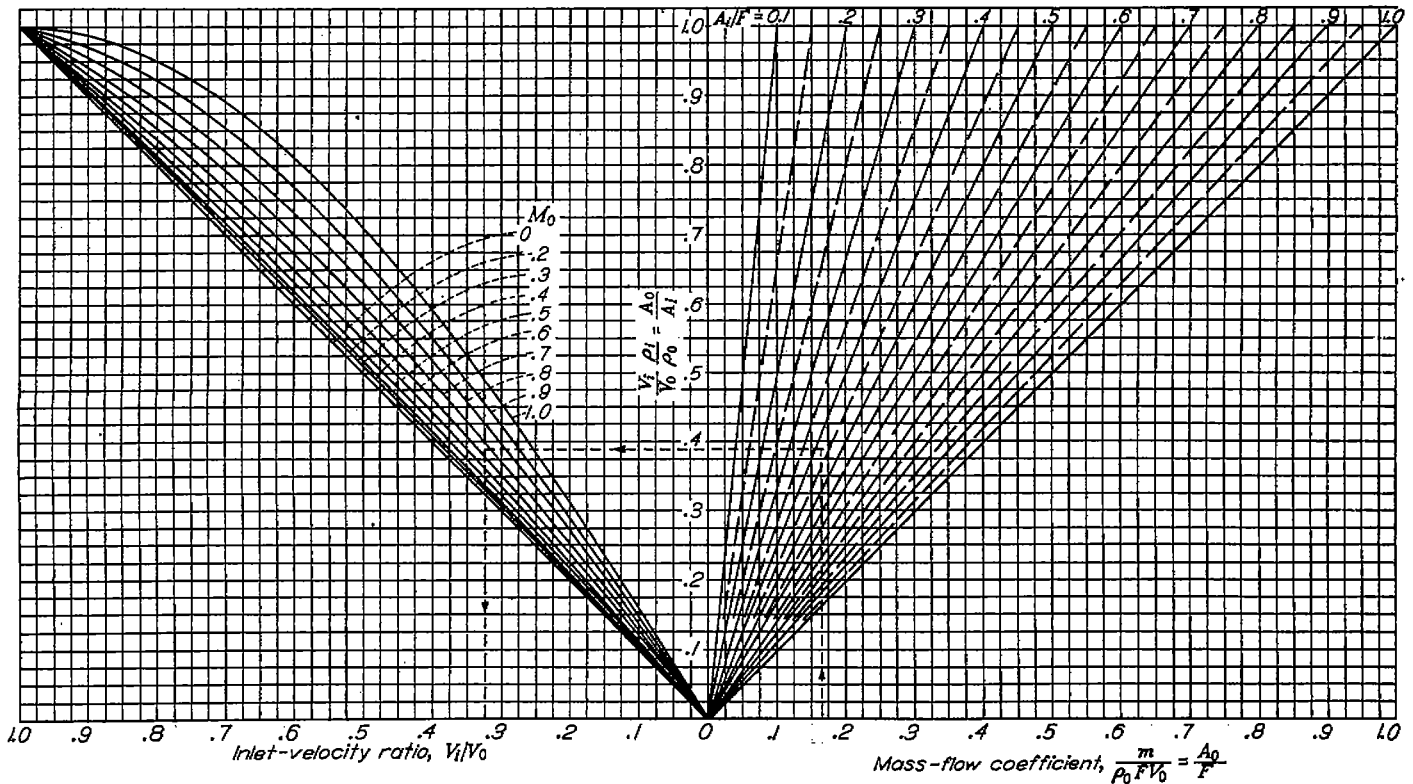


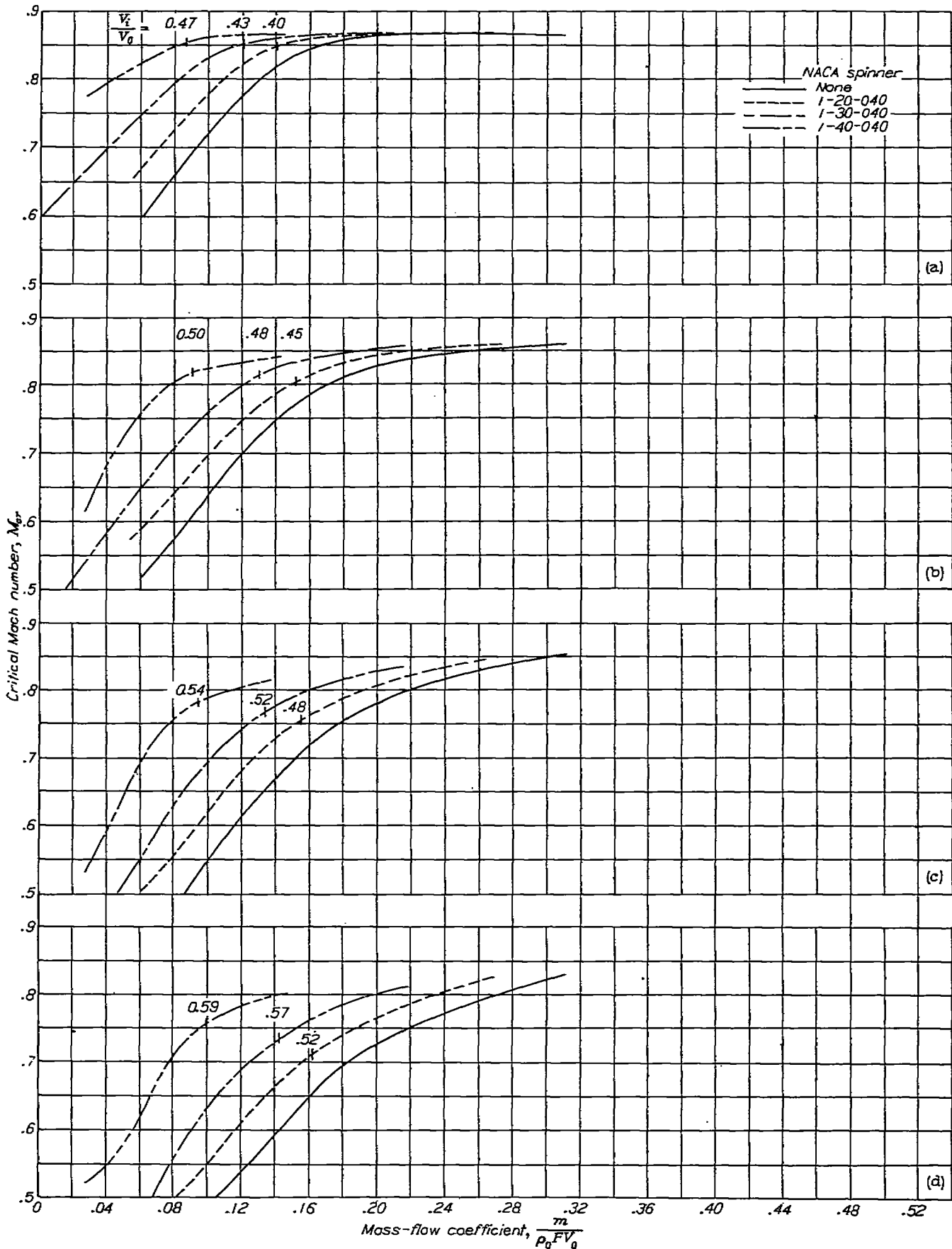
FIGURE 48.—Variation of inlet-velocity ratio with mass-flow coefficient for given Mach numbers and inlet-area ratios.

$$\frac{m}{\rho_0 F V_0} = \left(\frac{A_i}{F}\right) \left(\frac{V_i}{V_0}\right) \left[\frac{\gamma-1}{2} M_0^2 - \frac{\gamma-1}{2} M_0^2 \left(\frac{V_i}{V_0}\right)^2 + 1 \right]^{\frac{1}{\gamma-1}}$$

(See reference 1 or the appendix.)

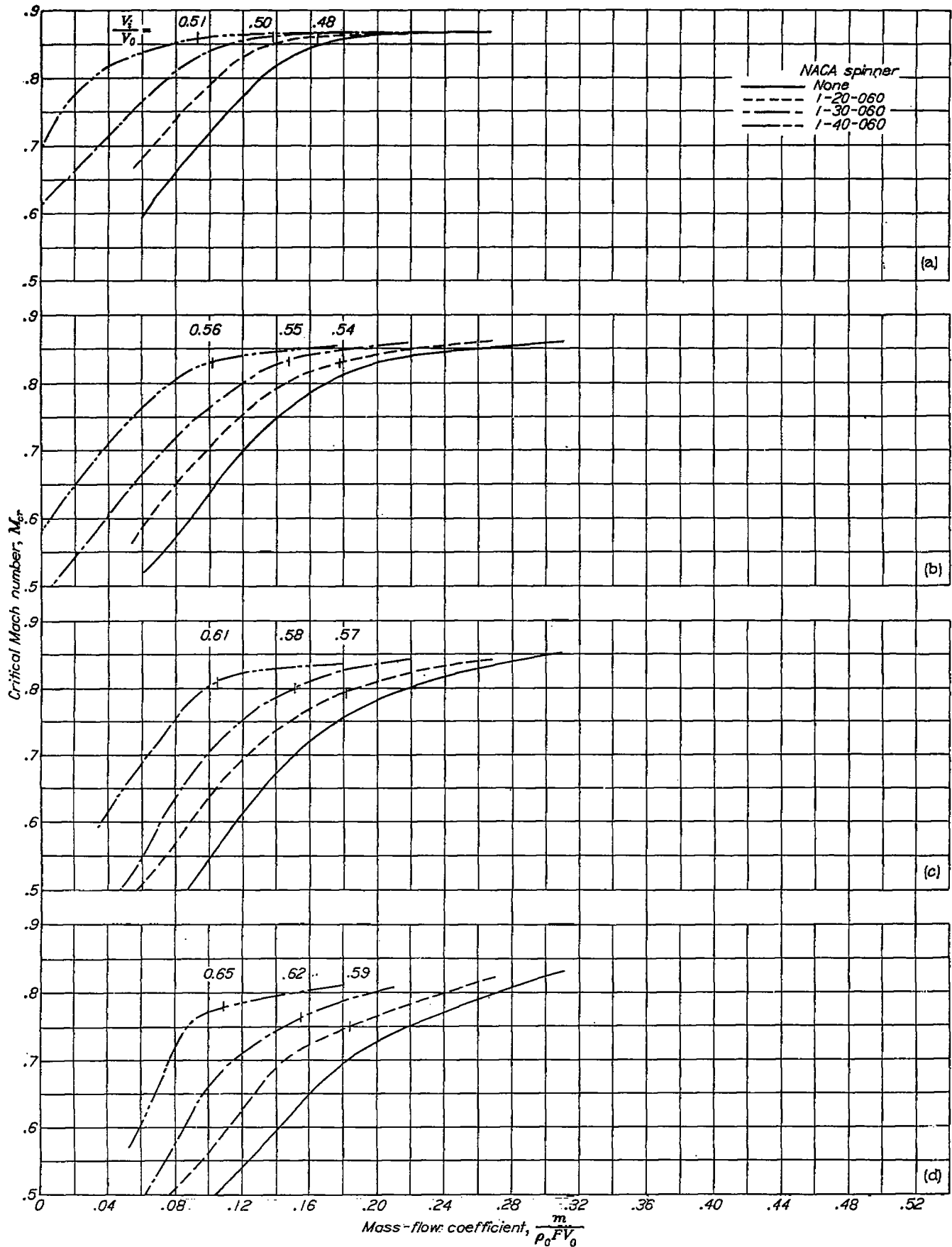
Effect of propeller operation.—Predicted critical Mach numbers for the NACA 1-series cowling-spinner combination tested with and without a propeller are presented in figures 87 and 88. The critical Mach number characteristics predicted for the propeller-installed condition from the pressure coefficient $P = \frac{p-p_0}{q_0}$ (fig. 87) are obviously in error since it has been shown previously that propeller operation effects increases in the maximum velocities along the cowling surface. Reasonable values of critical Mach numbers are obtained, however, if fictitious critical Mach numbers are first predicted from pressure coefficients based on the dynamic pressure in the slipstream just outside the cowling boundary layer $\frac{p-p_0}{H_u-p_0}$ and are then converted to values based on the free-stream velocity by multiplying the predicted values by $\frac{V_u}{V_\infty} = \sqrt{\frac{q_0}{H_u-p_0}}$. (See fig. 88.) Such values decrease regularly with increases in propeller thrust disk-loading coefficient as required by the accompanying increases in velocity along the cowling surface.

The knees of the curves of M_{cr} plotted against $(V_i/V_0)_{cr}$ for the propeller-installed condition always occurred at lower inlet-velocity ratios than was the case for the propeller-removed condition regardless of the computational method used. (See figs. 87 and 88.) This shift is believed to have been caused in part by the contraction of the slipstream, which changed the flow direction in the vicinity of the inlet lip, and in part by the static pressure gradient imposed by the slipstream. The inlet-velocity ratios which correspond to the selection points for the propeller-removed conditions therefore appear to be amply conservative for design purposes. A cross plot at the propeller-removed design value of inlet-velocity ratio (fig. 89) also indicates that within the high-speed range of flight conditions the decrease in critical Mach number due to propeller operation is negligible; thus, the propeller-removed critical Mach number characteristics of the present report are directly applicable without correction for the purpose of design. It is interesting to note in figure 89 that the decrease in critical Mach number due to the propeller was only about half as large when computed from the measured pressure data as when computed on the basis of uniform propeller thrust disk loading.



(a) $\alpha = 0^\circ$.
 (b) $\alpha = 2^\circ$.
 (c) $\alpha = 4^\circ$.
 (d) $\alpha = 6^\circ$.

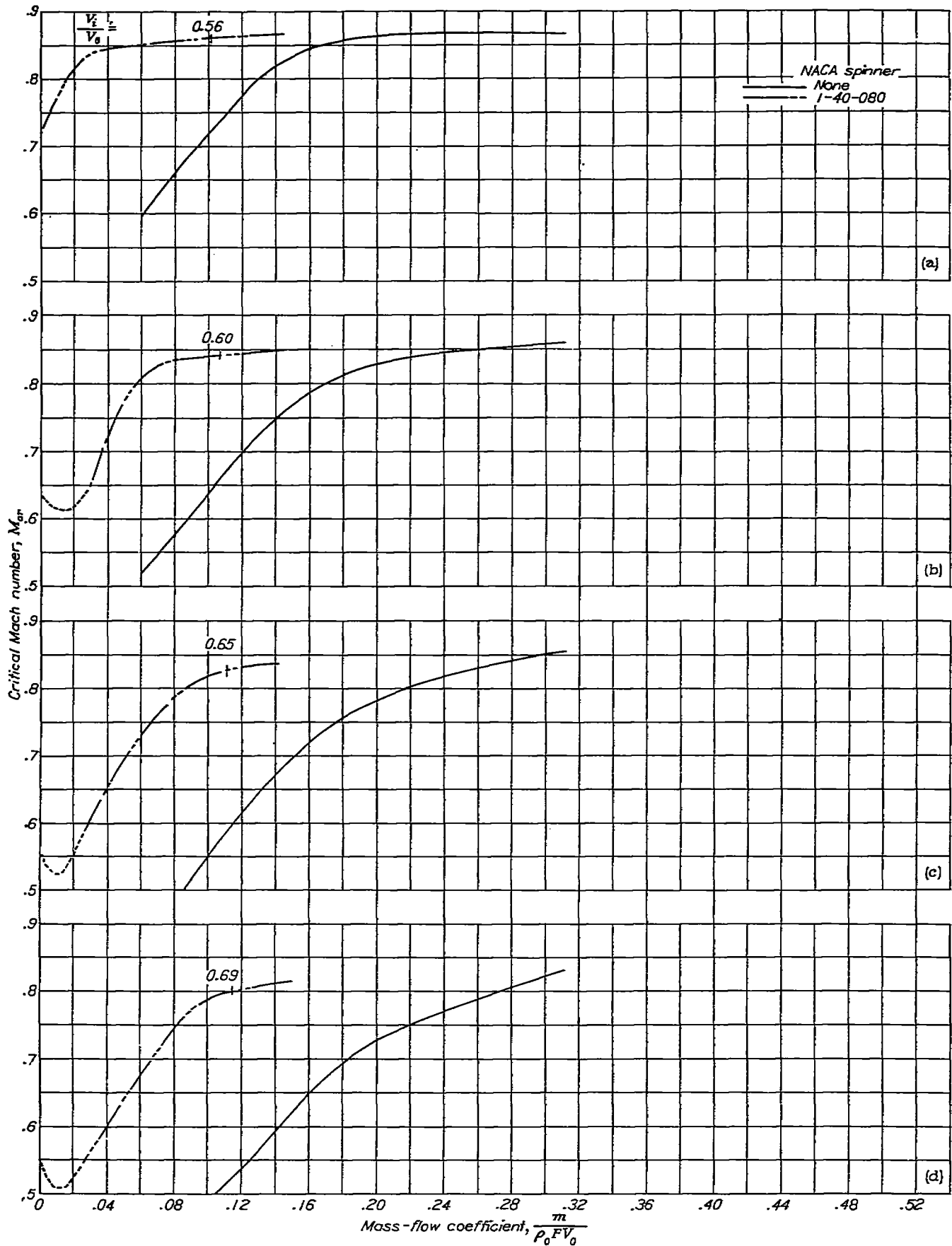
FIGURE 49.—Predicted critical Mach numbers for the NACA 1-55-150 cowling. (Ticks locate minimum design values of V_c/V_0 determined by separation from spinners.)
 Propeller removed; $\frac{V_c}{D_c} = 0.40$.



- (a) $\alpha=0^\circ$.
- (b) $\alpha=2^\circ$.
- (c) $\alpha=4^\circ$.
- (d) $\alpha=8^\circ$.

FIGURE 50.—Predicted critical Mach numbers for the NACA 1-55-150 cowling. (Ticks locate minimum design values of V_i/V_0 determined by separation from spinners.)

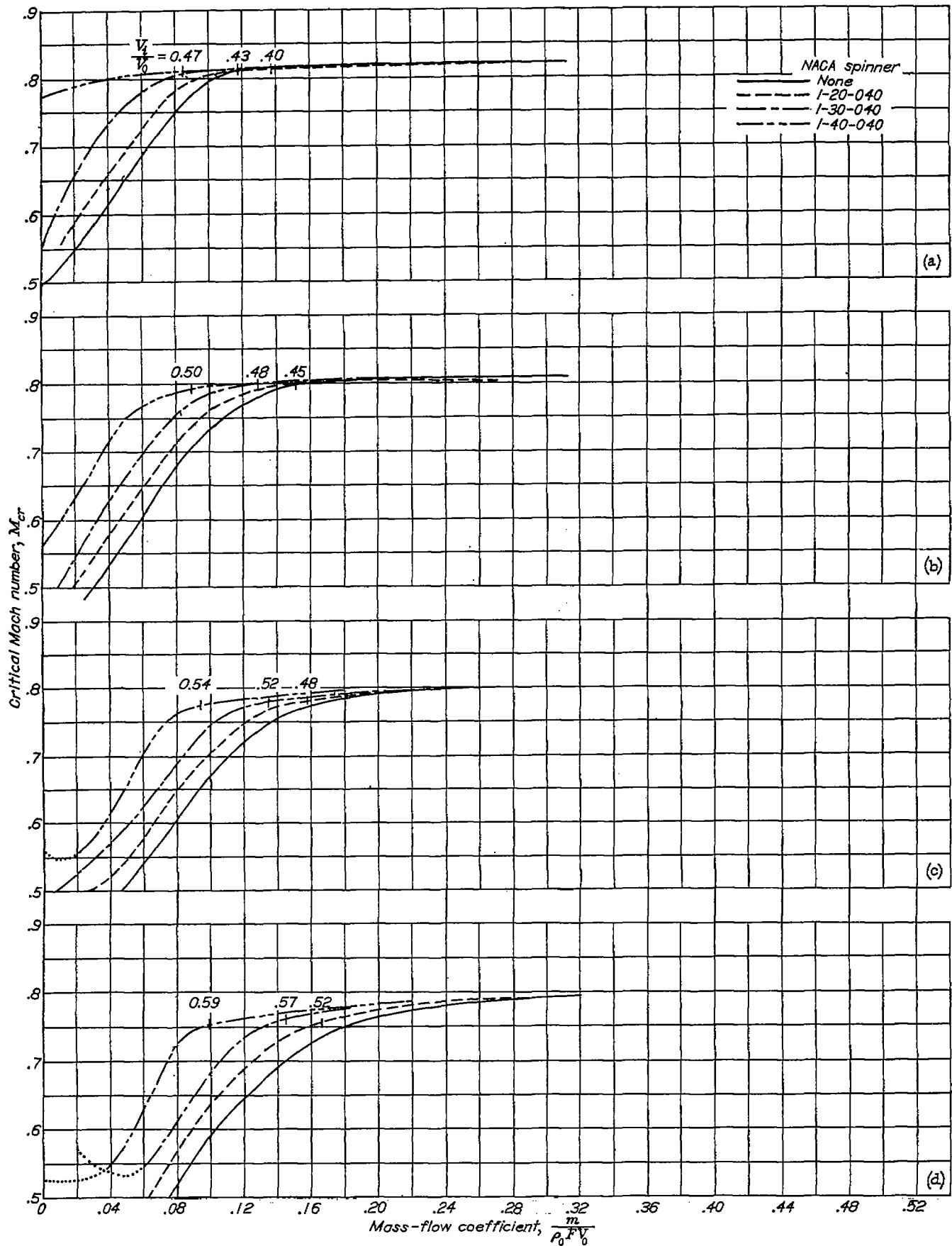
Propeller removed; $\frac{X_1}{D_c} = 0.60$.



- (a) $\alpha=0^\circ$.
- (b) $\alpha=2^\circ$.
- (c) $\alpha=4^\circ$.
- (d) $\alpha=8^\circ$.

FIGURE 51.—Predicted critical Mach numbers for the NACA 1-55-150 cowling. (Ticks locate minimum design values of V_i/V_0 determined by separation from spinners.)

Propeller removed; $\frac{X_s}{D_s}=0.80$.



- (a) $\alpha = 0^\circ$.
- (b) $\alpha = 2^\circ$.
- (c) $\alpha = 4^\circ$.
- (d) $\alpha = 6^\circ$.

FIGURE 52.—Predicted critical Mach numbers for the NACA 1-55-100 cowling. (Ticks locate minimum design values of V_d/V_0 determined by separation from spinners.)

Propeller removed; $\frac{X_1}{D_1} = 0.40$.

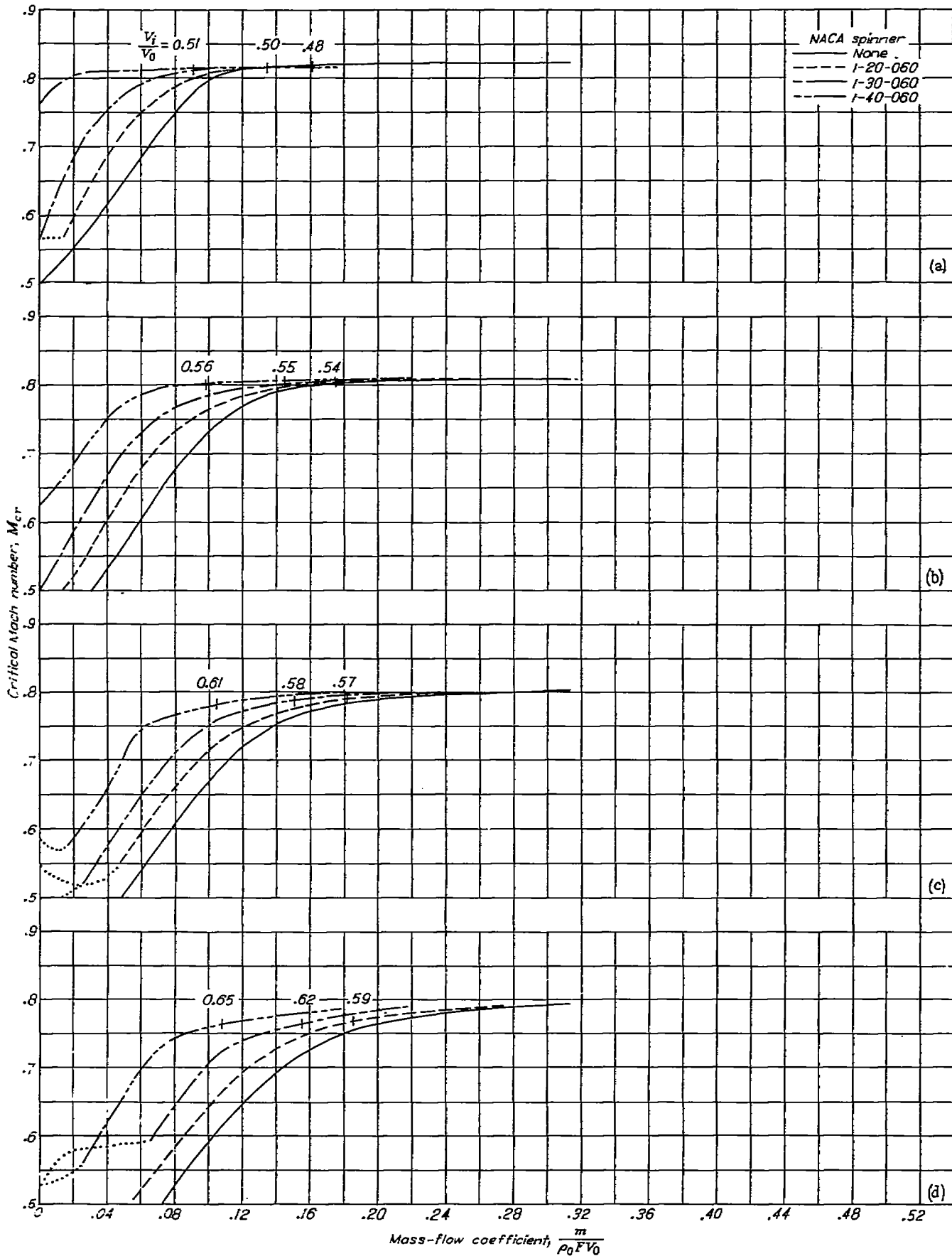


FIGURE 53. Predicted critical Mach numbers for the NACA 1-53-100 cowlings. (Ticks locate minimum design values of V_i/V_0 determined by separation from spinners.)

Propeller removed; $\frac{X_c}{D_c} = 0.60$.

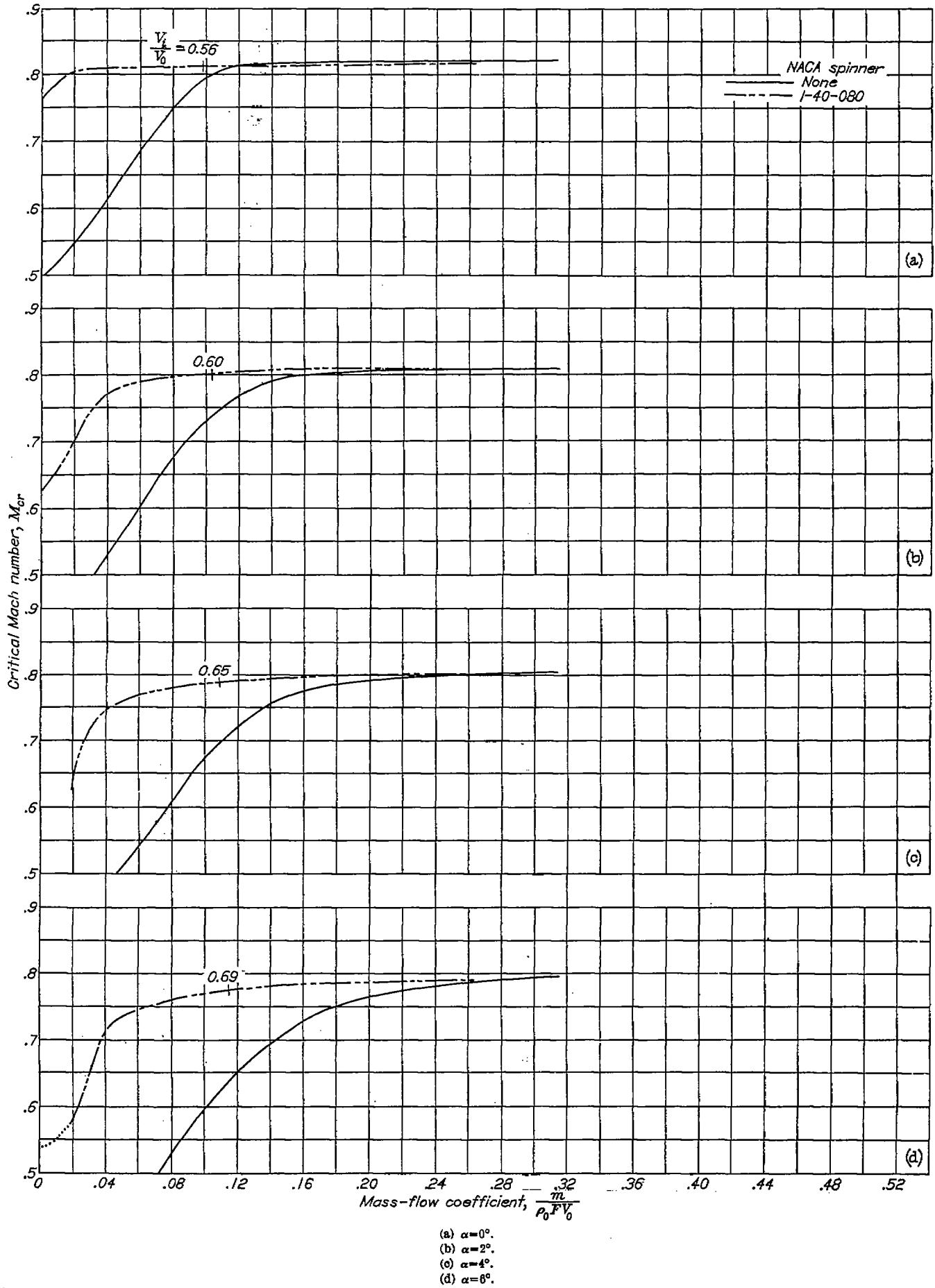


FIGURE 54.—Predicted critical Mach numbers for the NACA 1-56-100 cowling. (Ticks locate minimum design values of V_1/V_0 determined by separation from spinners.)

Propeller removed; $\frac{X_c}{D_c} = 0.80$.

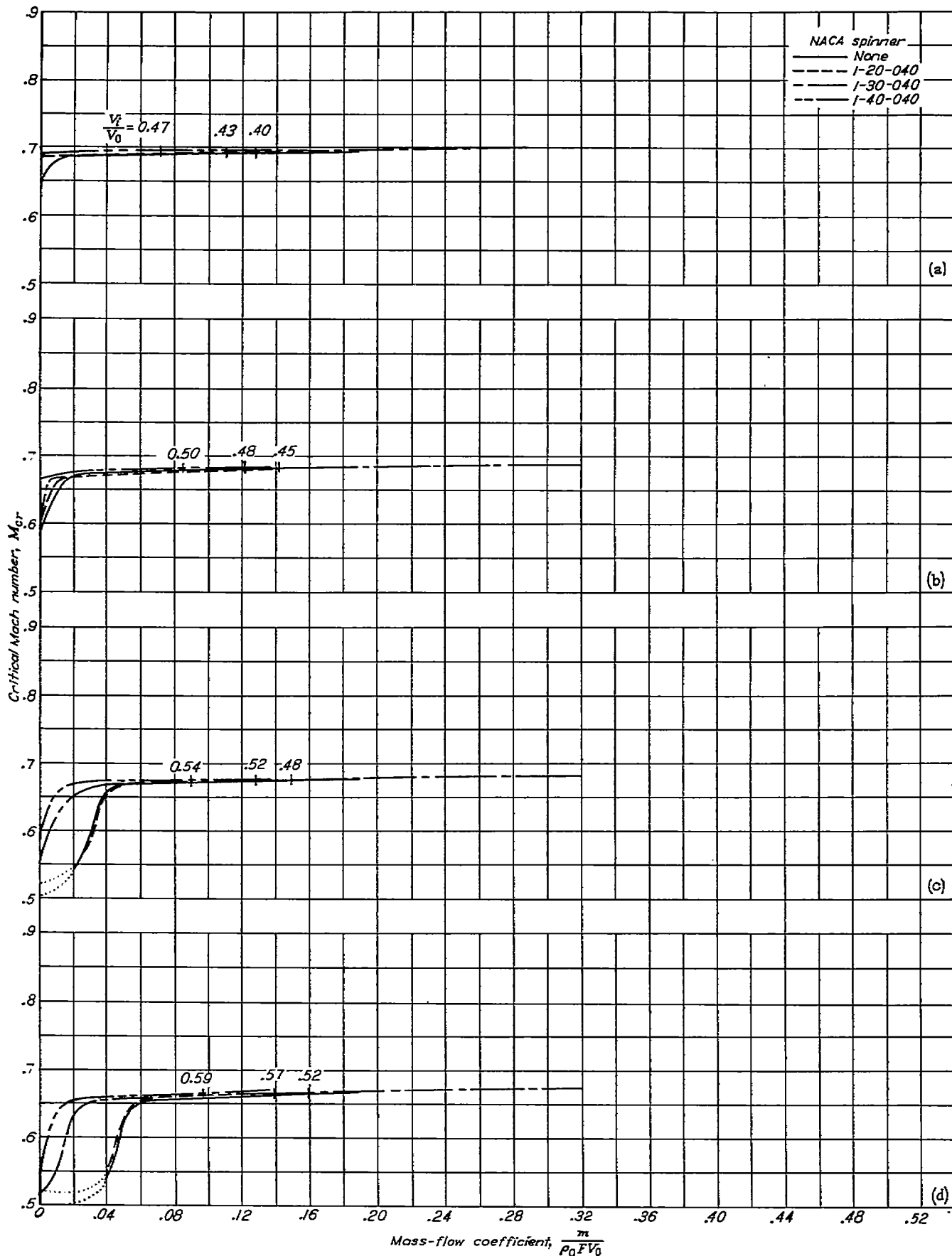
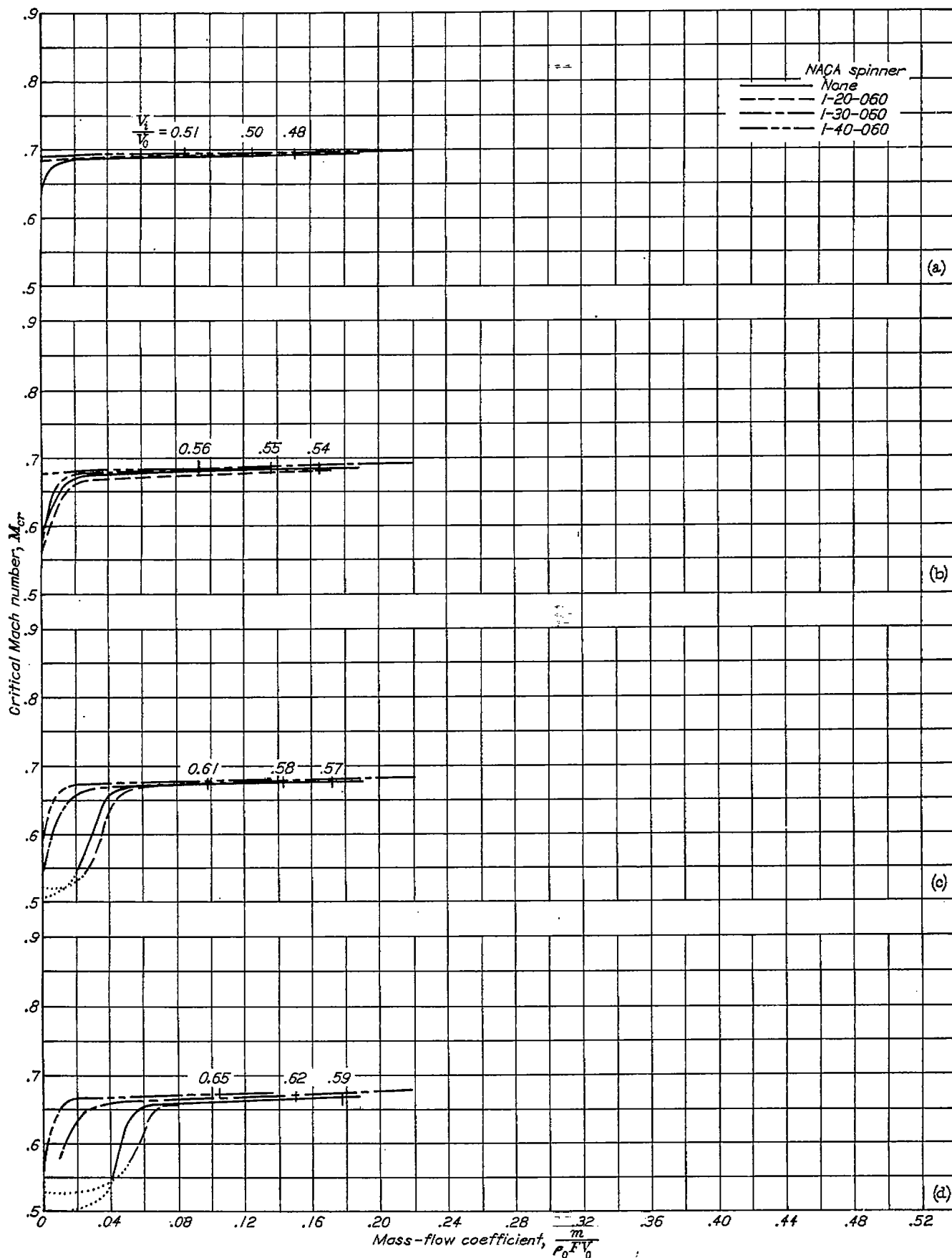


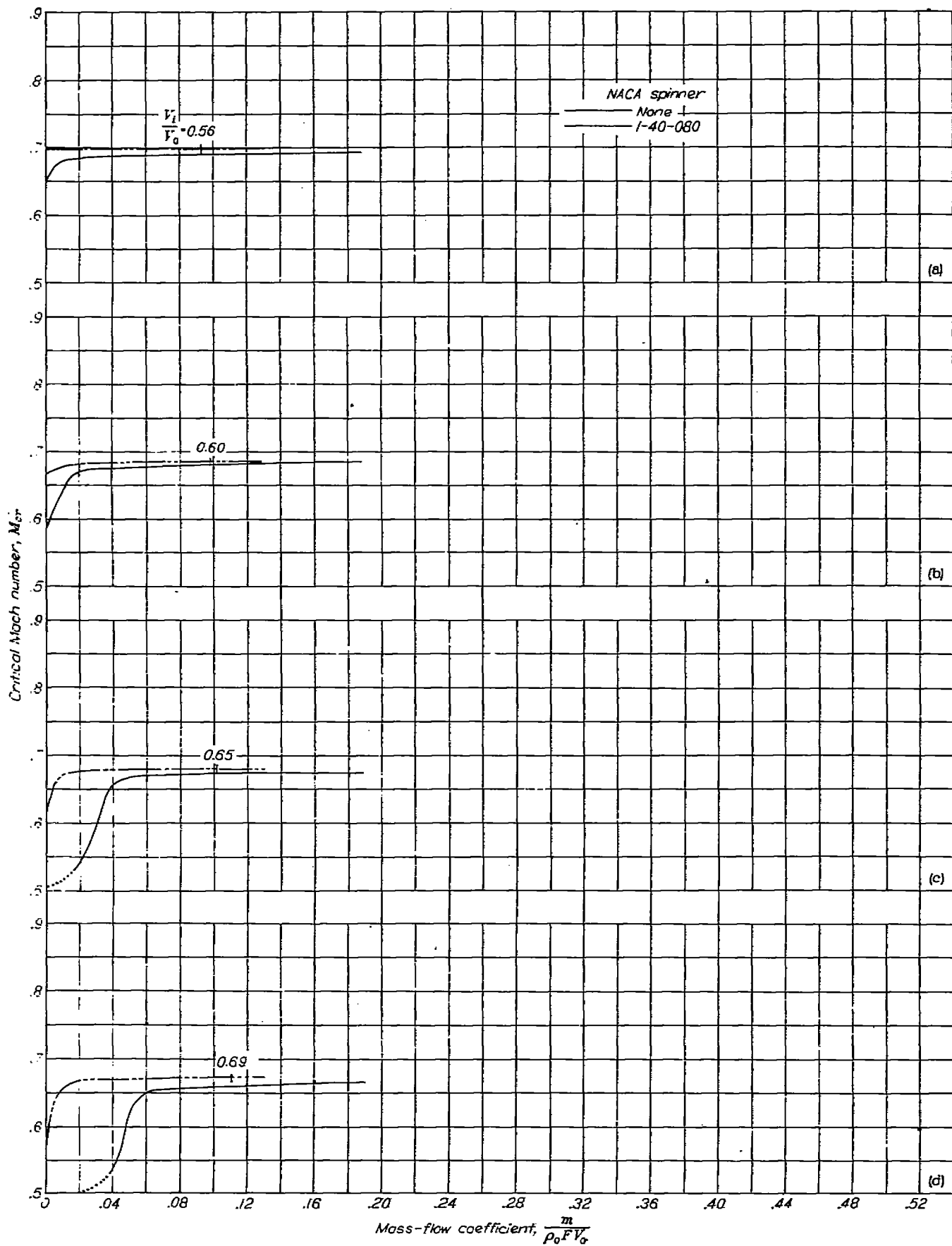
FIGURE 55.—Predicted critical Mach numbers for the NACA 1-55-030 cowling. (Ticks locate minimum design values of V_c/V_0 determined by separation from spinners.) Propeller removed; $X_c/D_c = 0.40$.



- (a) $\alpha = 0^\circ$.
- (b) $\alpha = 2^\circ$.
- (c) $\alpha = 4^\circ$.
- (d) $\alpha = 6^\circ$.

FIGURE 56.—Predicted critical Mach numbers for the NACA 1-55-080 cowling. (Ticks locate minimum design values of V_1/V_0 determined by separation from spinners.)

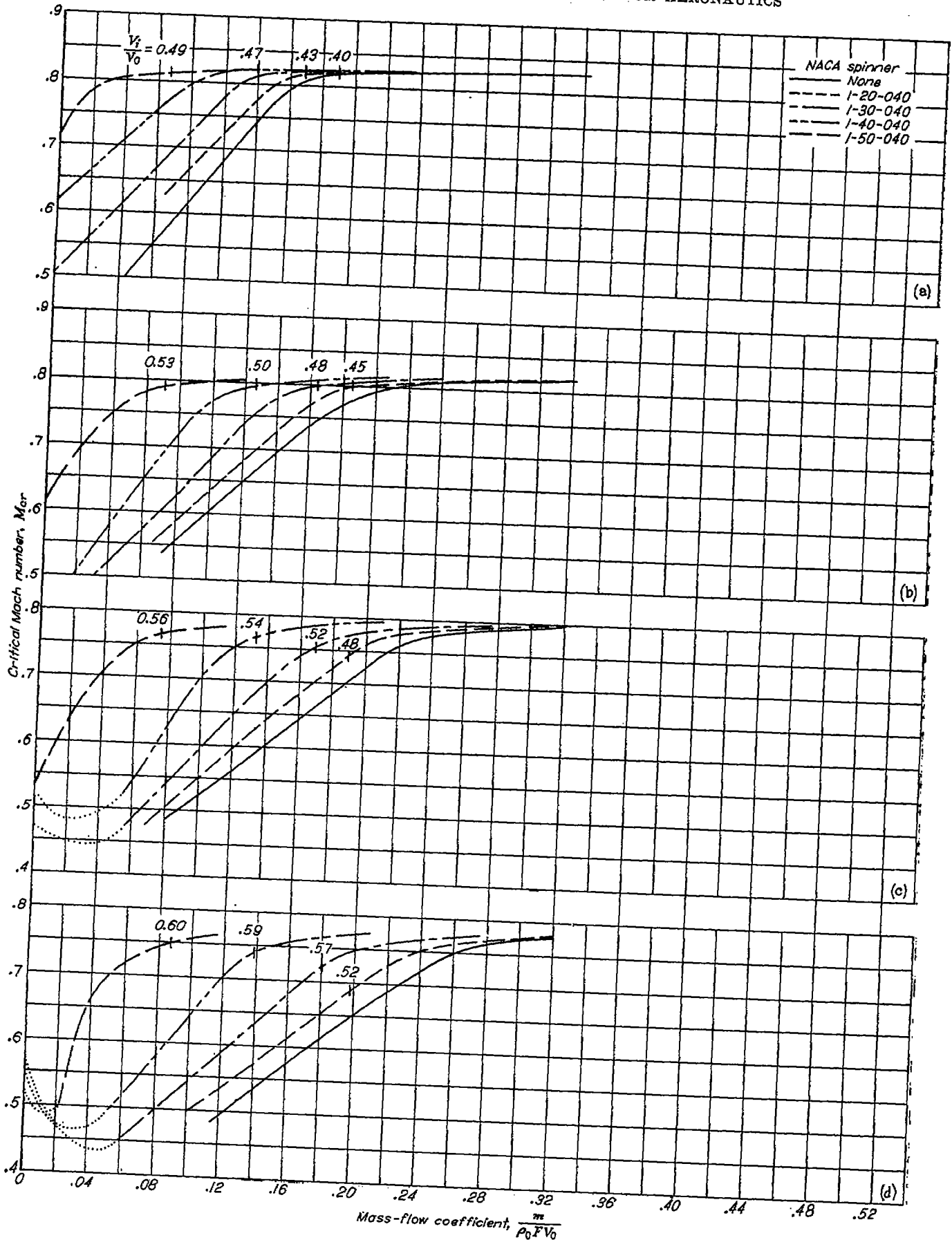
Propeller removed; $X/D_1 = 0.60$.



- (a) $\alpha = 0^\circ$.
- (b) $\alpha = 2^\circ$.
- (c) $\alpha = 4^\circ$.
- (d) $\alpha = 6^\circ$.

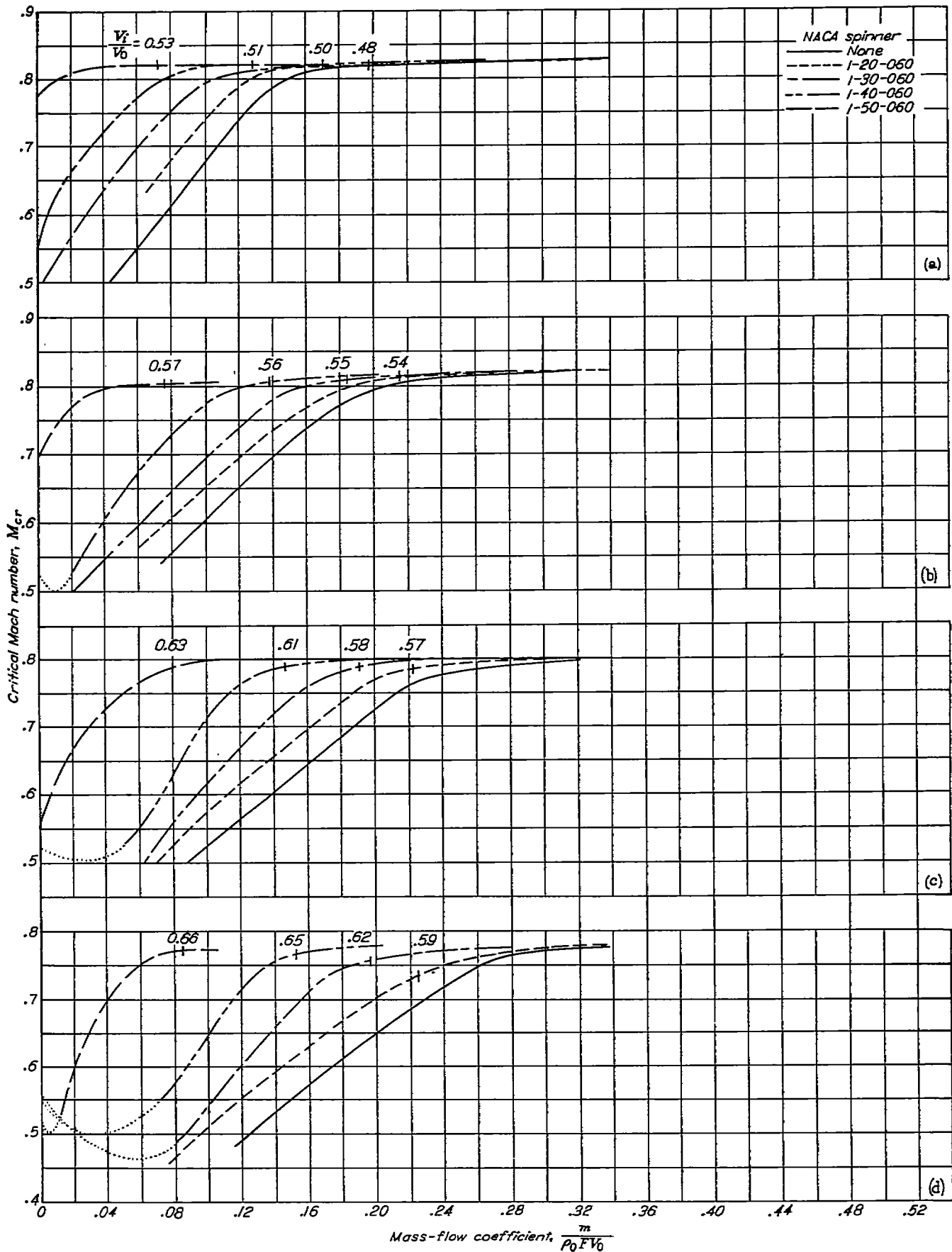
FIGURE 57.—Predicted critical Mach numbers for the NACA 1-55-050 cowl. (Ticks locate minimum design values of V_1/V_0 determined by separation from spinners.)

Propeller removed; $\frac{X_1}{D} = 0.80$.



- (a) $\alpha = 0^\circ$.
- (b) $\alpha = 2^\circ$.
- (c) $\alpha = 4^\circ$.
- (d) $\alpha = 6^\circ$.

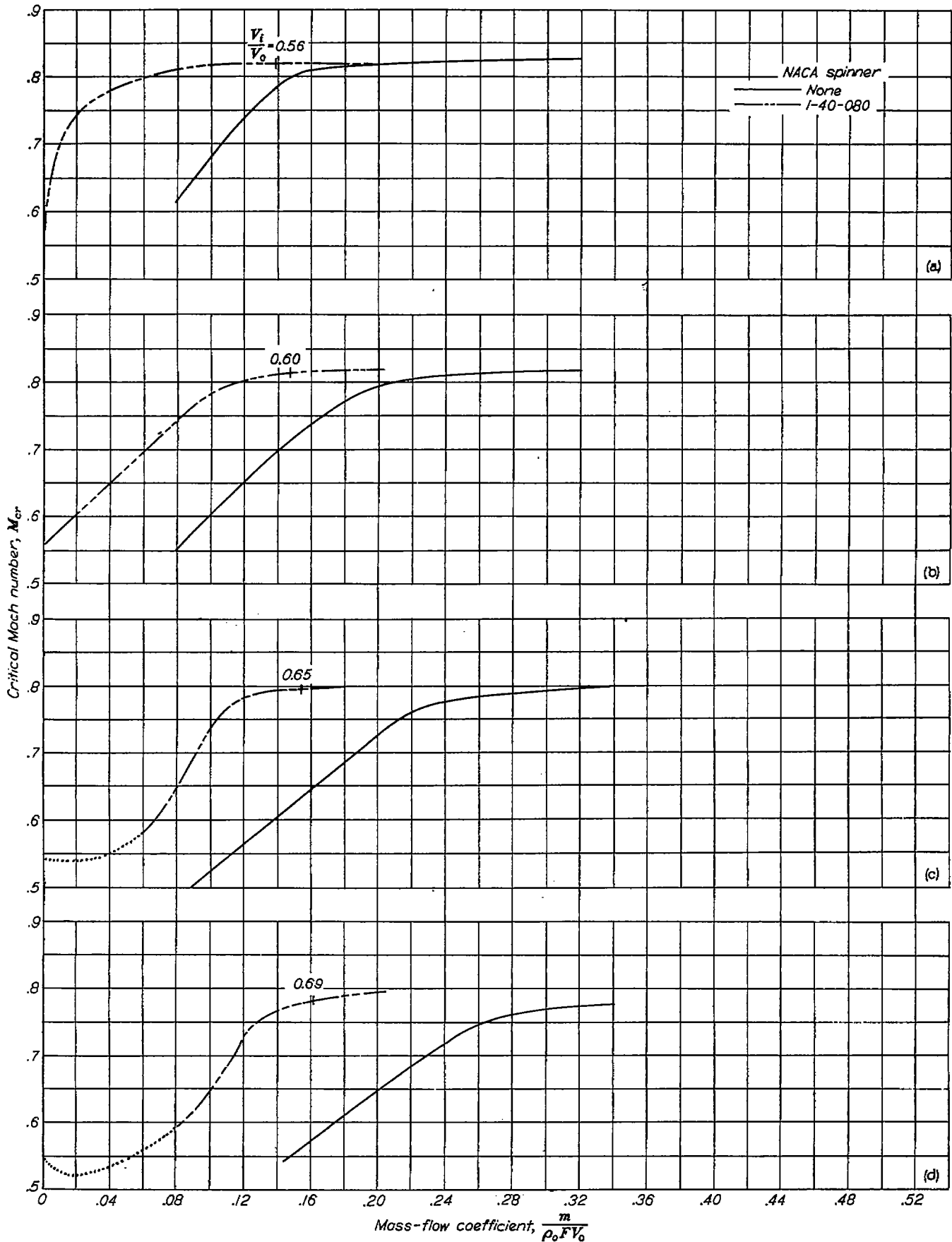
FIGURE 58.—Predicted critical Mach numbers for the NACA 1-60-100 cowling. (Ticks locate minimum design values of V_1/V_0 determined by separation from spinners.) Propeller removed; $\frac{X_c}{D} = 0.40$.



- (a) $\alpha = 0^\circ$.
- (b) $\alpha = 2^\circ$.
- (c) $\alpha = 4^\circ$.
- (d) $\alpha = 6^\circ$.

FIGURE 59.—Predicted critical Mach numbers for the NACA 1-60-100 cowl. (Ticks locate minimum design values of V_i/V_0 determined by separation from spinners.)

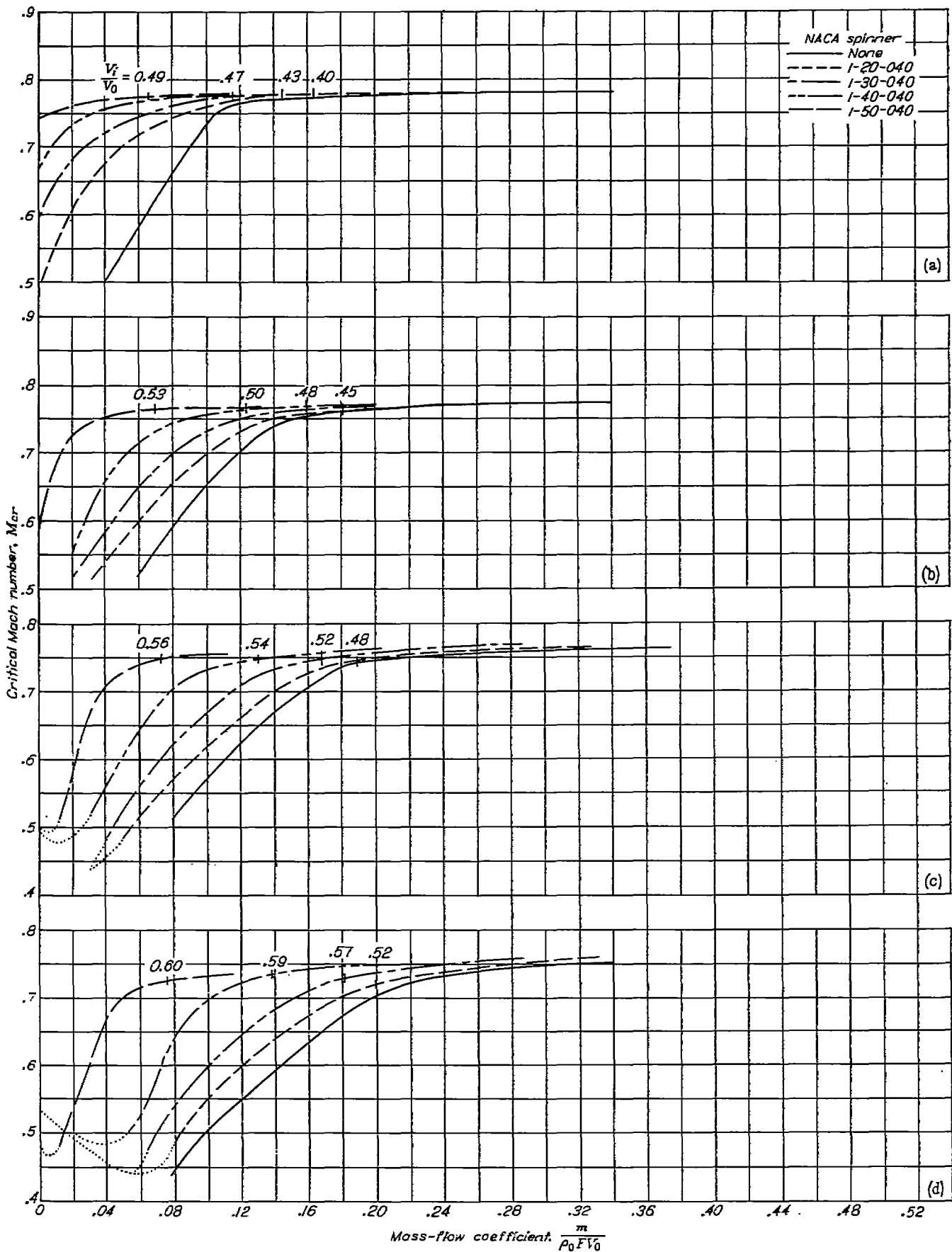
Propeller removed; $\frac{X_i}{D_s} = 0.80$.



- (a) $\alpha = 0^\circ$.
- (b) $\alpha = 2^\circ$.
- (c) $\alpha = 4^\circ$.
- (d) $\alpha = 6^\circ$.

FIGURE 60.—Predicted critical Mach numbers for the NACA 1-60-100 cowling. (Ticks locate minimum design values of V_f/V_0 determined by separation from spinners.)

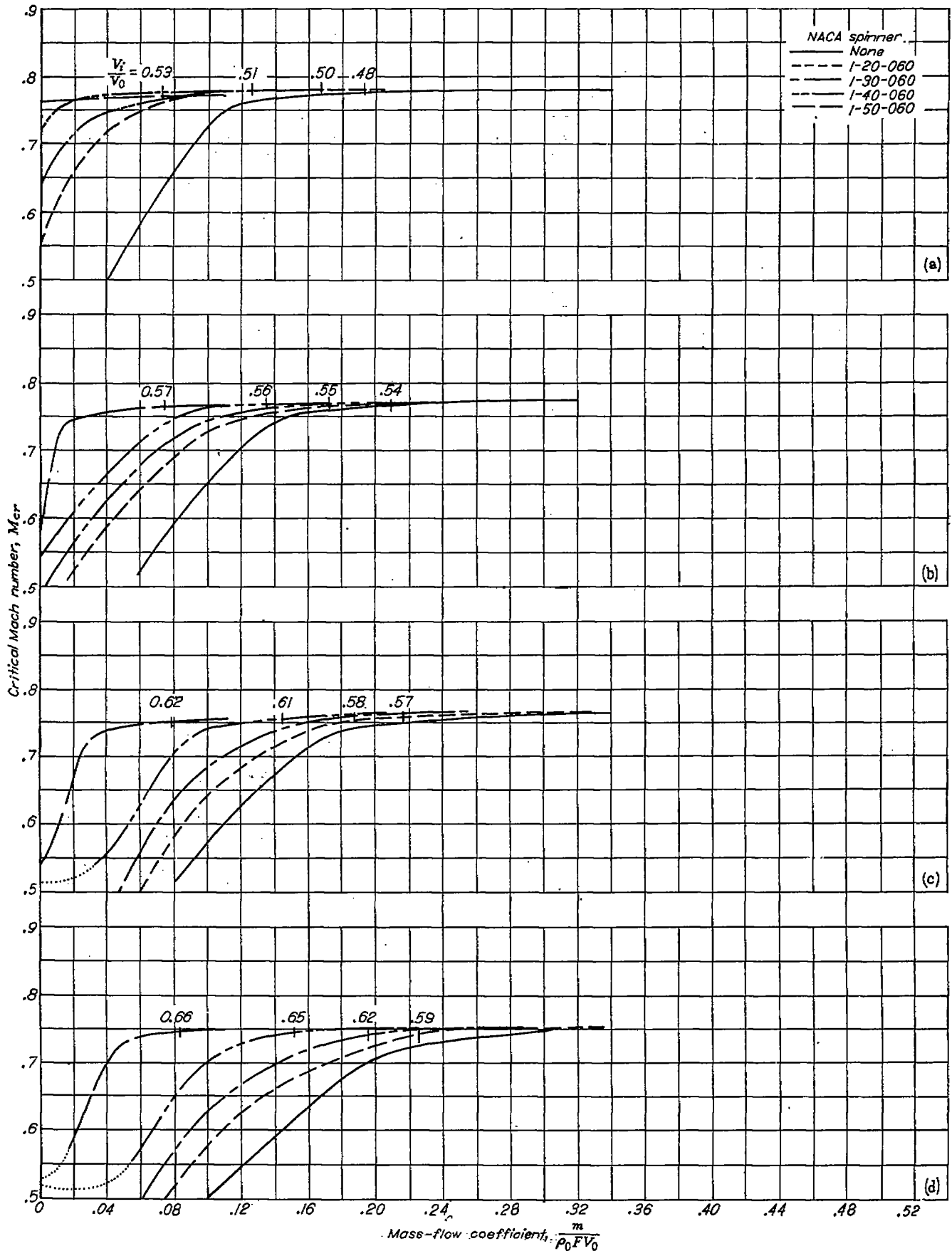
Propeller removed; $\frac{X_s}{D_s} = 0.90$.



- (a) $\alpha = 0^\circ$.
- (b) $\alpha = 2^\circ$.
- (c) $\alpha = 4^\circ$.
- (d) $\alpha = 6^\circ$.

FIGURE 61.—Predicted critical Mach numbers for the NACA 1-60-075 cowling. (Ticks locate minimum design values of V_c/V_0 determined by separation from spinners.)

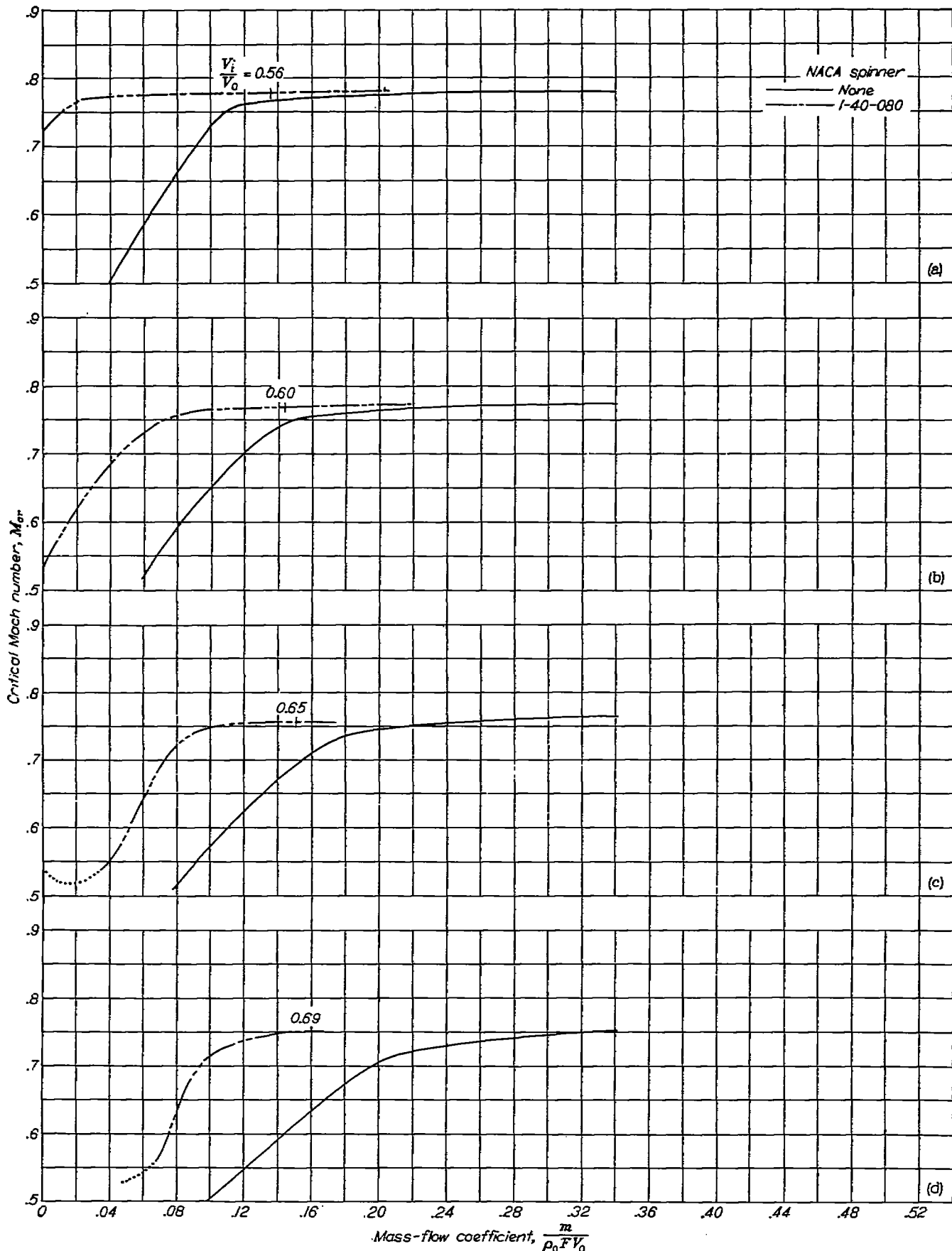
Propeller removed; $\frac{X_1}{D} = 0.40$.



- (a) $\alpha = 0^\circ$.
- (b) $\alpha = 2^\circ$.
- (c) $\alpha = 4^\circ$.
- (d) $\alpha = 6^\circ$.

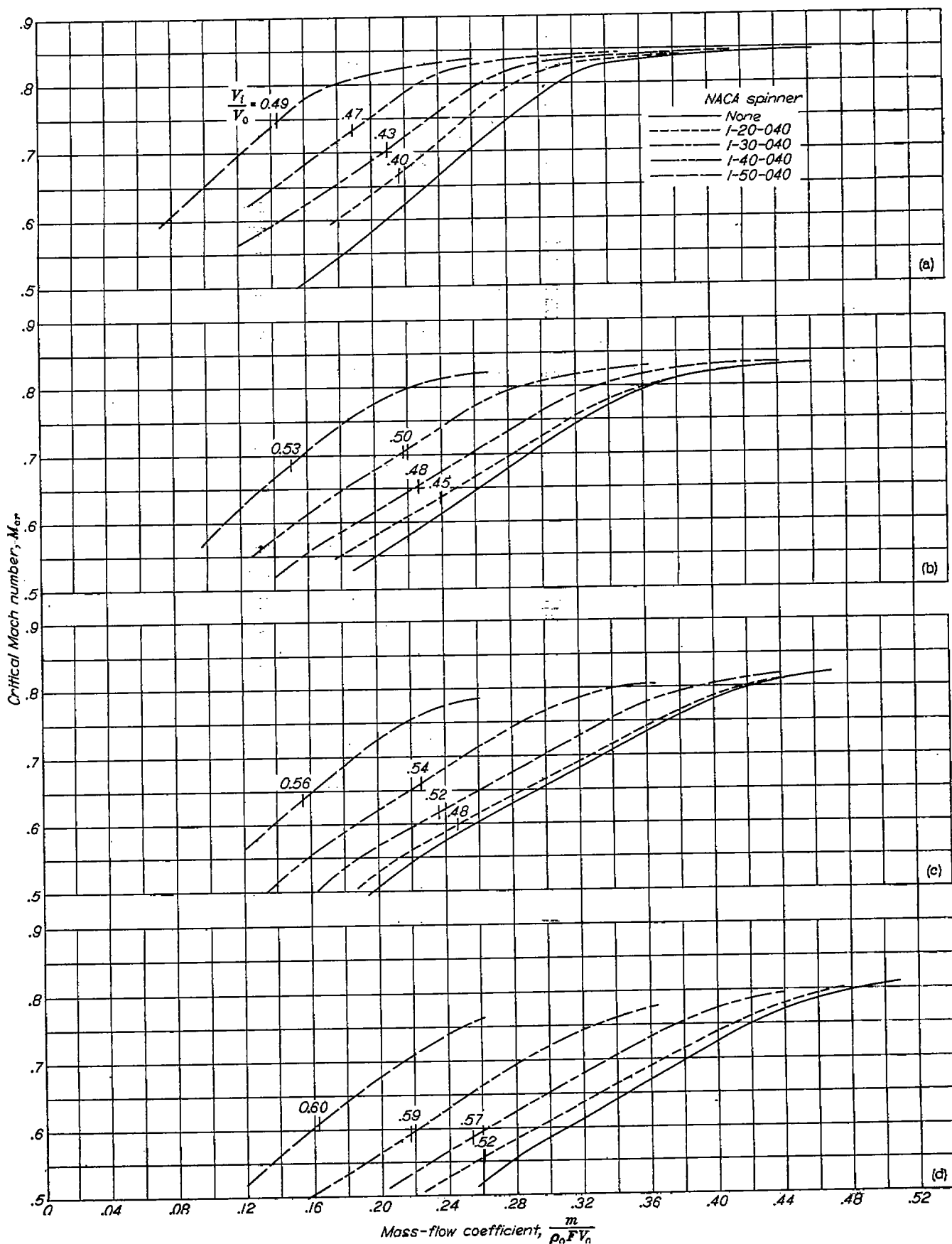
FIGURE 62.—Predicted critical Mach numbers for the NACA 1-60-075 cowling. (Ticks locate minimum design values of V_i/V_0 determined by separation from spinners.)

Propeller removed; $\frac{X_c}{D_c} = 0.60$.



- (a) $\alpha = 0^\circ$.
- (b) $\alpha = 2^\circ$.
- (c) $\alpha = 4^\circ$.
- (d) $\alpha = 6^\circ$.

FIGURE 63.—Predicted critical Mach numbers for the NACA 1-80-076 cowling. (Ticks locate minimum design values of V_i/V_0 determined by separation from spinners.) Propeller removed; $\frac{X_c}{D_c} = 0.80$.



- (a) $\alpha = 0^\circ$.
- (b) $\alpha = 2^\circ$.
- (c) $\alpha = 4^\circ$.
- (d) $\alpha = 6^\circ$.

FIGURE 64.—Predicted critical Mach numbers for the NACA 1-70-100 cowling. (Ticks locate minimum design values of V_1/V_0 determined by separation from spinners.)

Propeller removed; $\frac{X_2}{D} = 3.40$.

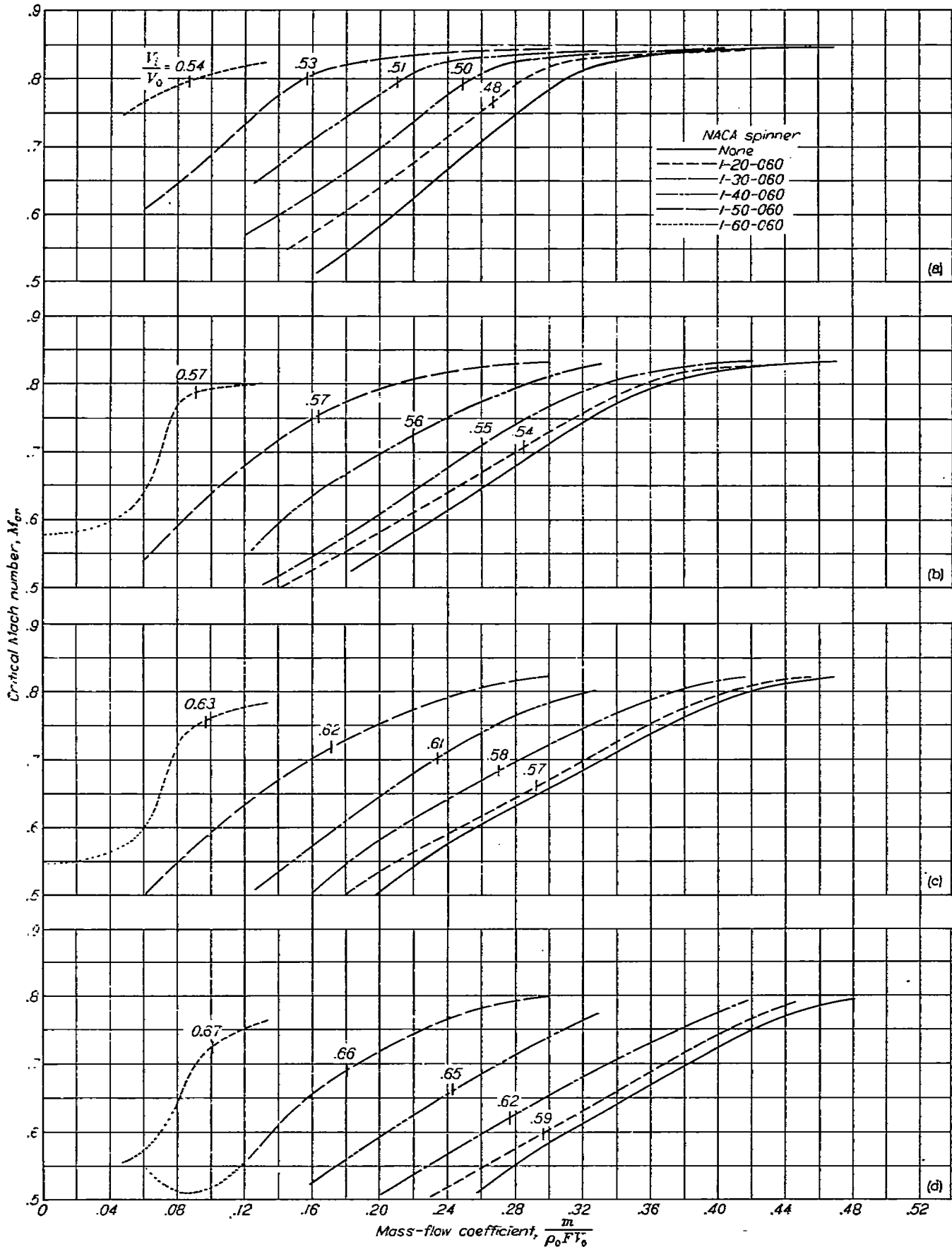
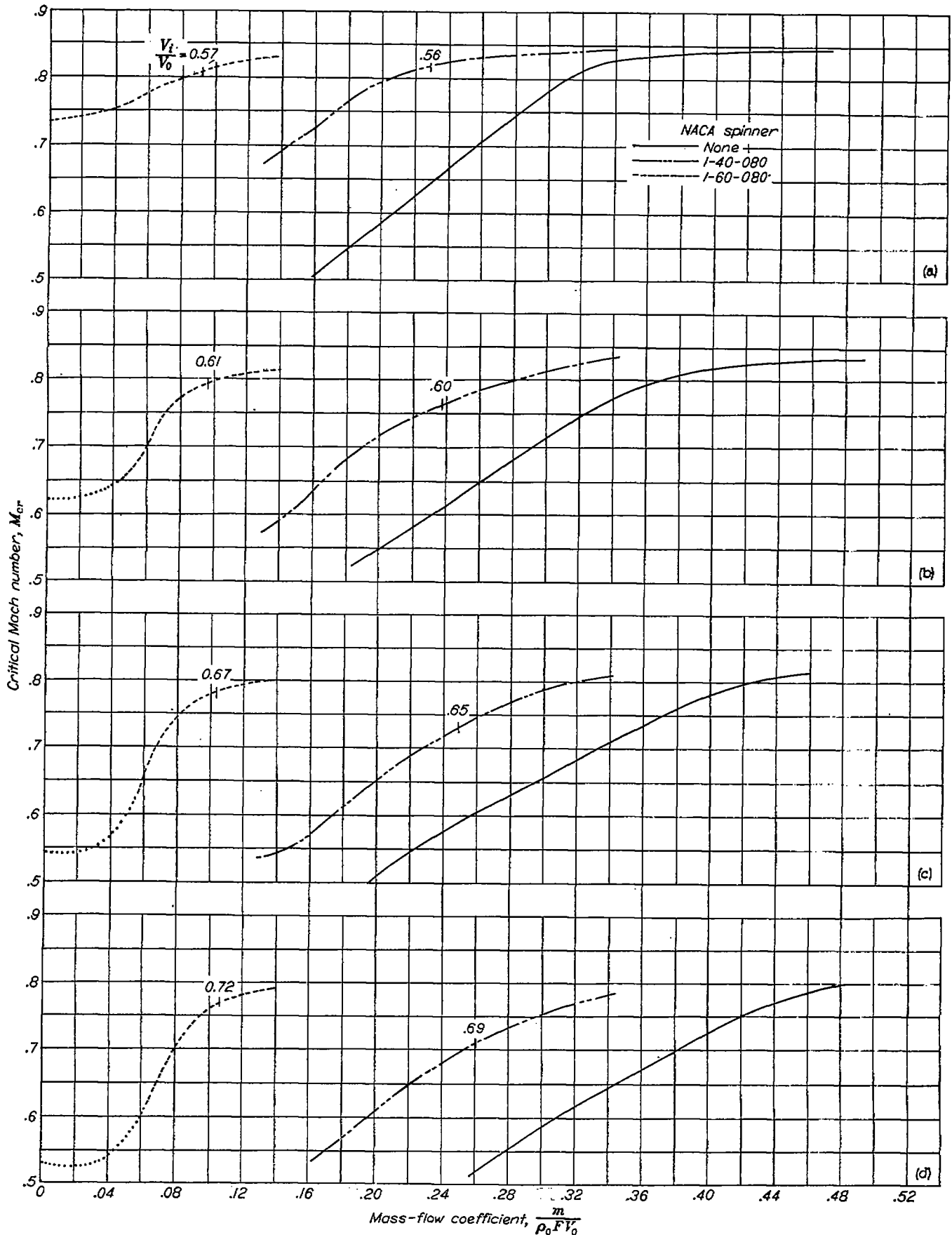


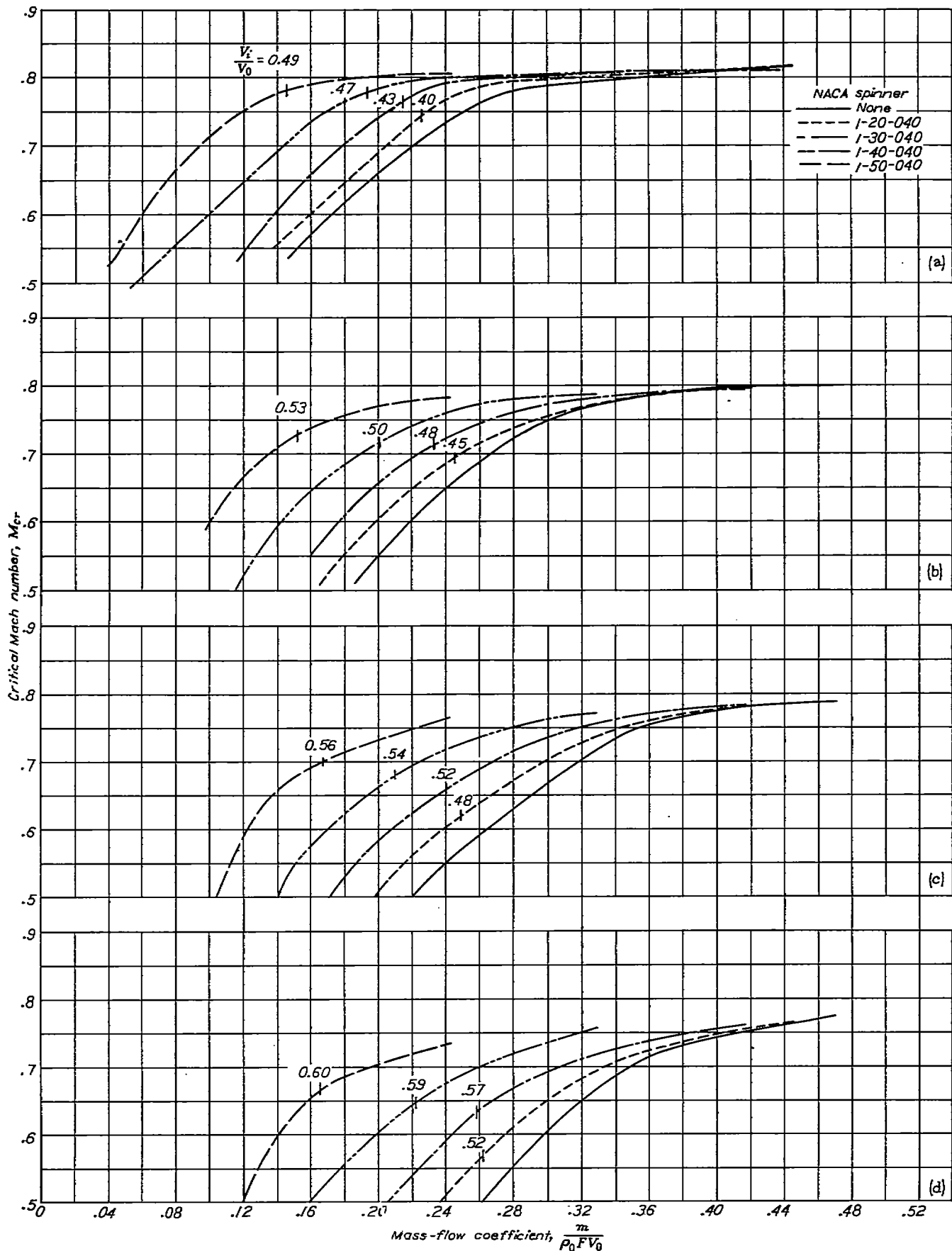
FIGURE 65.—Predicted critical Mach numbers for the NACA 1-70-100 cowling. (Ticks locate minimum design values of V_1/V_0 determined by separation from spinners.)
 Propeller removed; $\frac{X_1}{D} = 0.60$.



- (a) $\alpha = 0^\circ$.
- (b) $\alpha = 2^\circ$.
- (c) $\alpha = 4^\circ$.
- (d) $\alpha = 6^\circ$.

FIGURE 66.—Predicted critical Mach numbers for the NACA 1-70-100 cowling. (Ticks locate minimum design values of V_i/V_0 determined by separation from spinners.)

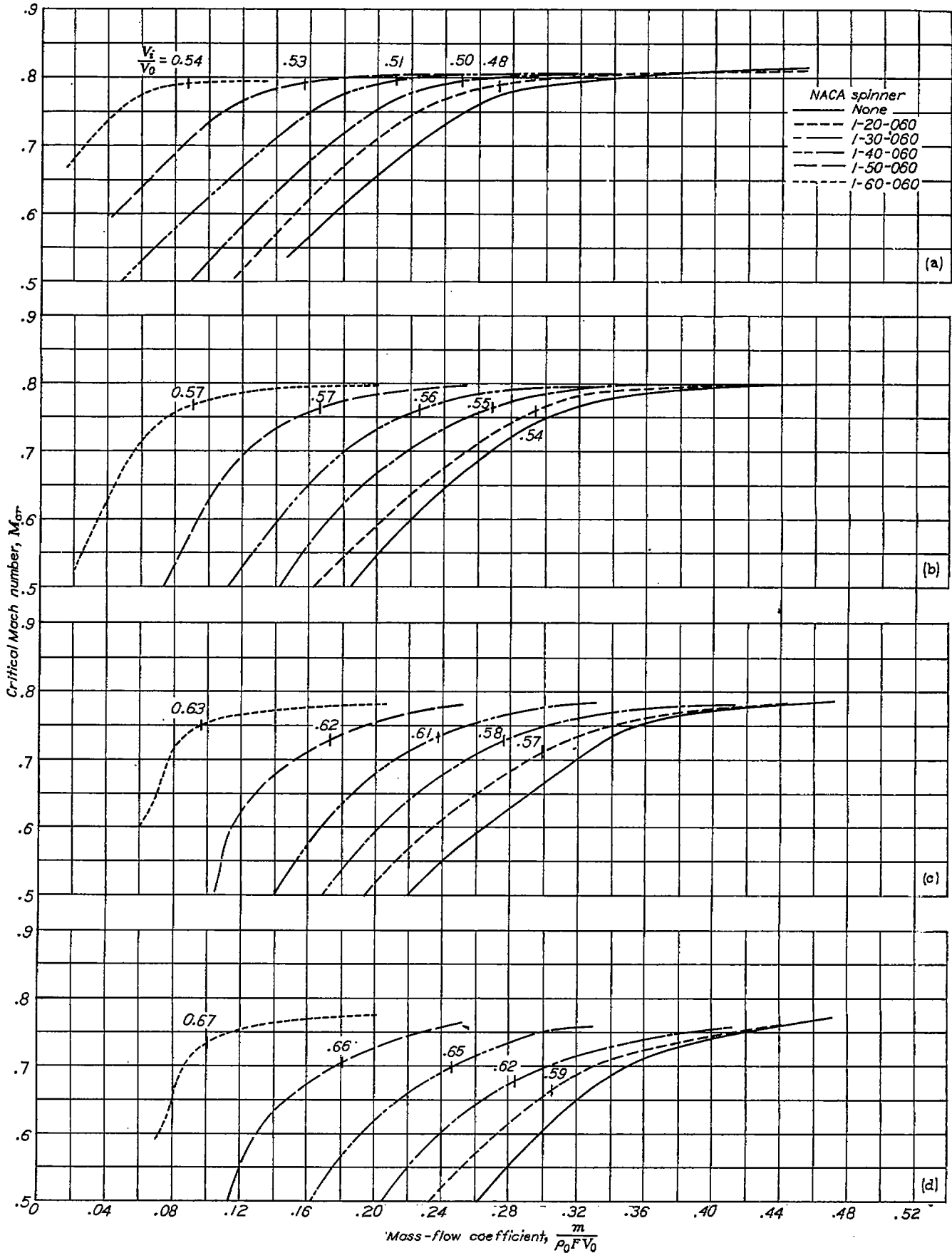
Propeller removed; $\frac{X_1}{D_c} = 0.80$.



- (a) $\alpha = 0^\circ$.
- (b) $\alpha = 2^\circ$.
- (c) $\alpha = 4^\circ$.
- (d) $\alpha = 6^\circ$.

FIGURE 67.—Predicted critical Mach numbers for the NACA 1-70-075 cowling. (Ticks locate minimum design values of V_i/V_0 determined by separation from spinners.)

Propeller removed; $\frac{X_c}{D} = 0.40$



- (a) $\alpha = 0^\circ$.
- (b) $\alpha = 2^\circ$.
- (c) $\alpha = 4^\circ$.
- (d) $\alpha = 6^\circ$.

FIGURE 68.—Predicted critical Mach numbers for the NACA 1-70-075 cowling. (Ticks locate minimum design values of V_i/V_0 determined by separation from spinners.)

Propeller removed; $\frac{X_2}{n} = 0.60$.

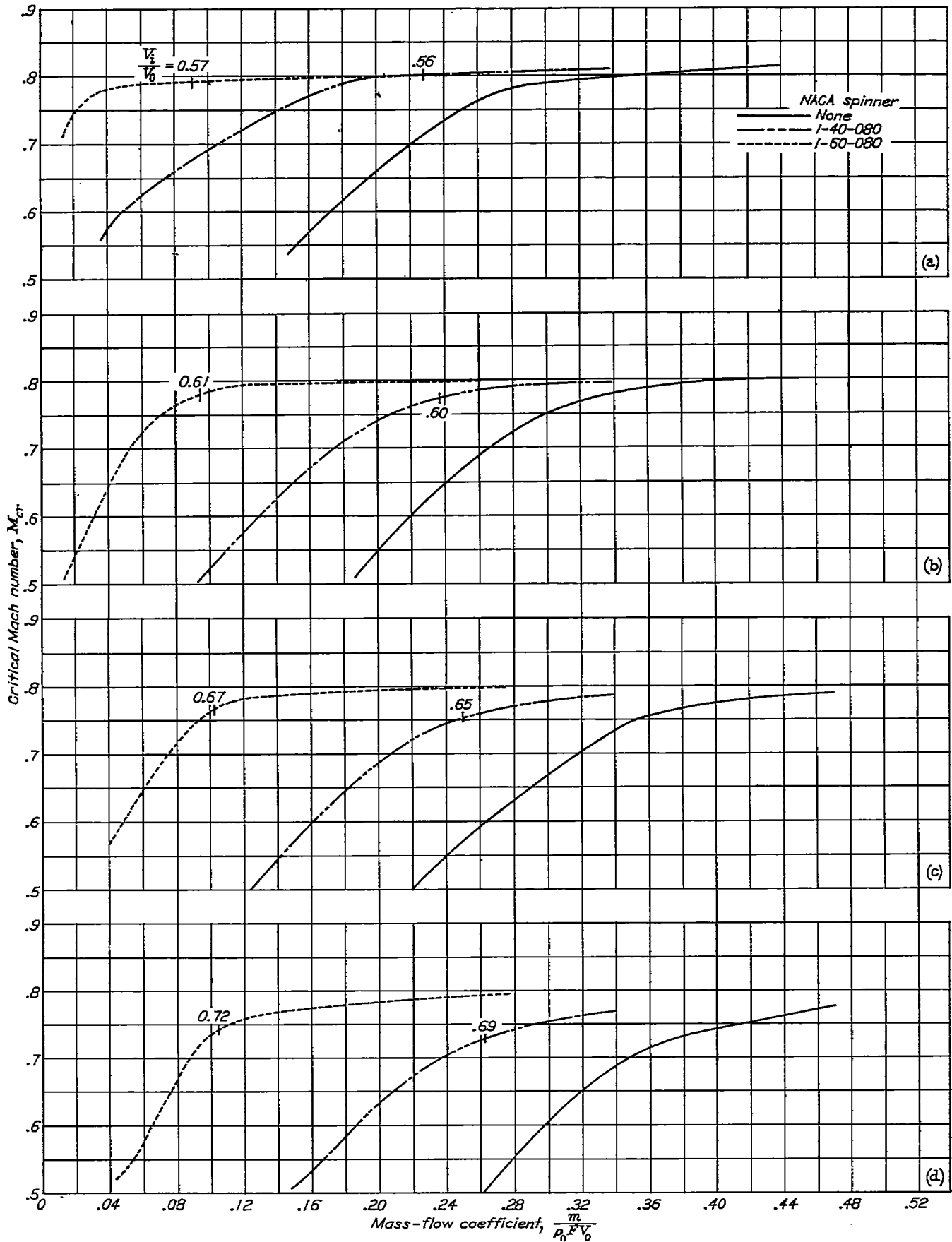


FIGURE 69.—Predicted critical Mach numbers for the NACA 1-70-075 cowlings. (Ticks locate minimum design values of V_2/V_0 determined by separation from spinners.)
 Propeller removed; $\frac{X_1}{D_c} = 0.90$.

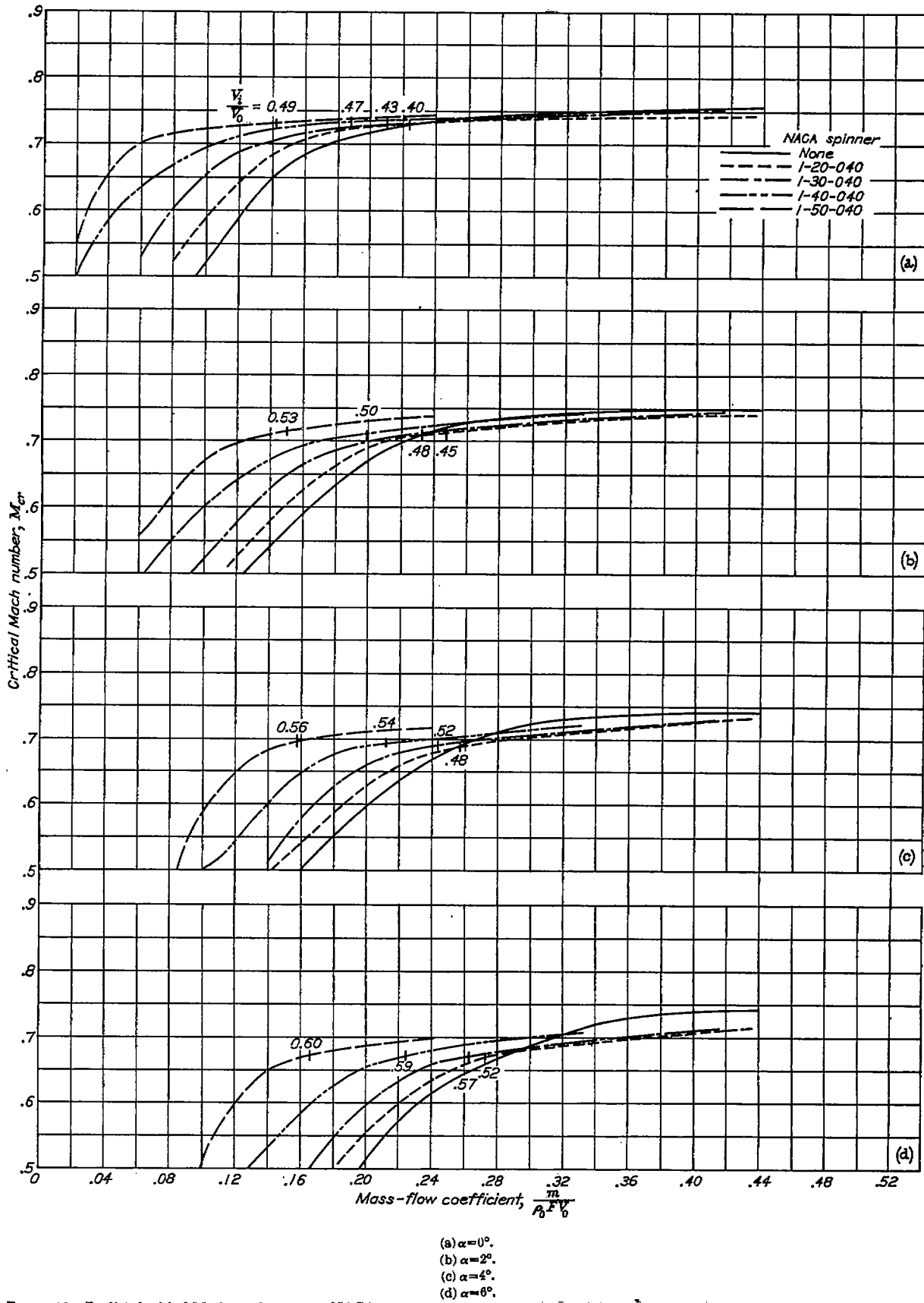
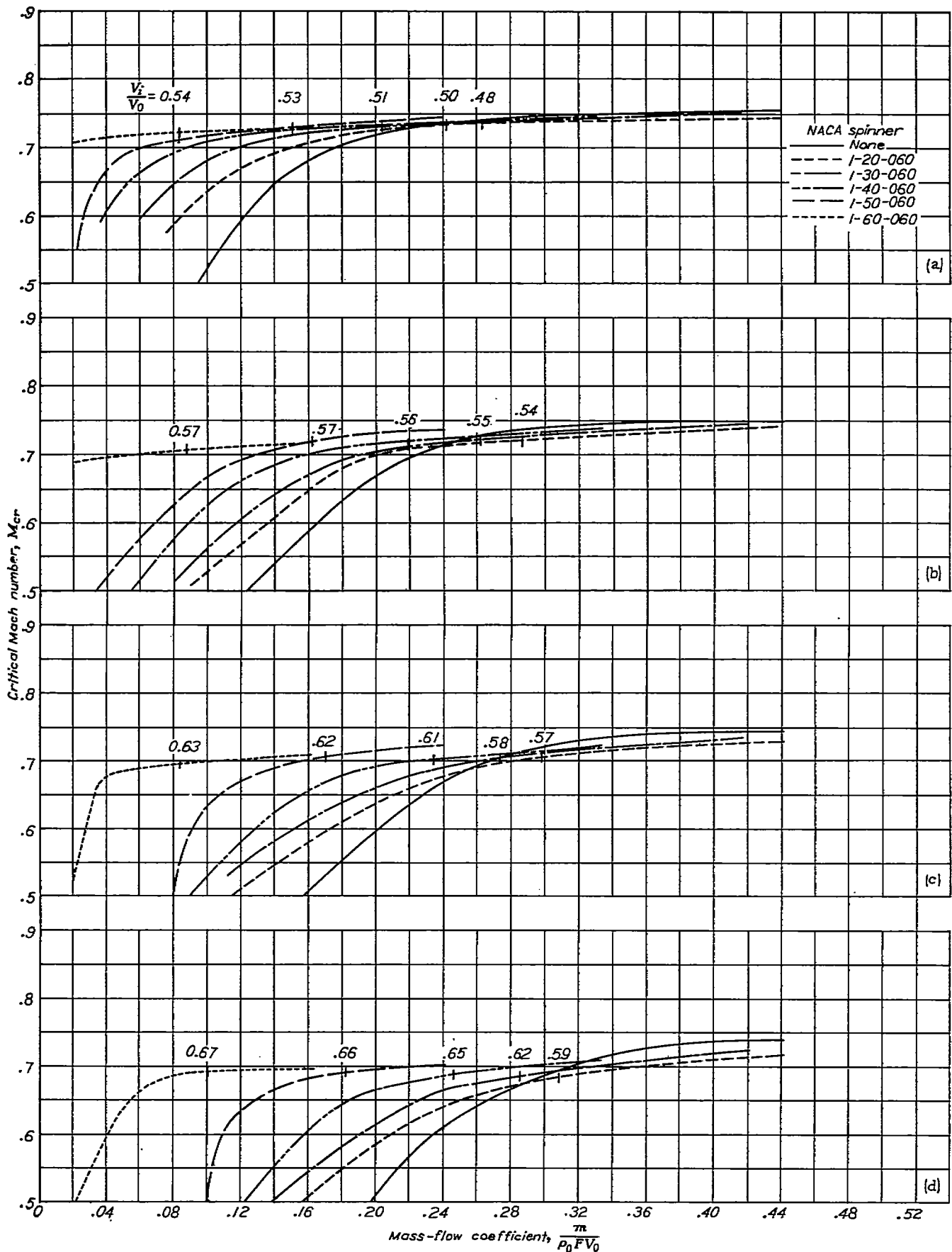


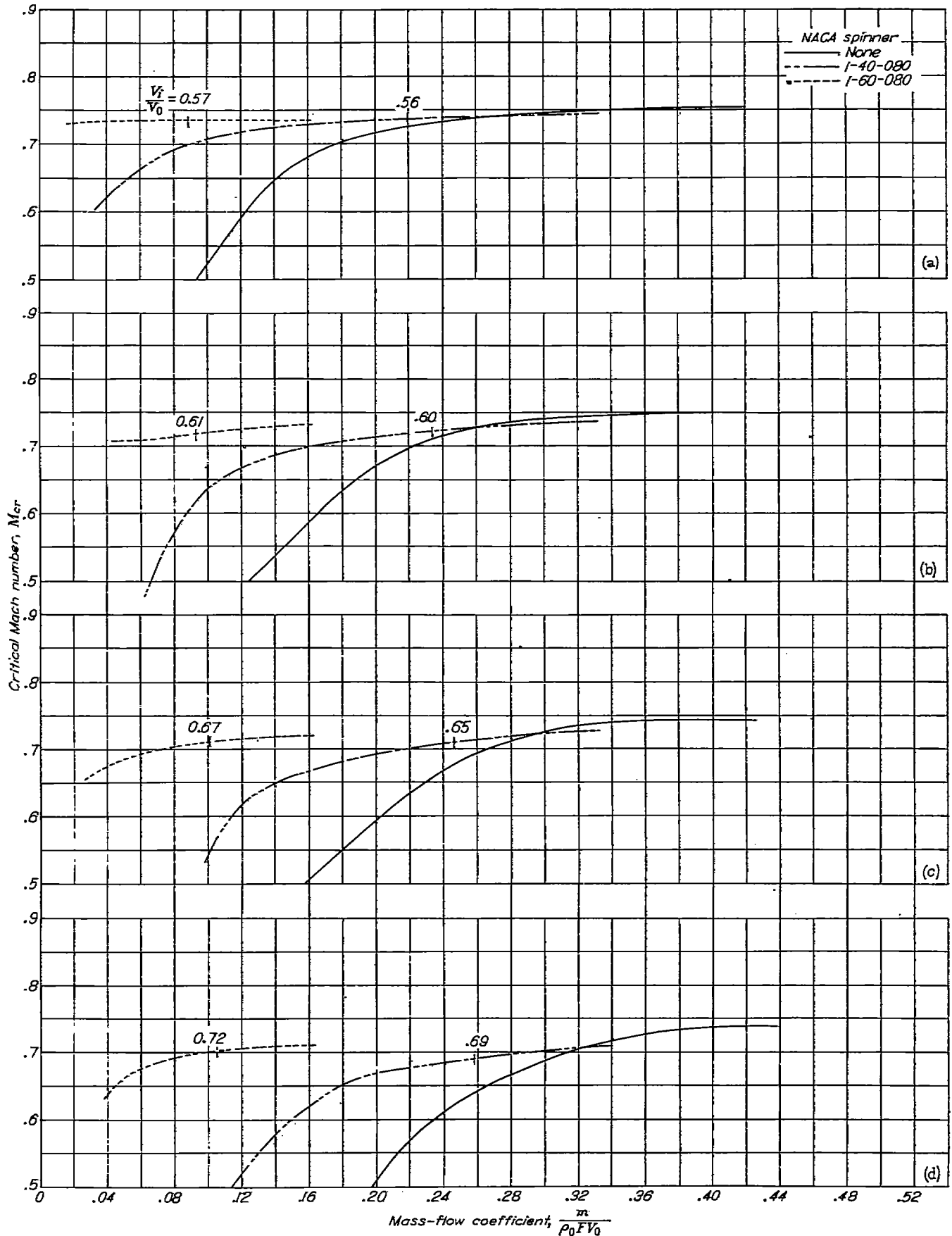
FIGURE 70.—Predicted critical Mach numbers for the NACA 1-70-050 cowling. (Ticks locate minimum design values of V_1/V_0 determined by separation from spinners.) Propeller removed; $\frac{X_c}{D_c} = 0.40$.



- (a) $\alpha = 0^\circ$.
- (b) $\alpha = 2^\circ$.
- (c) $\alpha = 4^\circ$.
- (d) $\alpha = 6^\circ$.

FIGURE 71.—Predicted critical Mach numbers for the NACA 1-70-050 cowling. (Ticks locate minimum design values of V_2/V_0 determined by separation from spinners.)

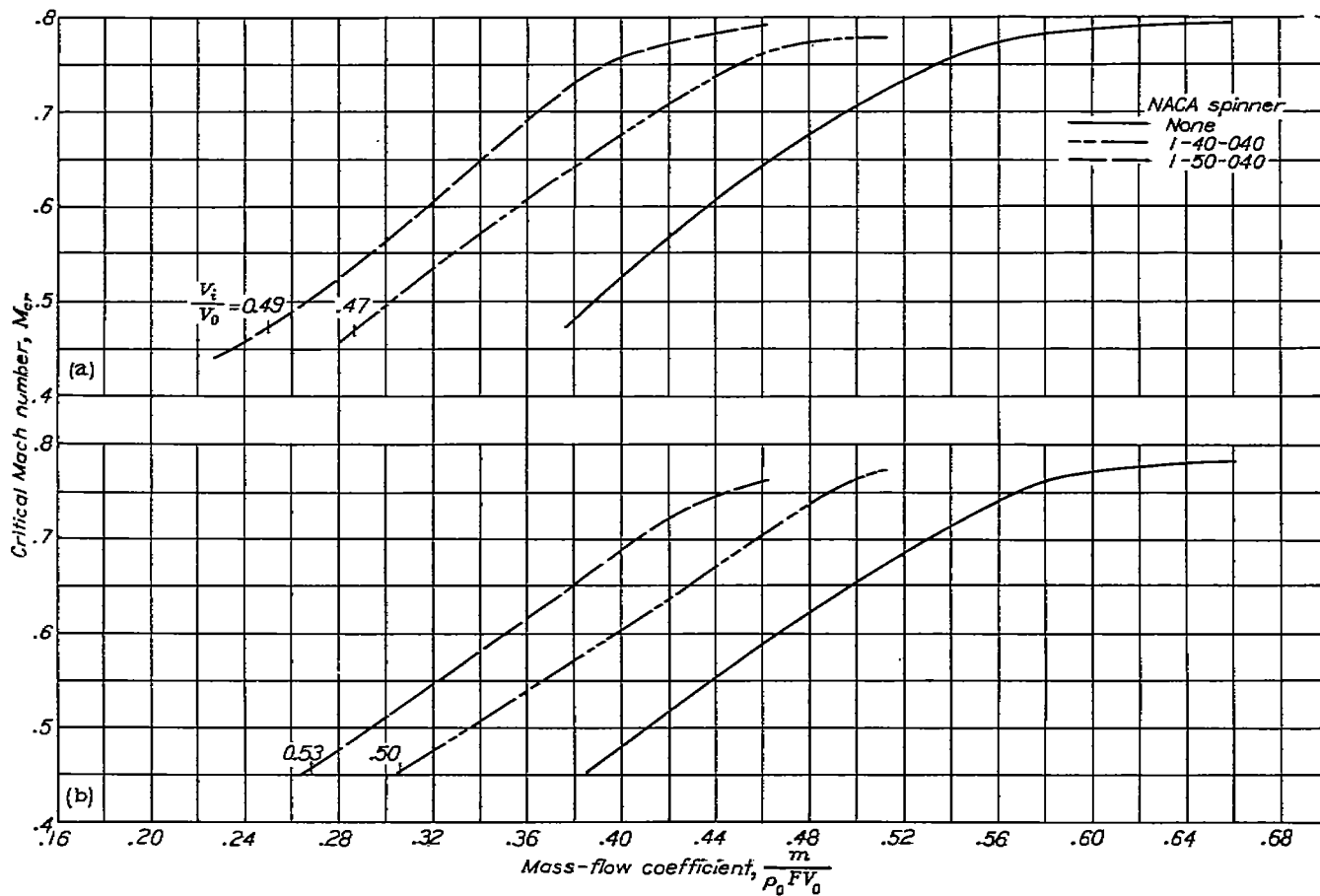
Propeller removed; $\frac{X_2}{D} = 0.60$.



- (a) $\alpha=0^\circ$.
- (b) $\alpha=2^\circ$.
- (c) $\alpha=4^\circ$.
- (d) $\alpha=6^\circ$.

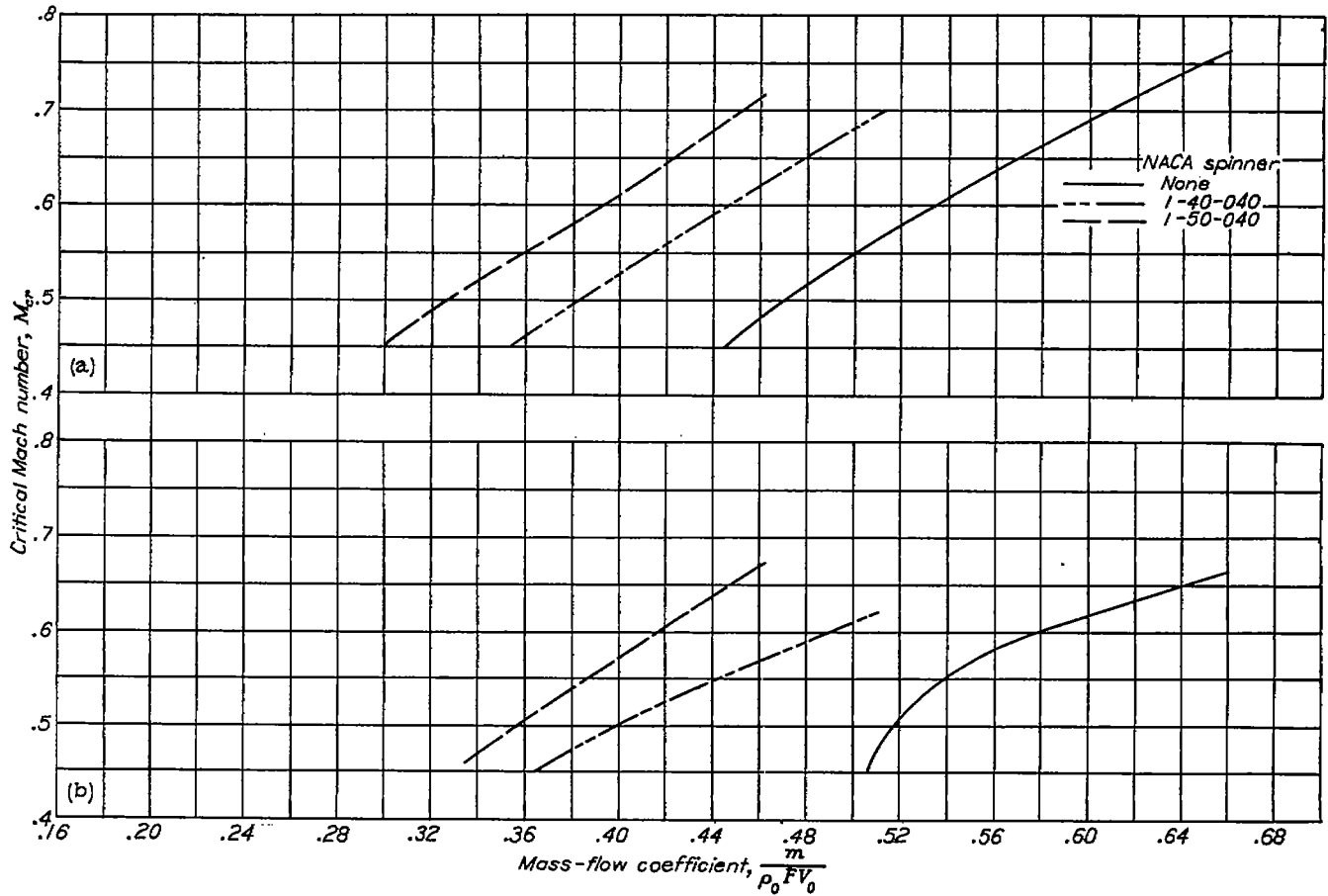
FIGURE 72.—Predicted critical Mach numbers for the NACA 1-70-050 cowling. (Ticks locate minimum design values of V_i/V_0 determined by separation from spinners.)

Propeller removed; $\frac{X_r}{D} = 0.80$.



(a) $\alpha = 0^\circ$.
 (b) $\alpha = 2^\circ$.

FIGURE 73.—Predicted critical Mach numbers for the NACA 1-65-050 cowl. (Ticks locate minimum design values of V_0/V_c determined by separation from spinners.)
 Propeller removed; $\frac{X_c}{D_c} = 0.40$.

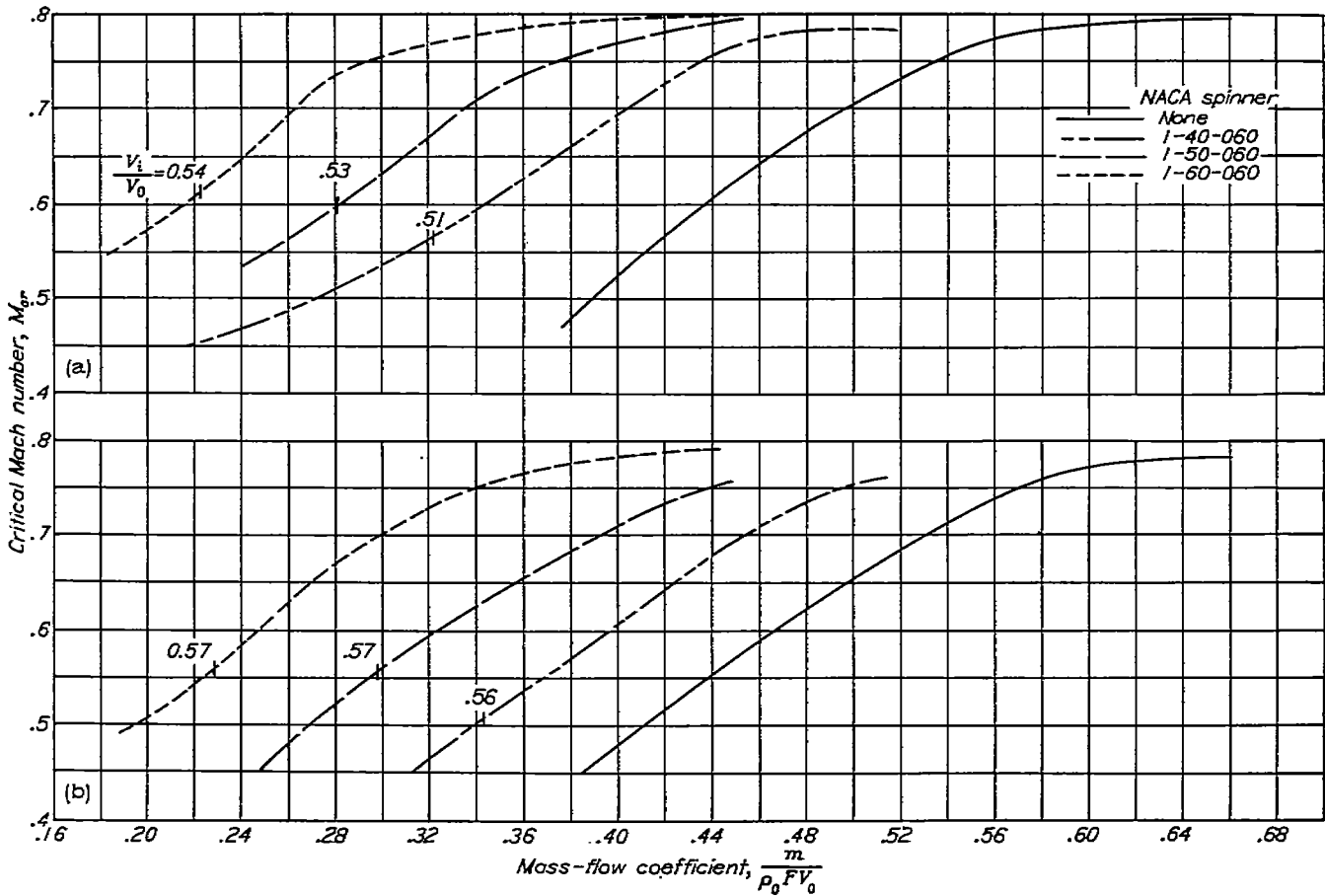


(a) $\alpha = 4^\circ$.

(b) $\alpha = 8^\circ$.

FIGURE 74.—Predicted critical Mach numbers for the NACA 1-85-050 cowling. (Ticks locate minimum design values of V_i/V_0 determined by separation from spinners.)

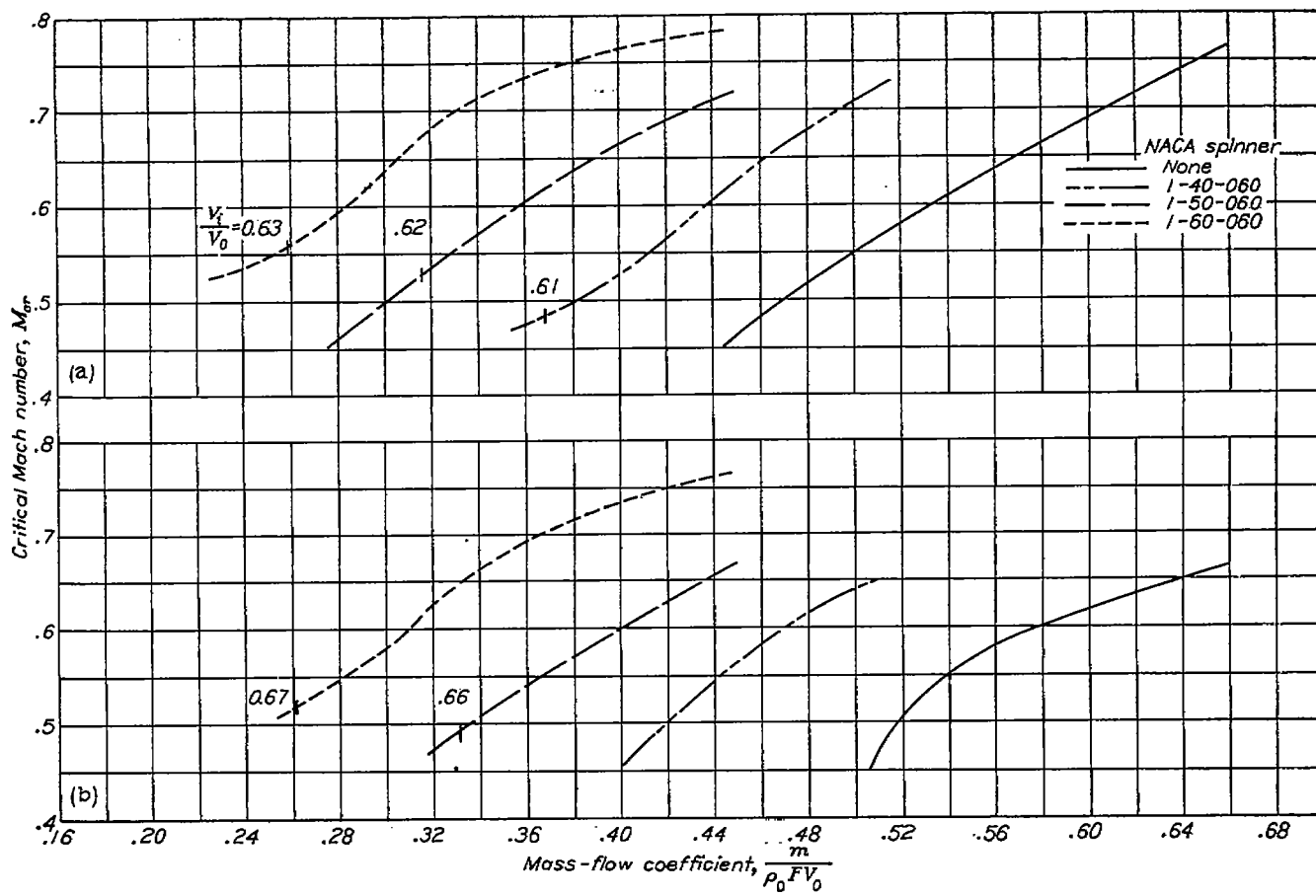
Propeller removed; $\frac{X_s}{D_s} = 0.40$.



(a) $\alpha = 0^\circ$.
 (b) $\alpha = 2^\circ$.

FIGURE 75.—Predicted critical Mach numbers for the NACA 1-85-050 cowling. (Ticks locate minimum design values of V_i/V_0 determined by separation from spinners.)

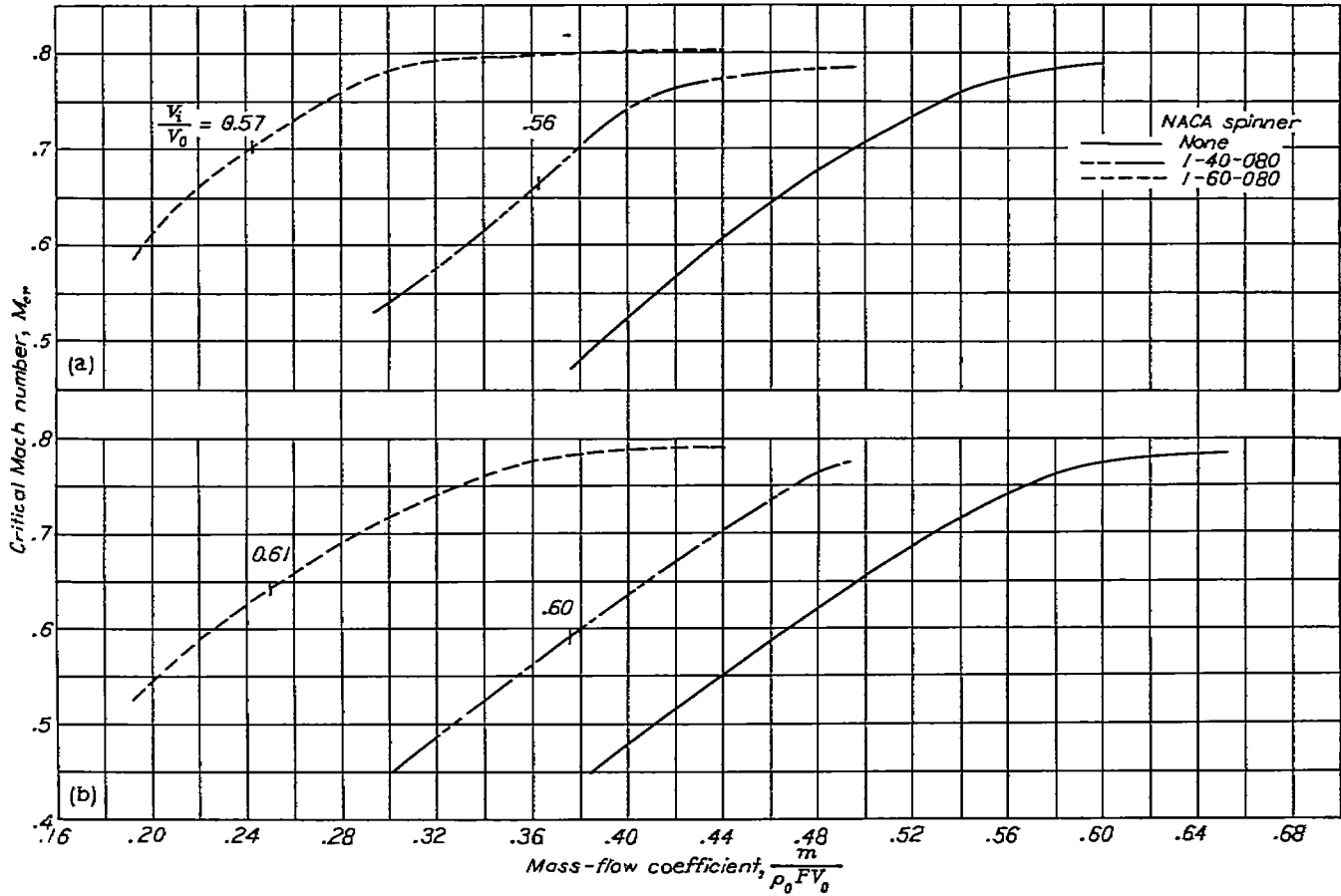
Propeller removed; $\frac{X_2}{D_0} = 0.60$.



(a) $\alpha = 4^\circ$.
 (b) $\alpha = 6^\circ$.

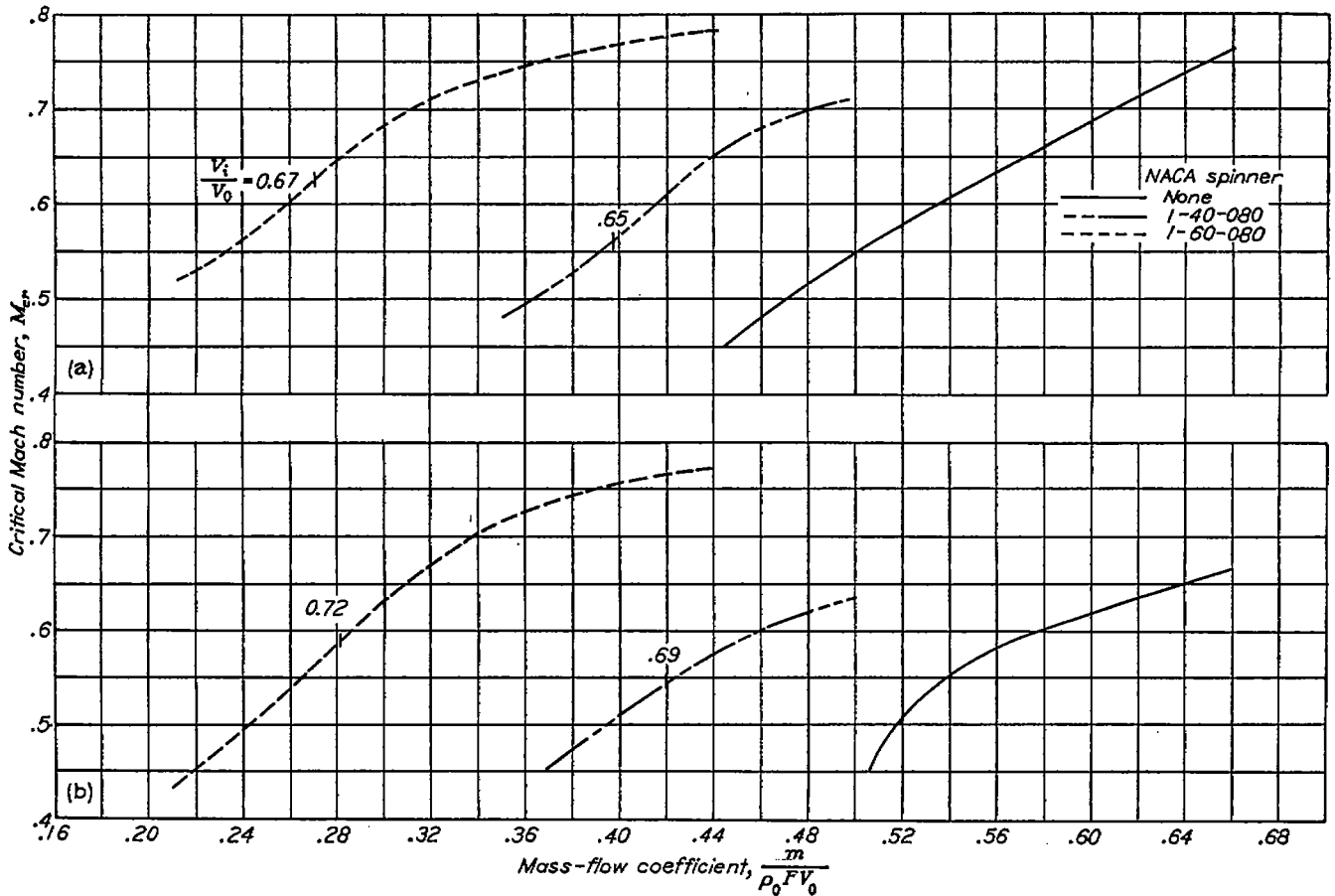
FIGURE 76.—Predicted critical Mach numbers for the NACA 1-85-050 cowling. (Ticks locate minimum design values of V_1/V_0 , determined by separation from spinners.)

Propeller removed; $\frac{X_1}{D_0} = 0.60$.



(a) $\alpha = 0^\circ$.
 (b) $\alpha = 2^\circ$.

FIGURE 7.—Predicted critical Mach numbers for the NACA 1-85-050 cowling. (Ticks locate minimum design values of V_2/V_0 , determined by separation from spinners.)
 Propeller removed; $\frac{X_s}{D_s} = 0.80$.

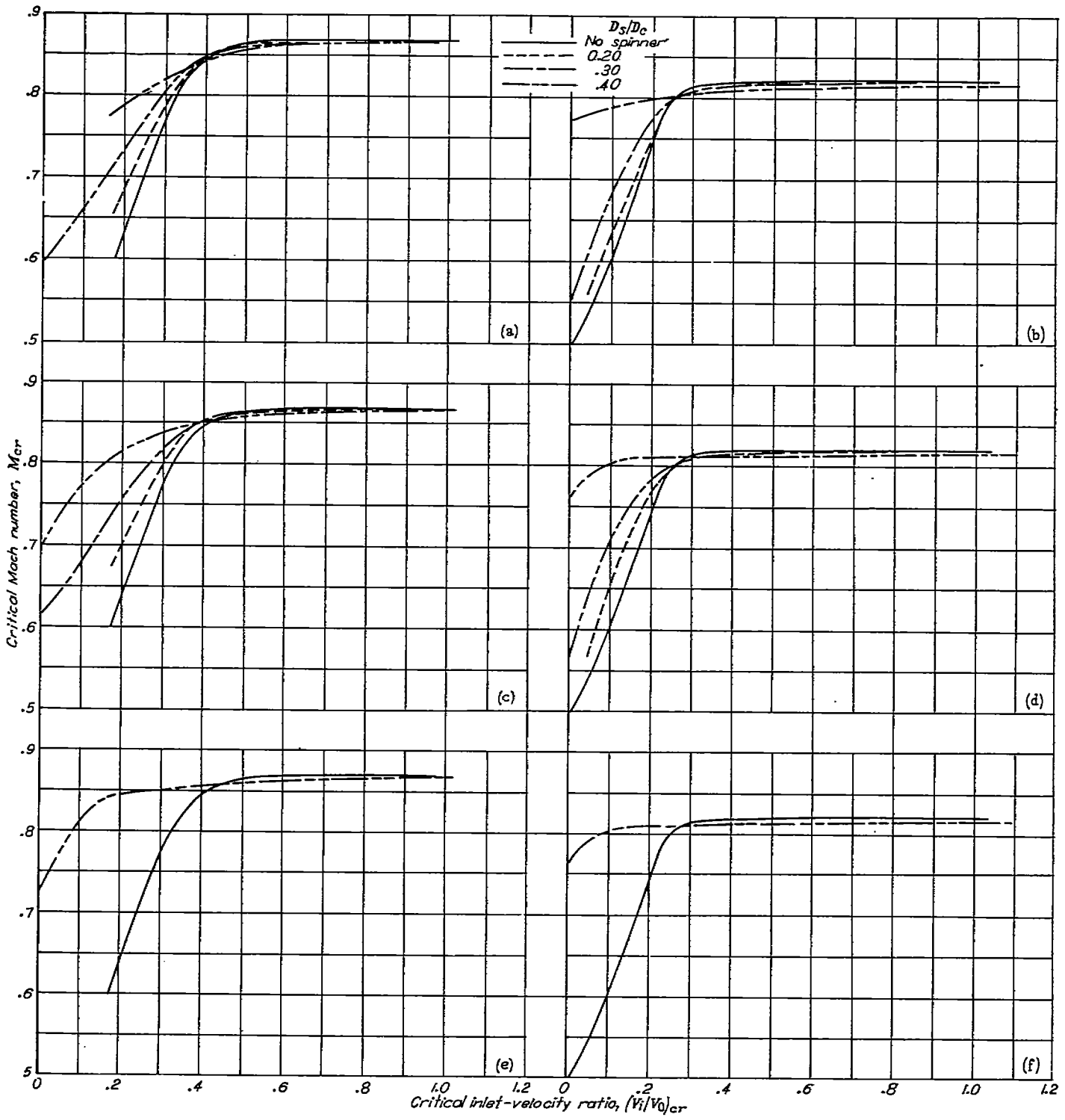


(a) $\alpha = 4^\circ$.

(b) $\alpha = 8^\circ$.

FIGURE 78.—Predicted critical Mach numbers for the NACA 1-85-050 cowling. (Ticks locate minimum design values of V_i/V_0 determined by separation from spinners.)

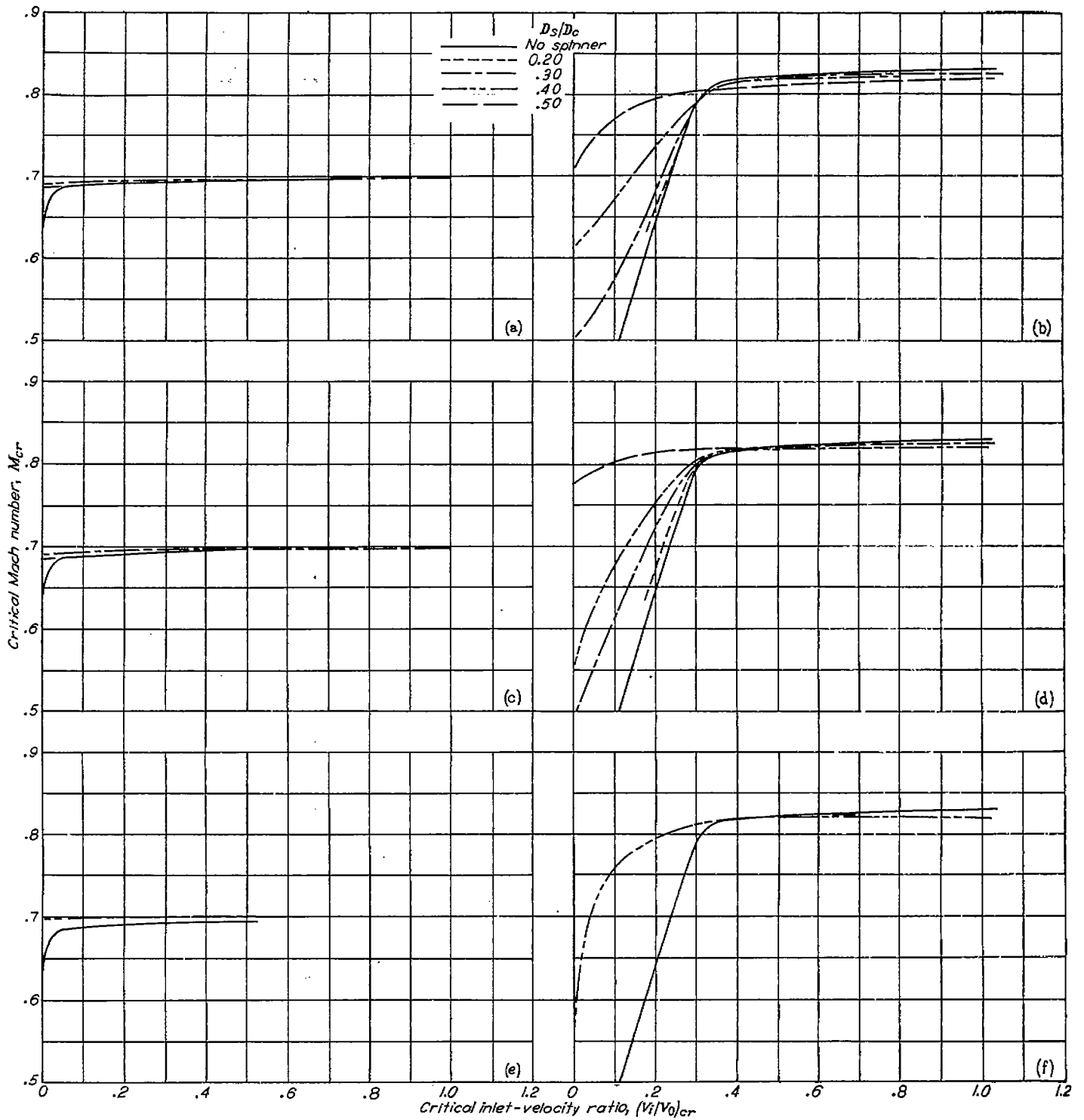
Propeller removed; $\frac{X_r}{D_s} = 0.80$.



- (a) NACA 1-55-150 cowling; $\frac{X_s}{D_c} = 0.40$.
- (c) NACA 1-55-150 cowling; $\frac{X_s}{D_c} = 0.60$.
- (e) NACA 1-55-150 cowling; $\frac{X_s}{D_c} = 0.80$.

- (b) NACA 1-55-100 cowling; $\frac{X_s}{D_c} = 0.40$.
- (d) NACA 1-55-100 cowling; $\frac{X_s}{D_c} = 0.60$.
- (f) NACA 1-55-100 cowling; $\frac{X_s}{D_c} = 0.80$.

FIGURE 79.—Predicted critical Mach numbers for the NACA 1-series cowlings and cowling-spinner combination as a function of inlet-velocity ratio. Propeller removed; $\alpha = 0^\circ$.



(a) NACA 1-55-050 cowling; $\frac{X_s}{D_c} = 0.40$.

(c) NACA 1-55-050 cowling; $\frac{X_s}{D_c} = 0.60$.

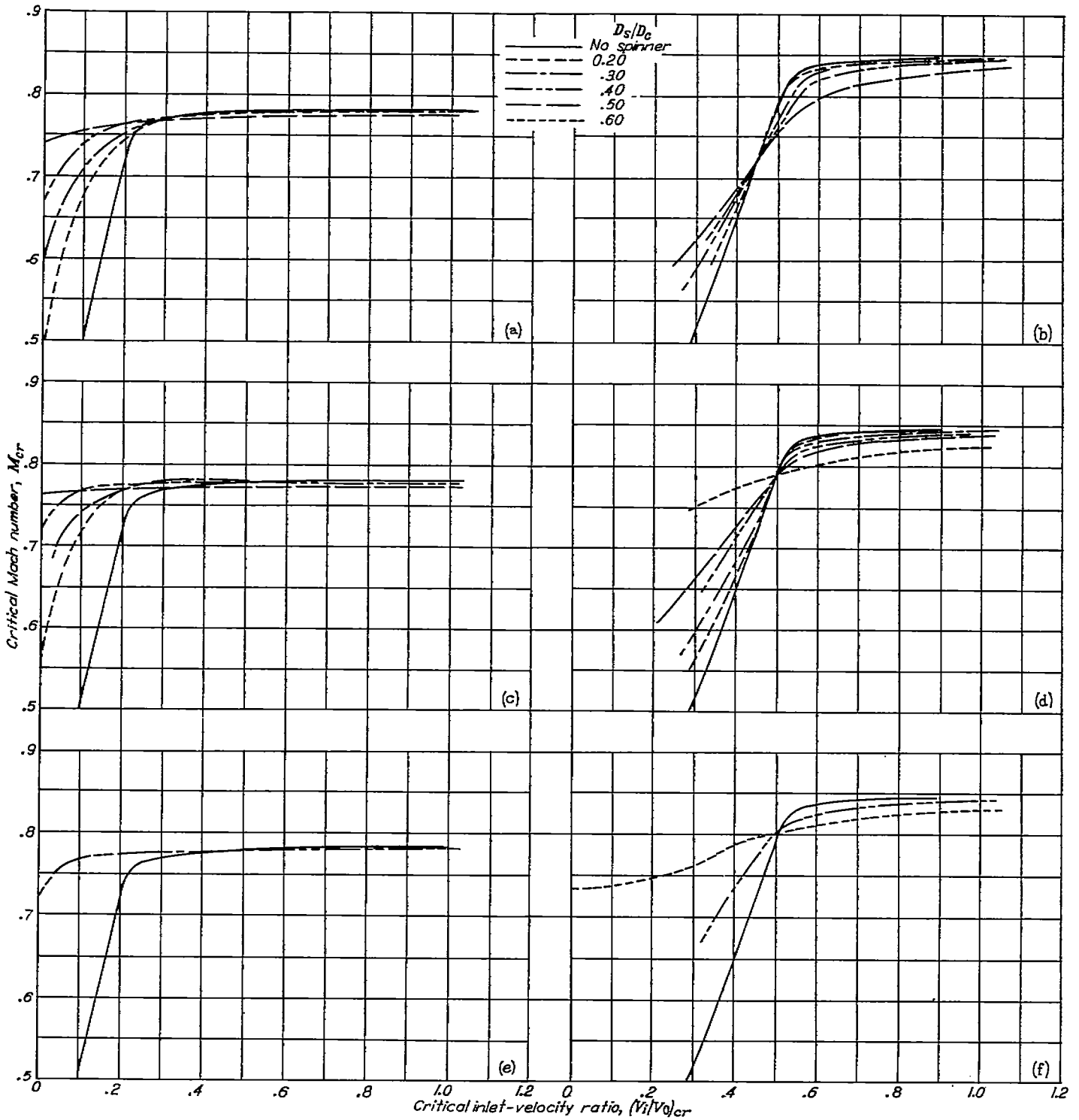
(e) NACA 1-55-050 cowling; $\frac{X_s}{D_c} = 0.80$.

(b) NACA 1-60-100 cowling; $\frac{X_s}{D_c} = 0.40$.

(d) NACA 1-60-100 cowling; $\frac{X_s}{D_c} = 0.60$.

(f) NACA 1-60-100 cowling; $\frac{X_s}{D_c} = 0.80$.

FIGURE 80.—Predicted critical Mach numbers for the NACA I-series cowlings and cowling-spinner combination as a function of inlet-velocity ratio. Propeller removed; $\alpha = 0^\circ$.



(a) NACA 1-60-075 cowling; $\frac{X_c}{D_c} = 0.40$.

(c) NACA 1-60-075 cowling; $\frac{X_c}{D_c} = 0.60$.

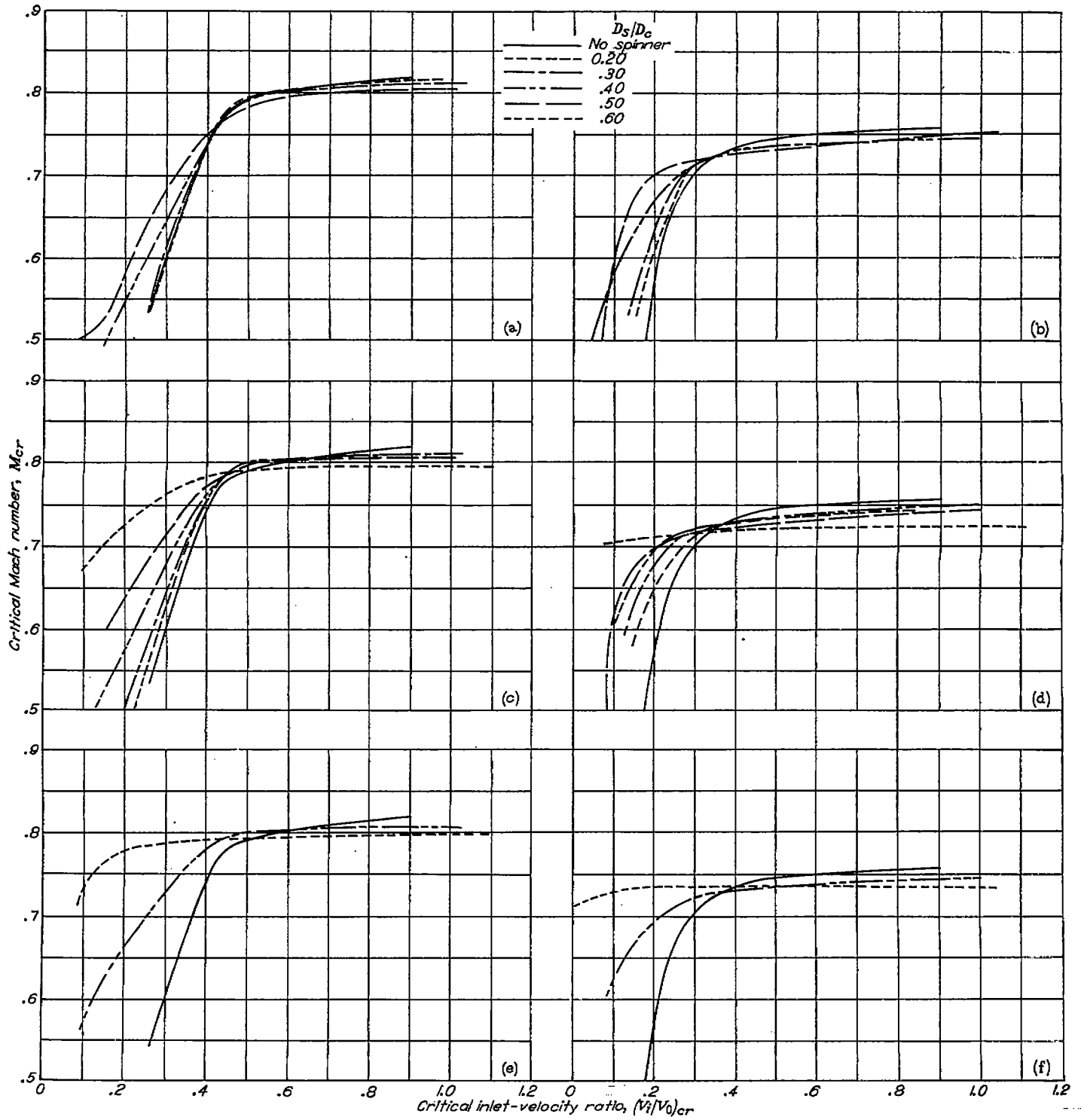
(e) NACA 1-60-075 cowling; $\frac{X_c}{D_c} = 0.80$.

(b) NACA 1-70-100 cowling; $\frac{X_c}{D_c} = 0.40$.

(d) NACA 1-70-100 cowling; $\frac{X_c}{D_c} = 0.60$.

(f) NACA 1-70-100 cowling; $\frac{X_c}{D_c} = 0.80$.

FIGURE 81.—Predicted critical Mach numbers for the NACA 1-series cowlings and cowling-spinner combination as a function of inlet-velocity ratio. Propeller removed; $\alpha = 0^\circ$



(a) NACA 1-70-075 cowling; $\frac{X_s}{D_c} = 0.40$.

(c) NACA 1-70-075 cowling; $\frac{X_s}{D_c} = 0.60$.

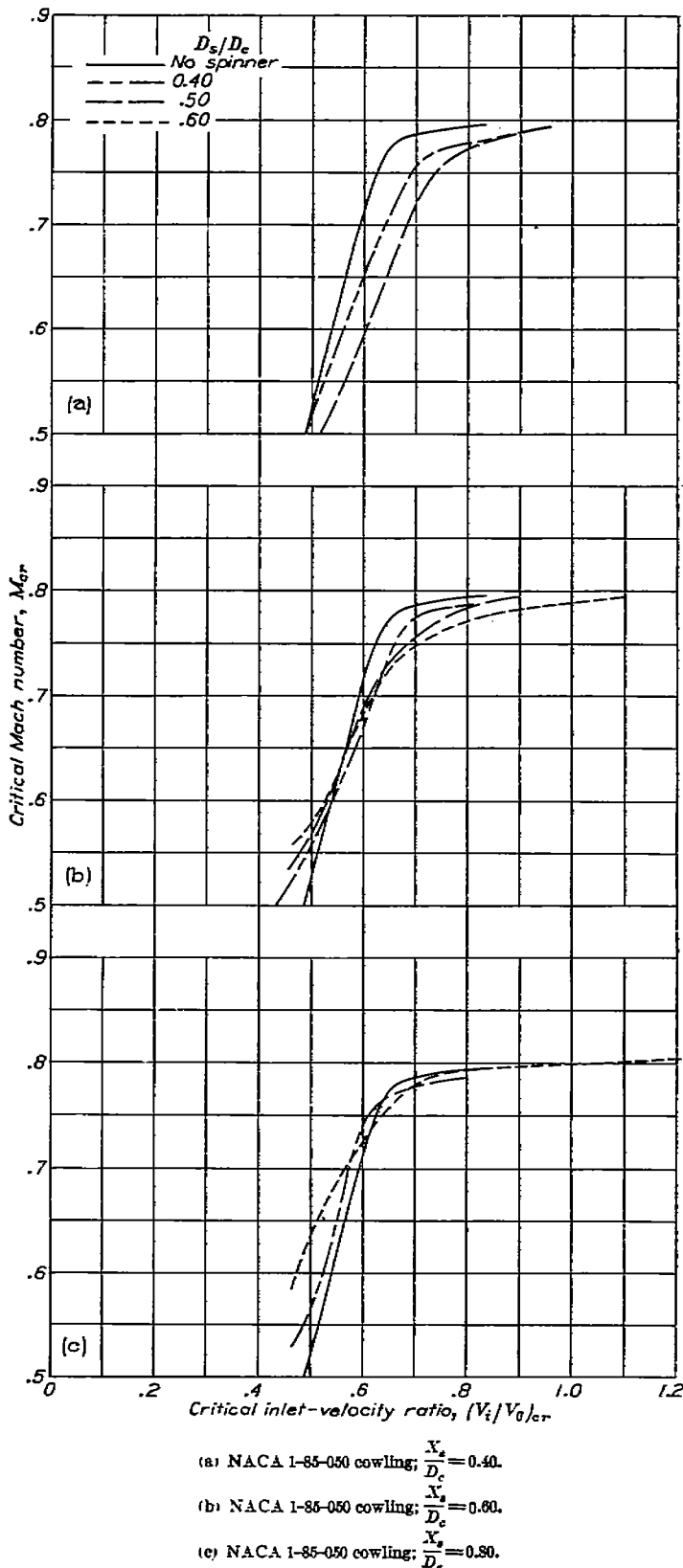
(e) NACA 1-70-075 cowling; $\frac{X_s}{D_c} = 0.80$.

(b) NACA 1-70-050 cowling; $\frac{X_s}{D_c} = 0.40$.

(d) NACA 1-70-050 cowling; $\frac{X_s}{D_c} = 0.60$.

(f) NACA 1-70-050 cowling; $\frac{X_s}{D_c} = 0.80$.

FIGURE 82.—Predicted critical Mach numbers for the NACA 1-series cowlings and cowling-spinner combination as a function of inlet-velocity ratio. Propeller removed; $\alpha = 0^\circ$.



ENVELOPE VALUES OF M_{cr} AND $(V_i/V_0)_{cr}$

Typical construction plots, in which the critical Mach number characteristics of cowling configurations with the same inlet diameter and spinner were grouped together for the purpose of determining envelope curves of critical Mach number and inlet-velocity ratio, are shown in figures 90 to 92. As discussed in reference 1, the envelope curve for each such family of cowlings has important significance in that the cowling whose critical Mach number curve is tangent to this curve at a given point has the minimum inlet-velocity ratio for which the critical Mach number corresponding to the point of tangency can be obtained by any cowling of the family; with the given spinner, such a cowling is also the shortest cowling of any inlet diameter for which this critical Mach number can be obtained at this inlet-velocity ratio. Therefore, when the flow is not separated from the spinner or when this consideration is ignored, the design inlet-velocity ratio and the design critical Mach number for a given cowling are considered to be the values corresponding to the point of tangency of the critical Mach number curve for the cowling with its respective envelope curve.

Envelope values of critical Mach number and inlet-velocity ratio for the several NACA 1-series cowlings investigated are presented in figures 93 and 94 as a function of spinner proportions. The addition of spinners to the open-nose cowlings had an almost negligible effect on the envelope critical Mach numbers in most cases. However, in accordance with the previous discussion of the effect of spinners on the locations of the knees of the critical Mach number curves, the envelope inlet-velocity ratios for the cowling-spinner combinations were usually less than those for the open-nose cowlings when the flow was separated from the spinners and were usually higher than those for the open-nose cowlings when the flow was not separated from the spinners.

The envelope critical Mach numbers for the NACA 1-series cowling configurations investigated are shown in figure 95 as a function of an empirically determined parameter $\frac{Y'}{X} \frac{d}{D_c}$. All the open-nose cowling data exhibited an excellent degree of correlation on the basis of this parameter and were in good agreement with the higher Mach number data of reference 1. As would be expected on the basis of figures 93 and 94, the data for the several cowling-spinner combinations also correlated to an acceptable degree on the same line as the data for the open-nose cowlings. On the basis of the variation shown, it is evident that within the usual range of inlet-diameter ratios the envelope critical Mach number increases with increase in either cowling length or cowling inlet diameter. Usually increasing the cowling length is the more effective means for obtaining a required increase in critical Mach number.

FIGURE 83.—Predicted critical Mach numbers for the NACA 1-series cowlings and cowling-spinner combination as a function of inlet-velocity ratio. Propeller removed; $\alpha=0^\circ$.

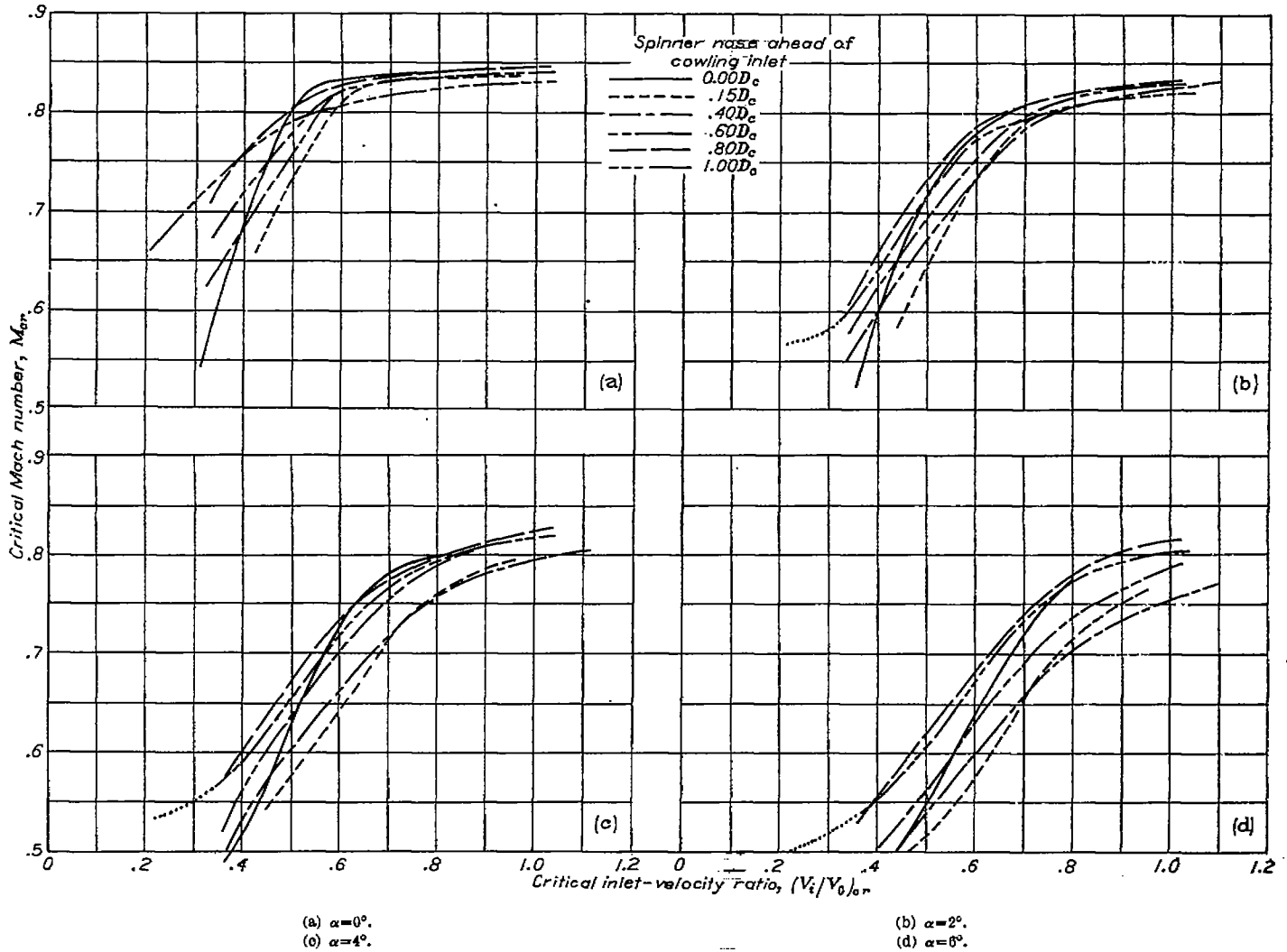


FIGURE 84.—Effect of spinner location on the predicted critical Mach number for the NACA 1-70-100 cowling with the 1-40-040 spinner. Propeller removed.

The surface pressure distributions over the NACA 1-series cowlings are not absolutely uniform at their envelope selection conditions. As a result, the envelope inlet-velocity ratios for these cowlings are somewhat higher than values calculated, by means of equation (10) of the appendix, for cowlings having the same critical Mach number and the same inlet diameter but having sharp inlet lips and absolutely uniform surface pressure distributions (fig. 96). As shown in figure 96, however, a fixed relationship exists between the two sets of inlet-velocity ratios. The inlet-velocity ratio for any given NACA 1-series open-nose cowling therefore may be estimated with acceptable accuracy by first calculating the inlet-velocity ratio required by the surface pressures on the corresponding theoretical open-nose cowling (by use of equation (10) of the appendix) and then by correcting the value obtained with reference to figure 96.

The insertion of an NACA 1-series spinner can be assumed to have a negligible effect on the envelope value of critical Mach number for any particular NACA 1-series open-nose cowling. (See figs. 93 to 95.) Also, the preceding paragraph has pointed out a means for calculating the envelope inlet-velocity ratios for the open-nose cowlings. It is necessary

only to establish the effect of spinner proportions on the required value of inlet-velocity ratio, therefore, in order to utilize the available NACA 1-series open-nose-cowling data in the design of NACA 1-series cowling-spinner combinations outside the range of cowling proportions investigated. As an approach to the problem of determining this effect of spinner proportions, an attempt was made to compute (by means of equation (4) of the appendix, with the skin-friction drag of the spinner being neglected) the inlet-velocity ratio required at the test Mach number to obtain a predicted critical Mach number for each cowling-spinner combination with unseparated spinner flow equal to the envelope critical Mach number for the open-nose cowling used as its basic component. When the actual pressure distributions on the cowling-spinner combinations were used in the calculations, the calculated and experimental values of required inlet-velocity ratio (fig. 97) were generally in good agreement at small values of spinner-diameter ratio. Appreciable discrepancies existed in some cases at large values of spinner-diameter ratio, however, probably because the minimum pressure peaks on the inner surface of the cowling, which contributed greatly to the thrust force on the cowling at the

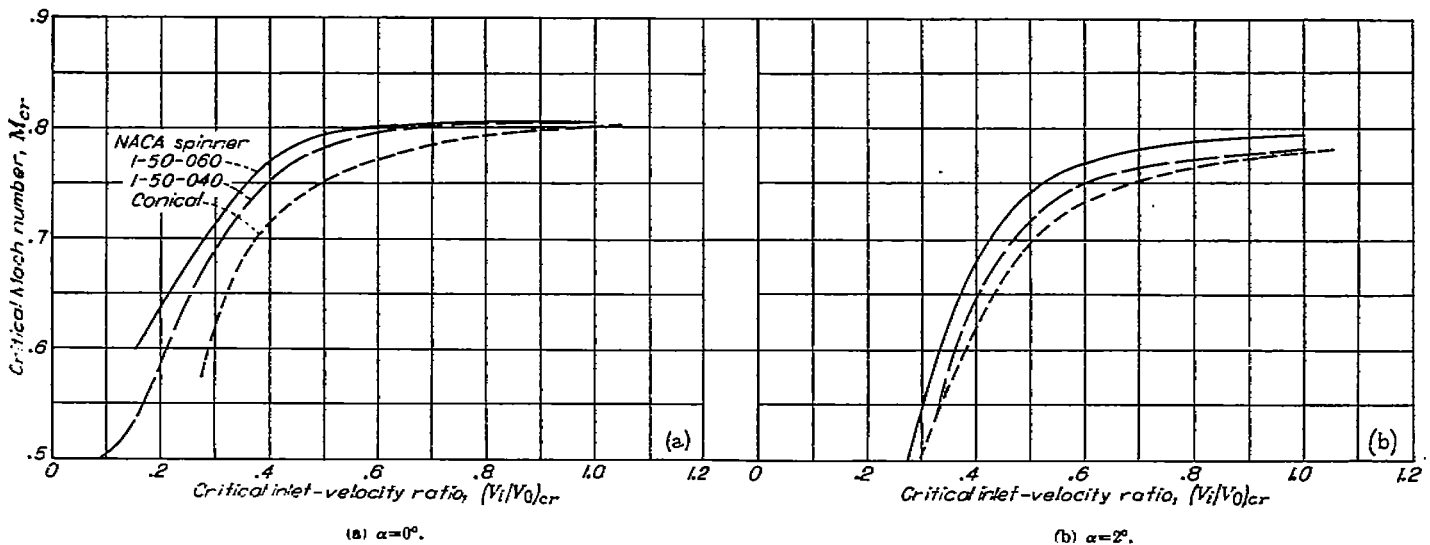
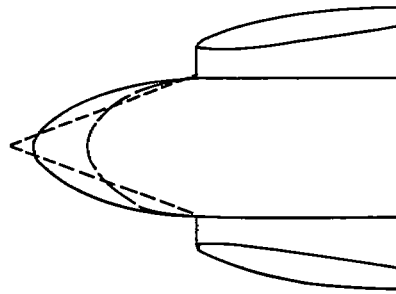


FIGURE 85.—Effect of spinner shape on the predicted critical Mach number for the NACA 1-70-075 cowling. Propeller removed.

higher inlet-velocity ratios, were very sensitive to small changes in lip contour such as may have existed at sections of the inlet lip outside the immediate region of the measuring station. When the measured pressures on the spinners were used in the calculations in conjunction with the average surface-pressure coefficients for the basic open-nose cowlings, the agreement between the calculated and the experimental values of required inlet-velocity ratio again was generally satisfactory at small values of spinner-diameter ratio where the insertion of the spinner would be expected to have only a small effect on the pressure distribution over the open-nose cowling. Thus, if the spinner diameter is small with respect to the inlet diameter of the proposed cowling and if pressure distributions over the spinner when inserted in a cowling of approximately the inlet diameter considered are existent, a rough estimate of the inlet-velocity ratio required by the proposed cowling-spinner combination (at the Mach number for which the test data are available) may be obtained as follows:

- (1) Calculate $P_{c_{av}}$ for the cowling at its envelope value of V_i/V_0 .
- (2) Calculate $P_{s_{av}}$ for the spinner at V_i/V_0 just greater than the envelope value for the cowling.
- (3) Use $P_{c_{av}}$ from step (1) and $P_{s_{av}}$ from step (2) and calculate V_i/V_0 for the cowling-spinner combination from equation (4) of the appendix.
- (4) Compare the calculated value of V_i/V_0 of step (3) with the value assumed in step (2). If the two values differ appreciably, assume a new spinner pressure distribution

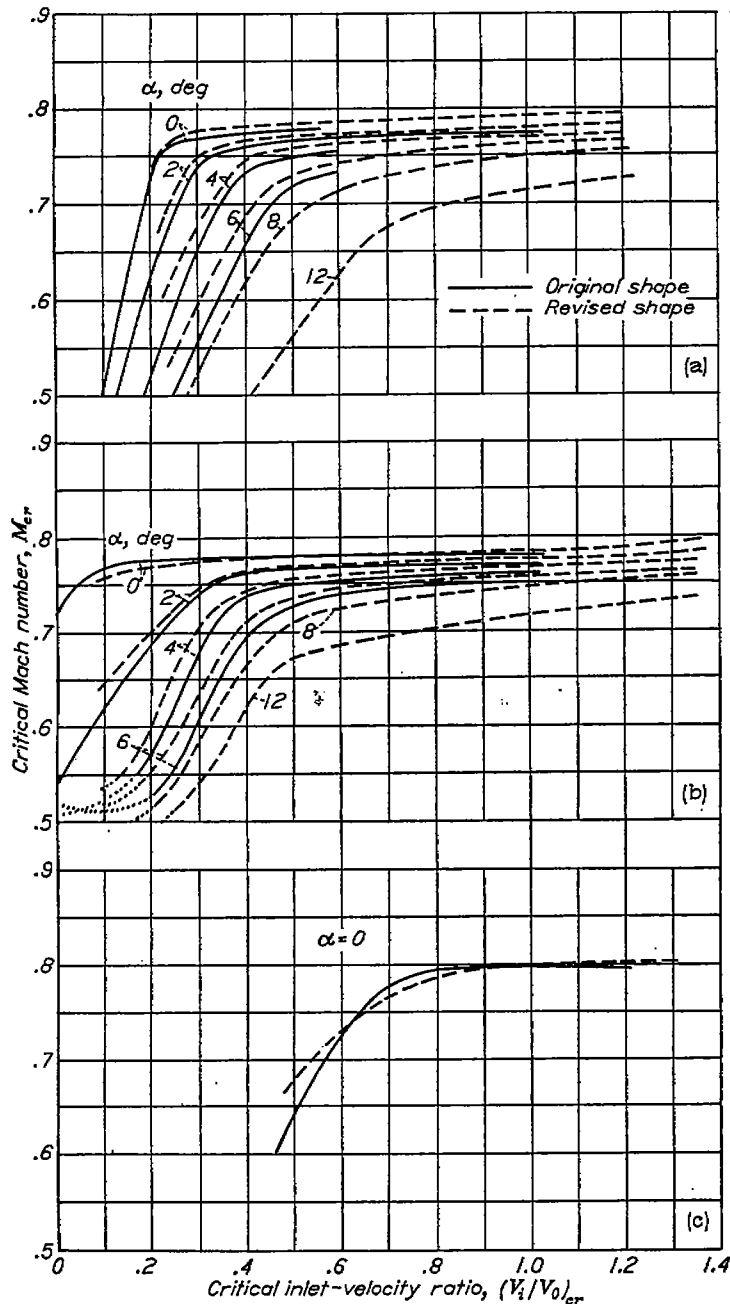
corresponding to V_i/V_0 obtained in step (3) and repeat steps (2) and (3).

(5) Repeat step (4) until the assumed and calculated values of V_i/V_0 agree. The V_i/V_0 finally obtained is the required value.

Inasmuch as equation (4) of the appendix predicts the effect of spinner proportions on the required inlet-velocity ratio for a given cowling with reasonable accuracy (fig. 97), equations (9) and (10) of the appendix can be used to study the effect of Mach number on the increments by which the envelope inlet-velocity ratios for the NACA 1-series open-nose cowlings must be increased to allow for the insertion of NACA 1-series spinners. Consider, for instance, the NACA 1-70-100 open-nose cowling and the NACA 1-70-100 cowling with the NACA 1-40-060 and 1-60-060 spinners installed. If for these configurations the measured pressure distributions are extrapolated by use of the Von Kármán relation to the predicted critical Mach number for the open-nose cowling (0.822) and the corresponding inlet-velocity ratios are calculated by use of equations (9) and (10) of the appendix, the following comparison with the low-speed values of figure 97 is obtained:

| NACA spinner | V_i/V_0 | | |
|--------------|------------|------------|-------------|
| | Test | Calculated | |
| | $M_0=0.13$ | $M_0=0.13$ | $M_0=0.822$ |
| None | 0.67 | 0.67 | 0.67 |
| 1-40-060 | .72 | .74 | .67 |
| 1-60-060 | 1.03 | 1.04 | 1.08 |

These results indicate that the change in required inlet-velocity ratio caused by the addition of a spinner is substantially the same at high speeds as at low speeds. The experimentally determined inlet-velocity-ratio increments of figures 93, 94, and 97 therefore appear to be directly applicable to the extrapolation problem discussed in the preceding paragraph.



(a) NACA 1-80-075 cowling.
 (b) NACA 1-80-075 cowling with 1-40-080 spinner.
 (c) NACA 1-85-050 cowling with 1-60-080 spinner.

FIGURE 86.—Effect of inner lip shape on predicted critical Mach number of top surface of cowling. Propeller removed.

DEVELOPMENT OF SELECTION CHARTS

The method used for selecting the design conditions for the NACA 1-series cowling-spinner combinations is illustrated in figure 98. The envelope values of critical Mach number and inlet-velocity ratio, labeled ①, were always used unless they fell to the left of the vertical line which identifies the minimum inlet-velocity ratio for which flow separation from the spinner was avoided (fig. 29). When the knee of the curve for a given cowling fell to the left of this vertical line, the design conditions corresponding to the points of intersection of the critical Mach number curves with this vertical line, labeled ②, were selected. The cowling-spinner combination with its knee curve tangent to the envelope curve at point ③ has the highest critical Mach number that can be obtained at the specified lower limiting value of inlet-velocity ratio by any cowling-spinner combination of the family; in accordance with the concepts of reference 1, such a configuration is hereafter referred to as an "optimum combination."

The separation-free design conditions for the NACA 1-series cowling-spinner combinations obtained as just discussed are presented in figures 99 and 100 as a function of spinner proportions. The slightly irregular variations in the design inlet-velocity ratios for several of the thinner-lip cowlings resulted from the variations in spinner proportions which caused changes in the flow phenomena on the spinner and, therefore, required changes in the selection method. It should again be noted that the values of inlet-velocity ratio and mass-flow coefficient specified in this figure are high enough to avoid appreciable negative pressure peaks on the cowling lips; further increases in the rate of internal flow will therefore increase the critical Mach number only a small amount.

Cowling selection charts based on the data of figures 99 and 100 are presented in figures 101 and 102. The dashed lines which divide the cowling-spinner charts into two parts define the optimum combinations having the maximum critical Mach number obtainable at the minimum inlet-velocity ratio for unseparated spinner flow. Above these lines, where the design conditions were determined by the locations of the knees of the curves of M_{cr} plotted against $(V_i/V_0)_{cr}$, the variations were established by cross-plotting the envelope data of figures 93 and 94 (extrapolated a reasonable amount) as a function of the cowling-inlet diameter and cowling-length ratios. Below the dashed lines, where the design conditions were determined by the consideration of avoiding flow separation from the spinners, the variations were obtained by similarly cross-plotting all the data in figures 99 and 100 for which the design inlet-velocity ratios were those defined in figure 29. The large areas below the dashed lines again point out the desirability of developing new families of spinners which can be used at lower values of inlet-velocity ratio than those of the NACA 1-series spinners without incurring flow separation ahead of the inlet.

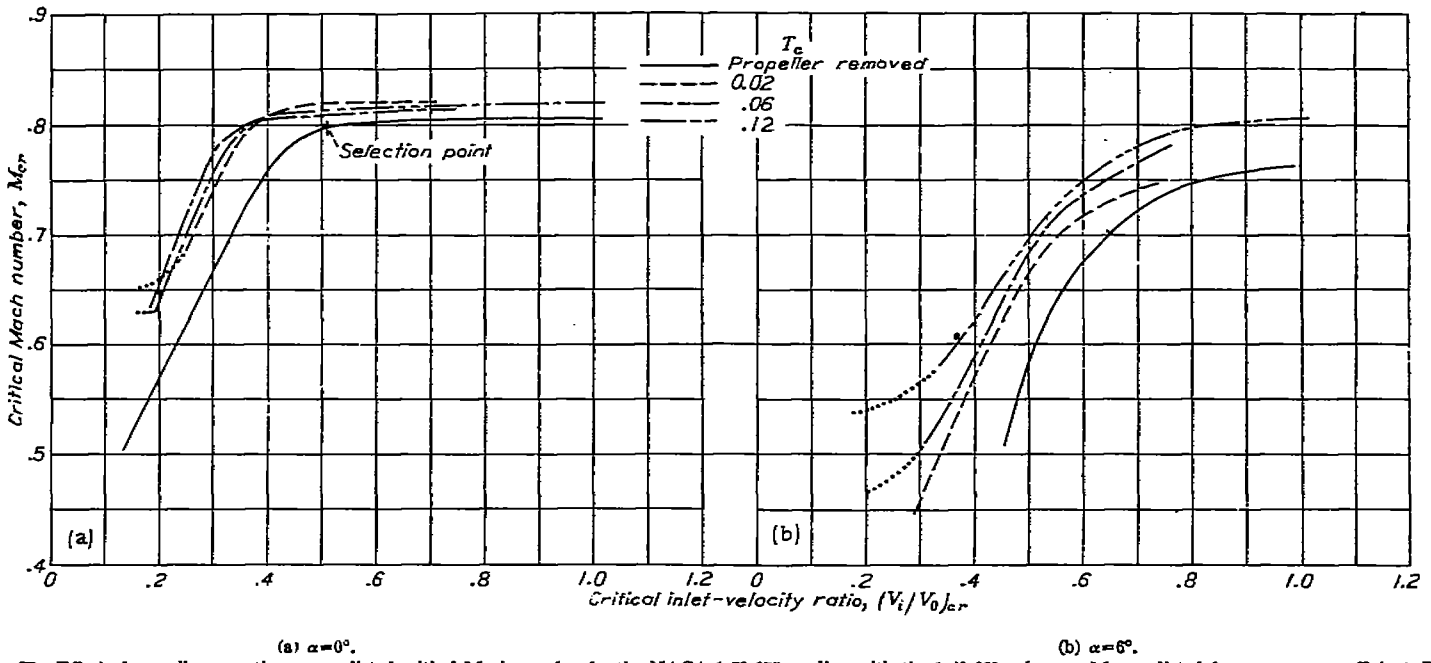


FIGURE 87.—Effect of propeller operation on predicted critical Mach number for the NACA 1-70-075 cowling with the 1-40-060 spinner. M_{cr} predicted from pressure coefficient P .

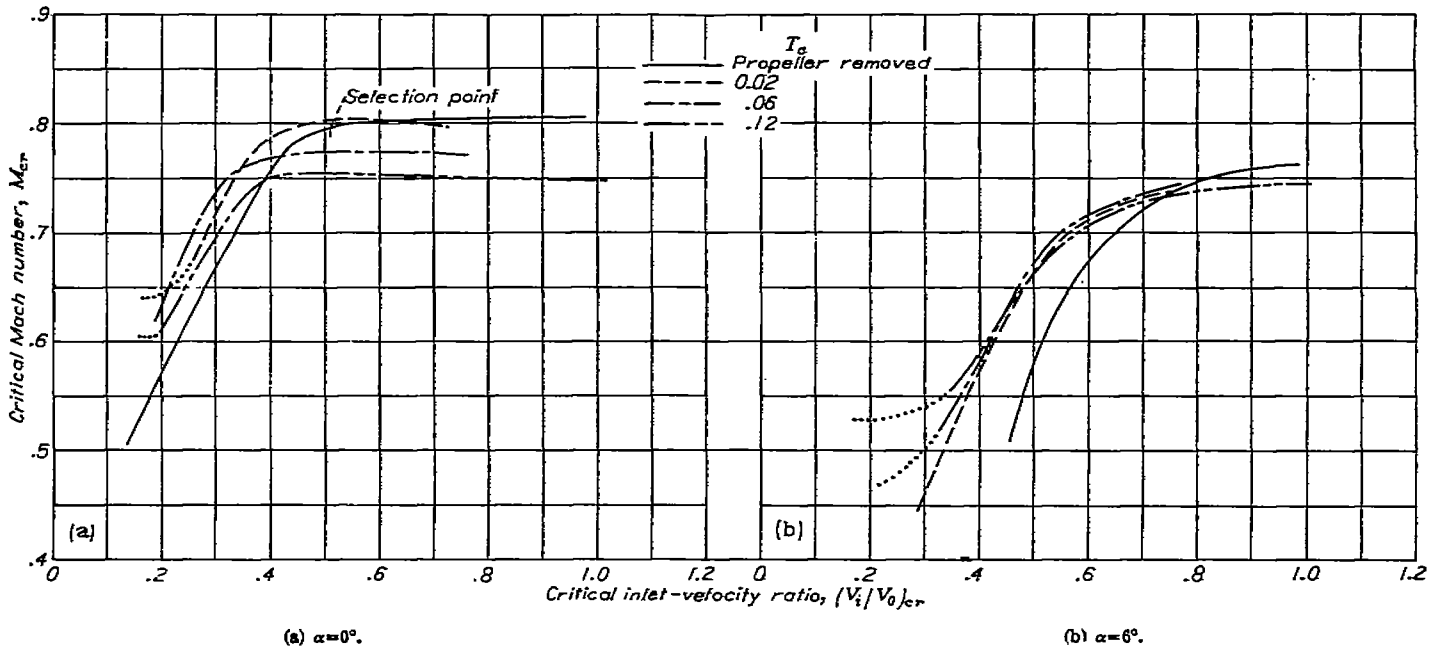


FIGURE 88.—Effect of propeller operation on predicted critical Mach number for the NACA 1-70-075 cowling with the 1-40-060 spinner.

$$M_{cr} = \left(M_{cr} \text{ predicted from pressure coefficient } \frac{p_c - p_0}{H_w - p_0} \right) \sqrt{\frac{g_0}{H_w - p_0}}$$

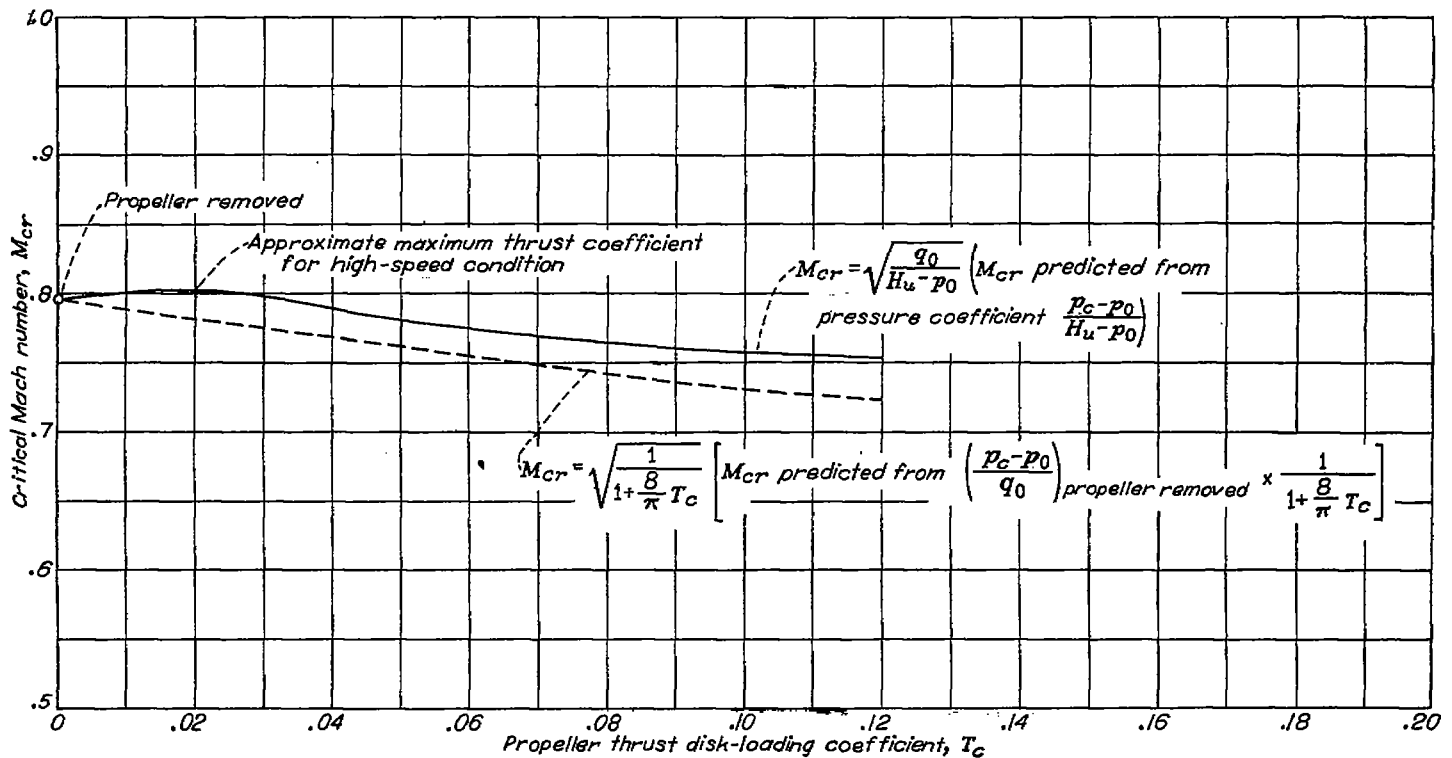


FIGURE 99.—Comparison of experimental and estimated propeller installed values of predicted critical Mach number for the NACA 1-70-076 cowling with the 1-40-000 spinner.

$$\alpha = 0^\circ; \frac{V_i}{V_0} = 0.51 \text{ (the selection point for the propeller-removed condition, figs. 87 and 88).}$$

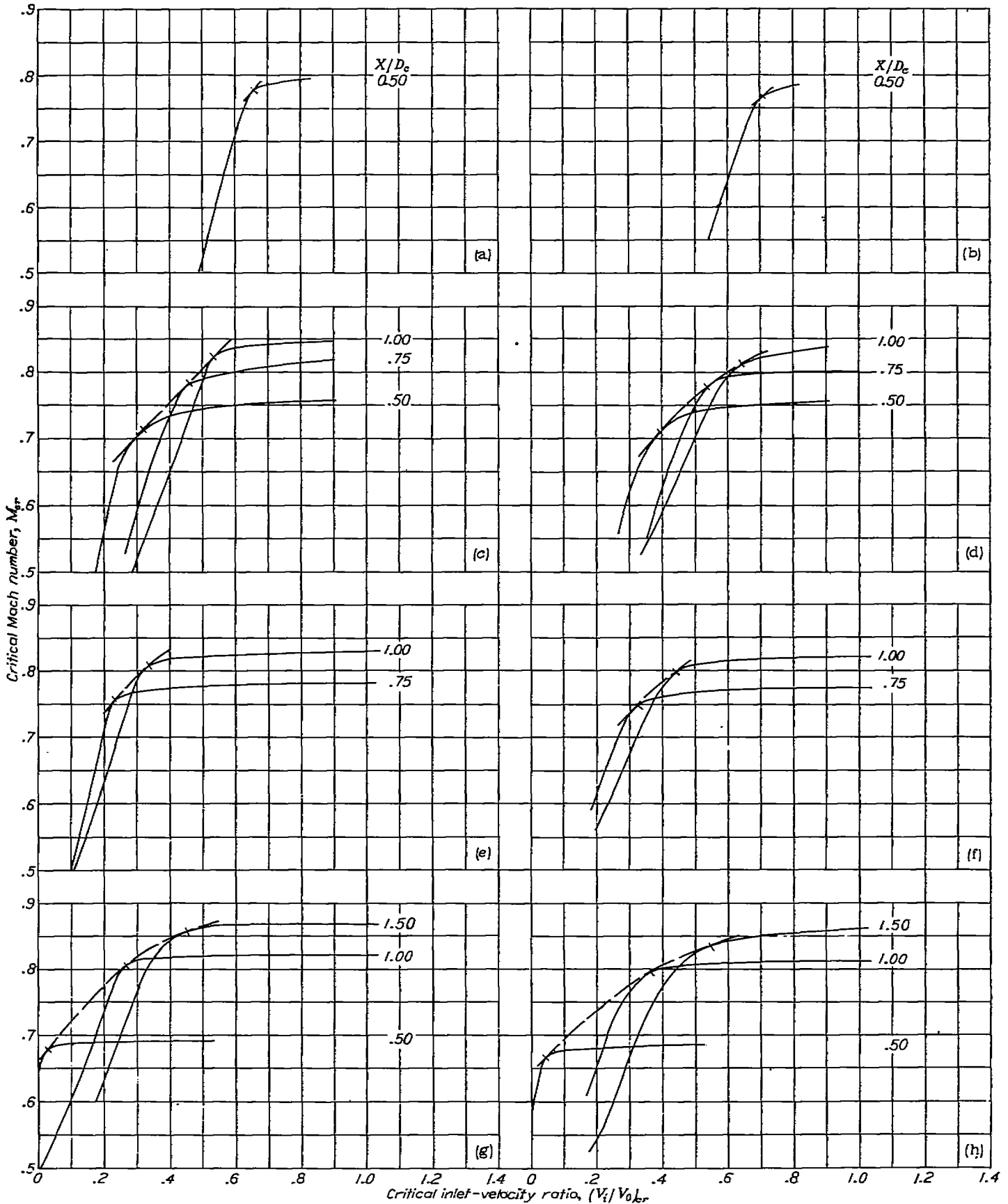
The large breaks in the critical Mach number contours of figures 101 and 102 may be explained by reference to figure 98. So long as the design inlet-velocity ratios fell to the right of the vertical line, the design critical Mach numbers followed the envelope curve with decreases in cowling length. When the cowling length decreased beyond that for the optimum combination (point ③), however, the design critical Mach numbers dropped below the envelope curve along the vertical line so that the critical Mach numbers changed less rapidly with further decreases in cowling length than would be the case if the design conditions were assumed to occur along the envelope curve. In other words, when the required inlet-velocity ratio was higher than that corresponding to the knee of the curve of M_{cr} plotted against $(V_i/V_0)_{cr}$, as is the case below the dashed lines of figures 101 and 102, the design critical Mach number was somewhat greater than that corresponding to the knee of the curve. The corresponding small breaks in the curves of $m/\rho_0 F V_0$ of figures 101 and 102 may be explained in a similar manner.

Design data for the NACA 1-series open-nose cowlings obtained in the present investigation are presented in figures 101 and 102 in the same form as the design data for the NACA 1-series cowling-spinner combinations. These data are also replotted in figure 103 with the parameter $m/\rho_0 F V_0$ replaced by the parameter $(V_i/V_0)_{cr}$ to facilitate the use of

these data in the general design procedure outlined in the next section of the report. The values of critical Mach number and inlet-velocity ratio for particular cowlings given in figure 103 are approximately the same as those specified in the selection charts of reference 1; some differences exist, however, because of differences in the methods used to extrapolate the test data.

COWLING SELECTION

The optimum cowling-spinner combination for a given airplane is considered to be the one for which the operating inlet-velocity ratios are a minimum and for which, under all important flight conditions, the flow is unseparated from the spinner and the critical Mach number is equal to or greater than the free-stream Mach number. In the present section of the report, a procedure for the selection of the optimum NACA 1-series cowling-spinner combination is first presented. A generalized procedure permitting selection of NACA 1-series cowlings for use with any spinner-propeller configuration for which certain application data are available is then developed and illustrated. Finally, a method is outlined for extrapolating the present cowling-spinner design data through the use of figure 95, figure 96, and equation (10) of the appendix in conjunction with the general design procedure.



(a) $\frac{d}{D_c} = 0.85; \alpha = 0^\circ.$

(c) $\frac{d}{D_c} = 0.70; \alpha = 0^\circ.$

(e) $\frac{d}{D_c} = 0.60; \alpha = 0^\circ.$

(g) $\frac{d}{D_c} = 0.55; \alpha = 0^\circ.$

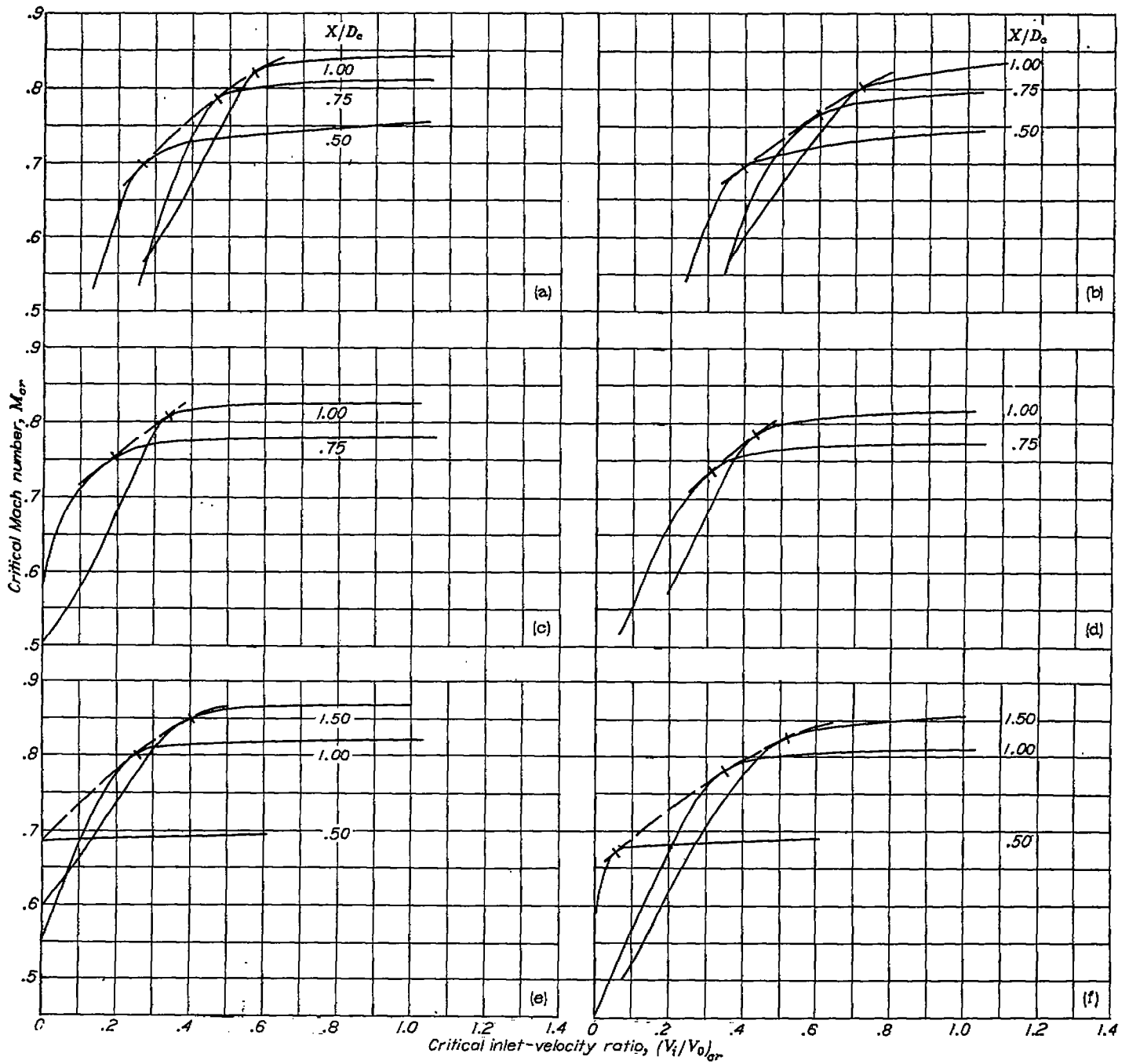
(b) $\frac{d}{D_c} = 0.85; \alpha = 2^\circ.$

(d) $\frac{d}{D_c} = 0.70; \alpha = 2^\circ.$

(f) $\frac{d}{D_c} = 0.60; \alpha = 2^\circ.$

(h) $\frac{d}{D_c} = 0.55; \alpha = 2^\circ.$

FIGURE 90.—Construction curves for the determination of envelope values of predicted critical Mach number and inlet-velocity ratio. Propeller removed; open-nose cowlings.



(a) $\frac{d}{D_c} = 0.70; \alpha = 0^\circ.$

(c) $\frac{d}{D_c} = 0.60; \alpha = 0^\circ.$

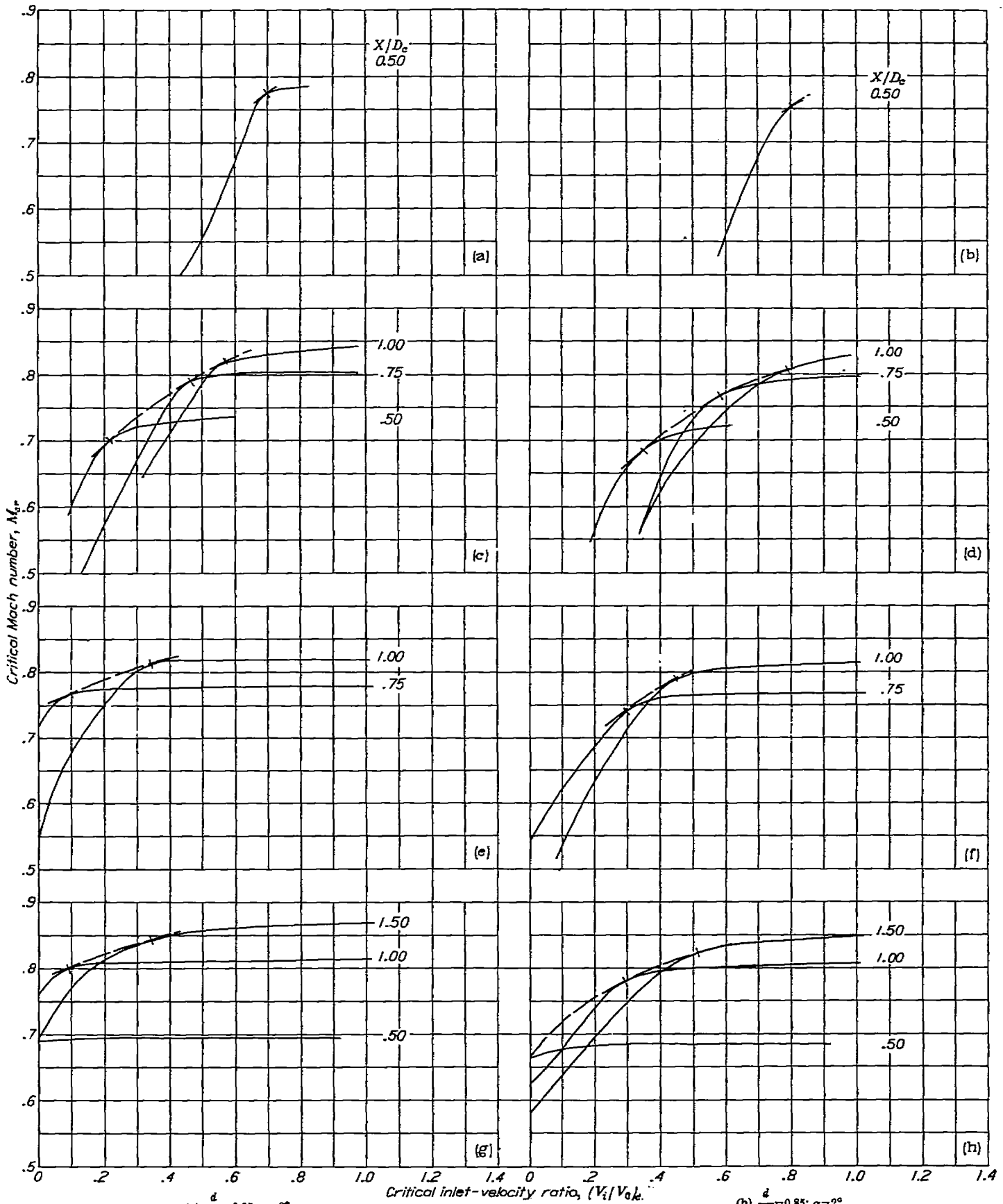
(e) $\frac{d}{D_c} = 0.55; \alpha = 0^\circ.$

(b) $\frac{d}{D_c} = 0.70; \alpha = 2^\circ.$

(d) $\frac{d}{D_c} = 0.60; \alpha = 2^\circ.$

(f) $\frac{d}{D_c} = 0.55; \alpha = 2^\circ.$

FIGURE 91.—Construction curves for the determination of envelope values of predicted critical Mach number and inlet-velocity ratio. Propeller removed; cowling-spinner combinations, NACA 1-30-040 spinner.



- (a) $\frac{d}{D_c} = 0.85; \alpha = 0^\circ.$
- (c) $\frac{d}{D_c} = 0.70; \alpha = 0^\circ.$
- (e) $\frac{d}{D_c} = 0.60; \alpha = 0^\circ.$
- (g) $\frac{d}{D_c} = 0.55; \alpha = 0^\circ.$

- (b) $\frac{d}{D_c} = 0.85; \alpha = 2^\circ.$
- (d) $\frac{d}{D_c} = 0.70; \alpha = 2^\circ.$
- (f) $\frac{d}{D_c} = 0.60; \alpha = 2^\circ.$
- (h) $\frac{d}{D_c} = 0.55; \alpha = 2^\circ.$

FIGURE 92.—Construction curves for the determination of envelope values of predicted critical Mach number and inlet-velocity ratio. Propeller removed; cowlings-spinner combinations, NACA 1-40-060 spinner.

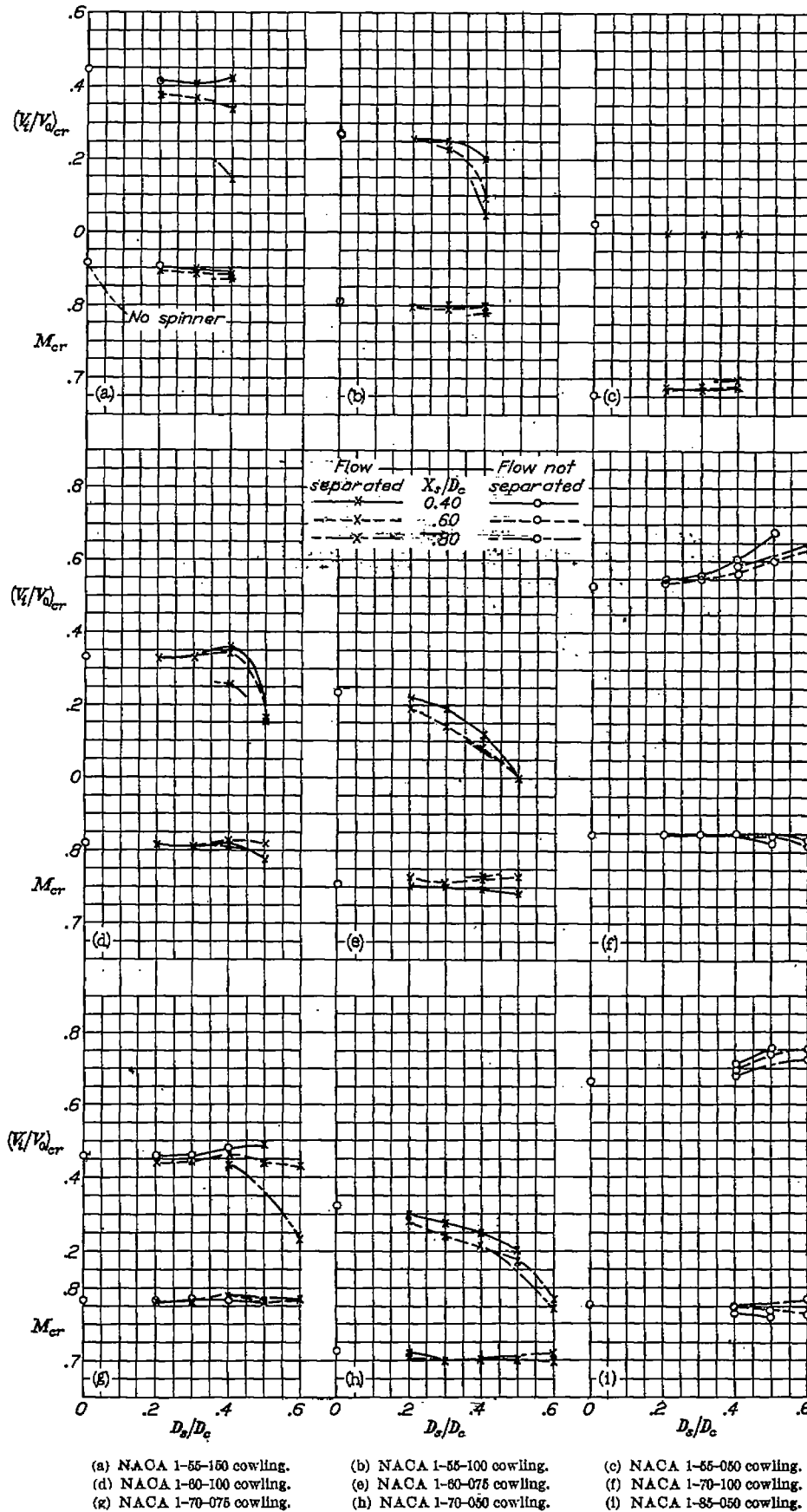


FIGURE 93.—Envelope values of predicted critical Mach number and inlet-velocity ratio as a function of spinner proportions. Propeller removed; $\alpha=0^\circ$.

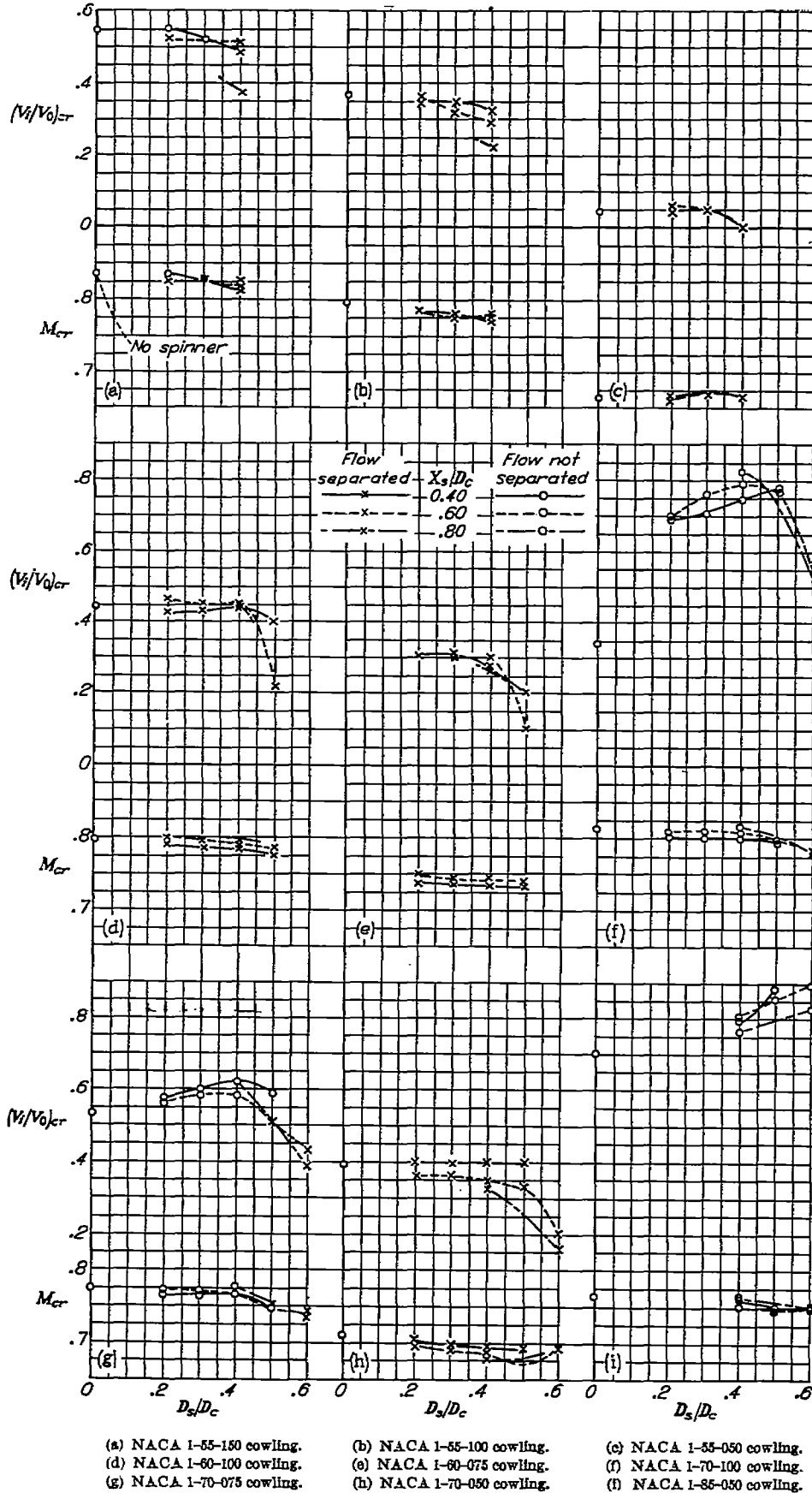
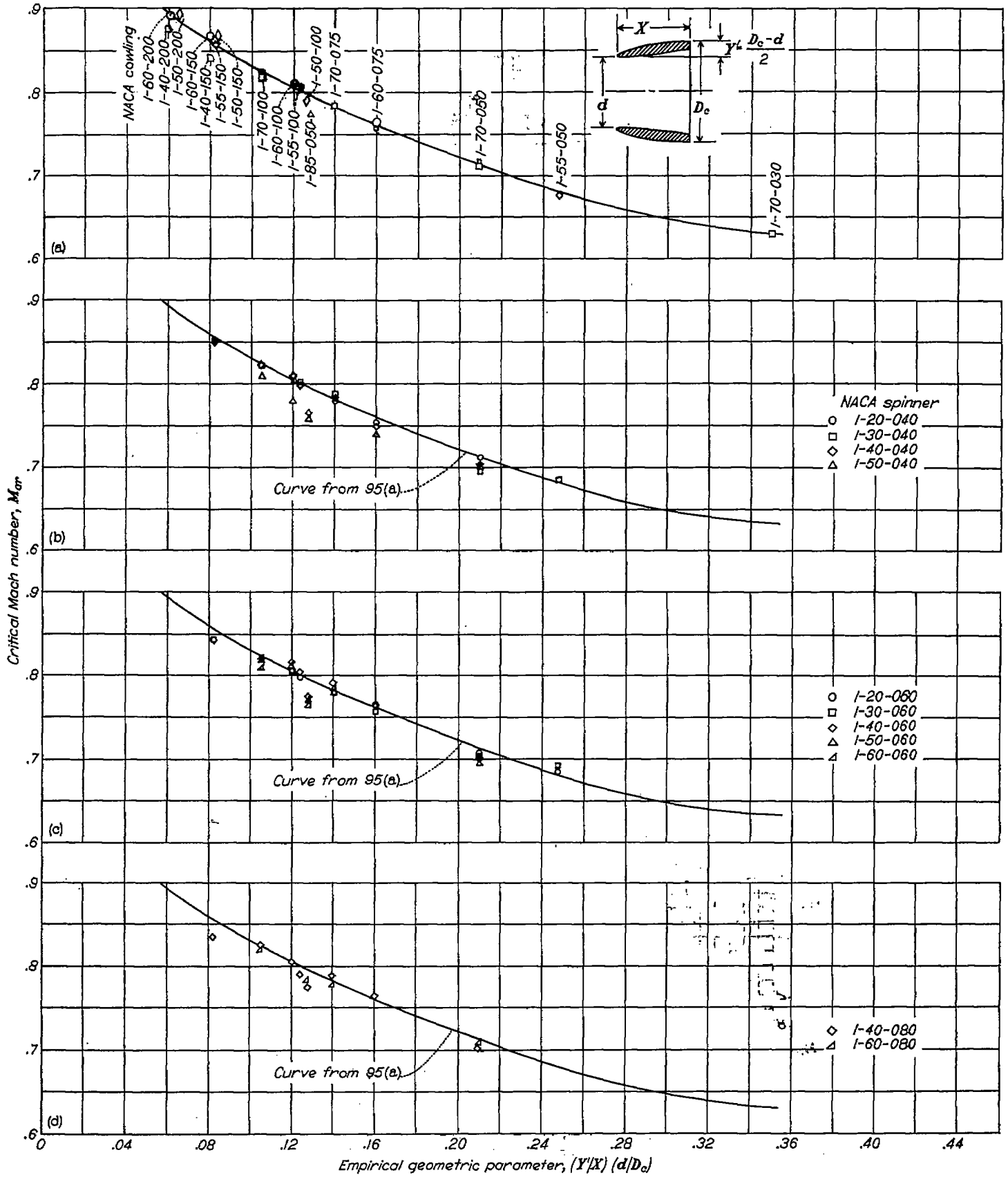


FIGURE 94.—Envelope values of predicted critical Mach number and inlet-velocity ratio as a function of spinner proportions. Propeller removed; $\alpha=2^\circ$.



(a) Open-nose cowlings (large symbols are for data obtained from reference 1).

(b) Cowlings with spinners; $X_2/D_c = 0.40$.

(c) Cowlings with spinners; $X_2/D_c = 0.60$.

(d) Cowlings with spinners; $X_2/D_c = 0.80$.

FIGURE 95.—Effect of geometric proportion of NACA 1-series cowlings on envelope values of predicted critical Mach number. Propeller removed; $\alpha = 0^\circ$.

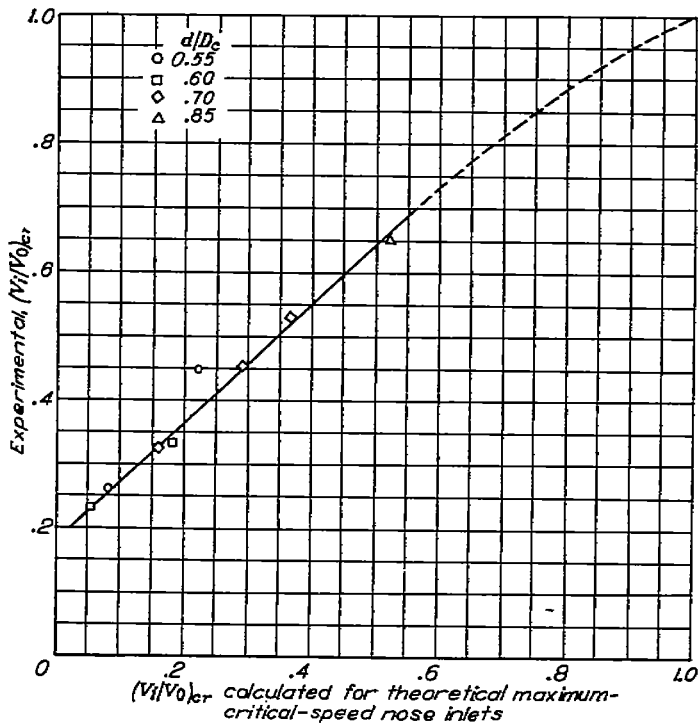


FIGURE 96.—Comparison of envelope values of $(V_1/V_0)_{cr}$ for NACA 1-series open-nose cowlings with values calculated for equal critical Mach number cowlings having same inlet diameters, sharp inlet lips, and absolutely uniform surface pressure distributions. $\alpha=0^\circ$.

Design procedure for NACA 1-series combinations.—NACA 1-series cowling-spinner combinations within the range of proportions investigated may be selected by the use of figures 101 and 102 provided that the propeller-shank configuration is similar to the one investigated. For example, assume that it is desired to design a cowling-spinner combination for a 3,000-horsepower gas-turbine unit to be mounted in a 40-inch-diameter nacelle (frontal area, $F=8.73$ sq ft). Also, assume that the effective angle of attack of the cowling axis and the engine air-flow requirements are known for all flight conditions. The required design procedure is then as follows:

(1) Select for consideration the following high-speed operating condition which appears to offer the most severe combination of high flight Mach number and low inlet-velocity ratio:

| | |
|---|----------|
| Operating altitude, feet..... | 35,000 |
| Air density at altitude, ρ_0 , slug per cubic foot..... | 0.000736 |
| Flight speed, V_0 , feet per second (538 mph)..... | 790 |
| Effective angle of attack of cowling center line, α , degree.... | 0 |
| Flight Mach number, M_0 | 0.81 |
| Total combustion and cooling air flow, m , slug per second.... | 0.762 |
| Mass-flow coefficient, $m/\rho_0 F V_0$ | 0.15 |

(2) From a layout of the propeller hub and the engine installation, determine that the NACA 1-45-050 spinner is the smallest spinner which will enclose the propeller hub and will fair smoothly to the fixed ducting of the engine. The data of figure 29 show that this minimum-size spinner should be used as it has a lower separation value of inlet-velocity ratio than that of longer or larger diameter NACA 1-series spinners.

(3) With $\alpha=0^\circ$, $M_0=0.81$, and $\frac{m}{\rho_0 F V_0}=0.15$, select in

figures 101 and 102 the following optimum cowling proportions for spinners bracketing the NACA 1-45-050 spinner:

| NACA spinner | Cowling proportions | |
|--------------|---------------------|-------|
| | d/D | X/D |
| 1-40-040 | 0.641 | 0.632 |
| 1-40-060 | .626 | .908 |
| 1-50-040 | .677 | 1.023 |
| 1-50-060 | .689 | .929 |

(4) Determine by cross interpolation that the NACA 1-66-095 cowling is optimum for the design conditions considered.

(5) Construct curves of M_{cr} plotted against $m/\rho_0 F V_0$ for the NACA 1-66-095 cowling with the 1-45-050 spinner (for angles of attack of 0° , 2° , 4° , and 6°) by interpolation of the data presented in figures 49 to 78.

(6) Check all known operating conditions against the curves of step (5). If, in any important flight condition, the critical Mach number is less than the flight Mach number or the mass-flow coefficient is lower than the minimum value for avoiding flow separation from the spinner, repeat steps (3) to (6) (use the more critical design conditions so determined) to select a new cowling.

Additional considerations may necessitate the choice of a different cowling. For instance, if the inner-lip fairing of figure 4 is to be applied to a large percentage of the inner-cowling-lip surface to reduce the likelihood of flow separation, it is desirable, where the design inlet velocity is determined by the consideration of flow separation from the spinner, to use a slightly larger inlet-diameter cowling in order to allow for the inlet area blocked by the revised fairing. Also, it may be found that the exterior lines of the cowling initially selected do not clear the engine installation. In such a case it is necessary to start with a larger-diameter spinner and thereby choose a cowling with a larger inlet diameter; if this process leads to the use of an excessively high inlet-velocity ratio, it may also be desirable to increase the maximum diameter of the nacelle.

General design procedure.—A number of design considerations are automatically taken into account in the preceding cowling-selection method. A more fundamental design procedure utilizing figures 47, 48, and 103 or the comparable design charts of reference 1 will now be presented to explain these considerations. This procedure, which treats the individual effects of the spinner and the propeller on the performance of the open-nose cowling separately, is essentially that presented in reference 1 with the addition of the following quantitative application data for the particular family of spinners and the propeller tested:

(1) The minimum inlet-velocity ratio for unseparated inlet flow (fig. 29)

(2) The effect of the spinner on the envelope critical Mach number of the cowling (figs. 84, 93, and 94)

(3) The effect of the spinner on the envelope inlet-velocity ratio of the cowling (figs. 84, 93, and 94)

(4) The effect of the propeller on the design conditions (figs. 25, 26, and 88)

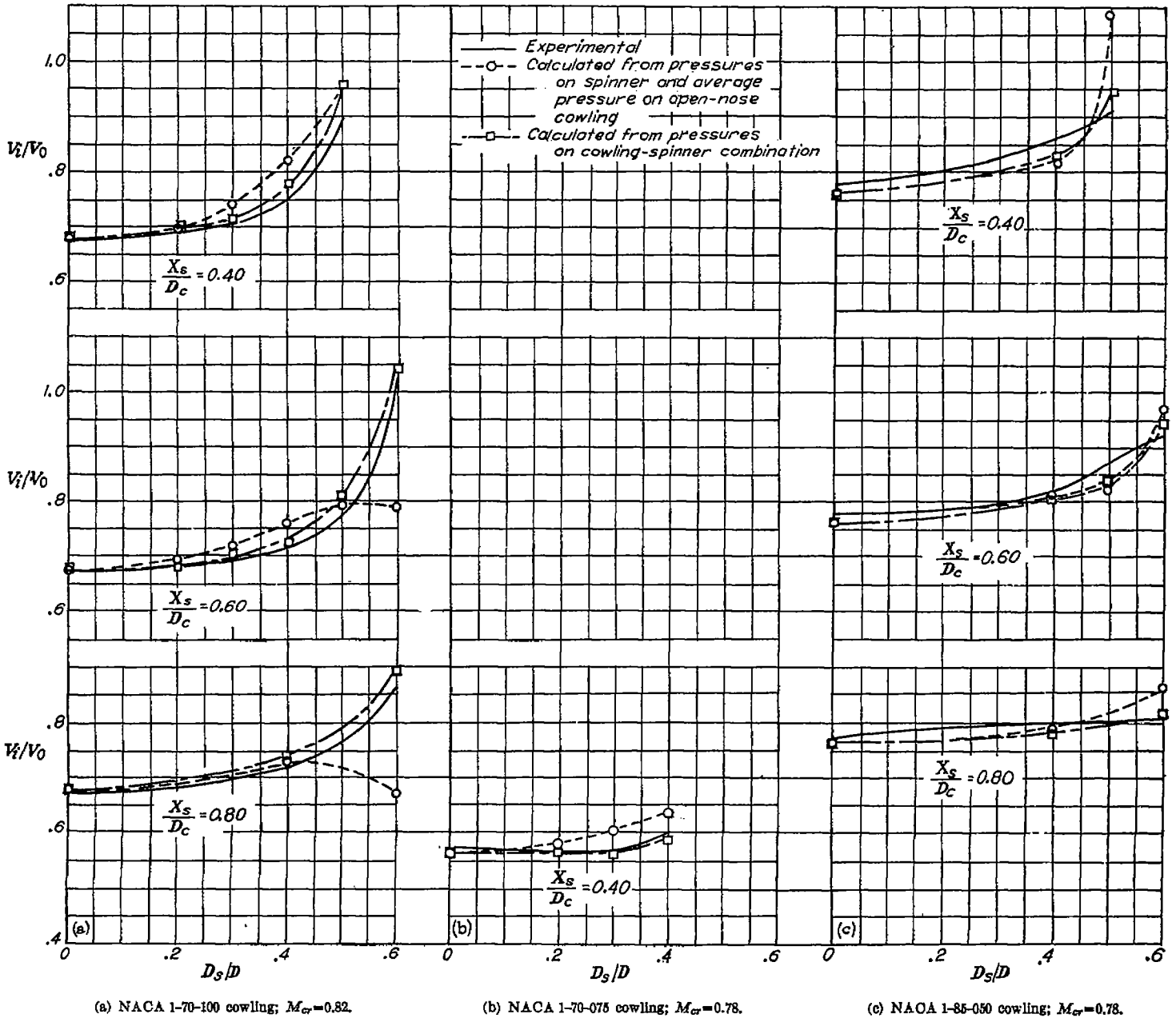


FIGURE 97.—Experimental and calculated effects of spinner proportions on inlet-velocity ratio required to obtain a critical Mach number equal to the design value for the open-nose cowling. Flow over spinners not separated; $\alpha=0^\circ$.

As pointed out in the preceding discussion, some application data for hemispherical-nose spinners are given in reference 4, data on the particular conical spinner of the present investigation are presented in figures 20, 30, and 85, and data presented in references 2 and 3 afford a beginning to the solution of the propeller-cowling interference problem. The method considered therefore has immediate application to the design of NACA 1-series cowlings for use with hemispherical-nose spinners and conical spinners similar to the one investigated. When the existing application data are supplemented by the recommended spinner-shape and propeller-interference research, this method then can be used in

the design of NACA 1-series cowling configurations incorporating desirable changes in spinner and propeller geometry.

The proposed general design method assumes that inlet-flow stability determines the minimum inlet-velocity ratio. Thus, after due allowance is made for the usually small effects of the spinner and propeller on the selection value of critical Mach number, an NACA 1-series cowling is selected for the inlet-diameter ratio corresponding to this critical value of inlet-velocity ratio. Then, the envelope inlet-velocity ratio for the cowling so selected is corrected for the presence of the spinner and the resulting value compared with the separation inlet-velocity ratio. If the envelope

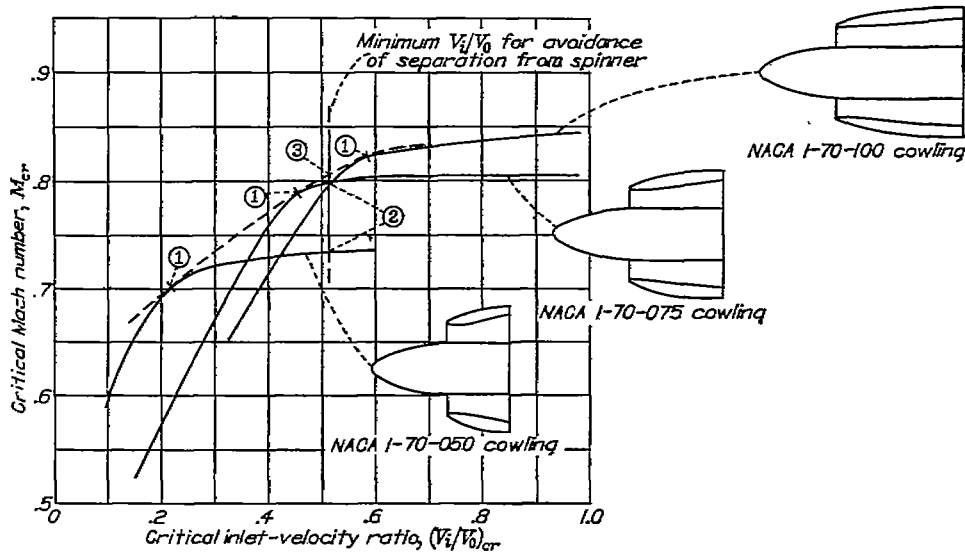


FIGURE 98.—Illustration of method used for selecting design points. NACA 1-40-060 spinner; $\frac{d}{D_c} = 0.70$; propeller removed; $\alpha = 0^\circ$.

inlet-velocity ratio for the cowling-spinner combination is lower than the separation inlet-velocity ratio, the selected cowling is the one required. However, if the envelope inlet-velocity ratio exceeds the separation inlet-velocity ratio, the selection procedure must be repeated, with the intermediate values of inlet-velocity ratio being used, until both design criteria are satisfied at the design mass-flow coefficient. As an illustration of this design method, assume that the spinner considered has the same maximum diameter ratio and design characteristics as the NACA 1-40-060 spinner and that the propeller is similar to the one investigated. Also, assume that the design critical Mach number is 0.82, the design mass-flow coefficient is 0.23, and the design angle of attack is 0° . The selection procedure is then as follows:

- (1) From figure 29 or equivalent, determine $\left(\frac{V_i}{V_0}\right)_{min}$ for unseparated inlet flow to be 0.51.
- (2) With $\left(\frac{V_i}{V_0}\right)_{min}$, M_{cr} , and $m/\rho_0 F V_0$ known, determine A_d/F to be 0.36 from figure 48.
- (3) Read $\frac{d}{D_c} = 0.72$ from figure 47.
- (4) From unseparated-spinner-flow data of figure 93 or equivalent, determine that for open-nose cowlings with $\frac{d}{D_c} \approx 0.7$ and $M_{cr} \approx 0.8$ addition of the spinner considered does not change M_{cr} (as is typical for spinners which are essentially cylindrical for a short distance ahead of the inlet) but increases $\left(\frac{V_i}{V_0}\right)_{cr}$ by 0.04.
- (5) From figure 88 or equivalent, determine that propeller operation also does not change M_{cr} but decreases $\left(\frac{V_i}{V_0}\right)_{cr}$ by 0.07.

(6) From steps (4) and (5) determine that addition of the spinner causes a ΔM_{cr} of zero and a $\Delta \left(\frac{V_i}{V_0}\right)_{cr}$ of -0.03 .

(7) With $\frac{d}{D_c} = 0.72$ and $M_{cr} + \Delta M_{cr} = 0.82$, select from figure 103 the NACA 1-72-094.5 open-nose cowling with $\left(\frac{V_i}{V_0}\right)_{cr} = 0.57$. For the cowling-spinner combination,

$$\left(\frac{V_i}{V_0}\right)_{cr} = 0.57 + \Delta \left(\frac{V_i}{V_0}\right)_{cr} = 0.54$$

a value greater than the assumed value of 0.51 which corresponds to the design $m/\rho_0 F V_0$. Thus, a second selection must be made.

(8) For the second selection, start with

$$\left(\frac{V_i}{V_0}\right)_{cr} = \frac{0.51 + 0.54}{2} = 0.525$$

and repeat steps (2) and (3) to obtain $\frac{d}{D_c} = 0.712$. Then from figure 103 select the NACA 1-71.2-096 open-nose cowling with $\left(\frac{V_i}{V_0}\right)_{cr} = 0.555$. Since

$$\left(\frac{V_i}{V_0}\right)_{cr} = 0.555 + \Delta \left(\frac{V_i}{V_0}\right)_{cr} = 0.525$$

the assumed value for the cowling-spinner combination, this cowling satisfies the design conditions.

Extrapolation of cowling-selection data.—When the design critical Mach number appreciably exceeds the range covered in figure 103, figures 44, 95, 96, and 97 and equation (10) of the appendix may be used to extrapolate the experimental design data to obtain longer or larger-inlet-diameter cowlings.

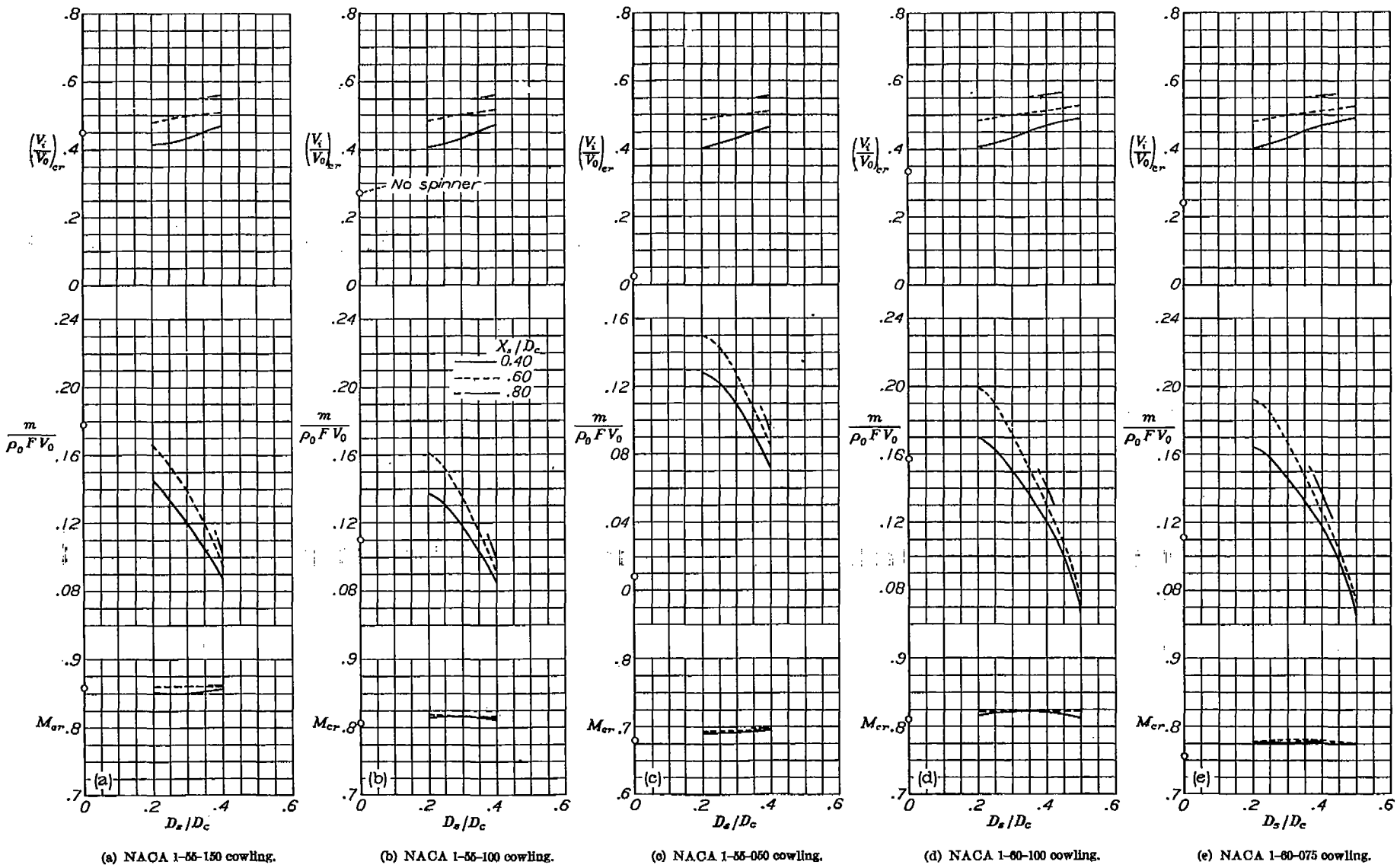


FIGURE 99.—Design conditions for NACA 1-series cowling-spinner combinations as a function of spinner proportions. Propeller removed; $\alpha=0^\circ$.

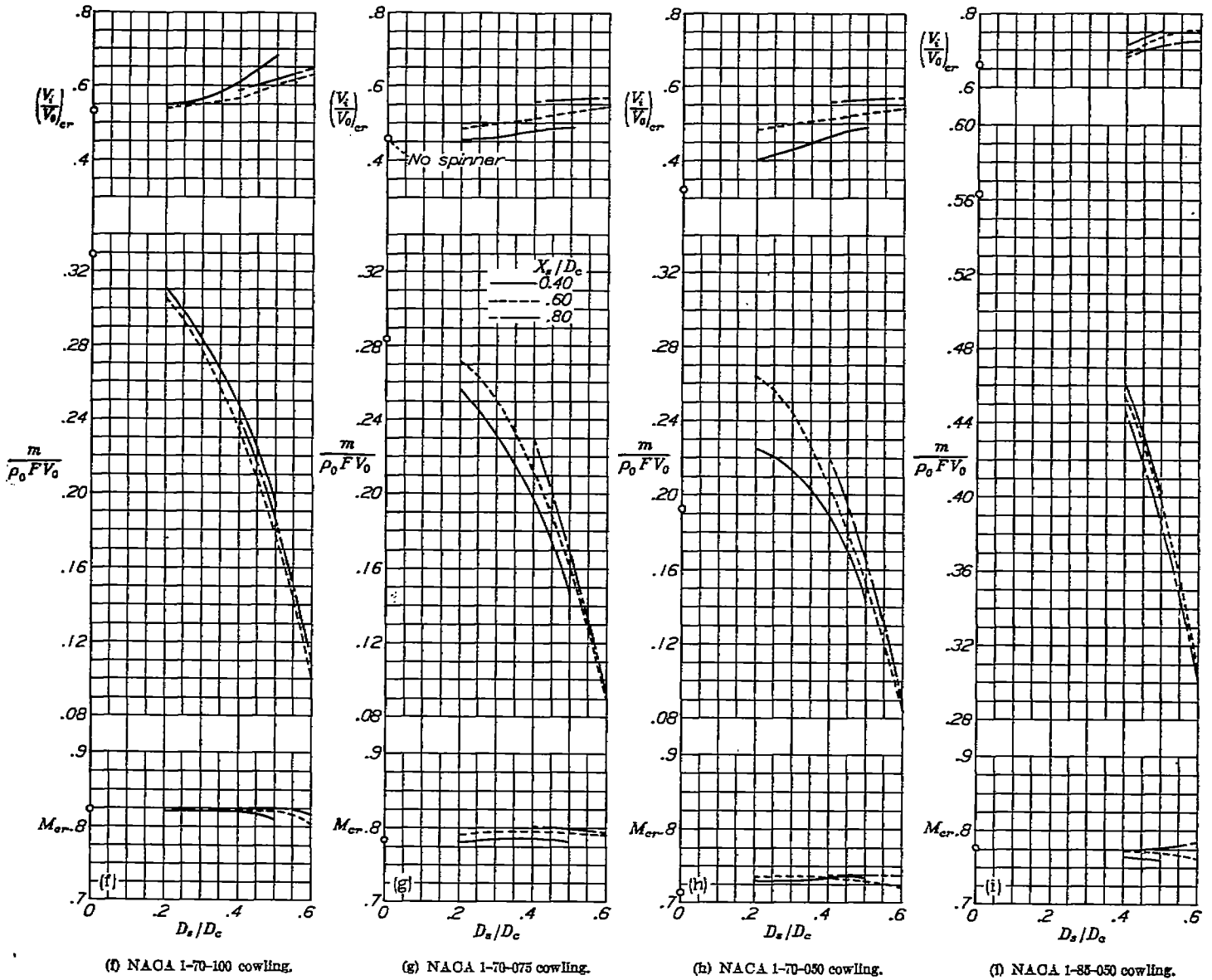


FIGURE 99.—Concluded.

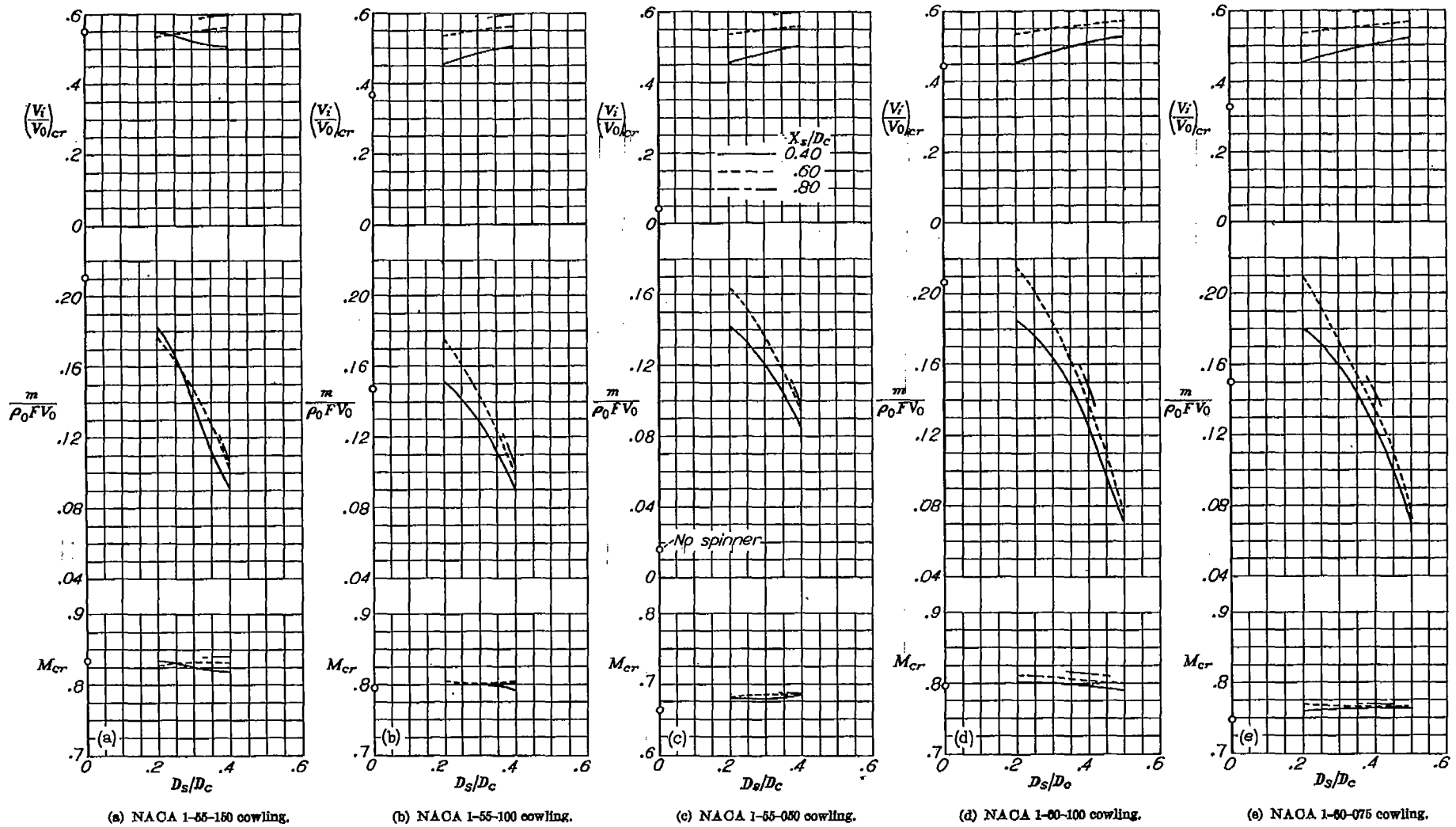
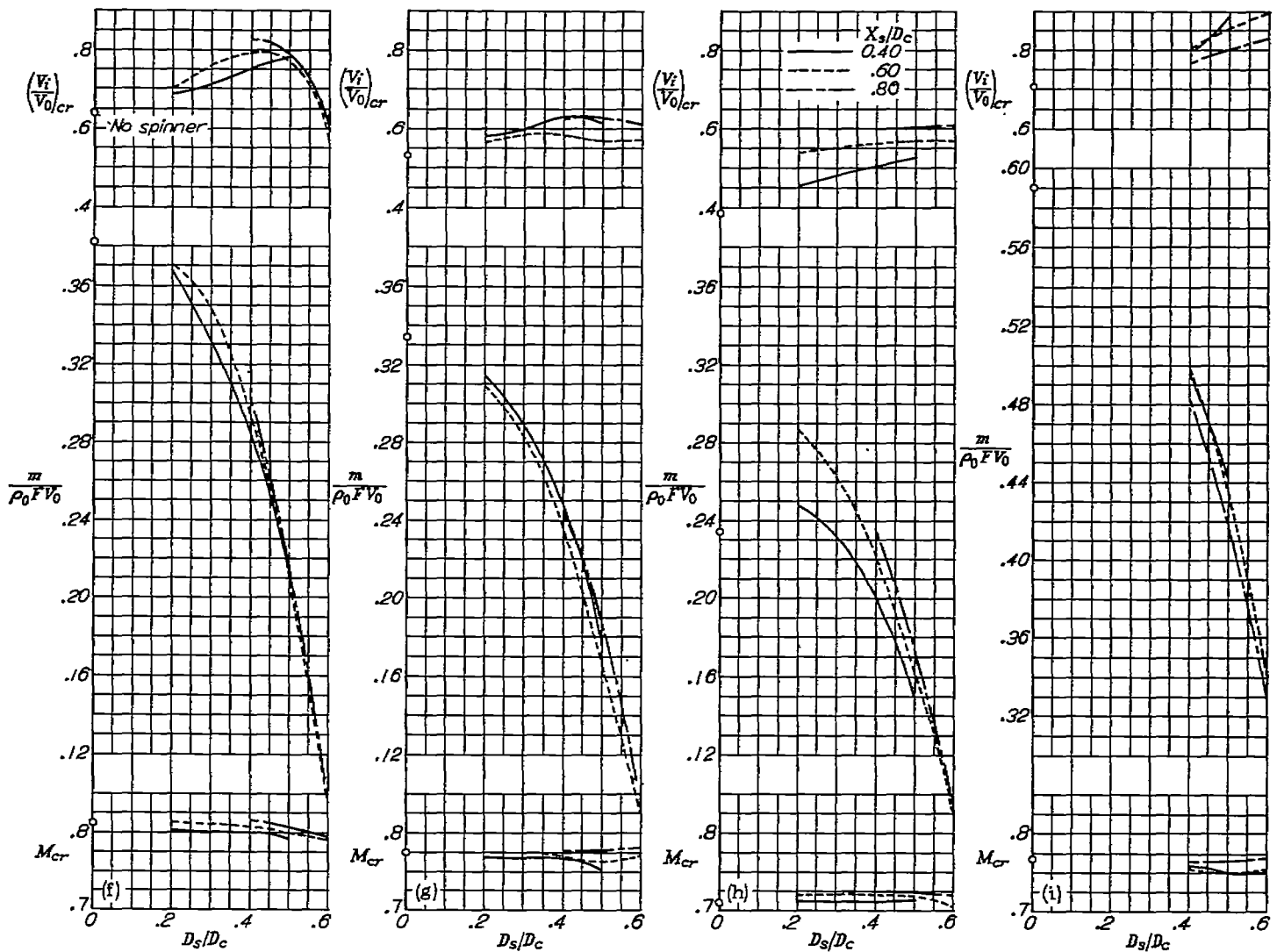


FIGURE 100.—Design conditions for NACA 1-series cowling-spinner combinations as a function of spinner proportions. Propeller removed; $\alpha=2^\circ$.



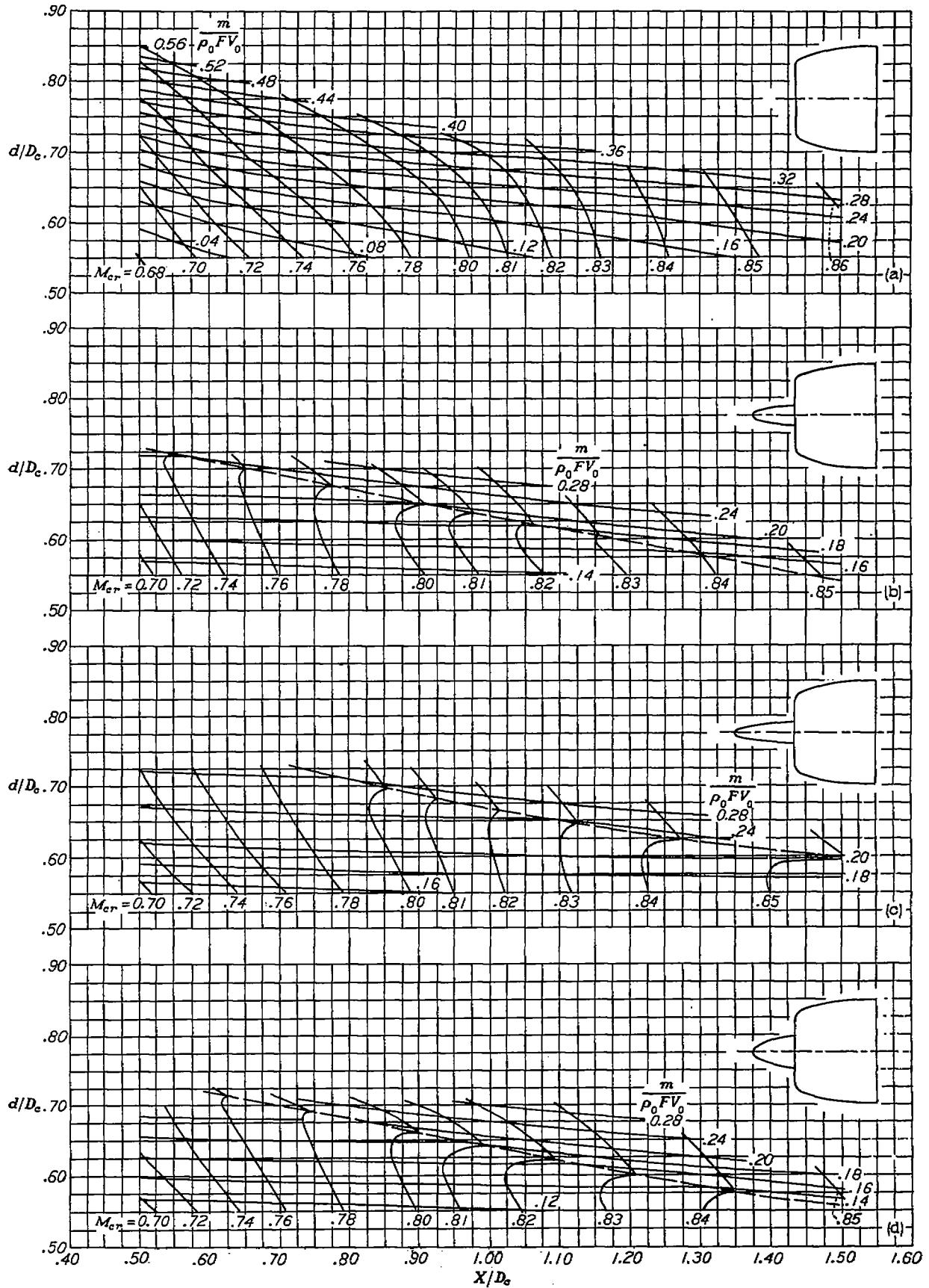
(f) NACA 1-70-100 cowling.

(g) NACA 1-70-075 cowling.

(h) NACA 1-70-050 cowling.

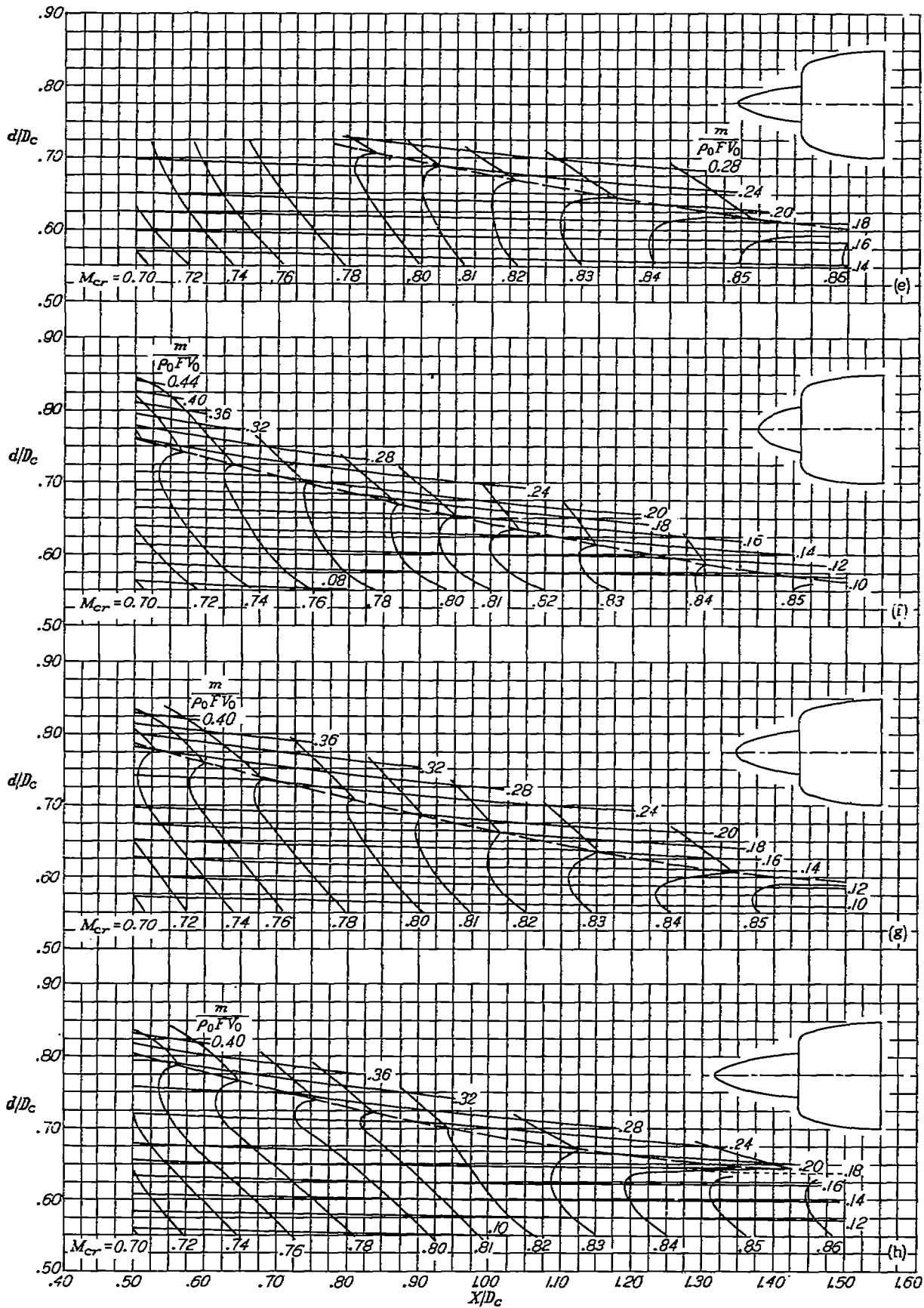
(i) NACA 1-85-050 cowling.

FIGURE 100.—Concluded.



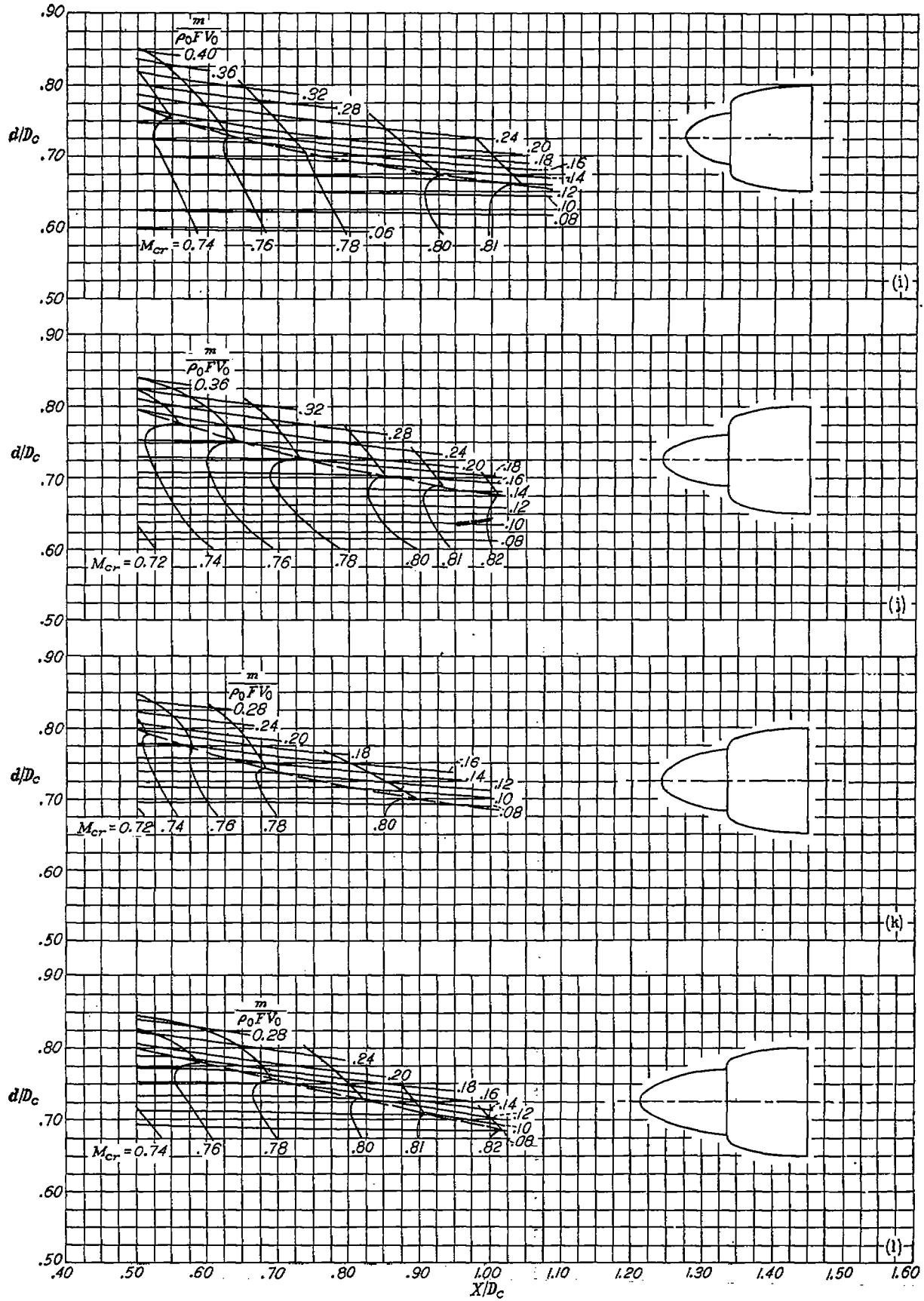
- (a) No spinner.
- (b) NACA 1-20-040 spinner.
- (c) NACA 1-20-080 spinner.
- (d) NACA 1-30-040 spinner.

FIGURE 101.—Selection charts for NACA 1-series cowling configurations. $\alpha = 0^\circ$.



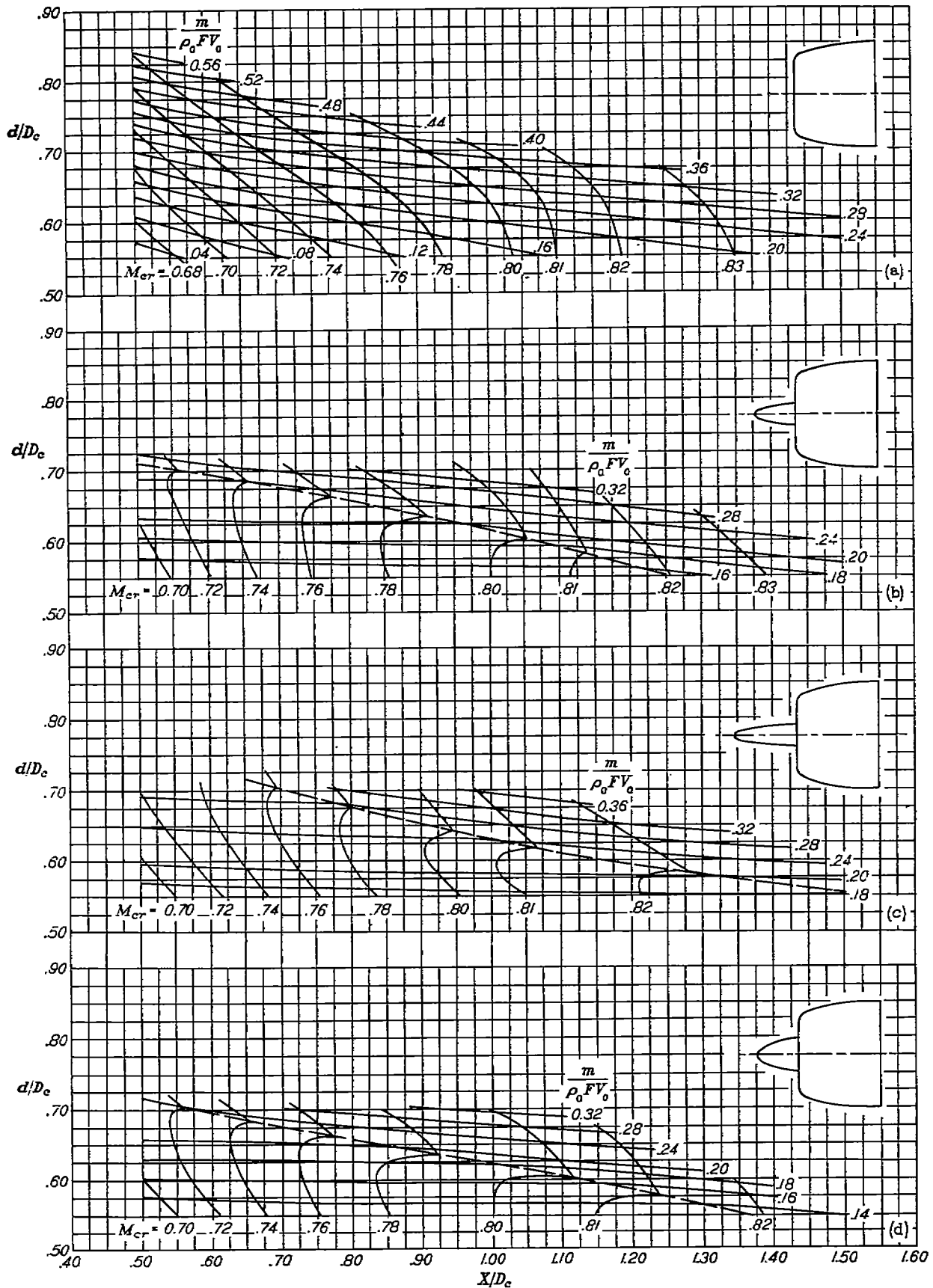
(e) NACA 1-30-060 spinner.
 (f) NACA 1-40-040 spinner.
 (g) NACA 1-40-060 spinner.
 (h) NACA 1-40-080 spinner.

FIGURE 101.—Continued.



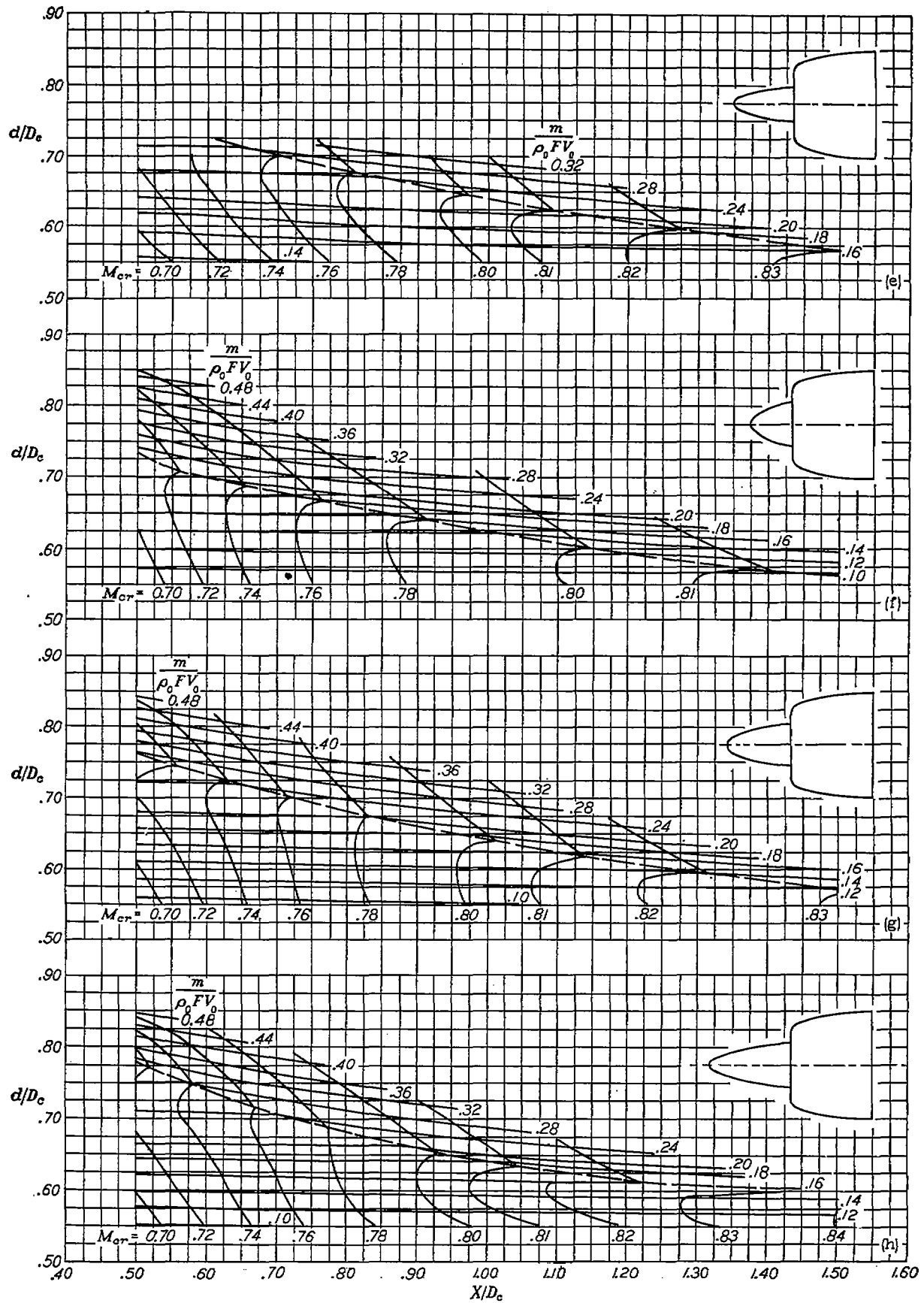
- (j) NACA 1-50-040 spinner.
- (k) NACA 1-50-060 spinner.
- (l) NACA 1-60-060 spinner.
- (m) NACA 1-60-080 spinner.

FIGURE 101.—Concluded.



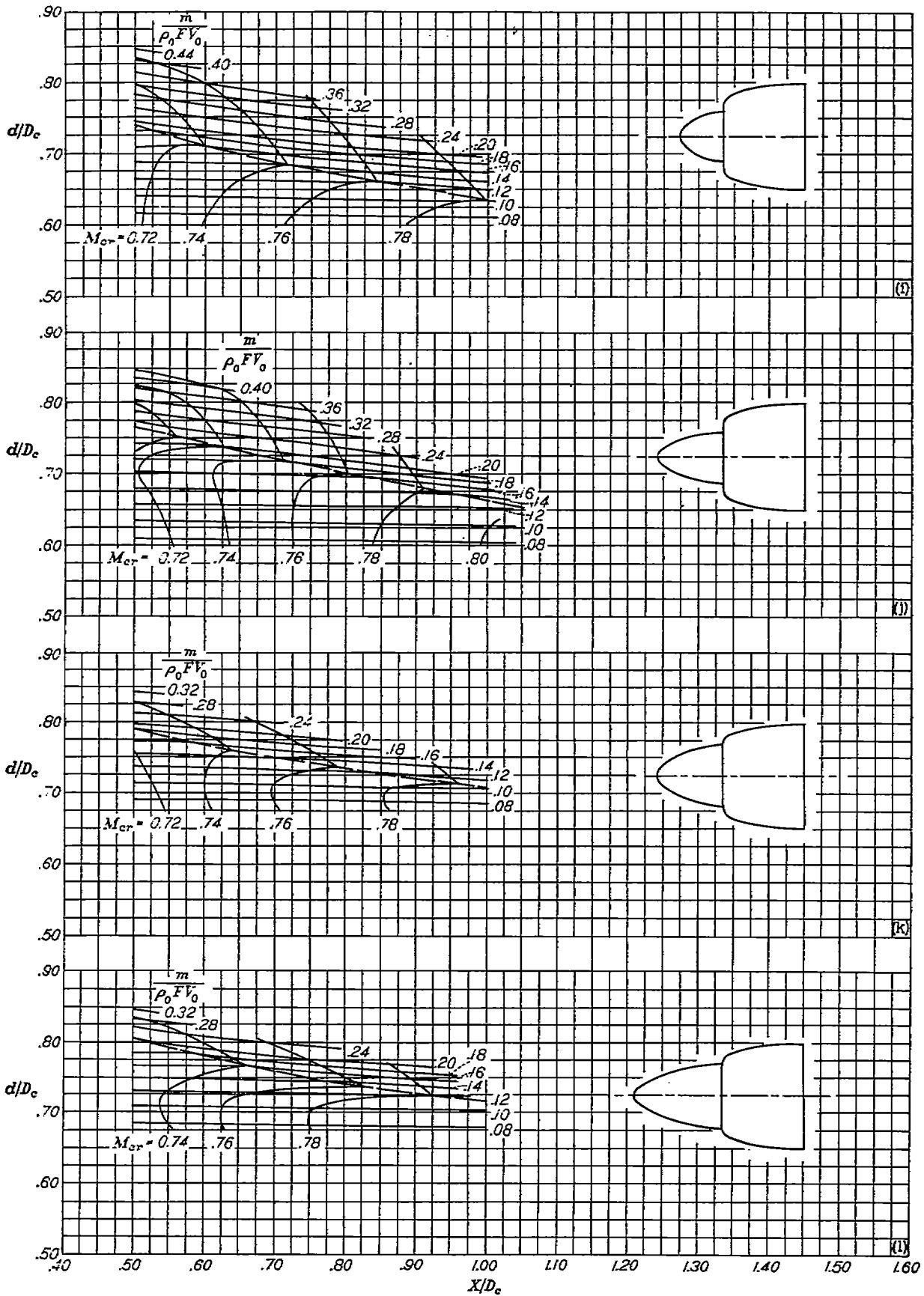
- (a) No spinner.
- (b) NACA 1-20-040 spinner.
- (c) NACA 1-20-060 spinner.
- (d) NACA 1-30-040 spinner.

FIGURE 102.—Selection charts for NACA 1-series cowling configurations. $\alpha = 2^\circ$.



(e) NACA 1-30-060 spinner.
 (f) NACA 1-40-040 spinner.
 (g) NACA 1-40-060 spinner.
 (h) NACA 1-40-080 spinner.

FIGURE 102.—Continued.



(i) NACA 1-50-040 spinner.
 (j) NACA 1-50-060 spinner.
 (k) NACA 1-60-080 spinner.
 (l) NACA 1-60-080 spinner.

FIGURE 102.—Concluded.

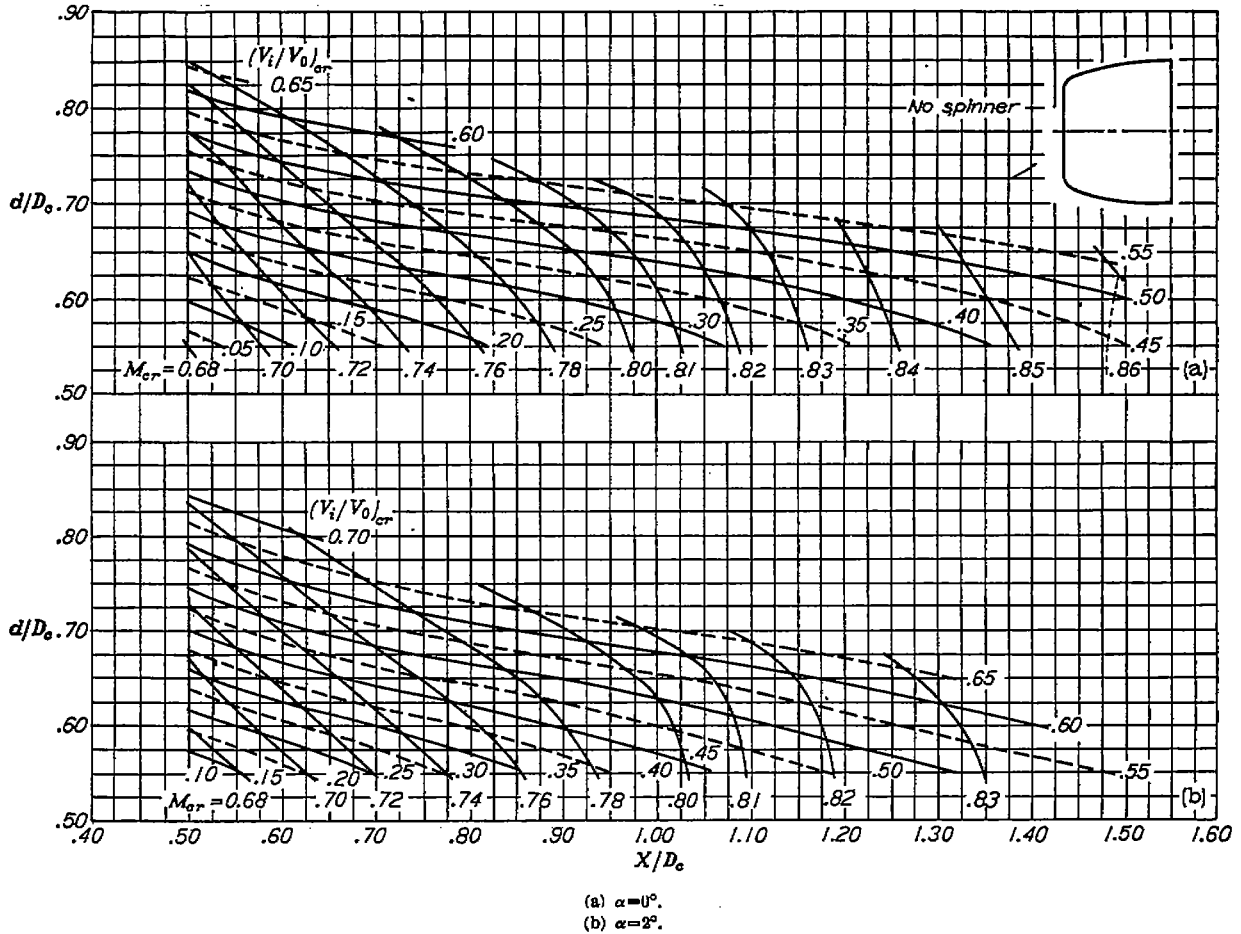


FIGURE 108.—Design values of critical Mach number and inlet-velocity ratio for NACA 1-series open-nose cowlings.

As an illustration of the proposed extrapolation procedure, take all the conditions of the preceding example except the critical Mach number and assume a new required critical Mach number of 0.90. Then proceed as follows:

(1) From figure 95 (a), determine required X/D_c for each of several values of d/D_c . (For example, $\frac{X}{D_c} = 1.87$ for $M_0 = 0.90$ and $\frac{d}{D_c} = 0.70$.)

(2) From figure 44 and equation (10) of the appendix, calculate required values of $\left(\frac{V_t}{V_0}\right)_{cr}$ for theoretical open-nose cowlings with sharp inlet lips, uniform surface pressure distributions corresponding to local $M = 1.0$ at $M_0 = 0.90$, and the same values of d/D_c as the cowlings selected in step (1). (For example, $\left(\frac{V_t}{V_0}\right)_{cr} = 0.51$ for $\frac{d}{D_c} = 0.70$.)

(3) Determine values of $\left(\frac{V_t}{V_0}\right)_{cr}$ for the NACA 1-series open-nose cowlings which correspond to values of $\left(\frac{V_t}{V_0}\right)_{cr}$ of step (2) by reference to figure 96. (For example, $\left(\frac{V_t}{V_0}\right)_{cr} = 0.66$ for $\frac{d}{D_c} = 0.70$, where $\left(\frac{V_t}{V_0}\right)_{cr} = 0.51$ for the theoretical cowling of this inlet-diameter ratio.)

(4) In order to allow for effect of the spinner on $\left(\frac{V_t}{V_0}\right)_{cr}$, add an increment of $\left(\frac{V_t}{V_0}\right)_{cr} = 0.04$ to values obtained in step (3) after reference to application data such as those of figure 97. Thus, for the NACA 1-series cowling-spinner combination with $\frac{d}{D_c} = 0.70$, $\left(\frac{V_t}{V_0}\right)_{cr} \approx 0.70$.

(5) Determine values of $\frac{A_t}{F}$ from figure 47. (For example, $\frac{A_t}{F} = 0.33$ for $\frac{d}{D_c} = 0.70$ and $\frac{D_t}{D_c} = 0.40$.)

(6) Determine design values of mass-flow coefficient from figure 48. (For example, $\frac{m}{\rho_0 F V_0} = 0.28$ for $\left(\frac{V_t}{V_0}\right)_{cr} = 0.70$, $M_{cr} = 0.90$, and $\frac{A_t}{F} = 0.33$.)

(7) Cross-fair the assumed values of d/D_c and the corresponding values of X/D_c from step (1) as a function of the mass-flow coefficients determined in step (6).

(8) At the required mass-flow coefficient of 0.23, determine from the cross fairing of step (7) that the NACA 1-66.5-198 cowling is the one required.

(9) From figure 48, determine that $\left(\frac{V_t}{V_0}\right)_{cr} = 0.65$ for the cowling-spinner combination of step (8). Then, note from figure 29 or equivalent that this value exceeds that necessary for avoiding separation from the spinner.

SUMMARY OF RESULTS

An investigation has been conducted in the Langley propeller-research tunnel to study cowling-spinner combinations based on the NACA 1-series nose inlets and to obtain systematic design data for one family of approximately ellipsoidal spinners. The more important conclusions of the investigation are summarized as follows:

1. For each spinner there is a single minimum inlet-velocity ratio below which boundary-layer separation from the spinner occurs at or ahead of the inlet. In the case of the NACA 1-series spinners, this inlet-velocity ratio is often higher than that necessary to obtain an essentially uniform pressure distribution on the cowling and, thus, determines the high-speed design conditions.

2. Short conical spinners are superior to comparable NACA 1-series spinners with regard to the minimum inlet-velocity ratio for which flow separation is avoided.

3. Separation bubbles occur on the inner-lip surface of the NACA 1-series cowlings at high inlet-velocity ratios and, in the case of the open-nose cowlings, initiate important separation of the internal flow. In the case of the cowling-spinner combinations, propeller operation causes a strong outwardly increasing total-pressure gradient in the inlet which delays and tends to eliminate such separation. A revised inner-lip shape of the type investigated can be used to delay the formation of such separation bubbles to considerably higher inlet-velocity ratios.

4. Within the usual range of proportions, the addition of NACA 1-series spinners to NACA 1-series cowlings does not change appreciably the design critical Mach numbers for the cowlings but frequently causes large changes in the inlet-velocity ratios required to obtain essentially uniform pressure distributions on the cowlings. Where the design conditions are not determined by the flow-separation characteristics of the spinner, the design inlet-velocity ratio increases rapidly with increases in the slope of the spinner surface just ahead of the inlet; important increases may be obtained when short conical spinners are substituted for conventional spinners of the same over-all proportions.

5. With a propeller having approximately oval shanks, propeller operation retards flow separation from the spinner

and inner cowling-lip surface and, within the usual range of high-speed operating conditions, does not reduce the design critical Mach number.

6. Increases in flight Mach number reduce the effective angle of attack of the cowling lip for given values of inlet-velocity ratio less than unity and, thus, reduce the minimum value of inlet-velocity ratio for which a near-uniform surface pressure distribution on the cowling is obtained and tend to make the inner cowling-lip surface more susceptible to flow separation.

Inasmuch as the present tests were conducted at low test airspeeds, the investigation necessarily included a study of the procedure required to determine the design operating conditions at the design flight Mach number from the low-speed test results. In this study, existing relations for open-nose cowlings were generalized to the case of the cowling-spinner combination and extended to the case of compressible flow. The derived relations were then used to calculate the effect of Mach number on the design inlet-velocity ratio and to establish a simple correction procedure.

The design conditions for the NACA 1-series cowlings and cowling-spinner combinations are presented in the form of charts from which, for wide ranges of spinner proportions and rates of internal flow, cowlings with near-maximum pressure recovery can be selected for critical Mach numbers ranging from 0.70 to about 0.85. In addition, the characteristics of the spinners and the effects of the spinners and the propeller on the cowling design conditions are presented separately to provide initial quantitative data for use in a general design procedure through which NACA 1-series cowlings can be selected for use with spinners of other shapes. By use of this general design procedure, correlation curves established from the test data, and the equations of the appendix, NACA 1-series cowlings and cowling-spinner combinations can be designed for critical Mach numbers as high as 0.90.

LANGLEY MEMORIAL AERONAUTICAL LABORATORY,
NATIONAL ADVISORY COMMITTEE FOR AERONAUTICS,
LANGLEY FIELD, VA., February 4, 1948.

APPENDIX

EQUATIONS RELATING INLET-VELOCITY RATIO WITH SURFACE PRESSURES AND FRONTAL AREAS OF COWLING AND SPINNER

P. Ruden in references 4 and 5 presents incompressible-flow equations relating the inlet-velocity ratio, inlet-area ratio, and surface-velocity ratios for a nose inlet. Because of their importance to the present investigation, these equations are herewith generalized to cover the case of the cowl-spinner combination. The scheme used in the basic derivations is also used to obtain similar compressible-flow relations for both open-nose cowlings and cowl-spinner combinations.

Consider in figure 104 the volume of reference, which encloses the cowling for a distance aft of the maximum-diameter station great enough to allow the external velocities to return to the free-stream value and which is so large that the pressures on its boundaries outside of the cowling are everywhere equal to the free-stream pressure. In steady flight, this volume must be in equilibrium; hence, the difference between axial forces on the ends of this volume must equal the rate of change of momentum of the internal flow. On the external surface of the cowling, the skin friction corresponds approximately to the momentum loss in the boundary layer so that both may be neglected in setting up the force equation. Thus, the axial pressure force on the spinner plus the pressure force on the inlet area plus the axial pressure force on the cowling minus the product of the free-stream pressure and the cowling frontal area plus the skin-friction drag of the spinner must equal the rate of change of momentum of the internal flow. If forces which tend to push the reference volume in the thrust direction are defined as positive, this relation can be expressed algebraically as follows:

$$2\pi \int_0^{D_s/2} p_s r dr + 2\pi \int_{D_s/2}^{d/2} p_f r dr + 2\pi \int_{d/2}^{D_c/2} p_c r dr - p_0 F + f_s = \rho_t A_t V_t (V_0 - V_t) \quad (1)$$

If the free-stream pressure is taken as the reference pressure and all terms are divided by q_0 , the following expression in terms of the pressure coefficient is obtained:

$$2\pi \int_0^{D_s/2} P_s r dr + 2\pi \int_{D_s/2}^{d/2} P_f r dr + 2\pi \int_{d/2}^{D_c/2} P_c r dr + \frac{f_s}{q_0} + \frac{\pi(d^2 - D_s^2)}{2} \left(\frac{\rho_t}{\rho_0}\right) \left(\frac{V_t}{V_0}\right) \left(\frac{V_t}{V_0} - 1\right) = 0 \quad (2)$$

Then, if the local pressure coefficients in the three terms on the left are replaced by average pressure coefficients weighted with respect to frontal area and all terms are then divided

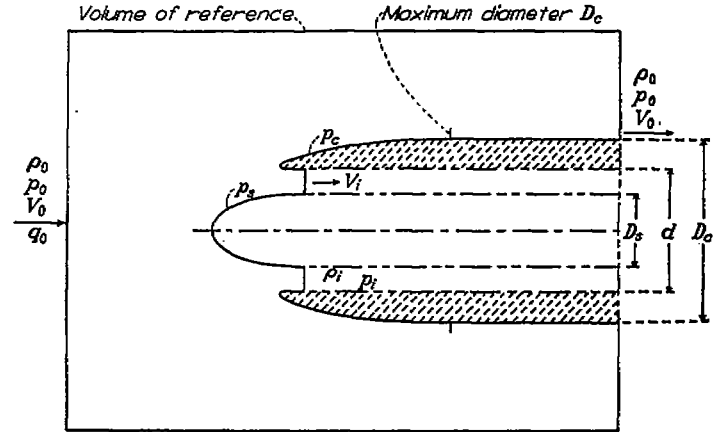


FIGURE 104.—Schematic diagram defining quantities considered in theoretical calculations of the appendix.

by $F = \frac{\pi D_c^2}{4}$, equation (2) becomes

$$\left(\frac{D_s}{D_c}\right)^2 P_{s,av} + \left[\left(\frac{d}{D_c}\right)^2 - \left(\frac{D_s}{D_c}\right)^2\right] P_c + \left[1 - \left(\frac{d}{D_c}\right)^2\right] P_{c,av} + \frac{f_s}{q_0 F} + 2 \left[\left(\frac{d}{D_c}\right)^2 - \left(\frac{D_s}{D_c}\right)^2\right] \left(\frac{\rho_t}{\rho_0}\right) \left(\frac{V_t}{V_0}\right) \left(\frac{V_t}{V_0} - 1\right) = 0 \quad (3)$$

Incompressible-flow case.—If the flow is incompressible so that $\rho_t = \rho_0$, $P_t = 1 - \left(\frac{V_t}{V_0}\right)^2$. Therefore, the second and fourth terms can be combined and the following general incompressible-flow expression for the average surface pressure coefficient on a cowl-spinner combination obtained:

$$P_{c,av} = \frac{\left(\frac{D_s}{D_c}\right)^2 P_{s,av} + \left[\left(\frac{d}{D_c}\right)^2 - \left(\frac{D_s}{D_c}\right)^2\right] \left(1 - \frac{V_t^2}{V_0^2}\right) + \frac{f_s}{q_0 F}}{\left(\frac{d}{D_c}\right)^2 - 1} \quad (4)$$

where the term $f_s/q_0 F$ can be neglected unless the spinner diameter is very large with respect to the maximum diameter of the cowl. It will be noted that the inlet-velocity ratio occurs only as $\left(1 - \frac{V_t^2}{V_0^2}\right)$ so that a given set of pressures would appear to correspond to two different inlet-velocity ratios, one greater than unity and one less than unity.

Equation (4) can be used to compute the average surface pressure coefficient on one component of the cowl-spinner combination if the surface pressure distributions on the other component, the inlet-velocity ratio, and the frontal dimensions of the inlet are known. Similarly, with the surface

pressures and frontal dimensions of one component known, the required frontal area of the other component for stipulated average surface pressure coefficients can be calculated for arbitrary values of inlet-velocity ratio. Also, as in the present report, this relation can be used to compute the inlet-velocity ratio from the frontal proportions of the installation and the surface pressure distributions.

In the case of the open-nose cowling, the spinner-diameter ratio goes to zero so that equation (4) for this special case becomes

$$P_{c_{ar}} = \frac{\left(1 - \frac{V_i^2}{V_0^2}\right)^2}{1 - \left(\frac{D_s}{d}\right)^2} \quad (5)$$

This equation can be transformed directly into the forms given in references 4 and 5.

Compressible-flow case.—An examination of equations (2) and (3) shows that all terms of these general relations are affected by a departure from the assumption of incompressible flow. However, it is possible to calculate the effects of compressibility on the inlet-static-pressure coefficient P_i and on the inlet-density ratio ρ_i/ρ_0 as a function of inlet-velocity ratio. Therefore, the same method of analysis can be used to obtain compressible-flow expressions relating the inlet-velocity ratio to the surface pressure coefficients and frontal areas of the spinner and cowling.

Consider the energy equation,

$$\frac{V_0^2}{2} + \frac{\gamma}{\gamma-1} \frac{p_0}{\rho_0} = \frac{V_i^2}{2} + \frac{\gamma}{\gamma-1} \frac{p_i}{\rho_i}$$

or

$$\frac{p_i}{\rho_i} - \frac{p_0}{\rho_0} = \frac{\gamma-1}{\gamma} \left(\frac{V_0^2}{2} - \frac{V_i^2}{2} \right)$$

Since $\rho_i = \rho_0 \left(\frac{p_i}{p_0}\right)^{\frac{1}{\gamma}}$ for isentropic flow,

$$p_i^{\frac{\gamma-1}{\gamma}} - p_0^{\frac{\gamma-1}{\gamma}} = \left(\frac{\rho_0}{\rho_i}\right)^{\frac{\gamma-1}{\gamma}} \left(\frac{\gamma-1}{\gamma}\right) \left(\frac{V_0^2}{2} - \frac{V_i^2}{2}\right)$$

Then, since $\frac{p_0}{\gamma p_0} = \frac{1}{a_0^2}$ and $\frac{V_0^2}{a_0^2} = M_0^2$,

$$p_i^{\frac{\gamma-1}{\gamma}} - p_0^{\frac{\gamma-1}{\gamma}} = \frac{\gamma-1}{2} M_0^2 p_0^{\frac{\gamma-1}{\gamma}} \left[1 - \left(\frac{V_i}{V_0}\right)^2 \right]$$

Whence

$$\frac{p_i}{p_0} = \left[\frac{\gamma-1}{2} M_0^2 - \frac{\gamma-1}{2} M_0^2 \left(\frac{V_i}{V_0}\right)^2 + 1 \right]^{\frac{\gamma}{\gamma-1}} \quad (6)$$

Then, since $\frac{p_0}{q_0} = \frac{2}{\gamma M_0^2}$,

$$P_i = \frac{p_i - p_0}{q_0} = \frac{2}{\gamma M_0^2} \left\{ \left[\frac{\gamma-1}{2} M_0^2 - \frac{\gamma-1}{2} M_0^2 \left(\frac{V_i}{V_0}\right)^2 + 1 \right]^{\frac{\gamma}{\gamma-1}} - 1 \right\} \quad (7)$$

Also, from equation (6) since $\frac{p_i}{\rho_i} = \left(\frac{p_i}{p_0}\right)^{\frac{1}{\gamma}}$ for isentropic flow,

$$\frac{p_i}{\rho_i} = \left[\frac{\gamma-1}{2} M_0^2 - \frac{\gamma-1}{2} M_0^2 \left(\frac{V_i}{V_0}\right)^2 + 1 \right]^{\frac{1}{\gamma-1}} \quad (8)$$

With expressions (7) and (8), the second and fourth terms of equation (3), as in the incompressible-flow case, again can be combined into a single term

$$2 \left[\left(\frac{d}{D_c}\right)^2 - \left(\frac{D_s}{D_c}\right)^2 \right] \left(\frac{1}{\gamma M_0^2} \left\{ \frac{\gamma-1}{2} M_0^2 - \frac{\gamma-1}{2} M_0^2 \left(\frac{V_i}{V_0}\right)^2 + 1 \right\}^{\frac{\gamma}{\gamma-1}} - 1 \right) + \left[\left(\frac{V_i}{V_0}\right)^2 - \frac{V_i}{V_0} \right] \left[\frac{\gamma-1}{2} M_0^2 - \frac{\gamma-1}{2} M_0^2 \left(\frac{V_i}{V_0}\right)^2 + 1 \right]^{\frac{1}{\gamma-1}}$$

If a symbol C is assigned to the quantity within the large parentheses, the following compressible-flow expression for the average surface pressure coefficient on the cowling of a cowling-spinner combination can be obtained from equation (3):

$$P_{c_{ar}} = \frac{\left(\frac{D_s}{D_c}\right)^2 P_{c_{ar}} + 2C \left[\left(\frac{d}{D_c}\right)^2 - \left(\frac{D_s}{D_c}\right)^2 \right] + \frac{f_s}{q_0 F}}{\left(\frac{d}{D_c}\right)^2 - 1} \quad (9)$$

where, it is again noted, that the term $f_s/q_0 F$ can be neglected, unless the spinner diameter is very large with respect to the maximum diameter of the cowling. The corresponding expression for the open-nose cowling is then

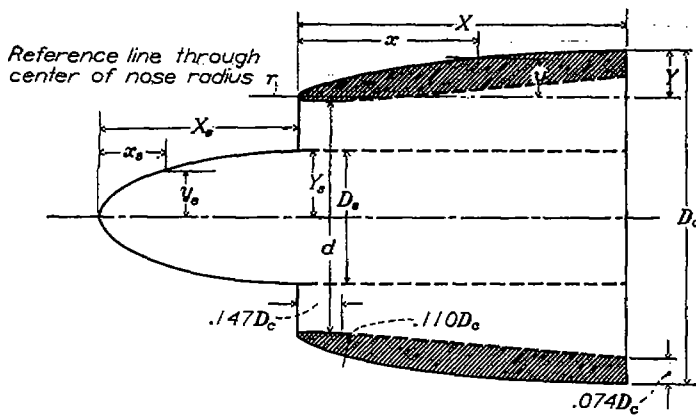
$$P_{c_{ar}} = \frac{2C}{1 - \left(\frac{D_s}{d}\right)^2} \quad (10)$$

As an aid to the solution of these equations, factor C is presented in figure 44 as a function of the free-stream Mach number and the inlet-velocity ratio.

Equations (9) and (10) when used with figure 44 have approximately the same field of application as incompressible-flow equations (4) and (5). Also, as developed in the text, it is possible by use of these equations to determine the approximate high-speed inlet-velocity ratio from low-speed test data by extrapolating the measured surface pressure coefficients by means of the Von Kármán relation. However, inasmuch as the Von Kármán relation does not accurately predict the variation of large positive pressure coefficients with Mach number, the latter application can give reasonably accurate results only so long as the region of large positive pressure on the cowling and spinner is small with respect to the region of negative pressure on the cowling.

TABLE I.—NACA 1-SERIES NOSE-INLET ORDINATES AS APPLIED TO COWLINGS AND SPINNERS

[Ordinates in percent, reference 1]



$$X = \left(\frac{X}{D_c}\right) D_c \quad X_c = \left(\frac{X_c}{D_c}\right) D_c$$

$$Y = \frac{D_c - d}{2} \quad Y_s = \frac{D_s}{2} = \frac{\left(\frac{D_s}{D_c}\right) D_c}{2}$$

For $r=0.025Y$: $Y = \frac{D_c - d}{2.05} = \frac{D_c \left(1 - \frac{d}{D_c}\right)}{2.05}$

| z/X or z_d/X_c | y/Y or y_d/Y_c |
|--------------------|--------------------|--------------------|--------------------|--------------------|--------------------|--------------------|--------------------|
| 0 | 0 | 13.0 | 41.94 | 34.0 | 69.08 | 60.0 | 89.11 |
| .2 | 4.80 | 14.0 | 43.66 | 35.0 | 70.08 | 62.0 | 90.20 |
| .4 | 6.63 | 15.0 | 45.30 | 36.0 | 71.05 | 64.0 | 91.23 |
| .6 | 8.12 | 16.0 | 46.88 | 37.0 | 72.00 | 66.0 | 92.20 |
| .8 | 9.33 | 17.0 | 48.40 | 38.0 | 72.94 | 68.0 | 93.11 |
| 1.0 | 10.38 | 18.0 | 49.88 | 39.0 | 73.85 | 70.0 | 93.95 |
| 1.5 | 12.72 | 19.0 | 51.31 | 40.0 | 74.75 | 72.0 | 94.75 |
| 2.0 | 14.72 | 20.0 | 52.70 | 41.0 | 75.63 | 74.0 | 95.48 |
| 2.5 | 16.57 | 21.0 | 54.05 | 42.0 | 76.48 | 76.0 | 96.16 |
| 3.0 | 18.21 | 22.0 | 55.37 | 43.0 | 77.32 | 78.0 | 96.79 |
| 3.5 | 19.94 | 23.0 | 56.66 | 44.0 | 78.15 | 80.0 | 97.36 |
| 4.0 | 21.48 | 24.0 | 57.92 | 45.0 | 78.95 | 82.0 | 97.87 |
| 4.5 | 22.95 | 25.0 | 59.15 | 46.0 | 79.74 | 84.0 | 98.33 |
| 5.0 | 24.30 | 26.0 | 60.36 | 47.0 | 80.50 | 86.0 | 98.74 |
| 6.0 | 27.01 | 27.0 | 61.52 | 48.0 | 81.25 | 88.0 | 99.09 |
| 7.0 | 29.47 | 28.0 | 62.67 | 49.0 | 81.99 | 90.0 | 99.40 |
| 8.0 | 31.81 | 29.0 | 63.79 | 50.0 | 82.69 | 92.0 | 99.65 |
| 9.0 | 34.03 | 30.0 | 64.89 | 52.0 | 84.10 | 94.0 | 99.85 |
| 10.0 | 36.13 | 31.0 | 65.97 | 54.0 | 85.45 | 96.0 | 99.93 |
| 11.0 | 38.15 | 32.0 | 67.03 | 56.0 | 86.73 | 98.0 | 99.98 |
| 12.0 | 40.09 | 33.0 | 68.07 | 58.0 | 87.95 | 100.0 | 100.00 |

Cowling nose radius: 0.025Y

TABLE II.—BASIC CRITICAL MACH NUMBER DATA FOR NACA 1-SERIES COWLING CONFIGURATIONS

| Figure (*) | Cowling | Spinner | |
|------------|----------|-------------------|------------------------------|
| | | $\frac{X_s}{D_s}$ | $\frac{D_s}{D_c}$ |
| 49 | 1-55-160 | 0.40 | 0.20, 0.30, 0.40 |
| 50 | 1-55-160 | .60 | 0.20, 0.30, 0.40 |
| 51 | 1-55-160 | .80 | 0.40 |
| 52 | 1-55-100 | .40 | 0.20, 0.30, 0.40 |
| 53 | 1-55-100 | .60 | 0.20, 0.30, 0.40 |
| 54 | 1-55-100 | .80 | 0.40 |
| 55 | 1-55-060 | .40 | 0.20, 0.30, 0.40 |
| 56 | 1-55-060 | .60 | 0.20, 0.30, 0.40 |
| 57 | 1-55-060 | .80 | 0.40 |
| 58 | 1-60-100 | .40 | 0.20, 0.30, 0.40, 0.60 |
| 59 | 1-60-100 | .60 | 0.20, 0.30, 0.40, 0.60 |
| 60 | 1-60-100 | .80 | 0.40 |
| 61 | 1-60-075 | .40 | 0.20, 0.30, 0.40, 0.60 |
| 62 | 1-60-075 | .60 | 0.20, 0.30, 0.40, 0.60 |
| 63 | 1-60-075 | .80 | 0.40 |
| 64 | 1-70-100 | .40 | 0.20, 0.30, 0.40, 0.60 |
| 65 | 1-70-100 | .60 | 0.20, 0.30, 0.40, 0.60, 0.60 |
| 66 | 1-70-100 | .80 | 0.40, 0.60 |
| 67 | 1-70-075 | .40 | 0.20, 0.30, 0.40, 0.60 |
| 68 | 1-70-075 | .60 | 0.20, 0.30, 0.40, 0.60, 0.60 |
| 69 | 1-70-075 | .80 | 0.40, 0.60 |
| 70 | 1-70-050 | .40 | 0.20, 0.30, 0.40, 0.60 |
| 71 | 1-70-050 | .60 | 0.20, 0.30, 0.40, 0.60, 0.00 |
| 72 | 1-70-050 | .80 | 0.40, 0.60 |
| 73, 74 | 1-85-060 | .40 | 0.40, 0.60 |
| 75, 76 | 1-85-050 | .60 | 0.40, 0.60, 0.60 |
| 77, 78 | 1-85-050 | .80 | 0.40, 0.60 |

* Data for open-nose condition are presented in each figure for purpose of comparison.

REFERENCES

1. Baals, Donald D., Smith, Norman F., and Wright, John B.: The Development and Application of High-Critical-Speed Nose Inlets. NACA Rep. 920, 1948.
2. Boswinkle, Robert W., Jr., and Bryant, Rosemary P.: An Experimental Investigation of Flow Conditions in the Vicinity of an NACA D_s-Type Cowling. NACA MR L6H14, 1946.
3. Boswinkle, Robert W., Jr.: Air-Flow Surveys in the Vicinity of Representative NACA 1-Series Cowlings. NACA RM L8A15a, 1948.
4. Ruden, P.: Windkanalmessungen an einem rotationssymmetrischen Fangdiffusor. Forschungsbericht Nr. 1427/1, Deutsche Luftfahrtforschung (Hannover), 1941.
5. Ruden, P.: Ebne symmetrische Fangdiffusoren. Forschungsbericht Nr. 1209, Deutsche Luftfahrtforschung (Hannover), 1940.
6. Smith, Norman F., and Baals, Donald D.: Wind-Tunnel Investigation of a High-Critical-Speed Fuselage Scoop Including the Effects of Boundary Layer. NACA ACR L5B01a, 1945.
7. Von Kármán, Th.: Compressibility Effects in Aerodynamics. Jour. Aero. Sci., vol. 8, no. 9, July 1941, pp. 337-356.